A.L.A. Kerver

Computer Assisted Surgical Anatomy Mapping

Applications in

Surgical Anatomy Research
Tailor-Made Surgery
Personalized Teaching

COMPUTER ASSISTED SURGICAL ANATOMY MAPPING

Applications in Surgical Anatomy Research, Tailor-Made Surgery and Personalized Teaching

Anton Leo Albert Kerver

ISBN: 978-94-91462-39-9
EAN: 9789491462399

Cover: Anton L.A. Kerver. Original image by “Packt Publishing”
Lay-out: Anton L.A. Kerver.
Contact: antonkerver@gmail.com
Print: Canon - De Studio

Computer Assisted Surgical Anatomy Mapping

Applications in surgical anatomy research,
tailor-made surgery and personalized teaching.

C A S A M

Toepassingen in chirurgisch-anatomisch onderzoek,
gepersonaliseerde chirurgie en geïndividualiseerd onderwijs.

Proefschrift

ter verkrijging van de graad van doctor aan de
Erasmus Universiteit Rotterdam
op gezag van de
rector magnificus

Prof.dr. H.A.P. Pols

en volgens besluit van het College voor Promoties.

De openbare verdediging zal plaatsvinden op
dinsdag 12 september 2017 om 15.30 uur

door

Anton Leo Albert Kerver
geboren op 17 april 1986
te Utrecht

Promotiecommissie:

Promotor:	Prof.dr. G.J. Kleinrensink
Overige leden:	Prof.dr. S.E.R. Hovius Prof.dr. M.H.J Verhofstad Prof.dr. D.J.O. Ulrich
Copromotoren:	Dr. E.T. Walbeehm Dr. D. Den Hartog

TABLE OF CONTENTS

01101001 01101110 01110100
01110010 01101111 01100100
01110101 01100011 01110100
01101001 01101111 01101110

General introduction and Outline of this thesis

INTRODUCTION

One of the major difficulties in surgery is a safe approach of the operation site. The vast amount of different surgical approaches for the same procedure exemplifies the constant surgical dilemma between exposure and tissue sparing. Iatrogenic damage to nerves and vessels still is a common complication of surgery, resulting in a wide array of postoperative complaints such as impaired wound healing and neuropathic pain. Meanwhile general public opinion appears to become less forgiving and surgeons are held accountable for iatrogenic damage. In this thesis several examples of iatrogenic damage to nerves or vessels are being linked to the clinical research questions that preceded these studies. Damage to arteries of the lateral ankle during calcaneal surgery results in high complication rates, with the rate of infection reported in up to 21%[1-5], and superficial necrosis reported in up to 14% of cases[4, 6]. Damage to motor nerves such as the intercostal- and subcostal nerves results in flank bulge after lumbotomy in up to 49%[7] as parts of the abdominal muscles are no longer innervated[8-10]. Sensory nerve damage may result in minor complaints such as numbness or paresthesia but also highly invalidating neuropathic pain or symptomatic neuroma`s are regular complications[11, 12]. For example, up to 10% of sural nerve injury[13] is reported after ankle surgery. In addition, in knee surgery 28% of the patients report irritating paresthesia after open meniscectomy[14] and it is a common complication after arthroscopy[15-17]. Furthermore, in total knee arthroplasty numbness of the anterolateral part of the knee is reported in as much as 55 to 100 %[18-19]. Especially in the knee these sensory, afferent nerves are also essential for transporting proprioceptive information. A lack of joint position perception can contribute towards joint instability which in turn leads to osteoarthritis. Less invasive techniques such as endovenous thermal ablation of the short saphenous vein in varicosis of the leg are also not without risk of complications. Since the sensory sural nerve is located closely to the vein which is ablated, thermal damage to the nerve can be a serious complication.

In the everlasting surgical dilemma between tissue sparing and exposure, iatrogenic damage to vessels, nerves and other anatomical structures can be inevitable. Nevertheless, preventing complications is of primary interest to any surgeon. Insufficient knowledge of human anatomy should never be the cause of iatrogenic complications in surgery. Despite of what plastic anatomy models, 2D anatomy books or virtual 3D anatomy-app's[20] suggest, there is an endless variation in human anatomy. Even in twins there is a wide array of differences.

In addition, differences between left and right extremities are always present in every single person. Thus, normal anatomy does not equal anatomy that is without variation[21]. The word normal is derived from the Latin word normalis which means "conform to the rule of pattern" and in descriptive anatomy the word "normal" is used for an anatomical structure falling within a normal range of characteristics. Generally speaking in anatomy the range of "normal" characteristics is rather extensive. Everything beyond "normal anatomy" is considered an anomaly or malformation. It is estimated that the incidence of minor malformations ranges from 7-40%[22, 23] whilst major anomalies are present in 2-3% of the general population[24].

For any surgeon, memorizing all variations of what we perceive as normal anatomy is close to impossible. Nor can a surgeon take into account all the different and sometimes rare anatomical abnormalities. Modern society demands complication free surgery but novel developments such as minimal invasive surgery allow for less exploration and exposure of vulnerable structures during surgery. This inadvertently has impact on the anatomical knowledge of young surgeons as the conventional way of learning anatomy, by experience in the operating room, becomes inadequate as less anatomy is dissected during a day of training. Moreover, anatomical knowledge is even more important in minimally invasive surgery than in conventional surgery, as less exposure and visibility requires more knowledge of surgical landmarks and anatomical variation. In the small area of laparoscopic views, the course of structures cannot be used for identification of an anatomical structure since only fragments of the structure can be seen. Neither can palpation be used to identify pulsatile structures since haptic feedback has not yet been introduced to laparoscopic surgery.

Furthermore, there is the difference between 'looking in from the outside' versus 'looking from the inside out'. A completely new set of anatomical perspectives arise. The most well known example is probably the 'dorsal view anatomy' of the abdominal wall at the level of the inguinal region. The Totally Extraperitoneal Procedure (TEP) in inguinal hernia repair has introduced new surgical questions and hence new answers were given by the anatomist. A new branch on the Anatomical tree developed: the endoscopic anatomy.

Experience alone is not enough to learn anatomical variations. This is most apparently shown in learning the anatomy of nerves. In contrast to vascular damage in which immediate hemorrhage is a clear sign of damage, mostly no

direct feedback is given to the surgeon when a nerve is damaged during surgery. For instance lesions due to excessive tensile forces, such as traction by wrongly placed retractors, can stay obscure because the epineurium is usually not visibly damaged. In case of ulnar nerve traction resulting in 10% of elongation can lead to internal damage to the axons without visible damage to the epineurium and the conduction velocity of the nerve can be significantly decreased[25, 26]. Unless this is noted directly postoperatively, damage to the nerve is usually only observed in the outpatient clinic, days, weeks or even months after surgery. Again, in contrast to arterial damage during surgery; as the artery starts to bleed the surgeon can quickly recollect what decisions led to the hemorrhage and he is able to learn anatomical variations in arteries by experience.

Therefore, to fulfill the increasing need for expert anatomy knowledge, a new method of mapping the variations that constitute normal anatomy needs to be developed. Complex data of multiple specimens need to be visualized and presented to residents and surgeons in an easily accessible and interpretable way. Vesalius was the first to note anatomical variations and differences. In fact, of the six anatomical structures carrying his name, only two can be considered as normal anatomy. Since then, the notion of variability has gained widespread acceptation. Mapping and comparing these variations is difficult as individual specimens never are of the same size. Contemporary ways of visualizing anatomy are drawings and photographs. Yet they lack the possibility to accurately show multiple variations and hence do not do justice to the surgical need for knowledge of the wide variation of normal anatomy.

Another way to compare variations in anatomy is to measure the location of certain structures and then adjust the measurements to, for instance, the length of a leg. Results are then presented in tables or schematic drawings. However, the shape of a specimen is not only dependent on its length, but also its width. As width usually depends on the amount of soft tissues it varies a lot and therefore the shape of a lower leg for instance differs significantly between people. Furthermore, research has shown[27, 28] that visual presentation of complex data is remembered better than when data is presented as text or tables. Moreover, text itself is memorized better when it is accompanied by a figure[29-31]. To paraphrase Confucius: “one picture tells us more than a thousand numbers”.

Computer Assisted Surgical Anatomy Mapping

In this thesis a novel anatomy mapping tool, Computer Assisted Surgical Anatomy Mapping (CASAM), is described. With this method the variation of anatomy, dissected in multiple specimens, can be compared and mapped. The complex data can then be processed and visual renditions can be made that represent the whole range of the anatomical term "norma". Currently CASAM can be applied in two main pillars of modern surgery;

1. Basic surgical anatomy research: CASAM allows anatomists and surgical researchers to compare and define anatomical variations better in structures such as muscles, nerves and vessels. To simplify the vast amount of data and highlight the clinical implications, renditions can be made to depict for instance "safe zones", in which a surgeon can make an incision without having the risk of damaging a certain nerve. Similarly it is possible to compute a "zone of interest" in which a certain muscle or arterial perforator is always located. Also "directionally anatomy zones" can be computed. These zones depict the position and direction of nerves, showing the surgeon in which direction to make an incision to best avoid damage to nerves of interest. Interestingly, when vessels are depicted by CASAM also "vascular safe zones" can be defined. In this case the reversed principle is seen. Whereas a nervous safe zone is defined as a zone with no or a few nerves, the vascular safe zone is defined as a zone in which as much vessels (and subsequent anastomoses and collateral vessels) as possible are found; the more vessels, the better the potential for optimal wound healing. When multiple different zones are depicted, a surgeon is provided with a vast amount of anatomical data gathered from multiple specimens. The goal of CASAM is not be a substitute for anatomical knowledge but to provide a tool to summarize complex and variable anatomy and subsequently allow the surgeon to make more informed decisions. In a 70 year old diabetic patient with peripheral atherosclerosis the vascular safe zone might be more important than the nervous safe zone whilst the opposite might be true for a healthy 20 year old Olympic gymnast.

2. Surgical teaching: not only can CASAM be used to teach complex anatomy, also trainees can add incision lines drawn for a specific type of surgery, such as for instance the extended lateral approach of the ankle for calcaneal fractures. These drawn incision lines can then be compared to the ones drawn by their peers, surgeons or the golden standard. The incision lines can also be compared to the anatomy of multiple dissected specimens, challenging a drawn incision

line to the scrutiny of variable anatomy. This is in contrast to conventional anatomy courses in which a drawn incision line is only compared to the anatomy of the specimen the trainee has at hand and not a vast library of the anatomy of multiple specimens. The web-based version of CASAM therefore is of added value during anatomy courses, giving a surgeon or surgical resident direct and personal feedback.

CASAM consists of multiple phases. First, the surgically relevant anatomic structures are dissected and photographed in a standardized way. Secondly, each specimen is outlined and its shape is delineated using so-called landmarks. From the location of the landmarks of multiple specimens an average shape can be computed. Then each original image of a specimen can be warped to match the computed average shape. Finally, since all specimens then have the same shape, the anatomy can be compared and renditions can be made to highlight the clinical relevance in everyday surgery.

The Aim of this dissertation is to prove the basic principles of CASAM are sound and applicable in two main pillars of surgery: Anatomy and Teaching. This thesis also lays the groundwork for a future web-based version of CASAM that has its application in 3D anatomy research and also in personalized teaching and Tailor-made Surgery.

OUTLINE OF THIS THESIS

First, a brief historical overview will describe the thoughts of previous anatomists that led to the development of CASAM. Current concepts of CASAM are explained in Part I, MATERIALS & METHODS. In the first sub-chapters the general principles of Image processing, Geometry and Warping are explained. Secondly, their role in CASAM is elucidated when the four phases of the method are explained; Dissection, Averaging, Warping and Renditions.

The application of CASAM in basic surgical research is shown in Part II, CASAM in SURGICAL ANATOMY. This part is divided into three subchapters, each describing different sorts of renditions dependent on the clinical research question. In Point distribution model, the perforating veins of the lower arm are mapped as they have an impact on survival of arteriovenous fistulae created for hemodialysis (chapter 2.1). In Multiple Line model the variations of nerves and arteries are mapped in relation to kidney surgery (chapter 2.2), ankle surgery (chapter 2.3) and knee surgery (chapter 2.4), showing how complex anatomy of multiple specimens can be mapped and applied to solve surgical problems encountered in everyday clinical practice. Furthermore, as the wrist is a common site for neuropathic pain after injury of the sensory nerves, two of the radially located superficial nerves were mapped in chapter 2.5. The anatomical relation between both nerves could be compared using CASAM. This possibly explains the high rates of post-operative neuroma formation and neuropathic pain after surgery of the dorso-radial side of the wrist.

In chapter 2.6 the mapping of a Multiple area model is combined with the anatomy of the sural nerve and the short saphenous vein. The nerve partially runs below a protective fascia layer and by mapping this area in 20 specimens, a safe-zone for laser surgery is defined. A “zone of interest” was mapped by defining a zone in which three arm muscles are present in all 20 specimens without overlap of other muscles and therefore a noninvasive preoperative test for tendon transfers in tetraplegic patients can now be developed (chapter 2.7). Finally, in chapter 2.8 similar zones of interest were mapped to showcase overlap between the nerves providing sensation to the hindpaw of a rat.

To further minimize the gap between basic anatomy research and everyday clinical practice, a web-based version of CASAM is developed. In Part III, CASAM in SURGICAL TRAINING the algorithms and computations used are

described and the structure of a central server, user features and general layout are outlined (chapter 3.1 and chapter 3.2). In chapter 3.3, incisions drawn for an approach of the tibia are mapped in relation to tibial nailing and chapter 3.4 discusses the inter- and intra surgeon variability in incisions drawn for an extended approach for the lateral calcaneus. Common variables in the placement of these incision lines such as experience, surgical specialty and exposure to calcaneal surgery are related to the ability of a surgeon to draw an incision according to the "gold standard".

Discussion and future perspectives further illustrates the application of CASAM in Teaching and Tailor made surgery. Reservations regarding image manipulation in basic research and data verification of CASAM renditions will be discussed. Finally, the future perspectives of a web-based and 3-Dimensional CASAM will be illustrated providing a platform for international anatomical data collection and in theater, real time visualization of complex anatomy on the patient.

REFERENCES

1) Benirschke SK, Sangeorzan BJ. Extensive intraarticular fractures of the foot. Surgical management of calcaneal fractures. Clin Orthop Relat Res. 1993 Jul;(292):128-34.
2) Thordarson DB, Latteier M.Open reduction and internal fixation of calcaneal fractures with a low profile titanium calcaneal perimeter plate. Foot Ankle Int. 2003 Mar;24(3):217-21.
3) Poeze M, Verbruggen JP, Brink PR. The relationship between the outcome of operatively treated calcaneal fractures and institutional fracture load. A systematic review of the literature. J Bone Joint Surg Am. 2008 May;90(5):1013-21.
4) Rammelt S, Amlang M, Barthel S, Zwipp H. Minimally-invasive treatment of calcaneal fractures. Injury. 2004 Sep;35 Suppl 2:SB55-63.
5) DeWall M, Henderson CE, McKinley TO, Phelps T, Dolan L, Marsh JL. Percutaneous reduction and fixation of displaced intra-articular calcaneus fractures. J Orthop Trauma. 2010 Aug;24(8):466-72.
6) Zwipp H, Rammelt S, Barthel S. Calcaneal fractures--open reduction and internal fixation (ORIF). Injury. 2004 Sep;35 Suppl 2:SB46-54.
7) Chatterjee, S., Nam, R., Fleshner, N., Klotz, L. Permanent flank bulge is a consequence of flank incision for radical nephrectomy in one half of patients (2004) Urologic Oncology: Seminars and Original Investigations, 22 (1), pp. 36-39.
8) Gardner, G.P., Josephs, L.G., Rosca, M., Rich, J., Woodson, J., Menzoian, J.O. The retroperitoneal incision: An evaluation of postoperative flank 'bulge' (1994) Archives of Surgery, 129 (7), pp. 753-756.
9) Korenkov, M., Rixen, D., Paul, A., Köhler, L., Eypasch, E., Troidl, H. Combined abdominal wall paresis and incisional hernia after laparoscopic cholecystectomy (1999) Surgical Endoscopy, 13 (3), pp. 268-269.
10) Hoffman, R.S., Smink, D.S., Noone, R.B., Noone Jr., R.B., Smink Jr., R.D. Surgical repair of the abdominal bulge: Correction of a complication of the flank incision for retroperitoneal surgery (2004) Journal of the American College of Surgeons, 199 (5), pp. 830-835.
11) Dellon AL, Mont MA, Mullick T, Hungerford DS. Partial denervation for persistent neuroma pain around the knee. Clin Orthop Relat Res. 1996;(329):216-22.
12) Berg P, Mjöberg B. A lateral skin incision reduces peripatellar dysaesthesia after knee surgery. J Bone Joint Surg Br. 1991;73(3):374-6.
13) Harvey EJ, Grujic L, Early JS, Benirschke SK, Sangeorzan BJ. Morbidity associated with ORIF of intra-articular calcaneus fractures using a lateral approach. Foot Ankle Int. 2001 Nov;22(11):868-73.
14) Johnson RJ, Kettelkamp DB, Clark W, Leaverton P. Factors effecting late results after meniscectomy. J Bone Joint Surg Am. 1974;56(4):719-29.
15) Mochida H, Kikuchi S. Injury to infrapatellar branch of saphenous nerve in arthroscopic knee surgery. Clin Orthop Relat Res. 1995;(320):88-94.
16) Poehling GG, Pollock FE Jr, Koman LA. Reflex sympathetic dystrophy of the knee after sensory nerve injury. Arthroscopy. 1988;4(1):31-5.

17) Katz MM, Hungerford DS. Reflex sympathetic dystrophy affecting the knee. J Bone Joint Surg Br. 1987;69(5):797-803.

18) Sundaram RO, Ramakrishnan M, Harvey RA, Parkinson RW. Comparison of scars and resulting hypoaesthesia between the medial parapatellar and midline skin incisions in total knee arthroplasty. Knee. 2007;14(5):375-8.

19) Borley NR, Edwards D, Villar RN. Lateral skin flap numbness after total knee arthroplasty. J Arthroplasty. 1995;10(1):13-4.

20) http://applications.3d4medical.com/essential_anatomy_3/

21) JR sanudo, R. Vazquez and J Puerta. Meaning and clinical interest of the anatomical variations in the 21st century.

22) Arey LB (1940). Developmental anatomy. W.B. Saunders Company, Philadelphia and London.

23) Holmes LB (1976). Congenital malformations. N Eng J Med, 295: 204-207

24) Stevenson RE and HALL JG (1993). Terminology. Vol I. In: Stevenson RE, Hall JG and Goodman RM (eds). Human malformations and related anomalies. Oxford University Press, London, pp 21-30.

25) SUNDERLAND S. Rate of regeneration of motor fibers in the ulnar and sciatic nerves. Arch Neurol Psychiatry. 1947 Jul;58(1):7-13.

26) SUNDERLAND S, HUGHES ES. Metrical and non-metrical features of the muscular branches of the ulnar nerve. J Comp Neurol. 1946 Aug;85:113-25.

27) Abhaji Eabadi, 2011. The effect of image generation on remembering story details in Iranian EFL learners. The Iranion EFL Journal, 7(2), 149-166.

28) RN. Carney, JR Levin. Pictorial Illustrations still improve students`learning from text. Educational Psychology Review. March 2002, Volume 14, Issue 1, pp 5–26

29) William E. Hockley. The picture superiority effect in associative recognition. Memory and Recognition. 2008, 36 (7), 1351-1359.

30) William E. Hockley, Tyler Bancroft. Extensions of the picture superiority effect in associative recognition. Canadian journal of experimental Psychology. 2011, vol 65, No. 4, 236-244.

31) Boldini A1, Russo R, Punia S, Avons SE. Reversing the picture superiority effect: A speed-accuracy trade-off study of recognition memory. Mem Cognit. 2007 Jan;35(1):113-23.

33) https://www.fuel-3d.com/nl/shop/

01101000 01101001 01110011 01110100
01101111 01110010 01101001 01100011
01100001 01101100 00100000 01101111
01110110 01100101 01110010 01110110
01101001 01100101 01110111

Historical Overview

Kerver, A.L.A., Kleinrensink, G.J.

INTRODUCTION

To know where you are and where you are going means knowing where you come from. Therefore this thesis starts with a historical overview explaining the thoughts of our predecessors that led to the eventual development of CASAM. In Dissection the works of the founding fathers of modern anatomy and surgery such as “The first known anatomist”, “the father of modern Surgery”, and “the restorer of anatomy” are described giving an historic overview of human dissection. Averaging describes how scientists such as Leonardo Da Vinci have long tried to capture the shapes of anatomy and reduce them to average and ideal proportions. Warping illustrates “how thinking outside the box” leads to exceptional theories; A Scottish biologist reduced the differences in shapes of related species (such as ape and man) to simple mathematical functions. In essence this was the basis for the application of algorithms in the description of variations in anatomy and species.

DISSECTION

Although the interest in human anatomy has been of all times, the opportunity for human cadaver dissection has been controversial till date. Without the monumental works of past visionary anatomists, human dissection as we know it today would not be possible. Also, current concepts of surgery, embalming techniques and dissection legislation have been greatly influenced by them.

Ancient Greece

The Greek Physician (335-280 BC) Herophilos[1,2] is to be considered as the first anatomist[3]. Born in Chalcedon Herophilos attended the medical faculty located at Cos, founded by Hippocrates himself. Having finished his education Herophilos moved to Alexandria where he and his companion Eristratus started the school of Aleksandria. Both had been given permission from Ptolemy the First to perform vivisections ("vivus" means alive and "section" means cutting) on convicted criminals[4]. They often performed such vivisections publicly as to better demonstrate the actual effects of their dissections and it is said that both vivisected at least 600 prisoners[1]. The vivisections were not without controversy as people such as Celcus[5] and Tertullian were publicly opposed to them.

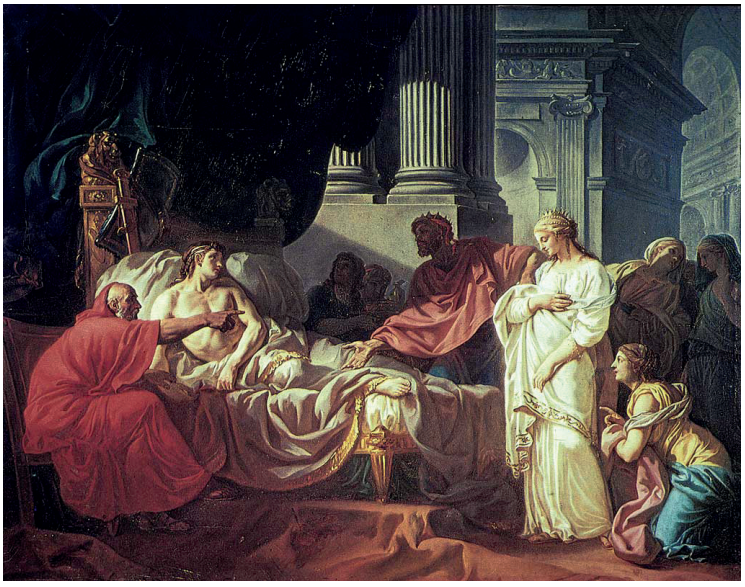

Figure 1. Erasistratus discovers the cause of the illness of Antiochus. Jacques_Louis Davis (1774)

Ancient Rome

In ancient Roman times the dissection of human specimen had been banned from 150 BC[7] as interference with the dead body was considered to be impious and offending to the gods. The act of crucifixion for instance was the most horrible form of punishment as the victim`s remains were left to rot and could not be buried.

Aelius Galenus (AD 129 – c. 200/c. 216), also known as Galen, was a physician and surgeon in the Roman Empire who advocated anatomy dissection on animals as a substitute to human dissection. He mostly dissected primates and especially the Barbary macaque as he considered their anatomy to be closest related to that of humans. His most valuable anatomic work was on the difference between venous blood (dark) and arterial blood (bright red), an observation he made during vivisections of primates and pigs[8]. His work however was not flawless. He for instance, deduced from his dissections that venous blood was made in the liver, distributed by veins and arterial blood was created in the heart being distributed through arteries. Galen also did multiple experiments in which he ligated nerves to support his theory that muscles are controlled via cranial and peripheral nerves[9].

Galen`s anatomical work, although based on animal dissection and Greek anatomy books greatly influenced Islamic surgery[10,11] and was uncontested and considered as human anatomy even in the Western World until the 1500`s AD.

Islamic World

Abu al-Qasim Khalaf ibn al-Abbas Al-Zahrawi (936–1013), is not only considered the greatest medieval surgeon of the Islamic World but has also been described as “the father of modern surgery”[12]. Among many medical and surgical

Figure 2. Abū al-Qāsim Khalaf ibn al-‘Abbās az-Zahrāwī
Source: Wikipedia[15]

books his greatest work is the Kitab al-Tasrif, a thirty-volume encyclopedia full of medical practices[13]. In it he describes the equivalent of the "Kocher`s method" for treating a dislocated shoulder, or ligating the temporal artery for migraines and the stripping of varicose veins in such detail that even today, it reads as a modern surgical treatise. He also stated that "He who devotes himself to surgery must be versed in the science of anatomy"[14].

However it is still debated if al-Zahrawi performed any human dissections. Although he and his scholars regularly reference human dissection al-Zahrawi was also considered a devoted Muslim for whom the study of the human body would imply breaking the Sharia (Islamic law).

Medieval times

In contrast to the complete cultural, scientific and economic decline during the Dark Ages, human dissection revived. During the thirteenth century it even became an obligatory subject of the medical universities. Mondino de Liuzzi, (1270-1326), also known as "the restorer of anatomy"[16], reintroduced human cadaver dissection and made it an integral part of the medical curriculum. He was also the first to describe that "when studying the muscles of the limbs, a sun-dried body could be used as an alternative to the dissection of a rapidly decaying cadaver"[17]. Despite the human dissections, ancient views on anatomy as postulated by Galen would not be contested until the renaissance.

Renaissance

Until the works of the Belgian anatomist Andries van Wesel (1545-1564), better known as Andreas Vesalius, the works of the old Greeks were recited and the ancient anatomical work had not been verified for ages. Vesalius however began to again carry out his own dissections and urged students to perform dissections themselves[18]. Having the opportunity for human dissection Vesalius began to refute old Roman and Galen`s claims on anatomical subjects such as the purpose of arteries and veins. Vesalius` most important contributions to anatomy are his books "De Corporis Fabrica"(on the fabric of the human body) and "De humani corporis fabrica librorum epitome"(the students abbreviated version) both of which are based on human dissection. The books focus on the visual drawings instead of actual text and highlight the importance of human dissections in understanding the three dimensional complexity of anatomy[19]. Also, Vesalius made a point of doing his own dissections and was known for inviting students and publishers of his books to join the anatomy classes.

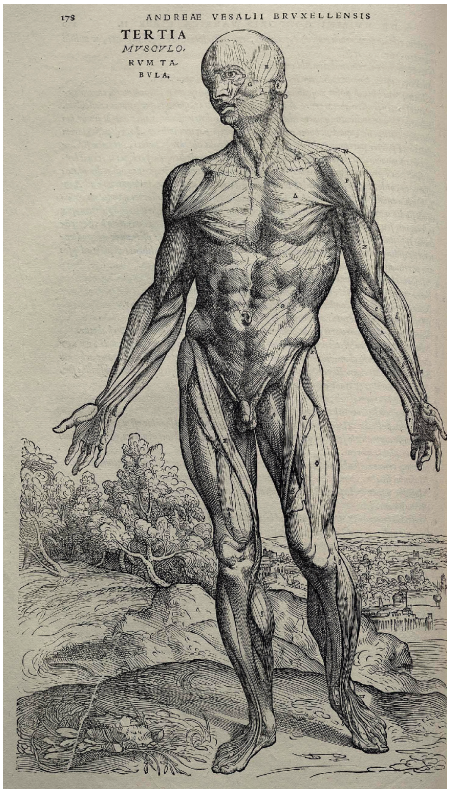

Figure 3. Andreas Vesalius, Illustration from De Corporis Fabrica[19], showing the muscular anatomy of man.

Vesalius` work however was also subject to much controversy as human dissection was forbidden by the Catholic Church. Also, Vesalius admitted the cadavers he used were gathered at graveyards and places of execution which stirred public emotions even more. Eventually Vesalius had to resign from his academic post and took a position as the imperial physician to Emperor Charles V. Vesalius` work however was not futile and his re-emphasis on human dissection slowly made anatomy again a central part in medical training and research.

Enlightenment

During the "age of enlightenment" (18th century) the thirst for knowledge and scientific progress further overcame centuries of ethical concerns regarding human anatomy research. The Scottish anatomist Alexander Monro "Primus" founded the Edinburgh Medical School[20] in which he openly participated in (and stimulated) dissection of the human body. His work on the human anatomy of bones, nerves and lacteal sac and duct is still being sold[21] and future generations of the Monro family (Alexander his son, "Secundus" and grandson, "Tertius")

have all taught at the Edinburgh Medical School, making it one of the oldest (and best)[22] medical schools in the English speaking world[23].

19th Century

At the start of the 19the century the Napoleonic Wars (1803-1815) led to an increased demand in medical and anatomical research. As a result of an increased demand for human specimen used for dissections, the disinterment of bodies at graveyards became more common and stirred public opinion so much that guards were placed at graveyards[24]. During this time William Burke and William Hare had killed 16 people, selling the bodies to anatomist Robert Knox[25]. Also the "London Burkers" a group of so called "resurrection-men"[26] tried to sell the body of a young Italian boy to a London surgeon[27]. The public outrage of these incidents eventually led to Great-Britain's 1832 Anatomy Act, legislating the donation of human cadavers to universities and medical schools. To this date the amended act is in use in Scotland and it has been the basis of Britain's Human Tissue Act of 2004 and similar acts in European countries and the U.S.[28].

Current times

Controversies surrounding anatomy and human dissection are also of modern times. Artist Damien Hirst stirred public opinion when he showcased his 'For the love of God", a human skull plated with 8601 diamonds[29] and Gunther von Hagen made international headlines when he performed the first televised public autopsy in 2002[30]. Millions of people of people visited the "body world" exhibition[31], showcasing human specimen plastinated using a technique created by dr. Von Hagen himself[32]. The exhibition was controversial by nature; it showcased human remains as pieces of art but also made anatomy accessible to the public. Interestingly, since the specimen were plastinated they legally weren't human cadavers anymore and could be classified as "objects of art" or "items in anatomical collections"[33].

If history teaches us anything it is that the general public opinion sets the boundaries for human dissection in anatomy research and anatomy teaching. The privilege anatomists currently have is most certainly fought hard over by our predecessors and not as ordinarily as most people think. The active preservation of the opportunity for human dissection should be of interest to any anatomist or surgeon and the impact of public opinion should not be underestimated.

Currently there are also new shifts in mapping 3d anatomy such as CT and MRI (see Warping). These techniques are evolving at a huge pace and become more accurate every day. And although some regard these new techniques as a replacement, they are currently best considered as good additions to conventional human dissection.

AVERAGING

The ambition of society to define and average the proportions and shapes of the human body has been long-standing and initially mostly driven by (divined) art. In ancient Egypt for instance the proportions of the body were recorded in "fists", meaning the length measured across the knuckles. The average length of an Egyptian was 18 fists[34,35]. In modern day drawing the head has been chosen as the basic unit of measurement and to establish the correct proportions of the rest of the body[36]. The head is measured from the top down to the most distal edge of the chin. Ideally the body then is 7.5 heads long with the hips being exactly halfway. Interestingly when gods or heroic figures were drawn they were typically 8 heads long with the extra length coming from longer legs and torso[37] (figure 4).

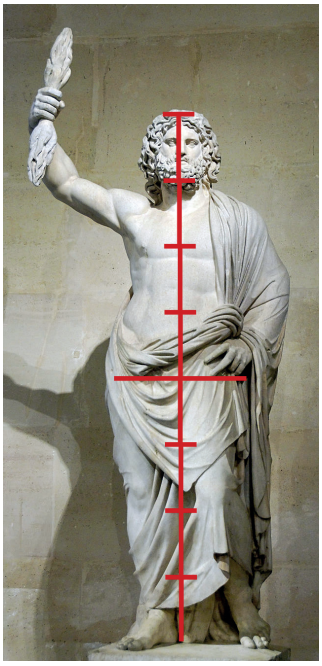

Figure 4. Jupiter of Smyrna (currentday Izmir, Turkey) currently exhibited in the Louvre paris. Exactly eight heads tall.

Famously, Leonardo da Vinci also tried to capture the proportions of our body in the "Vitruvian man" drawing[38] (figure 5). In this drawing and accompanying letters he correlated the ideal proportions of a human body to the basic laws of geometry as described by Vitruvius. In more recent studies on ideal features Pallett et al[40] found an amusing correlation that would forever change the meaning to the phrase "you are so average". In four experiments they set out to find the ideal facial proportions that would be able to theoretically "optimise" any given face. After having found the "golden facial ratios" they realised that these matched the proportions of an average face.

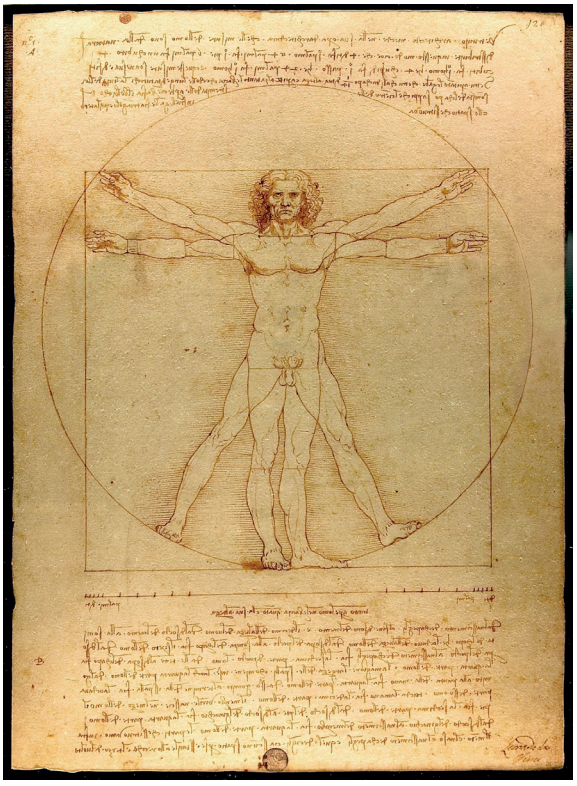

Figure 5.Vitruvian man C. 1492, pendrawing by Leonardo da Vinci. Photographed by Luc Viatour[39]

All methods of defining the human body so far had in common that they use an easy to identify measuring unit to describe the length of the entire body or certain parts of that body. In other words, the measurements are all relative (for instance to the fist or to the head).

To define a specific body part easily identifiable landmarks are used that define its borders. Although the exact definitions have changed over time the

general principle is still being used not only in art but also in science and product designs[37,38] such as tables and clothes.

WARPING

One of the founding fathers of what we currently call Bio-Mathematics was the Scottish biologist and mathematician Sir D`Arcy Wentworth Thompson[41,42]. Besides holding the record for having a professorial chair for the period of 64 years at the university of St. Andrews (and Dundee), Thompson`s main work was the 1917 book "On Growth and Form" [43], in which he explains the mathematical patterns and physical laws by which plants and animals are evolutionary formed. Using multiple examples he explains how biological forms are related to purely mechanical phenomena, for example he observed that phyllotaxis (the way leaves are organised on a stem) is based on the Fibonacci sequence (figure 6). He also stated that Darwinism is inadequate to explain the origin of new species and he regarded the phenomenon of "natural selection" to be secondary to the biological form[44].

Figure 6. Phyllotaxis. The leaves grown follow a pattern conform the Fibonacci sequence. (41,53)

The most (in-) famous part of his book is Chapter XVII, on the theory of transformations, or the comparison of related forms[45]. In this chapter he showcases linear and non-linear mathematical functions that transform the shape of one creature into a genetically related one and thus abridge evolution to simple calculations and functions. For instance he used simple shear mapping, a linear function, to display the similarity between two familiar fishes belonging to a different genus (figure 7). Using landmarks in a Cartesian coordinate system of the left fish and putting it at a 70 degree angle you have mathematically described the changes that form the second, related fish.

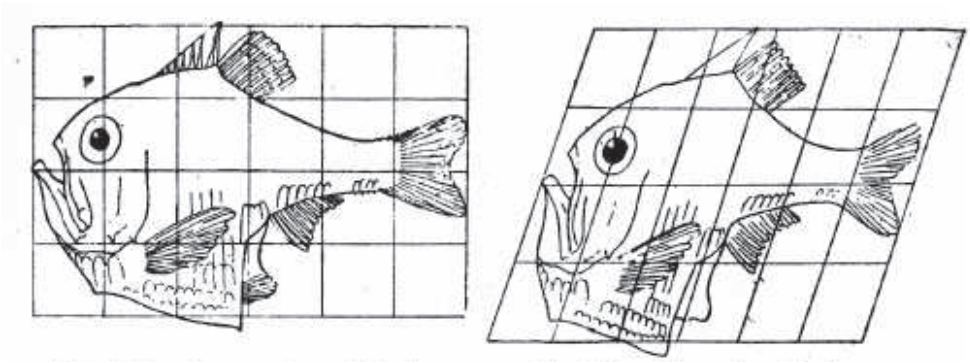

Figure 7. Shear mapping one genus of fish into another.
Argyropelecus Olfersi (left) and Sternoptyx diaphana (right)
From "On Growth and Form"[43]

When regarding human anatomy he related the human skull to that of a chimpanzee (higher ape) and a baboon (lesser ape) (figure 8). He uses the human skull as a reference, defining its shape by certain landmarks and creating a grid. When the same landmarks are defined on the chimpanzee and connected by smoothly curved lines a projection of the human skull emerges over the chimpanzee visualising the changes evolution made over time. Interestingly, when the same thing is done to the skull of a baboon it is clear that the transformation shown only differs in an increased intensity. The areas of the grid that represent the skull, mandibula, etc. increase gradually over evolution, following an approximately logarithmic order. This shows that the different parts of the skull all follow a continuous and integral process that can be mathematically explained.

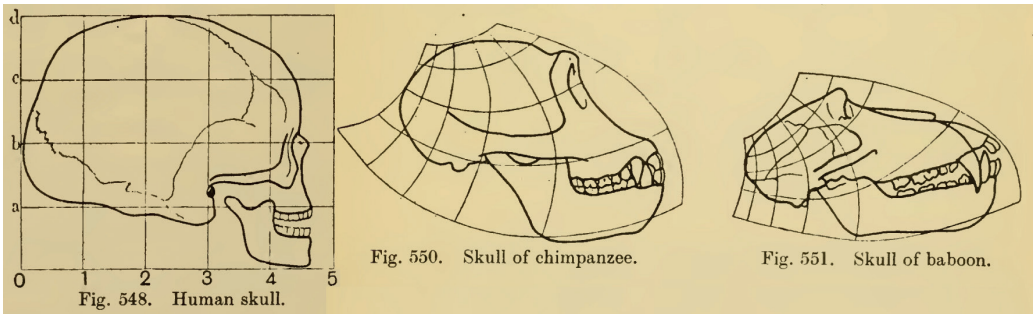

Figure 8. The human skull compared to that of a chimpanzee and a baboon.
From "On Growth and Form"[43].

This conclusion however is controversial as it contradicts with Darwinism. In Darwinism form is changed by environment. The environment however is subject to violent and abrupt changes and therefore form should also be subject to sudden changes; contrasting Thompson`s statement that form changes continuously following mathematical and mechanical functions.

In a way Thompson also laid the foundation for comparative anatomy mapping; he compared the Caucasian scapula (shoulder bone) to that of what he called "older or more remote races" showing the regularity of transformations over time (figure 9). Subsequently he demonstrated the inter-human variation of bony anatomy and laid the groundwork for quantifying anatomical differences using mathematical functions. In essence he explained warping in the year 1917, before images were even digitised.

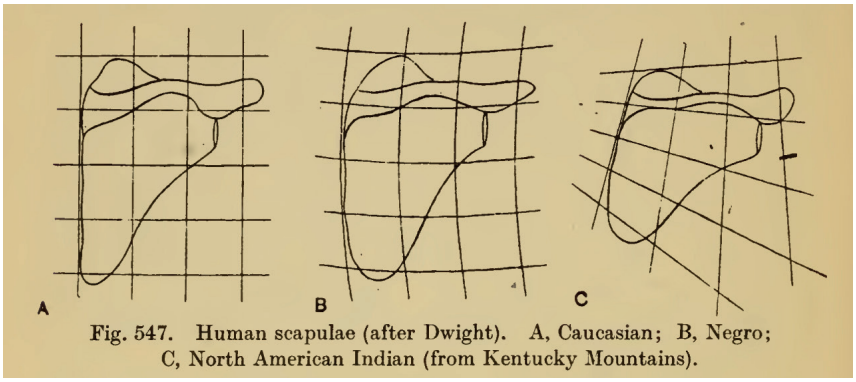

Fig. 547. Human scapulae (after Dwight). A, Caucasian; B, Negro; C, North American Indian (from Kentucky Mountains).

Figure 9. Human scapulae. a) Caucasian, of which the grid is used as a reference. b) African. c) North American Indian.
From "on growth and Form"[43].

Unsurprisingly, the works of Thompson inspired many people including biologists such as Julian Huxly, mathematicians such as Alan Turning and many artists and painters.

CT and (f)MRI

Another recent development in the mapping of 3D anatomy also uses geometry and mathematics. In computed tomography (CT) "digital geometry processing" is used to compute a 3D rendition from a series of circular 2D x-rays. The three-dimensional equivalent to a pixel in CT-scanning is called a Voxel. First developed by British engineer Geoffrey Hounsfield[46] the original CT took hours for the raw data to be collected and computing a single slice often took days. Currently however CT-scanning has evolved immensely and is part of regular

diagnostic practice. Magnetic resonance imaging also is a novel way of mapping the 3D anatomy, mainly of soft tissues. First introduced by Paul C Lauterbur in 1971[47] it uses strong and uniform magnetic fields to measure water molecules inside the body. The gathered data are then used to compute a 3D image.

Algorithms similar to those used in CASAM, such as the thin-plate-splines, are used when 3D renditions of CT and MRI images are being compared or combined to visualize structures best captured by either one of the techniques (bones for CT and soft tissues for MRI).

These algorithms are also used in the computation of a generic, average brain, using MRI, CT and anatomical data[48-50]. Such a brain can be used as a reference to identify, for example the area that is active when a functional (fMRI) is made. The department of Biomedical Engineering in Eindhoven (The Netherlands) already used these algorithms to map the anatomy of a brain (derived from basic anatomy dissections) to the MRI of patients so that specific parts of the brain are easier to identify[51,52].

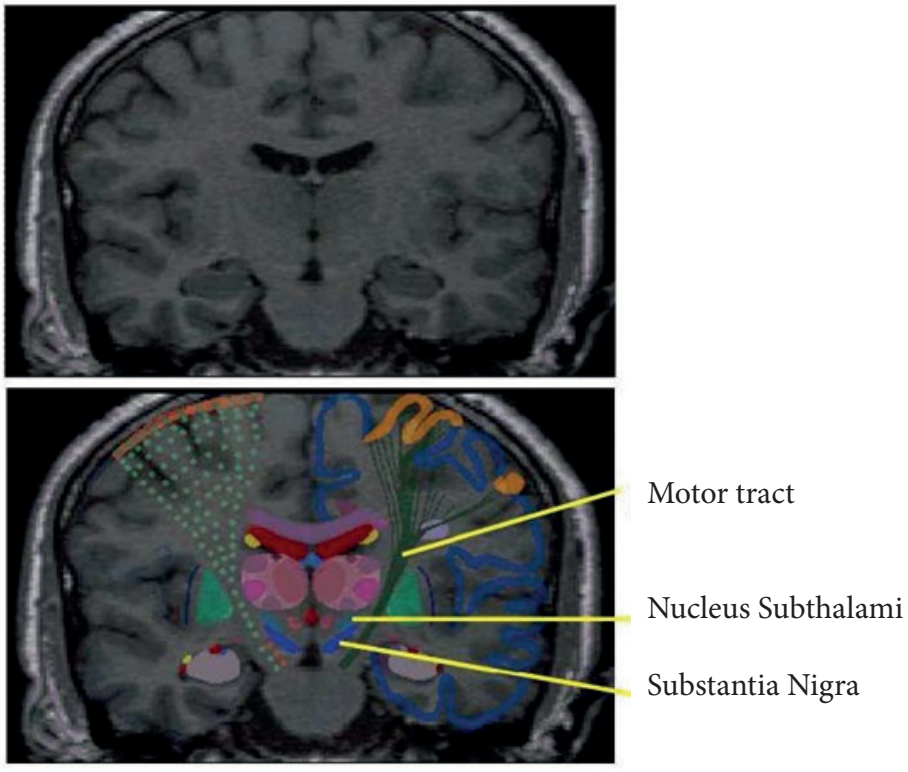

Figure 10. warping a neuro-anatomy atlas on 3D MRI data[51]

Further examples of the use of algorithms in everyday clinical practice will be discussed in the discussion of this thesis. However, these applications of geometry and mathematics in the imaging of 2D and 3D anatomy illustrate that these algorithms are becoming a part of everyday diagnostics and surgical procedures. Interestingly, although most clinicians use CT and or MRI images and their renditions on a regular basis, they are not informed on how these algorithms are being applied.

REFERENCES

1) Castiglioni, Arturo; Translated by E.B. Krumbhaar (1941). A History of Medicine. New York: Knopf.
2) Kornell, Monique (1989). "Fiorentino and the anatomical text". The Burlington Magazine 131 (1041): 842–847.
3) Wilson, Luke (1987). "The performance of the body in the Renaissance theater of anatomy". Representations (17): 62–95.
4) Dobson JF: Herophilus of Alexandria. Proc R Soc Med 18 (Sect Hist Med):19–32, 1925.
5) von Staden H: The discovery of the body: human dissection and its cultural contexts in ancient Greece. Yale J Biol Med 65:223–241, 1992.
6) Bynum, edited by W.F.; Porter, Roy (1997). Companion Encyclopedia of the History of Medicine (1st pbk. ed. ed.). London: Routledge. p. 281. ISBN 978-0415164184.
7) 'Tragically, the prohibition of human dissection by Rome in 150 BC arrested this progress and few of their findings survived', Arthur Aufderheide, 'The Scientific Study of Mummies' (2003), page 5
8) Arthur John Brock (translator), Introduction. Galen. On the Natural Faculties. Edinburgh 1916
9) Frampton, M., 2008, Embodiments of Will: Anatomical and Physiological Theories of Voluntary Animal Motion from Greek Antiquity to the Latin Middle Ages, 400 B.C.–A.D. 1300, Saarbrücken: VDM Verlag. pp. 180 – 323
10) Dear P. Revolutionizing the Sciences: European Knowledge and Its Ambitions, 1500–1700. Princeton, NJ: Princeton University Press (2001), 37–39
11) [Lindberg, D. C. (2007). The beginnings of western science: The European scientific tradition in philosophical, religious, and institutional context, prehistory to A.D. 1450. Chicago: University of Chicago Press.]
12) Ahmad, Z. (St Thomas' Hospital) (2007), "Al-Zahrawi - The Father of Surgery", ANZ Journal of Surgery 77 (Suppl. 1): A83, doi:10.1111/j.1445-2197.2007.04130_8.x
13) al-Zahrāwī, Abū al-Qāsim Khalaf ibn 'Abbās; Studies, Gustave E. von Grunebaum Center for Near Eastern (1973). Albucasis on surgery and instruments
14) Jones, PM. "Medieval medical miniatures." London: The British Library, in association with The Wellcome Institute for the History of Medicine; 1984 - Page 27 – 29

15) https://en.wikipedia.org/wiki/Al-Zahrawi
16) http://en.wikipedia.org/wiki/Mondino_de_Liuzzi#CITEREFWilson1987
17) Kornell, Monique (1989). “Fiorentino and the anatomical text”. The Burlington Magazine 131 (1041): 842–847.
18) http://en.wikipedia.org/wiki/Andreas_Vesalius
19) Image from Andreas Vesalius’s De humani corporis fabrica (1543), page 178.
20) Eddy, Matthew Daniel (2008). The Language of Mineralogy: John Walker, Chemistry and the Edinburgh Medical School, 1750-1800 Ashgate.
21) http://www.bol.com/nl/p/the-anatomy-of-the-human-bo/1001004010444104/
22) http://www.bol.com/nl/p/the-anatomy-of-the-human-bo/1001004010444104/
23) http://en.wikipedia.org/wiki/University_of_Edinburgh_Medical_School#cite_note-1
24) Lisa Rosner (2010), The Anatomy Murders. University of Pennsylvania Press
25) “William Burke, Confessions”. West Port Murders. Edinburgh: Thomas Ireland. 1829.
26) One or more of the preceding sentences incorporates text from a publication now in the public domain: Chisholm, Hugh, ed. (1911). “Body-Snatching” . Encyclopædia Britannica 4 (11th ed.).
27) Sarah Wise (2004). The Italian Boy. Metropolitan Books.
28) Anatomy Laws V. Body-Snatching” (1896). British Medical Journal Vol. 2, No. 1878, p. 1845
29) Damien Hirst: Beyond Belief exhibition” , White Cube. Retrieved 19 June 2009.
30) “Controversial autopsy goes ahead” b. BBC News. 20 November 2002. Retrieved 8 May 2009.
31) “Exhibitions”. Bodyworlds.com. Retrieved 2013-02-27.
32) “The Idea behind plastination” . Institute for Plastination. 2006. Retrieved 1 May 2012.
33) Warenverzeichnis für die Außenhandelsstatistik (List of goods for statistics on exports), 1998 Edition of the Federal Bureau of Statistics.
34) Smith, W. Stevenson, and Simpson, William Kelly. The Art and Architecture of Ancient Egypt, pp. 12-13 and note 17, 3rd edn. 1998, Yale University Press (Penguin/Yale History of Art), ISBN 0300077475
35) Clagett, Marshall (1999). Ancient Egyptian science, a Source Book. Volume Three: Ancient Egyptian Mathematics.. Philadelphia: American Philosophical Society. ISBN 978-0-87169-232-0.
36) http://en.wikipedia.org/wiki/Body_proportions
37) Japanese industrial standard, Ecronomics-Basic human body measruements for technological design. translation. ICS 13.180 JIS Z 8500: 2002
38) Basic human body measurements for technological design — Part 3: Worldwide and regional design ranges for use in ISO product standards. Élément introductif — Élément central — Partie 3: Titre de la partie. ISO TC 159/SC 3 416. 2013
39) Luc Viatour http://www.lucnix.be/main.php
40) Vision Res. 2010 Jan;50(2):149-54. doi: 10.1016/j.visres.2009.11.003. Epub 2009 Nov
41) http://app.dundee.ac.uk/pressreleases/2006/prmar06/thompson.html
42) http://en.wikipedia.org/wiki/D%27Arcy_Wentworth_Thompson

43) “ on growth and Form”, D`Arcy Wentworth Thompson, book. ISBN-10: 146358735X, CreateSpace Independent Publishing Platform (June 15, 2011)

44) Margaret A. Boden. (2008). Mind as Machine: A History of Cognitive Science. Oxford University Press. p. 1255. ISBN 978-0199543168

45) John Milnor. “Geometry of Growth and Form: Commentary on D’Arcy Thompson”. video. Institute for Advanced Study. Retrieved 31 March 2012.

46) Wells, P. N. T. (2005). “Sir Godfrey Newbold Hounsfield KT CBE. 28 August 1919 - 12 August 2004: Elected F.R.S. 1975”. Biographical Memoirs of Fellows of the Royal Society 51: 221–210.

47) Lauterbur PC (1973). “Image Formation by Induced Local Interactions: Examples of Employing Nuclear Magnetic Resonance”. Nature 242 (5394): 190–1. Bibcode:1973Natur.242..190L. doi:10.1038/242190a

48) Probabilistic Brain Atlas Construction: Thin-Plate Spline Warping via Maximization of Mutual Information. • C. R. Meyer • J. L. Boes • B. Kim • P. H. Bland. Medical Image Computing and Computer-Assisted Intervention – MICCAI’99 Lecture Notes in Computer Science Volume 1679, 1999, pp 631-637

49) Brain Mapping: The Methods: The Methods . Door Arthur W. Toga,John C. Mazziotta. BOOK. second edition. Elsevier science (USA).

50) Thin Plate Spline Registration in the Intrinsic Geometry of the Cortical Surface Cortical Surface Anand A. Joshi. David W. Shattuck, Paul M. Thompson,Richard M. Leahy. http://sipi.usc.edu/~ajoshi/anand_hbm05_poster.pdf

51) Warping a neuro−anatomy atlas on 3D MRI data with Radial Basis Functions. Joris Korbeeck, Edwin Bennink, Arjan Jansen, Marc Koppert, Roger Lahaije, Thomas Plantenga, Bart Janssen, Bart M. ter Haar Romeny

52) Warping a neuro−anatomy atlas on 3D MRI data with Radial Basis Functions. H.E. Bennink, J.M. Korbeeck, B.J. Janssen, B.M. ter Haar Romeny. Proc. Intern. Conf. on Biomedical Engineering (Biomed 2006, Kuala Lumpur, Malaysia, 11-14-December 2006.

53) hoto of ‘’Aloe polyphylla’’ at the University of California Botanical Garden, taken March 2006 by Stan Shebs

01001101 01100001 01110100 01100101
01110010 01101001 01100001 01101100
01110011 00100000 01100001 01101110
01100100 00100000 01001101 01100101
01110100 01101000 01101111 01100100
01110011 00001010 00001010

Chapter 1

Materials and Methods; Computer Assisted Surgical Anatomy Mapping

Kerver, A.L.A., Kleinrensink, G.J.

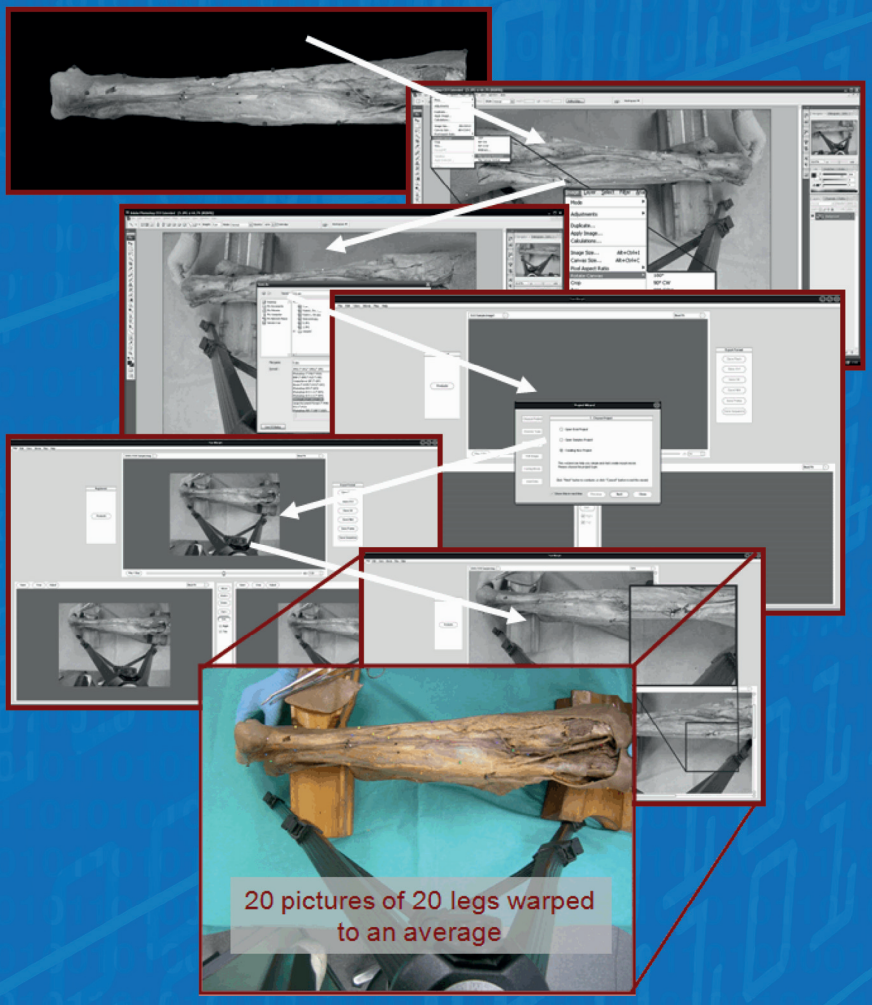
20 pictures of 20 legs warped
to an average

BACKGROUND OF IMAGE PROCESSING

It is imperative to first understand what a picture actually is; a picture consists of a (usually large) group of coloured dots placed on a flat surface, in this case representing the actual 3D anatomy of a photographed specimen. When computerised the coloured dots are called pixels and the pixels are laid out on a grid. One can look at a picture as a huge spreadsheet in which each box (or pixel) has the following information:

1) its location in the picture, defined by an X and Y coordinate.
2) its colour.

The X and Y coordinates follow the grid over each picture following the rules of a 2-dimensional Cartesian system, which is a specific kind of coordinate system.

Each picture therefore has a certain size which is defined by its height (X) and width (Y). The more pixels (or spreadsheet boxes) the image has, the higher its quality. The quality of digital images is usually reported as Dots per inch (DPI). The raw photographs made in the studies of this thesis were for example 17.067 x 12.800 inch with a resolution of 180 dots per inch resulting in a grid of 3.072 x 2.304 pixels. In total each pictures encompasses more than 7 million pixels, each with its own location and colour coded to it.

As an image can be viewed as a large Excel sheet with in each “box” a certain set of numbers, we can put formulas on the whole Excel sheet and thereby instantly change the appearance of the picture. An example is changing a colour picture to black-and-white or Sepia using a simple photo-editing apps. It is just a formula applied to the colour part of each “box” in the spreadsheet we call an image.

There are also formulas that can be applied to the location part of each “box” or pixel. These formulas are best explained and described using geometry.

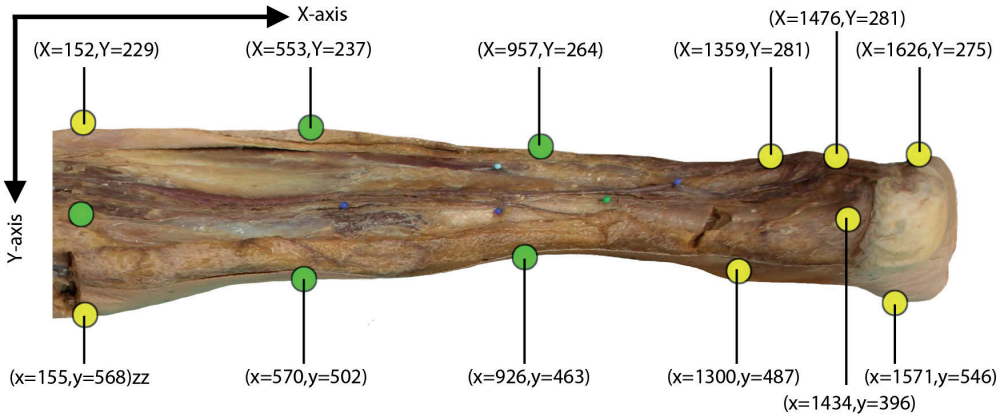

Figure 1. Grid-system.
X and Y quantify the width and height respectively.
(0,0) = the upper left corner.
(1686,720) = the lower right corner

BACKGROUND GEOMETRY

Geometry is a branch of mathematics that is focussed on the measurements of shape, size and the relative positions of a figure. In ancient Greek "geo" meant earth and "metron" meant measurements[3]. The classical part of geometry that encompasses the physical space is known as the Euclidian space (this in contrast to more modern geometry which has more abstract spaces). The Euclidian space is an abstraction and it is therefore not a real representation. Instead it can be viewed as a mathematical tool that can be used to explain and describe parts of the real world. Since the Euclidian space is a mathematical concept it is not tied to actual locations or measurement instruments. Distance for instance is measured in just numbers, not inches or meters.

The currentday basis of the Euclidian space has been formed by Euclid of Alexandria[1] who designed and described the axioms on which later theorems were based. An axiom is a statement or starting point of reasoning that is to be accepted without controversy[2] whilst a theorem needs to be proven based on previous theorems or axioms. The basic axioms (postulates) in Euclidian geometry are also called the Euclidean elements[4, 5]:

- Two points define a line (or you can always draw a line between two points).

- A line can be extended by continuing the line with a straight line
- A circle is defined by a centre and a radius
- All right angles are equal to each other
- The parallel postulate; if two lines are intersected by a third creating two right angles then the initial lines run parallel and never intersect.

Using these Euclidian elements Euclid began to mathematically deduce the properties of points, lines, planes and shapes such as triangles. For example he proved the theorem already described by Pythagoras on the relation of the three sides of a right triangle. It is believed that currently over a quarter of a million theorems are proven every single year[6].

To describe the location of a unique point in a certain plane the Cartesian coordinate system is used. How a point in the 2 dimensional space could be described using a X (horizontal) and Y (vertical) axis (figure 2) was first depicted by Rene Descartes[7, 8].

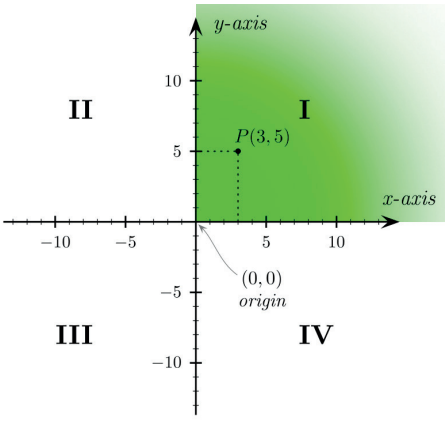

Figure 2. The Cartesian coordinate system.
Source: Wikipedia[9]

The advantage of such a coordinate system is that you can describe the location of a certain point (X, Y) and calculate with the coordinates. So point (x1, y1) can be moved two places to the right and its new coordinates will then be formed by the equation: (x1+2, Y1) in which x1 and Y1 are the old coordinates (figure3). It is also possible to calculate the distance between two points using the

Pythagorean theorem: Distance=√((x2-x1)²+(y2-y1)²)) or calculate an average point from three different points:

Average point (Xa,Yb)=(((x1+x2+x3))/3 ,((y1+y2+y3))/3) (figure 3). The pixels of an image are also located in such a Cartesian coordinate system and therefore it is possible to alter their location using formulas created from the principles of geometry and Euclidean space.

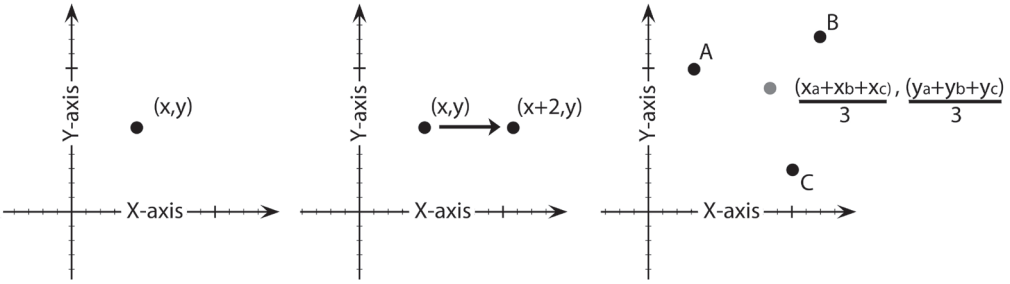

Figure 3. The Cartesian coordinate system.
Adapted from Wikipedia[9]

Rigid Transformations

In mathematics there are different forms of movement. Another mathematical name for moving (parts of-) an image is "warping". One of the simplest forms of movement is called a rigid transformation, meaning that the shape and size of an image or figure are preserved whilst moving. One form of a rigid transformation is moving the image horizontally or vertically. This is called translation. If the image of a house needs to be moved horizontally and vertically, a formula needs to be created to calculate the movement of all pixels. Given that the size and shape of the image are the same, only one corresponding pixel is needed to calculate the translation formula for all pixels. The corner of the house could be a useful landmark. Once a formula is computed that translates the coordinates of that one landmark to match the specified position (for instance (x1+4, y1+3) this formula can be applied to all pixels to move the entire image (figure 4). Rotation also is a rigid transformation. For a rotation however at least two corresponding landmarks are needed. Even though the formula becomes more difficult, the principle remains the same as for translation. The formulae that describe movement for both landmarks can be used to deduct the formula that can move all other pixels. Slightly controversial reflections can also be considered as rigid transformations. A minimum of three landmarks is needed for the third form of rigid transformations; either flipping an image vertically or horizontally.

Again the formulae describing the movement of all three landmarks can be used to compute the movement each pixel has to make.

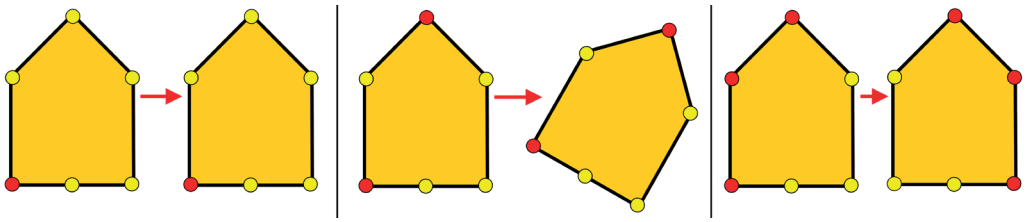

Figure 4. Rigid transformations;
Adapted from[10]
1: Translation (one landmark necessary)
2: rotation (two landmarks necessary)
3: reflection (three landmarks necessary).

Affine Transformations

Rigid transformations are a subset of affine transformations. In affine transformations points, straight lines and planes need to be preserved. However it is not necessary to preserve angles or distances between points[8]. For affine transformations up to three landmarks are necessary to compute the formula that moves all pixels of an image. Examples are scaling (making a picture bigger, figure 5.1), shear mapping (see bio-mathematics and figure 5.2) and squeeze mapping (making one direction of the image larger, figure 5.3). Since affine transformations are based on three landmarks deducing the formulas that move all other pixels in a picture is relatively simple.

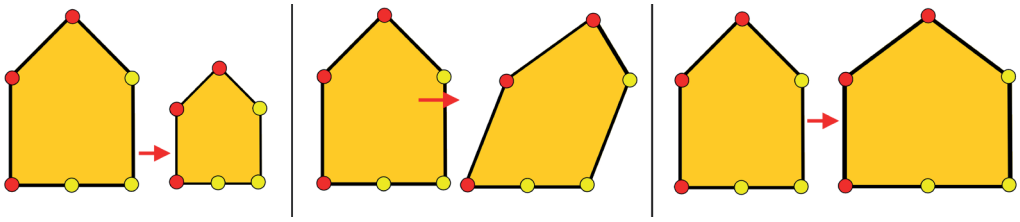

Figure 5. Affine transformations.
Adapted from[10]
1: Scaling.
2: Shear mapping.
3: Squeeze mapping.

Warping

The anatomy of a left ankle can be compared to the anatomy of a right ankle using simple affine transformations such as translation and reflection. Similarly it is also possible to scale a small ankle to match a larger ankle and even elongating a short leg for it to match a taller leg. However just scaling, reflecting and elongating the shape of a specimen will never allow for a complete matching of shapes between specimen.

In comparative anatomy it is imperative for all specimen to exactly match the average shape. In CASAM the shape of a specimen can therefore be delineated by up to 50 landmarks (instead of the relatively few numbers of a maximum of three landmarks used for affine transformations). This means that in order to move the pixels in that image the formulas calculating the new positions of pixels are dependent on the movements of all 50 landmarks. This tends to generate hugely complicated formulas and makes computation of average shapes virtually impossible.

Triangulation

One way to solve this problem is to break up the image into multiple smaller triangles, with the corners of a triangle located at landmarks. A triangle, by nature is defined by three landmarks. As described above this means that reshaping each individual landmark and all pixels within that landmark can be done with relatively simple affine transformations.

Although breaking up an image into triangles seems easy, it becomes more difficult when more landmarks are involved as there is an exponential number of triangulations possible for a growing set of points. Triangles most easy to warp are those that have relatively large areas and large angles. Creating these so called "finest triangles" between landmarks is called Delaunay triangulation and it adheres to the rule that no landmark is located inside the circumference of each triangle formed (figure 6).

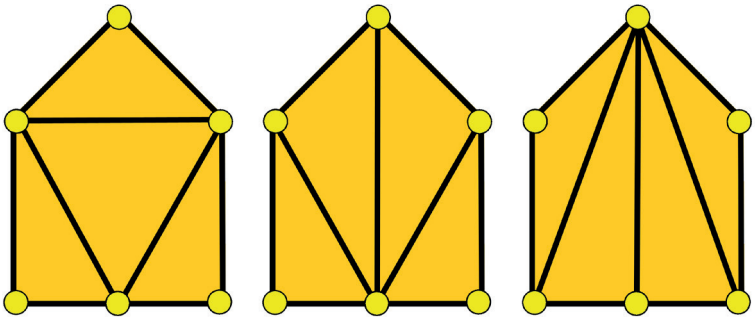

Figure 6. Triangulation
Adapted from[10]
1: Triangle conform Delaunay.
2: Bad triangulation.
3: Worst possible triangulation with skinny triangles.

Each pixel in each triangle then gets a coordinate within that triangle. In contrast to the Cartesian coordinate system, in which coordinates consist of x and y, in the Barycentric coordinate system[11] the pixels are located in relation to each side of the triangle, A, B, and C. The rules for moving a pixel however are the same and the formulas for moving pixels are still based on its three surrounding landmarks (figure 7).

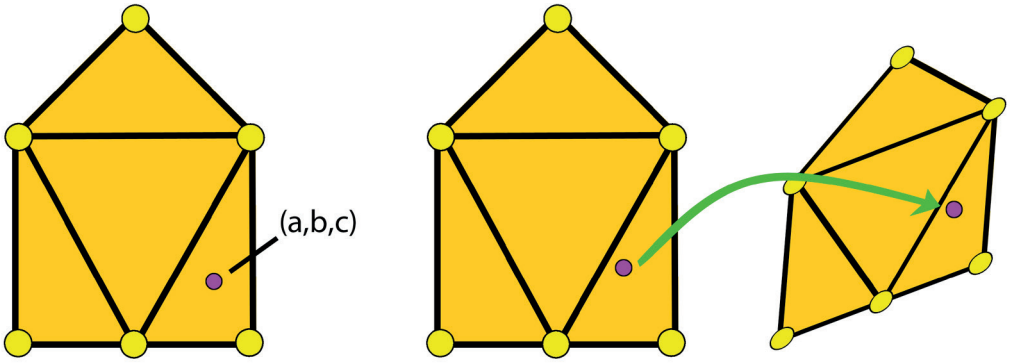

Figure 7. Barycentric coordinate system and related pixel relocation.
Adapted from[10]

Creating an average shape

Given the linear and simple nature of triangulation the algorithm can be used to compute an average shape between 2 or more different shapes.

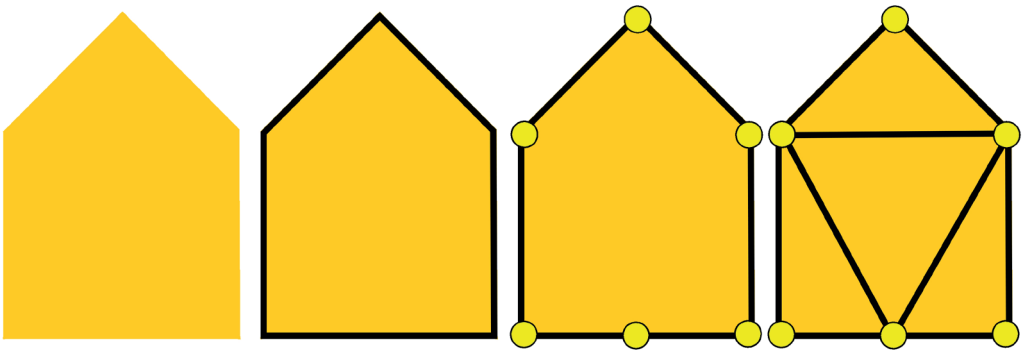

Figure 8. Shape defining by using landmarks.
Adapted from[10]

To create an average size from two differently shaped houses, house 1 (figure 9, yellow) and house 2 (figure 9, blue), the landmarks of each house are defined and Delaunay triangulation is used to describe the relation between the landmarks. Using the location on the coordinate system, the distance between the landmarks of house 1 and 2 can be deducted and also a vector (direction of the displacement) can be calculated. To calculate the average shape the landmarks of house 1 are moved 50% of the distance in the specified direction, thus creating the average shape between houses 1 and 2 (figure 9, green house)

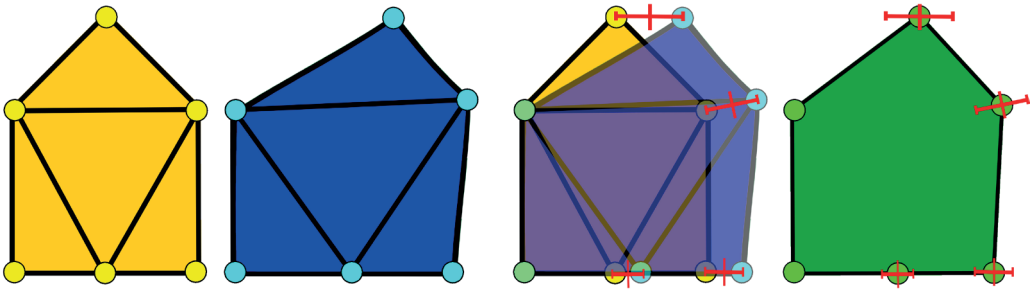

Figure 9. Computing an average shape.
Adapted from[10]

To calculate the average size of three houses, the just created "average" house (figure 9.4, green house) can be compared to a third house. This time however the landmarks of the green house are moved ⅔ of the distance (since the green house "counts' as two houses).

Folding

As discussed above, affine transformations adhere to certain rules. Two of the rules described were that points and planes needed to be preserved[8]. This means that no landmark can cross the base of its own triangle or the extension of its base as this would in fact delete either the landmark itself or the plane (triangle) that it is part of.

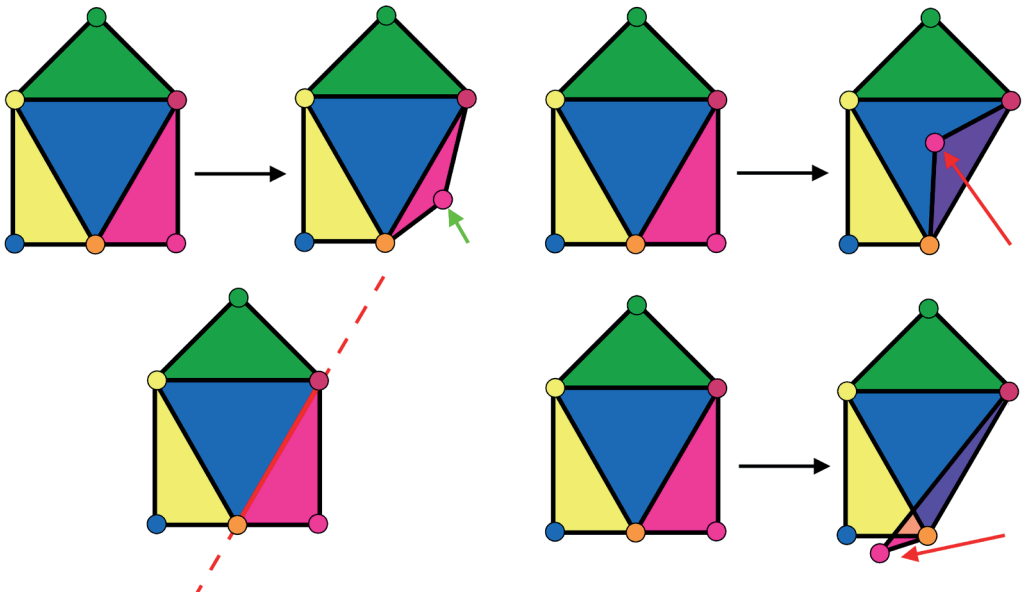

Figure 10. Folding.
Adapted from[10]

Hence that skinny triangles or triangles with a small surface are not preferred as they severely limit the range over which a landmark can move during warping.

Thin plate spline warp

Another way to solve the aforementioned problem of having up to 50 landmarks is to use a Thin Plate Spline transformation (TPS). In contrast to the triangulation technique a TPS does not divide the image into multiple triangles. Instead all the corresponding landmarks are used to calculate a "bend". The TPS was first introduced in geometry by Duchon[12] and later adapted by Goshtasby[13] and Bookstein[14]. The TPS is an algorithm that is currently used in many medical fields such as MRI and CT imaging in which it is important to describe deformation or differences in shape or creating similar images. It is also still being used in

zoology to describe shape differences and similarities between species, and the general principles are not that different to those that Thompson (introduction, bio-mathematics) described.

The essence of a TPS is best explained as a technique of interpolating datapoints whilst smoothing the transition between these data points. Fundamentally it works like this:

Figure 11 (green dots) shows an original image with certain landmarks (x,y) that needs to be reshaped to match the average shape (red dots) with landmarks located at (xi,yi). First a grid is placed over the original landmarks. Secondly affine transformations (blue lines) are used to get the location of original landmarks (x,y) to match those of the average landmarks as closely as possible. Then the grid is bended as if it were a thin metal sheet (hence the name thin-plate spline), with a certain resistance so that a smooth bend is created. When looking from above the original landmarks (x,y) must match the shape of the average landmarks(xi,yi) when the bend is finalised.

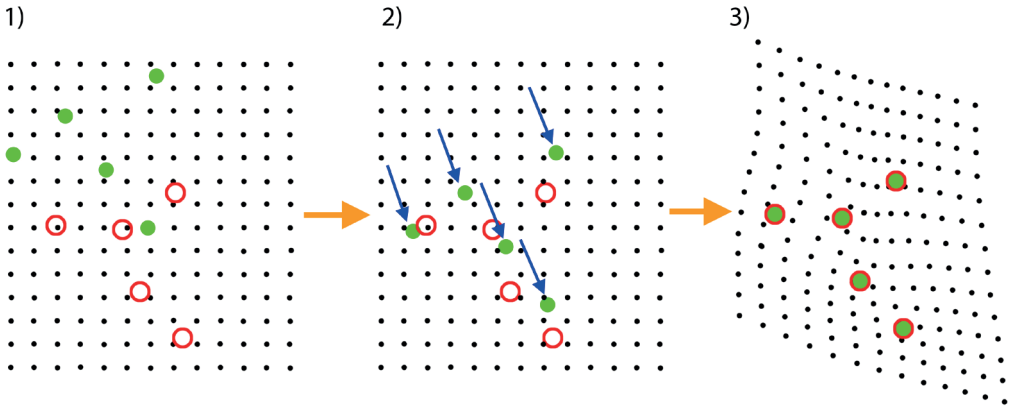

Figure 11. Thin plate spline transformation stages.
Adapted from[14-16]
1: put a grid over the landmarks. Green= original landmarks, red= average landmarks,
2: rigid transformation for alignment. Blue arrows=translation of original landmarks
3: bending of the grid so original (green) landmarks match the average (red) landmarks.

In other words the sheet is bended in such a way that when looking from above the landmarks are located at the same location. However when looking from the side there is a an elevation difference between the original (x,y) and average landmarks (xi,yi).

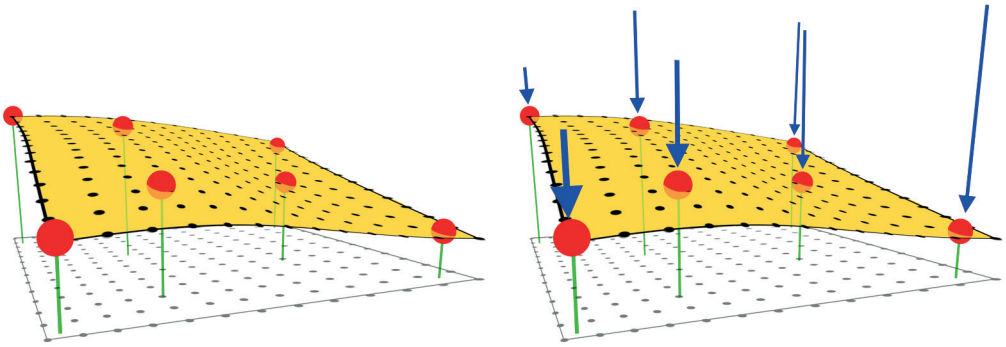

Figure 12. Side view of a thin plate spline
Adapted from Jarno Elonen[17]
A thin plate splines that passes through a set of control points (red dots). The blue lines represent the vertical "force" needed to bend the orinal picture so that it passes through the control points (average landmarks).

When put into a formula the TPS looks like this:

$$f(x,y) \quad = \quad a_1 + a_x x + a_y y + \sum_{i=1}^{p} w_i U\left(\|(x_i,y_i) - (x,y)\|\right)$$

The First part of the formula entails the general alignment using affine transformations of the original landmarks to best match the new average landmarks. The second part of the formula corresponds to the "bending forces" and is determined by P control points (= the number of landmarks) and the "stiffness" of the metal sheet. The third part of the formula calculates the distance between the original (x,y) and average (xi,yi) landmarks.

$a_1 + a_x x + a_y y +$ $\cdot \sum_{i=1}^{p} w_i$ ${}_i U\left(\|(x_i, y_i) - (x, y)\|\right)$

Since the third part of the formula (distance between original and average landmark) and P (the number of landmarks) are known it is possible to calculate the other, unknown coefficients. Since a1, ax, ay and Wi are dependent on the difference between a specific original and average landmark (third part of the formula) it is necessary to calculate these coefficients for each landmark individually.

$$f(x,y) = a_1 + a_x x + a_y y + \sum_{i=1}^{p} w_i U\left(\|(x_i, y_i) - (x, y)\|\right)$$

Once these coefficients are known for each landmark it is possible to deduct a formula that computes the height of each pixel on the bended sheet. The height of each pixel on the bended sheet is then used to calculate its horizontal and vertical displacement, thus calculating its final position in the average shape.

Combined techniques

A disadvantage of triangulation is that it is a piecewise method of warping; pixels warped in one triangle have no information of the movement of pixels in other surrounding triangles. This results in unsmoothed warping which sometimes results in unrealistic warps. Figure 13 shows the sudden change in angle of the blue line at the base of warped triangle.

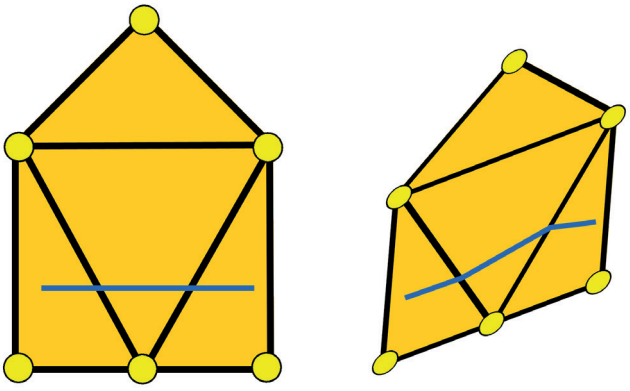

Figure 13. Warping a line using triangulation

Another disadvantage is that triangulation only allows for image registration within the convex hull of the outer landmarks. Although extrapolation of the algorithm to pixels outside the outer edge of the landmarks is possible it usually generates inconsistent results with multiple registration errors. Piecewise warping is however very robust in that it uses relatively easy algorithms and essentially only affine transformations are being applied. Especially pixels located near the sides of the triangle are warped reliably. Also triangulation allows for averaging multiple shapes. In TPS however no average shape can be calculated since the exact location of two landmarks (in different specimen) is needed to solve the other coefficients in the formula. Once an average shape is computed TPS results in a smooth warp most reliably representing reality.

Therefore in CASAM triangulation is used to compute an average shape from every specimen. Then the TPS is used to create a smooth and reliable warp from the original image to match the computed average size. Finally triangulation can again be used to verify the accuracy of the TPS created warp.

PREPARATION, PHOTOGRAPHY AND LANDMARKS

Population

All anatomical studies were performed at the anatomy department of the Erasmus MC, Rotterdam the Netherlands. The specimens originated from Dutch volunteers that contractually agreed for their bodies to be used in anatomical courses and anatomy studies after passing away. In The Netherlands specimens are bound to individual Universities and/or institutions and therefore we only used specimens from volunteers that had been assigned to aforementioned anatomy department. Dutch law prohibits the gathering of personal and and/or medical data of deceased patients without explicit permission by the patient ante-mortem or post mortem by the next of kin of the deceased. Therefore, in none of our studies we present data on medical history or population statistics. All specimens were checked for macroscopic signs of disease and unfit specimens not meeting the criteria of health were not used. This mainly applied to studies in which vascular access was paramount and vessels had to be free of atherosclerosis.

Choice of specimen

Three different kind of specimen were available; conventionally embalmed specimen, Anubifix[18] embalmed specimen and fresh frozen specimen. Depending

of the clinical subject being examined different specimens and different methods of embalming were used.

Most studies did not require for the specimen to be supple and therefore we used specimens which had been embalmed conventionally; the bodies are embalmed at room temperature and at low pressure with a mixture of 6% formaldehyde and 5% phenol to minimize shrinkage and embalming artefacts.

In two studies it was paramount to have specimens with normal joint mobility as the knee needed to be flexed to 90 degrees in order to best represent clinical practice. In one study the ankle needed to be held in 90 degrees in order to best represent clinical practice in calcaneal surgery and duplicate results gathered by conventional anatomy mapping. Specimens used in these studies had therefore been flushed with Anubifix[18]. Anubifix is being used as it reverts post-mortem rigidity whilst maintaining the ability to fully embalm the specimen. After preflushing these specimens were also embalmed at room temperature and at low pressure with a mixture of 6% formaldehyde and 5% phenol.

In one study the anatomy of the arterial supply of the hindfoot was studied in relation to calcaneal surgery. In order to dissect even the smallest arteries fresh frozen specimens were used. As soon as the specimens were thawed the popliteal artery and its branches were filled with FilloPaQ[19]. FilloPaQ is a filling-agent having a viscosity close to that of water, but still hardens in 8-10 minutes. It therefore is capable to even reach the smallest capillaries in the (hind-) foot when the right amount of pressure is used. Blue-green dye is added to FillOpaQ as it contrasts well to the red colour of muscle and the yellow colour of fatty tissue. Once set FilloPaQ is slightly flexible (rubber like consistency) and therefore less brittle than other filling agents such as Biodur. This allows for easier manipulation when dissecting. After mapping the arterial anatomy the specimens were again frozen so that data could be verified afterwards if need be.

Dissection

Especially when superficial cutaneous nerves are being dissected, dissection begins with the removal of skin, epidermis and dermis (figure 14).

Figure 14. De-epithelialisation.
Dissection of the dermis of the posterior side of the lower leg.

To ensure comparable exposures and results the dissection method was standardized for each study. Classification of the artery, nerve or vein started proximally and consequent branches are then dissected peripherally. Terminal branches are dissected using a 2,5 times magnifying loupe (figure 15).

Figure 15.
Dissection using a 2.5 times magnifying loupe.

The arterial wall of arteries filled with FiloPaQ[19] are cut open longitudinally and superficially removed so that the dyed FiloPaQ contrasts with surrounding tissue as much as possible (figure 16).

Figure 16. Two fresh frozen specimens filled with FiloPaQ.
1: Arterial wall intact.
2: Arterial wall incised longitudinally and peripherally removed so the (white) FiloPaQ is visible and contrasts to surrounding tissue.

Surrounding and underlying subcuticular tissues need to be meticulously preserved in order to avoid any alteration to the natural location of the nerve studied (figure 17). Care should be taken not to dissect at multiple levels at the same time as this will compromise the location of the anatomical structure. Instead the same specimen can be photographed multiple times at different stages of the dissection. The CASAM method allows for anatomical data gathered at multiple levels to be combined. In this way it is possible to visually map deeper anatomical structures without having to compromise data gathered superficially.

Figure 17.
Example of mapping the anatomy of multiple layers in multiple stages.
1: Dissection and mapping of the superficial branches of the short saphenous vein.
2: Dissection and mapping of the main branches of the short saphenous vein (located superficial to the fascia)
3: Dissection and mapping of the medial branch of the sural nerve (located deep to the fascia)

Photography

Standardized photography of the specimen is the most important step in CASAM. Although researchers mostly focus on dissection and the warping process, miniscule deviations to the standardized photography have a huge impact on the final visualisation.

All dissected specimen are photographed using a Canon 350D body[20]. Initially a Canon EF-S (Canon USA, Inc, San Jose, Calif) 18-55 mm lens was used. In more recent studies however the use of a Sigma (Sigma Corporation of America, Ronkonkoma NY) EX 50mm 1:2.8 DG macro lens is preferred. Macro-lenses are by nature 'flat' field lenses[21] whilst general lenses suffer from field curvature. In general lenses the focal-point will be at a slightly different distance at the corners of the frame when compared to the centre of the frame. A disadvantage of using macro-lenses is that depth of field is extremely shallow; meaning that merely centimetres away from the focal point of the lens an object can be out of focus. Another disadvantage of the macro lens is that it generally is difficult to get enough light. Therefore indirect lighting, a tripod and a remote are used. Hereby long exposure times can be achieved without any motion artefacts, allowing for adequate lighting whilst maintaining a small aperture. Using a small aperture results in a wider depth of field, thus having the majority of the specimen in focus.

Figure 18. Camera setup and alignment for standardized photography

A ruler is used as a reference for digital measurements. The distance of the ruler to the camera is very important. For instance placing the ruler really close to the camera would make it seem bigger in the image and therefore not representative to distances in the specimen. Therefore the ruler was placed exactly midway between the closest and furthest points of interest. Similarly to the example with the ruler, the distance between the specimen and the camera needs to be exactly the same for each specimen.

Landmarks are used to centre and align specimen to the camera in a standardized way. Then it is imperative to quantify the amount of rotation of the specimen relative to the camera position. Mal-alignment and rotation of the specimen have a big impact on the shape-defining landmarks as the outer edges of a specimen change depending on the angle at which they are observed.

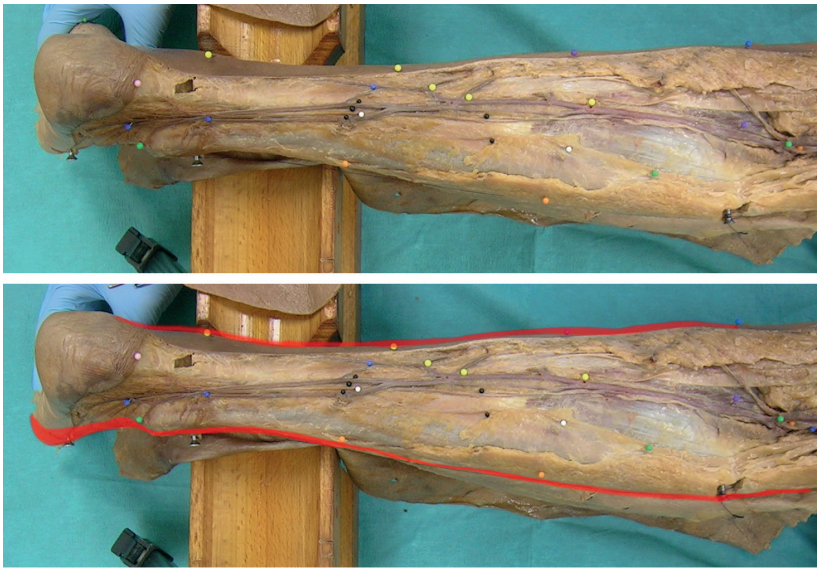

Figure 19. Malrotation resulting in wrong representation of shape
1) Normal alignment.
2) Malrotation and concurrent wrong representation of shape (red)

Landmarks

One of the first steps in using CASAM is to define the shape and size of each individual specimen. The most straightforward landmarks are based on the human bones. The length of the lower leg for instance (figure 20) can be easily defined as the distance between the tibia-plateau (superior part of the tibia)

and the lateral malleolus (=distal part of the fibula). Both of which are easily identifiable exteriorly. This makes these bony landmarks very reproducible and since the length of a bone correlates well to the actual length of a leg it is also very representative. In conventional anatomy research these bony landmarks are used to adjust gathered anatomical data for the length of each specimen so that otherwise incomparable data can now be marginally correlated.

Although these Bony landmarks correlate well to the length of a leg, they do not correspond at all to the width of the leg. A calf for instance can be very wide proximally but still be very narrow distally and its variation in width has no correlation with the length of the bones in that leg. However, for a researcher the information on the width of the leg at multiple levels will allow him to not only adjust his gathered anatomical data for the length of the leg but also for its width at multiple levels. This makes comparing anatomical data between specimens much more reliable as the location of an anatomical structure definitely correlates to the width of the specimen. Inadvertently but interestingly, by computing an average 'size', we might also be calculating the golden proportions for a leg[22].

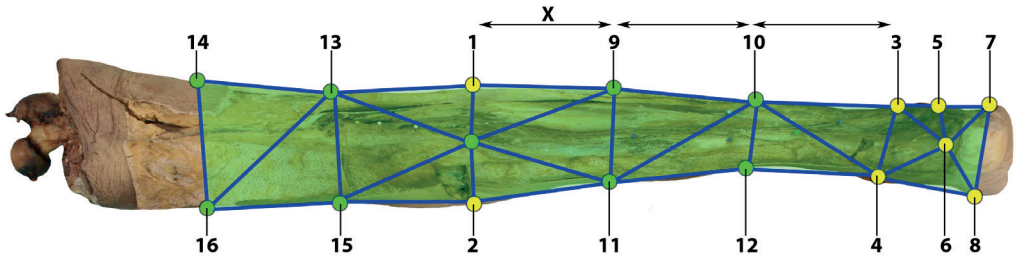

Figure 20 Landmarks
Shape-defining landmark 9 (green) is dependent on the width of the specimen at one thrd of the distance between Bony landmarks 1 (=tibia plateau) and 3 (=lateral malleolus).
yellow dots: bony landmarks
green dots: shape-defining landmarks
green area: area in which the anatomic structure to be studied needs to be located
blue lines: triangulation.

In CASAM, to define the width of a specimen, shape-defining (= non-bony) landmarks are calculated from the bony-landmarks. These shape defining landmarks delineate the specimen and are dependent on two variables: Two bony landmarks and the width of the specimen. For instance (figure 20) the location of shape-defining landmark 9 (green) is dependent on the width of the specimen

at one third of the distance between Bony landmarks 1 (=tibia plateau) and 3 (=lateral malleolus).

As the location of shape-defining landmarks is heavily dependent on the few bony landmarks, reproducibility of the placement of the bony landmarks is very important and therefore needs to be verified. Furthermore any anatomical structure to be studied needs to be located inside of both bony and shape-defining landmarks as otherwise it is not taken into account when being warped (figure 20 green area). Landmarks need to correspond between pictures and are assigned a specific number.

Landmark optimisation

Especially when studied specimens have more complex shapes, such as a hand with multiple fingers, it is imperative to optimise the number and location of the landmarks placed. Figure 21 shows the hindpaw of a rat in which we studied the innervation using evans blue extravasation. For this study it was therefore essential to also map the toes of the rat.

When only seven landmarks (figure 21.2) are used (on the tip of the toes and the base of the sole) some parts of the the paw are not mapped (red area) and the essential shape of the paw is not outlined well. Therefore the width of the toes is

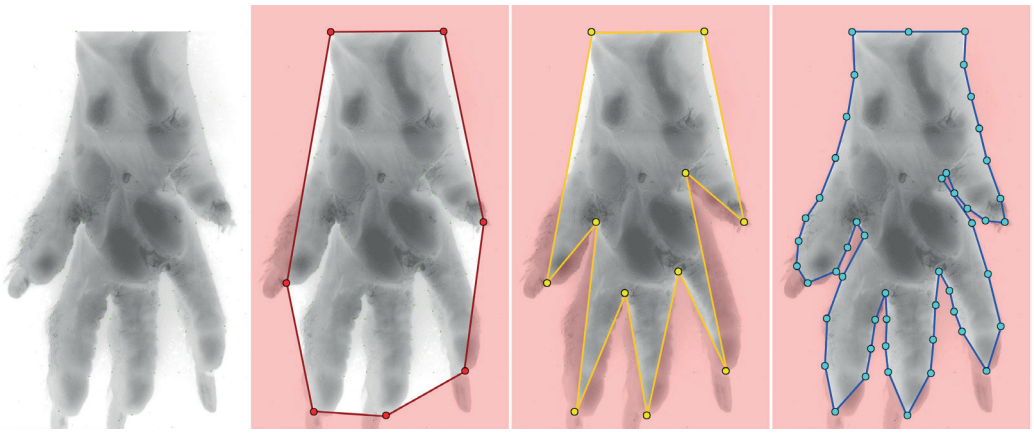

Figure 21 Defining the outlines of a specimen using 7, 11 and 49 landmarks.
Red area: area not taken into account as it lays outside the outer edges of the landmarks
1: Original image
2: Seven landmarks
3: Eleven landmarks
4: Forty-nine landmarks

not taken into account when warping, even though the width, as described earlier, is as essential to anatomy localization as length.

To further describe the outline of the hindpaw `s shape we then placed four additional landmarks (figure 21.3) to the most distal edge of the webspace between each toe. However in doing so, important parts of the toes could not be taken into account as they were localised outside the outer-most edges of the landmarks (red area).

To resolve this problem more landmarks were created in a similar way to the shape-defining landmarks used in other CASAM studies. These shape-defining landmarks were based on the width of the toes and hindpaw at a well defined location between the initially chosen eleven landmarks. The result of the additional 38 landmarks (figure 21.4) is that the shape of the hindpaw is outlined well. The width of the toes is well defined at different locations. Areas that could not be taken into account (as they laid outside the outer edges of the landmarks) were small and mostly included the toenails and distal tips of the toes.

A disadvantage of using these 49 landmarks is that when triangulating the image satisfying the Delaunay condition a total of 47 triangles are formed (figure 22.1). One disadvantage of so many triangles is the added time of computation. Secondly, creating too many triangles makes for skinny triangles without much surface and narrow corners.

Figure 22.2 shows two example landmarks, red and purple, and the similarly coloured boundaries that each landmark can not cross when it is going to be warped. Crossing these boundaries when warping would result in “folding” and creates a useless warp. The surface over which the red landmark is allowed to move is not that large as the three triangles that determine its range of motion are also small. The purple landmark for instance has a much higher degree of freedom because of two reasons; 1) it is a centrally placed landmark and can therefore move over more triangles. 2) Especially the proximal landmarks have a big surface. Distal movement (towards the toes of the hindpaw) is however severely limited as the triangles distal to the purple landmarks are really skinny and have narrow corners.

Previously we have already discussed that when warping a landmark it is not allowed to cross the basis of (any of) its triangles as it results in “folding”of the image and an utterly unusable and irrepresentative image. We therefore have to optimise triangulation by selectively deleting Landmarks that triangulate with many other landmarks and thus are most likely to form small and skinny triangles.

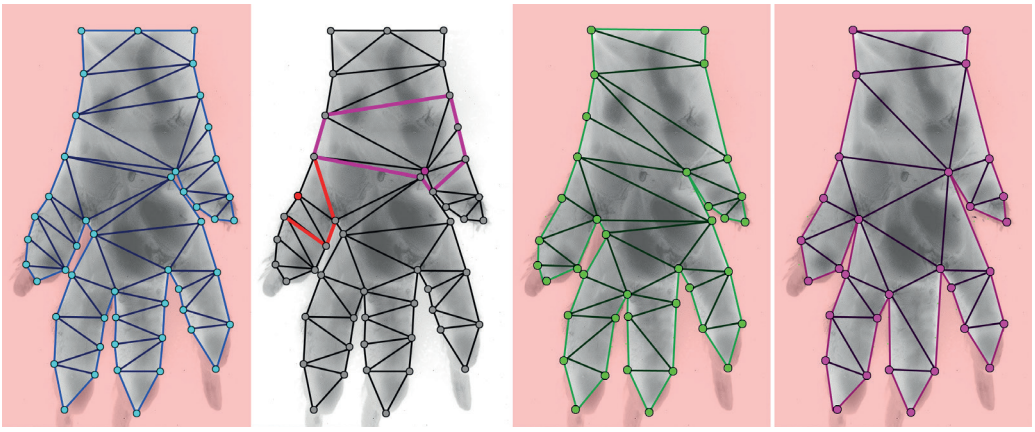

Figure 22. Optimising landmarks using triangulation and selective landmarks.
1: blue, 49 landmark triangulation.
2: Purple and red lines: limits of movement for corresponding landmarks.
3: Green, 38 landmark triangulation.
4: Purple, 31 landmark triangulation

In figure 22.3 the number of landmarks was selectively lowered to 38 resulting in 36 triangles. The general shape of the hindpaw is still well delineated and hardly differs from figure 22.2. At least four of the triangles however still have quite narrow angles. In figure 22.4 the number of landmarks has been further reduced to 31, resulting in 29 nicely shaped triangles, all having sufficient surfaces and decent corner angles. Most importantly, reducing the number of landmarks from 49 to 31 has hardly lowered the quality of delineating the shape of the hindpaw as it is still nicely represented in both length and width. Only the nails and tips of the toes can not be taken into account as they lay outside the outer border of the landmarks but these were of no interest in this study.

Landmark reproducibility

The whole background for CASAM is that specimens in general are not of the same shape. Therefore the landmark optimisation as described needs to be completed for at least three different specimens to establish which landmarks delineate the shape best without creating small and skinny triangles.

Secondly, reproducibility of landmark placement within the same specimen needs to be verified and only landmarks that can be consistently placed (usually within a 2 mm radius) should be used. If consistency within one specimen is hard to obtain, it most probably will be impossible to reliably place landmarks among

multiple specimen. If consistent landmark placement seems to be difficult, even when experienced, a different view sometimes solves reproducibility problems.

Thirdly, landmark placement, and especially the distribution of landmarks between specimens needs to be quantified. Therefore, three different specimens, each showing their own landmarks need to be aligned. Then the distribution of each landmark between all specimens can be visualised and landmark placement can be optimised. If for instance landmark 3 shows little variation between three different specimens it might be redundant. If landmark 5 for instance shows huge variation between three different specimens it might be of benefit to add an additional landmark so that the variation is divided. Furthermore when the spreading of a certain landmark is compared to the surfaces and angles of the surrounding triangles formed by Delaunay triangulation, the likelihood of folding can be estimated.

Finally, after warping the original images to match the computed average the landmarks of all three specimens need to be at the exact same location so that the shape of each specimen is the equal. Figure 23 shows a post-warping assessment of landmarks placed on the volar side of the fore arm. Four of the landmarks show variations between specimens (especially specimen 1, red) which suggests that landmark placement and/or warping still needs further optimisation.

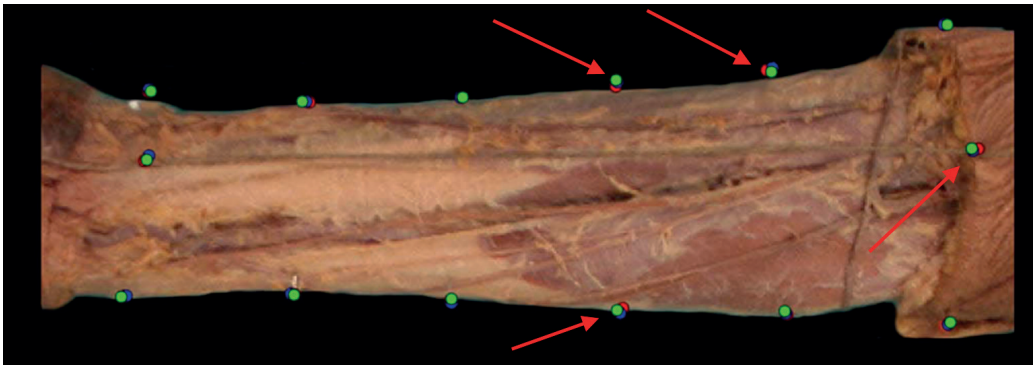

Figure 23. Post-warping to average assessment of landmarks
Red dots: specimen 1
Blue dots: specimen 2
Green dots: specimen 3

WARPING

Photoshop CS-4[23] is used to align the original images, MagicMorph[24] is used to create an average shape and then warp the original images to match the computed average shape. Photoshop CS-4 is then used to create renditions of the images.

Averaging the shapes of specimen

Multiple photographs are taken of each specimen. The most aligned and sharp image of each specimen is chosen. Photoshop is used to load the images into stack (File; scripts; load images into stack) so that they are loaded into the same file in different layers.

Landmarks are highlighted using a hard brush tool (B) in each image and if applicable shape-defining landmarks are calculated from bony landmarks using the ruler tool (Analysis; Ruler tool). If digital, absolute measurements need to be taken the ruler tool can be calibrated using the photographed ruler (Analysis; set measurement scale; custom). This way the number of pixels can be represented as actual millimetres. Intrinsic measurements (non-digital) are however preferred. Rigid transformations are applied to further centre each specimen . Pressing (Ctrl+A) selects the entire image of selected layer then (V) can be pressed to select the move tool. In order to compare left and right specimens (legs for example) images of either one need mirroring. To do so the entire image is selected (Ctrl+A) and then a horizontal reflection is made (images; image rotation; flip canvas horizontally). Finally, all aligned layers are then exported as individual images (Edit; transform; flip horizontal).

The images of the first two specimens are then loaded into magic morph. The warping software uses triangulation to compute virtual locations of landmarks when one image is gradually warped to match the second. This means that the software can be used to compute an average size (figure 24).

First corresponding landmarks are marked in specimen 1 (field 1) and specimen 2 (field 2). The exact coordinates of these landmarks are shown in the control point coordinate field. Then the morph mode needs to be changed to source warp, so that specimen 1 is warped to match the size of specimen 2. The output file (computed image) is shown on the right field. A slider-bar can be used to adjust the shape of the output file to either match specimen 1 (0%) or specimen 2 (100%). When put at 50 % the landmarks of the output file correspond to the average size of specimen 1 and 2. The coordinates of the computed average landmarks can be verified in the control point coordinate field. The computed average image of specimen 1 and 2 is then saved and loaded into field one. Specimen 3 is loaded into field two. The process of averaging is repeated, however this time the slider bar that adjusts shape of the output file is set to 33.3%. This means that the shape of the output file resembles the shape in field 1 more than the shape in field 2, thus representing the average shape of specimen 1, 2 and 3. The averaging process is repeated for all other specimens, finally resulting in an output file that represents the average shape of all specimens.

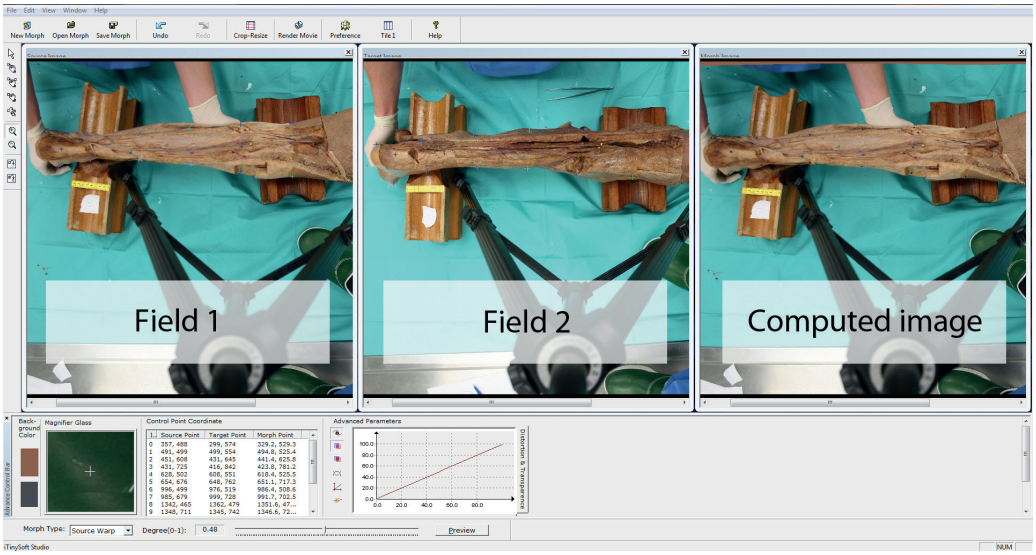

Figure 24. Warping software; using triangulation to average shapes.

Warping original images to match the average

The morphing software uses a TPS for the actual morph itself and can therefore be used to warp the original images of specimens to match the computed average size.

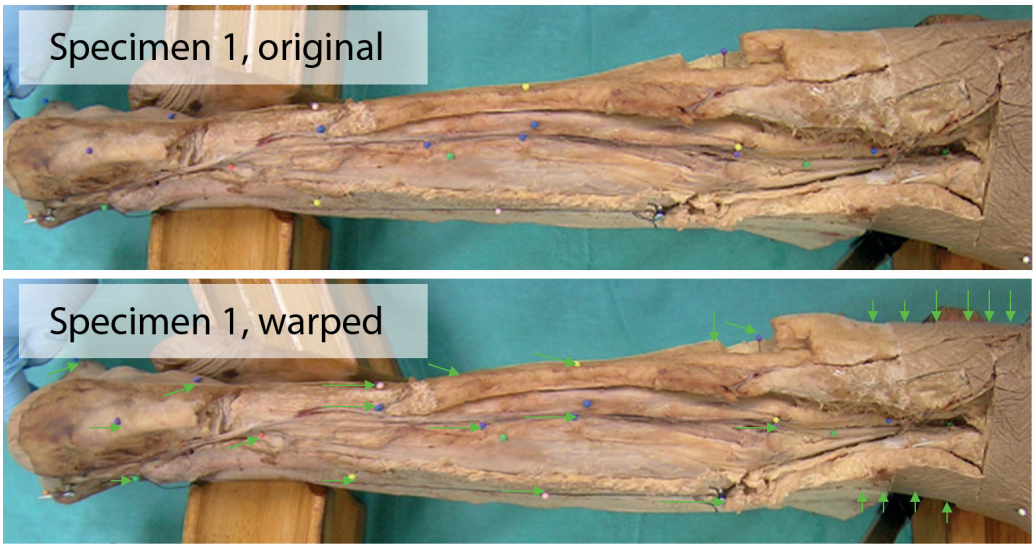

Figure 25. Specimen 1, original shape and warped to match the average

The image of specimen 1 is loaded into field 1, the averagely shaped image is loaded into field 2 and corresponding landmarks are marked. Since placement of the landmarks in the average image is extremely important and needs to be consistent each time an original image is warped and a custom script is written for each project. The script allows for automated and consistent landmark placement in field 2 (averagely shaped image) and is executed in Autohotkey[25]. When the landmarks are placed the morph mode is set to source warp and the slider determining the shape of the output file is set to 100%. This means that the output file depicts specimen 1 (field 1), but consists of the average shape (field 2). This process is repeated for all other original images of each specimen.

The quality of output files can be analysed using the TPS used in the web-based version of CASAM en through custom piecewise warping through triangulation.

RENDITIONS

So far, each specimen has been dissected, photographed, its shape delineated and then warped to match the average size of all specimens. Therefore all specimens now have the exact same (and average) shape and size. This allows for their anatomy to be mapped and compared. Renditions are made in Photoshop CS3 to CS6[23].

All warped images are loaded into the same file at different layers (files; scripts; load files into stack). Although the relevant anatomy of multiple specimens will be visualised, the rest of the images is not going to be used. Instead one of the averagely shaped specimens will be used as a background over which the anatomy will be displayed. One of the layers is chosen and non-relevant background is selected using the Quick selection tool (Q) and deleted resulting in a roughly edged specimen.

Figure 26. deleting irrelevant background

The edges of the specimen are then smoothed using the soft-edged Eraser tool (E)

Figure 27. Smoothing of the edges

Point distribution model

It is important that each structure is highlighted individually for each specimen in a separate layer (so the nerve, artery and fascia layer of specimen 1 are all highlighted in different, separate layers). First create a new layer (Ctrl+Alt+N) then enter the quick mask (Q). Quick mask allows for visualisation of the selected area and refine the edges or shape of the selected area). The brush tool (B) can then be used to select a certain area, such as the origin of the short saphenous vein. Exit the quick mask (press Q again) before filling the area with colour (edit; fill). To show aspecific point the selection is also outlined (edit; stroke).

Figure 28. Highlighting a specific point. Quick-mask selection, fill, stroke.

When corresponding points have also been selected for the other specimens (each in separate layers) all layers depicting, for instance, the origins of the short saphenous vein can be merged (layer; merge layers). The merged layer then shows the distribution of origins of the short saphenous vein and can be shown over the created background and saved as a separate rendition.

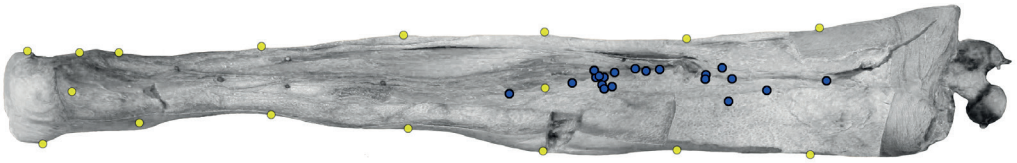

Figure 29. origins of the short saphenous vein of 20 dissected specimens.

Multiple line model

To highlight the complete course of a nerve it is first necessary to create a new layer (Ctrl+Alt+N). After the quick mask is entered (Q) the brush tool (B) can be used to roughly outline the course of the nerve. A sharp edged eraser tool (E) can then be used to deduce the selection to the actual outlines of the nerve. After exiting the quick mask (Q) the selection can be filled with a yellow colour (edit; fill).

Figure 30. Highlighting a nerve.

The opacity of the layer can be changed (layer; layer style; blending options) so that the background of the image is still visible.

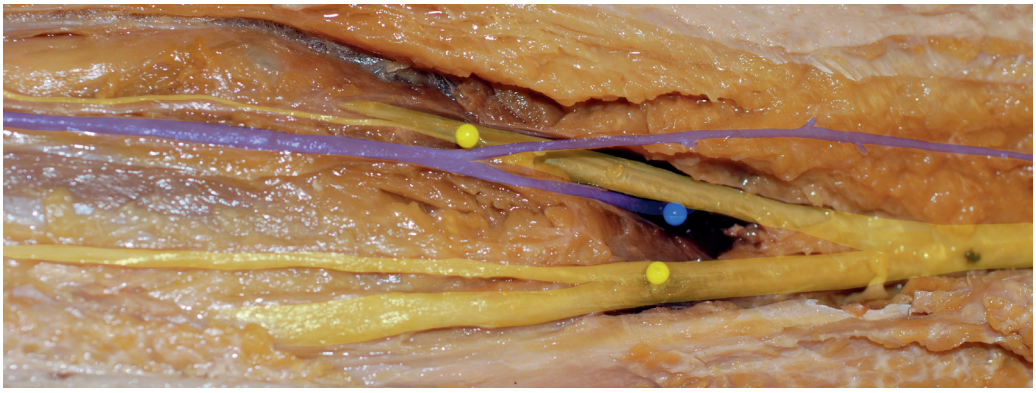

Figure 31. The opacity of layers highlighting the nerves and short saphenous vein is reduced to 40%.

When the nerves of other specimens have also been highlighted in separate layers, all layers can be merged (layer; merge layers). The merged layer then shows the area of distribution of the nerve.

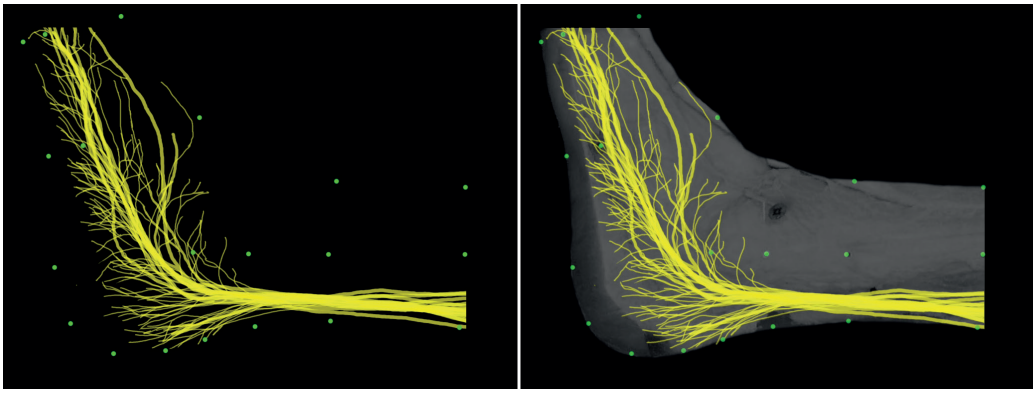

Figure 32. Distribution of the sural nerve on the lateral ankle of 10 specimens.

To visualise the location dependent direction of nerves, first all layers with highlighted nerves need to be merged (layer; merge layer). Then a grid of squares is placed over the computed area of spreading of all nerves. Within each individual square, the direction of all branches of the nerve is being measured in relation to the base-line of zero degrees. Angle measurements are taken using the ruler tool (Analysis; ruler tool) while holding (Alt).

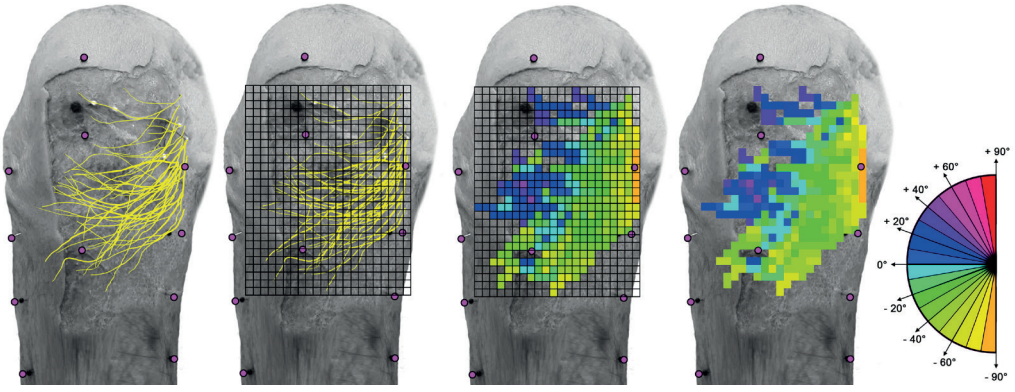

Figure 33. location dependent direction of nerves.

Multiple area model

To select a certain area in a specimen the specimen needs to be selected first. The magic wand tool (W) can be used to select the area surrounding the specimen. Then the selection needs to be inversed (Select; inverse) to select the specimen itself. After entering the Quick mask (Q) the areas of the specimen that are not being highlighted need to be removed using the sharp edge Eraser tool (E). After

exiting the Quick mask (Q) the selected area can be filled with colour (edit; fill) and the opacity of the layer can be adjusted (layer; layer style; blending options).

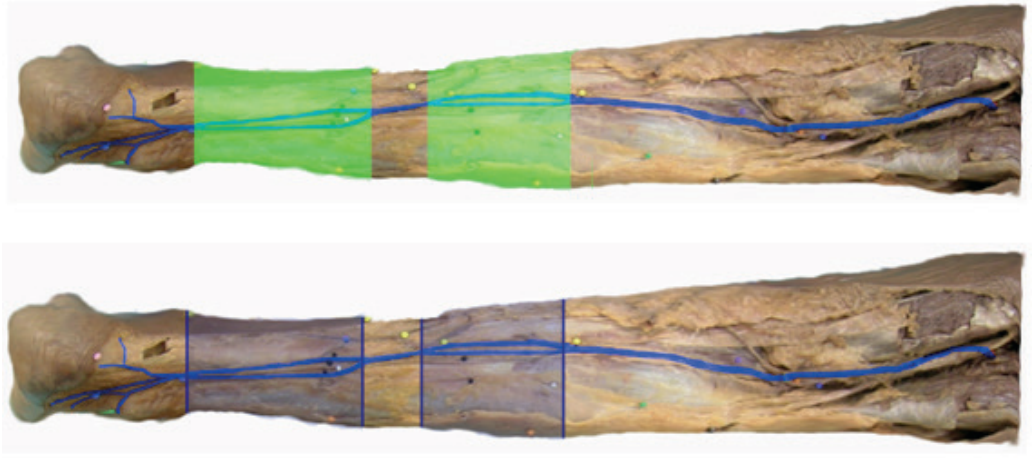

Figure 34. Showing the area in the lower leg in which the short saphenous vein has a duplicated trunk.

To make renditions of areas in multiple specimens the opacity of the individual layers of each specimen need to be adjusted. When 20 specimens are used the opacity of each layer needs to be set to 5% (=100%/20). Then the individual layers can be merged (layer; merge layers) and visualised over a background specimen. The combined opacity of the layers represents the amount of specimens in which the highlighted area is present. Figure 34 for example shows the area in the leg in which a vein has a duplicated trunk. In figure 35.1 when the combined opacity of selected areas is 100 % this represents that the vein has a duplicated trunk in all 20 specimens. If the combined opacity of the selected areas is just 10 % this represents that only 2 of the 20 specimens have a duplicated trunk.

Different opacities (or intensities) of the same colour are difficult to distinguish. Also most printers have trouble printing 20 different intensities of blue. To solve this problem the different intensities of blue can be given a certain colour. To create this rendition first the merged layer showing all areas with an opacity of 5 percent needs to be merged with a completely black layer. Then the magic wand tool (W) can be used to select the different intensity levels of blue (0,5,10,...., 100%). Finally each of the intensity levels, representing a certain number of specimens for that area) can be allocated a certain colour.

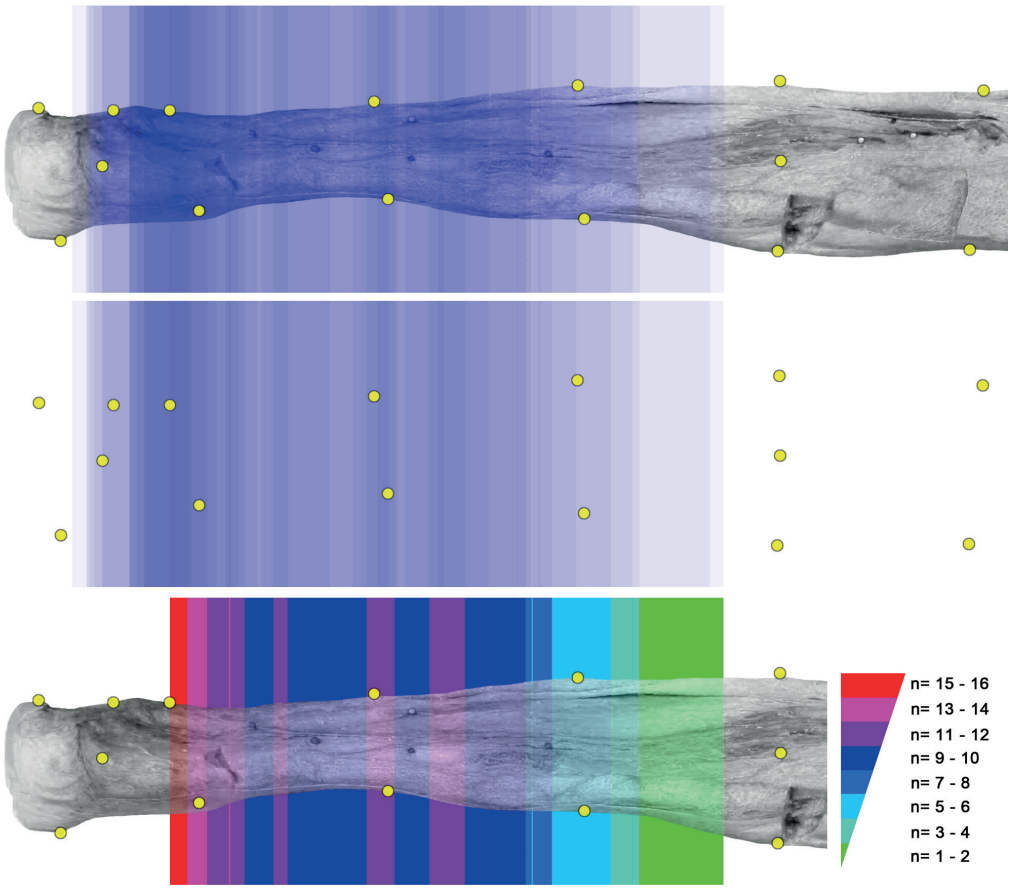

Figure 35. Rendition of 20 specimens. 1: original combined areas
2: areas overlay on a black background
3: final rendition. Each colour represents a certain number of specimens in which the short saphenous vein has a duplicated trunk.

REFERENCES

1) Ball, W.W. Rouse (1960) [1908]. A Short Account of the History of Mathematics (4th ed.). Dover Publications. pp. 50–62. ISBN 0-486-20630-0.
2) A proposition that commends itself to general acceptance; a well-established or universally conceded principle; a maxim, rule, law" axiom, n., definition 1a. Oxford English Dictionary Online, accessed 2012-04-28. Cf. Aristotle, Posterior Analytics I.2.72a18-b4.
3) http://en.wikipedia.org/wiki/Geometry
4) http://en.wikipedia.org/wiki/Euclidean_space
5) Euclid`s elements of Geometry, Richard fitzpatrick. translation. 2007 ISBN10: 0615179843
6) Hoffman, P. (1998). The Man Who Loved Only Numbers: The Story of Paul Erdős and the Search for Mathematical Truth. Hyperion, New York. ISBN 1-85702-829-5.
7) http://en.wikipedia.org/wiki/Cartesian_coordinate_system
8) O. Bottema & B. Roth (1990). Theoretical Kinematics . Dover Publications. reface. ISBN 0-486-66346-9. J. M. McCarthy (2013). Introduction to Theoretical Kinematics . MDA Press. reface.
9) https://en.wikipedia.org/wiki/Cartesian_coordinate_system
10) Alexey Tikhonov, http://slideplayer.com/slide/9681157/
11) Eric Weisstein, http://mathworld.wolfram.com/BarycentricCoordinates.html
12) J. Duchon, 1976, Splines minimizing rotation invariant semi-norms in Sobolev spaces. pp 85–100, In: Constructive Theory of Functions of Several Variables, Oberwolfach 1976, W. Schempp and K. Zeller, eds., Lecture Notes in Math., Vol. 571, Springer, Berlin, 1977
13) A. Goshtasby, Registration of image with geometric distortion," IEEE Trans. Geoscience and. Remote Sensing, vol. 26, no. 1, pp. 60{64, 1988.
14) F. L. Bookstein, Principal warps: Thin-plate splines and the decomposition of deformations.
15) http://www.cs.sjsu.edu/faculty/pollett/masters/Semesters/Spring05/wallun/index.shtml?Del3.html
16) Aseem Agarwala, Mira Dontcheva, Maneesh Agrawala, Steven Drucker, Alex Colburn, Brian Curless, David Salesin, Michael Cohen. Interactive Digital Photomontage. ACM Transactions on Graphics (Proceedings of SIGGRAPH 2004), 2004.
17) http://step.polymtl.ca/~rv101/thinplates/
18) Anubifix, http://www.anubifix.com/?id=311&id2=38
19) http://www.anubifix.com/?id=311&id2=35
20) Canon Group. http://www.canon.com
21) http://www.digitalcameraworld.com/2013/08/23/what-is-a-macro-lens-magnification-minimum-focus-distance/
22) Bogin, B; Varela-Silva, M. I. (2010). "Leg length, body proportion, and health: A review with a note on beauty". International Journal of Environmental Research and Public Health. 7 (3): 1047–75.doi:10.3390/ijerph7031047. PMC 2872302 . PMID 20617018.
23) Adobe crop. Adobe Photoshop CS-4; http://www.photoshop.com/

24) Effect Matrix Software Studio; http://www.effectmatrix.com/morphing/

25) AutoHotkey Foundation LLC. https://autohotkey.com/

01000011 01101000 01100001 01110000
01110100 01100101 01110010 00100000
00110010 00101110 00110001 00001010

Chapter 2.1

An Anatomical Approach to Arteriovenous Fistula Performance in the Forearm.

M.G. ten Berge, T.I. Yo, A. Kerver, A.A.E.A. de Smet, G.-J. Kleinrensink.

Eur J Vasc Endovasc Surg. 2011 May 6.

ABSTRACT

Background: Arteriovenous fistulae (AVFs) play a key role for people who rely on chronic haemodialysis. Stenosis in the venous outflow of the AVF will cause an alternative route of the subcutaneous blood flow via the deeper venous pathways by means of side branches and the perforating veins (PVs). The purpose for the present study was to define the number and anatomical localisation of the perforating veins in the forearm.

Methods: Twenty forearms were dissected to study the venous anatomy. The localisation, size and connections of the perforators were recorded and stored digitally.

Results: In total, 189 PVs were defined (mean, 9.5 per arm; range, 6–19), with 60 (32%) PVs connected to the cephalic vein, 97 (51%) connections to the basilic vein and 32 (17%) PVs to the median vein of the forearm. Most PVs originate from the basilic vein and connect with the ulnar venae comitans. The cephalic vein connects equally to the radial venae comitans, interossea veins and the muscles.

Conclusions: The cephalic vein has the fewest PVs and almost a third of them connect to the muscles. This is probably important for the maturation of the AVF, the superficial flow volume and the accessibility for puncture.

INTRODUCTION

Successful access for haemodialysis largely depends on the patient's venous flow in the upper extremity. To ensure vascular access with sufficient blood flow in patients who need chronic haemodialysis, an arteriovenous fistula (AVF) has to be created. Impaired vascular access is the main factor for surgical or radiological intervention.[1] The most distal site for a fistula is the anatomic snuffbox, followed by the Brescia–Cimino fistula.[2] In 15.3% of cases, the radiocephalic AVF fails due to early thrombosis and failure to mature.[3] The maturation depends, among other factors, on sufficient flow, by means of a good inflow pressure and a sufficient upstream resistance.[4, 5] This delicate balance could be easily disturbed, resulting in low inflow pressure or insufficient upstream resistance, caused by alternative routes, such as side branches and the perforating veins or communicating veins. Perforating veins as found in the leg are the connections between the superficial venous system, such as the cephalic, basilic and median vein, and the deep venous system, known as the venae comitans, near the radial and ulnar artery.[6-8] So far, no studies have examined the exact location and amount of the perforating veins in the forearm. It seems likely that they play a role in the direction of flow downstream of an AVF. To assess the relationship between the venous systems in the forearm, an anatomical study was performed to review the number, size and localisation of the perforators on the ventral and dorsal side in the forearm.

METHODS

Materials

In this study, 20 forearms (10 male and 10 female) from human embalmed specimens were dissected. The area of interest was between the styloid process of the ulna and radius and the medial and lateral epicondyl. We were especially interested in the venous pattern of the forearm because of its possible implications of primary AV fistula construction and performance. On the other hand, upper arm fistulae are usually created for secondary autogenous dialysis access.[9] In addition, the group contained 10 left and 10 right forearms. If a forearm showed any signs of surgical intervention or macroscopic signs of vascular disease, it was excluded from the study. We defined a perforating vein as a connection, through the fascia, between the superficial venous system and the deep venous system, as described above. The branches from the superficial system, which did not perforate the fascia, are defined as side branches. At the commencement of dissection, the skin and the subcutis were removed. The cephalic, basilic vein and

median antebrachial veins remained attached to the forearm and the perforators were marked by coloured pins.

Computer-Assisted Surgical Anatomy Mapping (CASAM)

All 20 forearms were photographed by using a standardised setting. The camera, a Canon 350D with a Zoom EF-S lens, was placed on a tripod 1 m above the forearms and horizontally aligned, so that all the photographs were comparable. To create an average forearm, all the pictures were marked by using bony landmarks, that is, the styloid process of the ulna and radius, the medial and lateral epicondyl. Magic Morph 1.90 (ITinySoft) software was used to warp 20 forearms into one average forearm. Hereafter, all the perforating vein markers are displayed on the average forearm with Photoshop CS3 to create an overview of the localisation of all perforating veins. In addition, the lumen-size diameter (<1 mm, 1≥ mm) and number of the perforators were identified by using a calliper. Besides the perforators, the localisation and size of the vena mediana cubiti profunda was defined by using the method mentioned above.

RESULTS

Topographic Anatomy

The cephalic veins connect equally with the radial venae comitans and interossea veins on the dorsal side of the forearm. A third of the cephalic vein perforators disappear in the muscles on both sides, in contrast to the basilic perforators, which connect mainly to the interossea veins on the dorsal side and the muscle fibres. The smallest number of perforators from the basilic vein

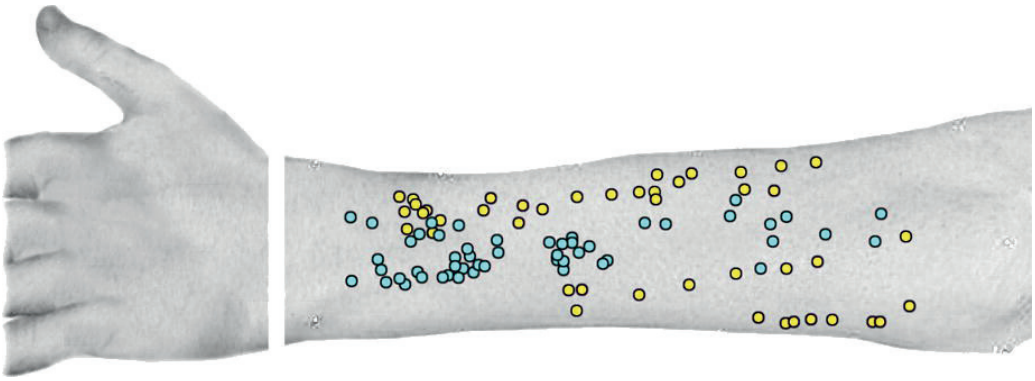

Figure 1. Localisation of the perforating veins at the dorsal side of the upper extremity.
Turquoise: PV which connect with the interossea vein, yellow: PV disappearing in the muscles.

connects to the ulnar venae comitans. Similar to the cephalic vein, 31 perforators connected with the basilic vein disappear in the muscle fibres.

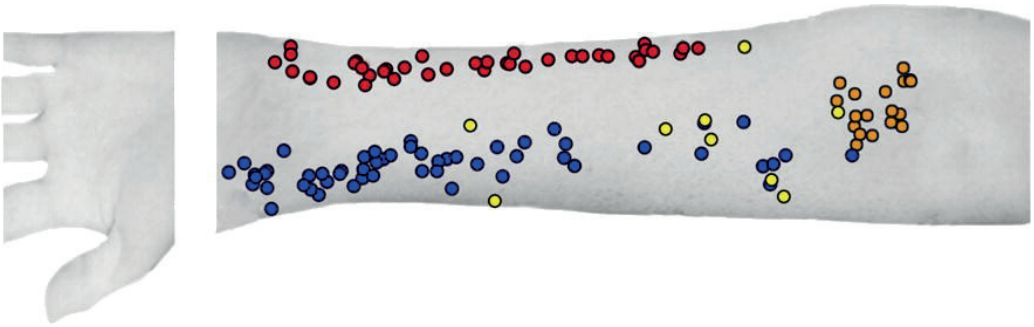

Figure 2. Perforating veins at the ventral side of the upper extremity.
The red dots depict the perforating veins to the a. ulnar venae comitans. Perforating veins that connect to the a. radial venae comitans are colored blue. The yellow dots are the perforating veins that disappear in the muscles and the orange dots are the cubiti media profunda veins.

	Cephalic vein Mean [range]	Basilic vein Mean [range]	Median antebra-chial vein Mean [range]
Perforating vein connections			
ulnar venae comitans	0	1.35 [1-5]	0
Radial venae comiatns	1.05 [0-4]	0	1.15 [0-3]
V. interossea	0.9 [0-2]	1.95 [1-4]	0
Muscles	1.05 [0-3]	1.55 [0-4]	0.45 [0-1]
Total	**3 [1-11]**	**4.85 [1-9]**	**1.6 [0-3]**
Side branches	**4.4 [1-7]**	**4.2 [1-8]**	**3.1 [1-5]**
Size of the perforating veins			
< 1 mm	1.7 [1-3]	3.05 [2-5]	0.9 [0-2]
≥ 1 mm	1.3 [0-2]	1.8 [1-4]	0.7 [0-1]

Table 1. Connections of the superficial venous system with the deeper venous system in the forearm. (Numbers, size and connections of the perforating veins in the forearm).

Median antebrachial veins connect mainly to the radial venae comitans (n = 23) and with a small number to the muscles. Most perforating veins originating from the three veins are <1 mm in diameter. The coordinates of the perforators on the dorsal side of 19 upper extremities are depicted in Figure 1. This diagram shows a more or less organised plot with most connections, based medial of the forearm, to the interossea vein and a higher density at the proximal part of the lower forearm. The diagram of the ventral perforators (Figure 2) of 19 forearms shows a different plot when compared with the dorsal side. Most perforators are located at radial or ulnar side on the ventral side of the forearm. In all 20 forearms, a media cubiti profunda vein was found with a mean diameter of 3.6 (range, 2–5) mm. In 70% of the cases, the media cubiti vein branched off the cephalic vein and 30% are connected to the median antebrachial vein with a connection with the comitant veins. A constant localisation of the media cubiti profunda (Figure 2) has been found at the fossa cubiti. In two cases, the media cubiti profunda vein was divided into two connections.

DISCUSSION

As most complications after AVF formation arise from stenosis or thrombosis of the fistula or the venous outflow of the fistula, the importance of patent venous blood flow in the forearm related to fistula maturation is clear. Similar to the venous circulation in the leg, the perforating veins of the forearm may play an important role in the fragile relationship between deep and superficial venous circulation. However, in contrast to the extensively studied situation of the leg with its well-known Cocket et al.[10] perforating veins, as far as we could find in literature, no study has described the exact anatomic location of the perforators on the dorsal and ventral side of the forearm. Other studies have confirmed the presence of perforators in the forearm, yet have never described the anatomy. An extensive study done by Taylor et al.[11] investigated the venous architecture of the integument and the deep tissues in six total-body human fresh-frozen anatomic specimen. The sites of the venous perforators were plotted and traced to their underlying parent veins that appear to accompany the source arteries. Further, a series of cross-sectional studies were performed to determine the course of the perforators between integument and deep tissue. Valentino et al.[6] confirm the connection between the radial venae comitans and the superficial system, and the presence of valves found in the perforating veins indicates a flow from superficial to deeper venous structures.

In the present study, a similar connection between the ulnar and radial vena comitans and the superficial system was observed. Due to the fact that, in this study, we registered the veins smaller than 1 mm, we found much more perforator veins than expected. Most of the cephalic perforator veins connect with the radial venae comitans and the muscles and on the opposite side, the basilic perforator veins connect mainly with the ulnar venae comitans vein and the interossea vein. Further, half of the connections have a diameter of 1 mm or greater, which probably has a significant role in the venous flow. The cephalic vein has fewer connections with the deeper venous system compared with the basilic vein. Aside from this, most connections are smaller than 1 mm. This can be a factor in maturation of a radiocephalic shunt. The mediana cubiti profunda vein was constant regarding its location and diameter in all arms. This vein was present in all arms, had a mean diameter of 3.6 mm and connected the deep comitant veins with the cephalic vein in 70% and with the median cubital vein in 30% of cases. This perforating vein is used as the anastomotic site with the brachial artery in the brachiocephalic elbow fistula,[12] Perforating veins as ascribed may play a role in the adjustment of the venous flow when the outflow is increased. On the other hand, perforating veins may have a detrimental effect on maturation by diverting blood to the deeper vascular structures. To establish which compensatory mechanisms apply to this situation, it would be useful to investigate the function of perforating veins during the maturation of the fistula. In this study, we therefore attempted to quantify and localise the perforating veins to be able to create a haemodynamic model in the future.

REFERENCES

1) Kidney disease outcomes quality initiative (DOQI). update 2006
2) Kidney disease outcomes quality initiative (DOQI). [online]. Available: National Kidney Foundation, Inc http://www.kidney.org/professionals/guideline_upHD_VA/va_guide2.htm; 2001 [accessed 25.08.08].
3) Rooijens, P.P.G.M., Tordoir, J.H.M., Stijnen, T., Burgmans, J.P.J., de Smet, A.A.E.A., Yo, T.I. Radiocephalic wrist arteriovenous fistula for hemodialysis: Meta-analysis indicates a high primary failure rate (2004) European Journal of Vascular and Endovascular Surgery, 28 (6), pp. 583-589.
4) Beathard, G.A., Settle, S.M., Shields, M.W. Salvage of the nonfunctioning arteriovenous fistula (1999) American Journal of Kidney Diseases, 33 (5), pp. 910-916.
5) Roy-Chaudhury, P., Spergel, L.M., Besarab, A., Asif, A., Ravani, P. Biology of arteriovenous fistula failure (2007) Journal of Nephrology, 20 (2), pp. 150-163.
6) Valentino, J., Funk, G.F., Hoffman, H.T., McCulloch, T.J. The communicating vein and its use in the radial forearm free flap (1996) Laryngoscope, 106 (5 I), pp. 648-651.
7) Wu, T.-Y.T., Brown, R.E. Antegrade venous drainage in a reverse radial forearm flap (2004) Plastic and Reconstructive Surgery, 113 (2), pp. 645-648.
8) Zhong, S.Z., Wang, G.Y., Yuan, L., Xu, D.C. Anatomic basis of venous drainage in donor flaps (1994) Surgical and Radiologic Anatomy, 16 (4), pp. 349-354.
9) Rivers, S.P., Scher, L.A., Sheehan, E., Lynn, R., Veith, F.J. Basilic vein transposition: an underused autologous alternative to prosthetic dialysis angioaccess (1993) Journal of Vascular Surgery, 18 (3), pp. 391-397.
10) Cockett, F.B. The pathology and treatment of venous ulcers of the leg (1955) Br J Surg, 43, pp. 260-278.
11) Taylor, G.I., Caddy, C.M., Watterson, P.A., Crock, J.G. The venous territories (venosomes) of the human body: Experimental study and clinical implications (1990) Plastic and Reconstructive Surgery, 86 (2), pp. 185-213.
12) Bender, M.H.M., Bruyninckx, C.M.A., Gerlag, P.G.G. The brachiocephalic elbow fistula: A useful alternative angioaccess for permanent hemodialysis (1994) Journal of Vascular Surgery, 20 (5), pp. 808-813.

01000011 01101000 01100001 01110000
01110100 01100101 01110010 00001010
00110010 00101110 00110010
00101110 00110010 00001010

Chapter 2.2

Surgical Anatomy of the 10th and 11th Intercostal, and Subcostal Nerves: Prevention of Damage During Lumbotomy.

Teunette van der Graaf, Paul C.M.S. Verhagen, Anton L.A. Kerver, Gert-Jan Kleinrensink.

J Urol. 2011 Jun 16.

ABSTRACT

Background: In a descriptive, inventorial anatomical study we mapped the course of the 10th and 11th intercostal nerves, and the subcostal nerve in the abdominal wall to determine a safe zone for lumbotomy.

Methods: We dissected 11 embalmed cadavers, of which 10 were analyzed. The 10th and 11th intercostal nerves, and the subcostal nerve were dissected from the intercostal space to the rectus sheath. Analysis was done using computer assisted surgical anatomy mapping. A safe zone and an incision line with a minimum of nerve crossings were determined

Results: The 10th and 11th intercostal nerves were invariably positioned subcostally. The subcostal nerve lay subcostally but caudal to the rib in 4 specimens. The main branches were located between the internal oblique and transverse abdominal muscles. The nerves branched and extensively varied in the abdominal wall. A straight line extended from the superior surface of the 11th and 12th ribs indicated a zone with lower nerve density. In 5 specimens the 10th and 11th intercostal nerves crossed this line from the superior surface of the 11th rib. In 5 specimens neither the 11th intercostal nerve nor the subcostal nerve crossed this extended line from the superior surface of the 12th rib up to 15 cm from the tip of the rib

Conclusions: Damage is inevitable to branches of the 10th or 11th intercostal nerve, or the subcostal nerve during lumbotomy. However, an incision extending from the superior surface of the 11th or 12th rib is less prone to damage these nerves. Closing the abdominal wall in 3 layers with the transverse abdominal muscle separately might prevent damage to neighboring nerves

INTRODUCTION

Flank bulge is a common complication after lumbotomy for renal surgery. The cause of this complication is often iatrogenic damage to the nerves supplying the abdominal wall musculature due to the initial incision or to closing sutures after the procedure. This denervation results in laxity and bulging of parts of the abdominal wall.[1-3] It is a clinically innocuous complication but also inconvenient and it can be esthetically disturbing for patients.[4]

The incidence of flank bulge after renal surgery has been reported with a large variability. In 1974 a 3% incidence of bulging was found after nephrectomy using a classic flank incision.[5] This was in accordance with a 3.6% incidence using a miniflank incision.[6] However, a 49% incidence of flank bulge after nephrectomy was reported in a telephone survey with patients who reported flank bulge.[4]

It is unclear how lumbotomy can be performed without nerve injury. The intercostal nerves are classically described to run in the subcostal groove.[7, 8] Others found that they run mid intercostally[1, 9] or more caudal in the intercostal space.[10] The lower intercostal nerves divide and give off 1) an anterior branch innervating the skin and the external oblique muscle, and 2) a posterior branch innervating the internal oblique and transverse abdominal muscles.[1, 8] The main trunk of the intercostal nerves runs a course between the internal oblique and transverse abdominal muscles.[11] The 9th to 12th intercostal nerves conjoin to form a plexus.[8, 12]

We mapped the course of n10, n11 and n12 in the lumbotomy area using the new analytical method, CASAM, and defined a safe zone for the lumbotomy incision.

METHODS

Materials

In this descriptive inventorial anatomical study 11 embalmed specimens, including 4 male and 7 female cadavers with intact flanks, were dissected unilaterally. All landmarks were assessed in situ at dissection and standardized photographs were taken (Figure 1). One male body was excluded from study due to dissimilar anatomy, ie poor pelvic alignment. In this case the analytical method caused distortion of the body contour and the nerves could not be analyzed properly.

The epidermis was removed from just below the iliac crest up to the 10th rib from the posterior intercostal space to the lateral edge of the rectus abdominis muscle. The neurovascular bundles of n10, n11 and n12 were identified below the ribs and followed through the abdominal wall to the rectus abdominis muscle. Surrounding tissue was removed while preserving the underlying tissue. Neurovascular bundle nerves were marked with yellow pins.

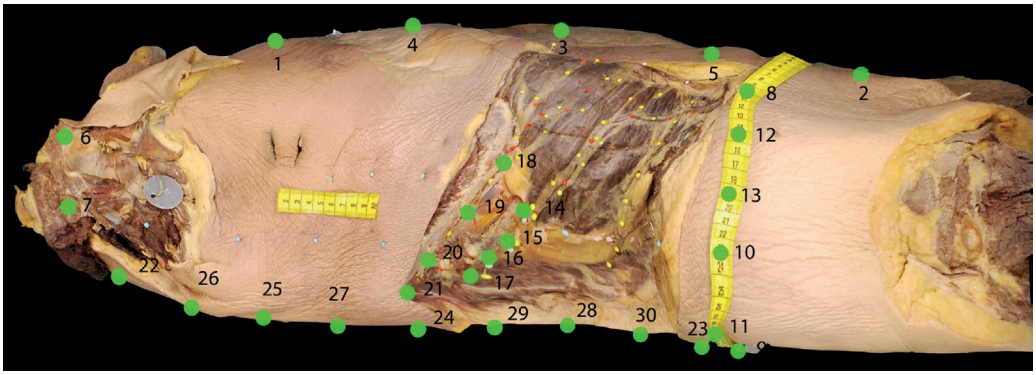

Figure 1.Landmarks (1 to 30, green circles) used for analysis

Measurements

General measurements were made in the specimens. The distance between the anterior superior and posterior superior iliac spines was measured to indicate the width of the body. The distance between the sternal angle (Louis' angle as landmark 1) and the pubic symphysis (landmark 2) were measured to assess the length of the body (Figure 1). The distance from n10, n11 and n12 to the caudal surface of the rib was measured. The number of branches of each nerve was counted. Nerve diameter was measured below the rib and in the abdominal wall. Branches with a diameter of less than 1 mm were considered small. An incision line with a minimum of crossing nerves was determined. The distance of the first branch passing this line was measured from the tip of the 11th or 12th rib.

Computer-Assisted Surgical Anatomy Mapping (CASAM)

All photos were taken according to a standardized protocol, which is a required condition to enter photos into CASAM. The cadaver was placed on a screen, which was marked with a cross to facilitate standardized positioning. The cadaver was placed on the contralateral flank, supported subcostally and fixed in a 90-degree position with 2 U-shaped constructions that were especially made for this study. To prevent rotation of the thorax and pelvis the back and pelvis were supported in

the U-shaped construction. Landmarks were marked with pins after positioning the specimens. A tape measure was pinned between the anterior superior and the posterior superior iliac spine to ensure that the landmarks between were on the same line.

All photographs were taken using a Nikon® D60 camera with a 50 mm 1:2.8 DGmacro lens (Sigma, Tokyo, Japan). The camera was set in a tripod and fixed in a position perpendicular to the specimen at 160 cm from the specimen. The camera flash was disabled and a self-timer was used to avoid any camera movement. The camera was centered on the middle of the line between the posterior tip of the acromion, and the middle of the anterior superior and posterior superior iliac spine.

CASAM was used to compare the photographs of the different cadavers and make clinically relevant information visible. Photographs of the left flank were mirrored to create the same view and make the right and left sides comparable.

To perform step 1 (morphing) Magic Morph was used. In this process the shape and size of each cadaver was defined using predetermined landmarks. This was followed by calculating and computing an average body shape and size. Thin plate spline transformation was used as a morphing algorithm.[13, 14] All bodies were shaped to exactly match the shape and size of the computed and calculated average body. Photoshop® CS4 was used to compile all data and visualize the relevant anatomy.

A safe zone was determined by coloring the nerve-free zones, excluding the ribs. Safe zones were compiled into 1 image and a gradient of free zones was visualized. These gradients were colored and a percent was assigned to each area.

RESULTS

Topographic Anatomy

The median distance between the anterior superior and the posterior superior iliac spine was 24 cm (range 19.8 to 30). The median distance from the pubic symphysis to the sternal angle was 48.5 cm (range 40 to 50). We found that n10 and n11 ran subcostally and were flush to the caudal surface of the rib in all specimens. In 6 specimens n12 was positioned subcostally. The subcostal nerve was found 1, 1.5, 2 and 3 cm caudal to the 12th rib in 4 specimens. In 8 of 10 specimens (80%) n10 and n12 branched. The 11th intercostal nerves branched in 9 specimens (90%). When n10, n11 or n12 branched, there were 2 to 4 branches. In 1 specimen (10%) n10 and n11 crossed, and in 3 (30%) n11 and n12 crossed.

In the anterior abdominal wall n10 and n11 ran together in 2 specimens (20%). In 4 specimens (40%) n11 and the subcostal nerve ran together in the abdominal wall. Average nerve diameter was 2.2 mm caudal to the rib and 2.1 mm in the abdominal wall.

Computer-Assisted Surgical Anatomy Mapping (CASAM)

All landmarks except the superior surface of the first thoracic vertebra were visible in all photographs. Since this landmark was not visible in the photographs of 3 specimens (30%), it was not used for computer analysis. However, landmarks between the superior surface of the first thoracic vertebra and the superior surface of the sacral bone were used. The tip of the 12th rib was not visible in the photos of 2 specimens (20%) because the rib was too small and the abdominal wall obstructed the view. Figure 2,A shows the course of 10 intercostal and subcostal

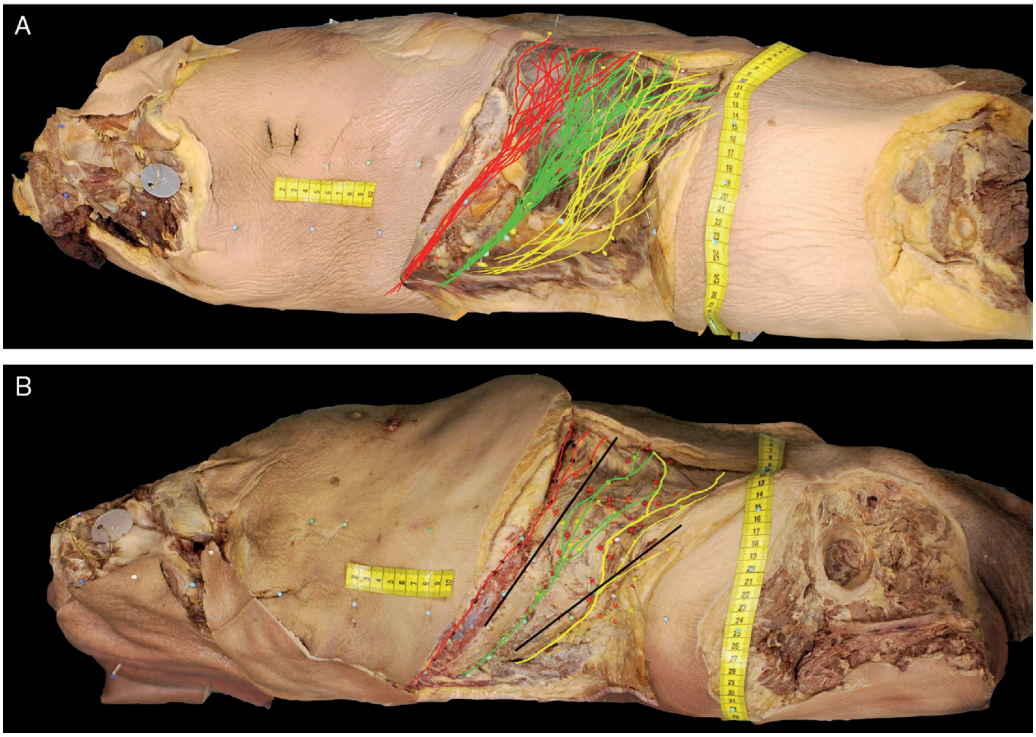

Figure 2. One standardized specimen created from 10 specimens shows n10 (red lines), n11 and n12.
A, abdominal wall. Yellow lines indicate n11. Green lines indicate subcostal nerve.
B, projection of extrapolated lines (black lines) from rib superior surface. Green lines indicate n11. Yellow lines indicate n12.

nerves visualized in 1 average body. Little variation was noted in the course of n10 and n11 in the intercostal space. The position of the 12th rib varied among specimens, resulting in variation of the position of n12 to the caudal surface of the 11th and 12th ribs. The nerves first branched in the abdominal wall and after this large variation existed in terminal branches. Figure 3,A shows safe zones in the abdominal wall with the percents assigned to these zones. A safe zone was found in the intercostal space between the 10th and 11th ribs, and below the 11th rib. The 11th and 12th ribs were part of this safe zone (Figure 3, B).

The safe zone, that is the zone with a low chance of nerve injury, for lumbotomy appeared to project in a straight line extrapolated from the superior surface of the 11th and 12th ribs. No absolute safe zone was identified. In our specimens we investigated how often the intercostal or subcostal nerve crossed this imaginary line.

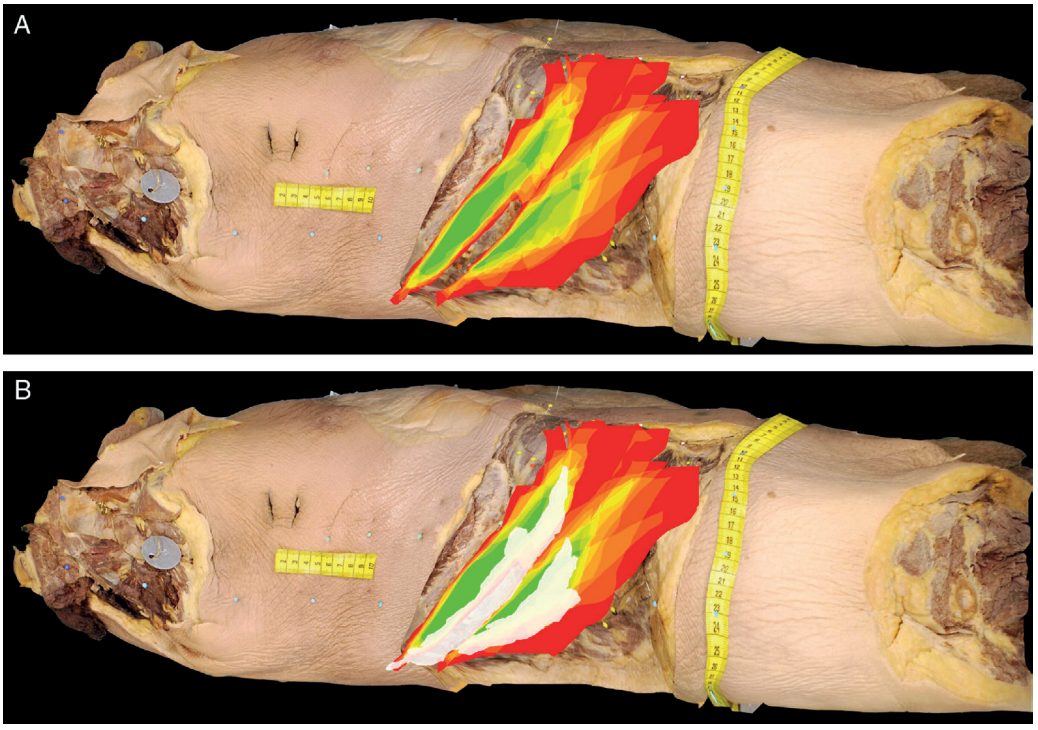

Figure 3. Safe zones in abdominal wall between n10 and n11, and n11 and n12.

A, 100% safety where no nerves run in certain parts of body (green areas).
B, additional white area represents position of 11th and 12th ribs, which partly overlaps safe zone. Red areas indicate 10% safety. Orange gradient from red to yellow represents 20% to 50% safety. Yellow areas indicate 60% safety. Yellow to green gradient represents 70% to 90% safety.

In 6 specimens (60%) neither n10 nor n11 crossed an extrapolated line from the superior surface of the 11th rib (Figure 2, B). When n10 or n11 crossed this line, the distance from the tip of the 11th rib to the first passing branch was 0.5 to 7 cm (Table 1). In 5 specimens (50%) n11 and n12 did not cross an extrapolated line from the superior surface of the 12th rib in the lumbotomy area, 15 cm from the tip of the rib. Only small branches crossed this line in 1 specimen (10%). The distance of the nerves crossing this line was 5 to 13.5 cm.

NR.	11th-n10 or n11*	12th-n11 or n12*
1	-	9.5*
2	-	6.7*
3	-	-
4	-	19.5
5	-	11.5*
6	4	4.5+
8	0.5	-
9	4.5	-
10	7	15
11	-	5*

Table 1. Distance from rib tip to first nerve branch crossing extrapolated line from superior surface of ribs
* Considered within lumbotomy area
+ Only small branches crossed line and no branch crossed extrapolated line from rib.

DISCUSSION

Flank bulge is a common, disturbing complication after lumbotomy.[4-6] It is caused by damage to intercostal and subcostal nerves supplying the abdominal wall musculature, resulting in paralysis and atrophy of these muscles.[1-3] It is not yet clear how nerve injury can be minimized during lumbotomy. Therefore, we mapped the course of n10, n11 and n12 in relation to relevant anatomical structures to define a safe zone for lumbotomy.

A new method of analysis was used to visualize structures of clinical interest in the abdominal wall. The essence of this method is an especially made computer program that uses body landmarks to calculate an average body. CASAM revealed that damage may be minimized using an incision extending from the superior

surface of the 11th or 12th rib. In 60% of specimens no or minimal damage to the intercostal and subcostal nerves would be expected if incision length was limited to 15 cm from the tip of the rib. Diblasio et al previously proposed an incision over the superior surface of the 11th rib, starting 5 cm ventral and ending 3 cm dorsal to the tip of the rib, to limit damage to the intercostal nerves.[6] This is in agreement with our findings (Figure. 2, A). If an incision is made over the superior surface of the ribs, damage to the intercostal nerves will be minimal.

An accurate safe zone cannot be defined with 100% certainty based on data on 10 specimens. Due to extensive variation in the course of the terminal nerve branches in the abdominal wall a 100% safe zone could not be defined. This means that damage to branches of the intercostal nerves during lumbotomy cannot be prevented in all cases.

However, certain aspects of positioning the anatomical specimens may have hampered analysis. The cadavers could not be placed in the flank position with lateral flexion of the lumbar region, which is common practice for lumbotomy. It might be possible in vitro that in this position the intercostal space and the space between the nerves in the abdominal wall are smaller than in a patient who undergoes lumbotomy. Furthermore, the tissue of embalmed cadavers is less voluminous than in a living individual since slight contraction occurs during the embalming procedure. Damaging cutaneous branches does not result in paralysis of the abdominal wall musculature and, thus, does not result in flank bulge. All of this might contribute to an underestimation of the safe zone in the intercostal space and abdominal wall.

It is unclear whether damage to the intercostal and subcostal nerves is caused by the initial incision alone. Nerve damage might also be caused by forces induced by the retractor. Peripheral nerves are prone to damage due to traction. In addition, nerve injury might be caused by closing the incision and, thus, by entrapment.[15] The intercostal nerves ran a course between the internal oblique and the transverse abdominal muscles in all specimens (the neurovascular plane). Closing the incision in 3 muscle layers separately, ie the transverse abdominal muscle separately, could decrease the risk of nerve entrapment.

Damage to nerves in the abdominal wall may not necessarily result in flank bulge. The intercostal nerves crossed, branched and ran together in the abdominal wall in some specimens, resulting in overlap of the areas innervated by individual nerves. Minimizing damage to intercostal nerve branches might prevent flank bulge. Further research must be done to evaluate this hypothesis.

Conclusion

Damage to branches of n10, n11 and n12 during lumbotomy can be minimized. Incisions extending from the superior surface of the 11th or 12th rib seem to be less prone to cause damage to the intercostal and subcostal nerves. Closing the abdominal wall in 3 layers with the transverse abdominal muscle separately might prevent damage to neighboring nerves.

REFERENCES

1) Gardner, G.P., Josephs, L.G., Rosca, M., Rich, J., Woodson, J., Menzoian, J.O. The retroperitoneal incision: An evaluation of postoperative flank 'bulge' (1994) Archives of Surgery, 129 (7), pp. 753-756.
2) Korenkov, M., Rixen, D., Paul, A., Köhler, L., Eypasch, E., Troidl, H. Combined abdominal wall paresis and incisional hernia after laparoscopic cholecystectomy (1999) Surgical Endoscopy, 13 (3), pp. 268-269.
3) Hoffman, R.S., Smink, D.S., Noone, R.B., Noone Jr., R.B., Smink Jr., R.D. Surgical repair of the abdominal bulge: Correction of a complication of the flank incision for retroperitoneal surgery (2004) Journal of the American College of Surgeons, 199 (5), pp. 830-835.
4) Chatterjee, S., Nam, R., Fleshner, N., Klotz, L. Permanent flank bulge is a consequence of flank incision for radical nephrectomy in one half of patients (2004) Urologic Oncology: Seminars and Original Investigations, 22 (1), pp. 36-39.
5) Ward, J.N., Lavengood Jr., R.W., Subramaniam, A.P., Draper, J.W. Lumbar approaches to kidney. Complications associated with procedure (1974) Urology, 3 (2), pp. 163-167.
6) DiBlasio, C.J., Snyder, M.E., Russo, P. Mini-flank supra-11th rib incision for open partial or radical nephrectomy (2006) BJU International, 97 (1), pp. 149-156.
7) Aubert, J., Koumare, K., Dufrenot, A. Anatomical study of the twelfth intercostal nerve and oblique lumbotomies [ETUDE ANATOMIQUE DU DOUZIEME NERF INTERCOSTAL ET DES LOMBOTOMIES BLIQUES. EXPLICATION CLINIQUE DE QUELQUES NEVRALGIES POSTOPERATOIRES] (1981) Journal d'Urologie, 87 (5), pp. 283-289.
8) Davies, F., Gladstone, R.J., Stibbe, E.P. The anatomy of the intercostal nerves (1932) J Anat, 66 (PART 3), pp. 323-333.
9) Hardy, P.A.J. Anatomical variation in the position of the proximal intercostal nerve (1988) British Journal of Anaesthesia, 61 (3), pp. 338-339.
10) Court, C., Vialle, R., Lepeintre, J.-F., Tadié, M. The thoracoabdominal intercostal nerves: An anatomical study for their use in neurotization (2005) Surgical and Radiologic Anatomy, 27 (1), pp. 8-14.
11) Schlenz, I., Burggasser, G., Kuzbari, R., Eichberger, H., Gruber, H., Holle, J. External oblique abdominal muscle: A new look on its blood supply and innervation (1999) Anatomical Record, 255 (4), pp. 388-395.

12) Rozen, W.M., Tran, T.M.N., Ashton, M.W., Barrington, M.J., Ivanusic, J.J., Taylor, G.I. Refining the course of the thoracolumbar nerves: A new understanding of the innervation of the anterior abdominal wall (2008) Clinical Anatomy, 21 (4), pp. 325-333.

13) Cootes, T.F., Taylor, C.J., Cooper, D.H., Graham, J. Active shape models - their training and application (1995) Computer Vision and Image Understanding, 61 (1), pp. 38-59.

14) Bookstein, F.L., Reyment, R.A. Microevolution in Miocene Brizalina (foraminifera) studied by canonical variate analysis and analysis of landmarks (1989) Bulletin of Mathematical Biology, 51 (6), pp. 657-679.

15) Loos, M.J., Scheltinga, M.R., Mulders, L.G., Roumen, R.M. The Pfannenstiel incision as a source of chronic pain (2008) Obstetrics and Gynecology, 111 (4), pp. 839-846.

01000011 01101000 01100001
01110000 01110100 01100101
01110010 00100000 00110010
00101110 00110011 00001010

Chapter 2.3

The neurovascular anatomy of the lateral hindfoot in relation to incisions for a lateral approach of the ankle and the calcaneus.

A.L.A. Kerver, M.H.J. Verhofstad, A.J.H. Kerver, A.H. van der Veen, D. den Hartog; G.J. Kleinrensink.

Submitted 2017

ABSTRACT

Background: Soft-tissue related complication rates following a lateral approach of the ankle are high and can result in neuropathic pain, wound necrosis or wound infections. Therefore this anatomy study aims to map both neural- and vascular safe zones, resulting in a safer approach of the lateral ankle.

Methods: In 10 embalmed and 10 fresh-frozen lower legs, the sural nerve and vascular anatomy was dissected. A novel method, Computer Assisted Surgical Anatomy Mapping (CASAM) was used to compare anatomy and compute both neural and vascular safe zones and relate them to different surgical approaches.

Results: Both the neural and vascular anatomy of the lateral hindfoot follow a relatively predictable pattern. The sural nerve is mainly at risk in an extended lateral approach or in an incision for the posterolateral portal in ankle arthroscopy. Damage to the main branch can easily be prevented moving the (proximal part of) the incision closer to the Achilles tendon. Damage to the distal sural nerve can be reduced when approaches to the fifth metatarsal are located inferior to the metatarsal head. In addition, the medial calcaneal branch of the postior tibial artery supplies a large part of the lower hindfoot and is easily damaged during an extended lateral approach, especially when the incision is placed further away from the sole of the foot. This results in impaired bloodflow to both the full-thickness skin-flap and the lateral-posterior calcaneus. The sinus tarsi approach is located in a neural safe zone and is situated in an area which is supplied by choke vessels of all three suppliying arteries: the anterior tibial, fibular and medial calcaneal branch of the posterior tibial artery. This may explain lower soft-tissue complication rates following this approach.

Conclusion: The neurovascular anatomy of the lateral hindfoot is relatively predictable and soft-tissue related complication rates can be further reduced by implementing effective changes to existing surgical approaches.

Clinical relevance: This study shows that the neurovascular anatomy of the lateral hindfoot is relatively predictable and soft-tissue related complication rates can be further reduced by implementing effective, anatomy based changes to existing guidelines on for instance the extended lateral approach of the calcaneus, the sinus tarsi approach, the approach to the fifth metatarsal and portal placement in ankle athroscopy.

INTRODUCTION

Research and innovation on surgical treatment of foot and ankle injuries has traditionally focused on mechanical aspects of the injury and primary repair techniques. Soft tissue complications such as wound necrosis, wound infection and neuropathic pain are major drawbacks of foot and ankle surgery. Fear for these complications has increased popularity of minimally invasive surgical techniques. However, it is not clear yet if small incisions are safer than large ones in this respect. Current gold-standard incisions for surgery in the lateral hindfoot are merely based on 'nervous safe zones' alone. Therefore the aim of this study is to combine anatomical data of multiple specimens and propose a combined neural and vascular safe-zone(s) for an optimal approach of the lateral side of the ankle and hindfoot.

Traditionally, surgical safe zones in foot and ankle surgery are implicitly seen as 'nervous safe zones'. These zones are anatomical areas in which little or no nerves are encountered during the surgical approach. Of the three sensory nerves running distally, the sural nerve is of particular interest. It innervates the lateral part of the foot. Especially in the lower leg the sural nerve has a variable course mostly located between both gastrocnemius muscles[1,2] whereas more distally it runs close to the Achilles tendon. The sural nerve is at risk for iatrogenic damage in both open and minimally invasive (postero-)lateral approaches for the surgical treatment of talar fractures, ruptured anatomic ankle ligaments, calcaneus fractures, malleolar fractures, percutaneous Achilles tendon repair and ankle arthroscopy[3-7]. Iatrogenic damage to the distal part of the sural nerve can lead to a wide spectrum of postoperative complaints varying from local skin numbness to sharp and invalidating or even causalgic pain[8,9]. Moreover, the sural nerve is considered to recover slower from injury than other cutaneous nerves and appears to have the highest possibility of developing painful neuromas interfering drastically with daily routine and quality of life[3].

Uncomplicated wound healing requires adequate vascularization of a surgical wound. Therefore 'vascular safe zones' are as important as 'nervous safe zones'. The use of watershed areas in ankle surgery in order to preserve perfusion of soft tissues, is relatively new. The main arteries supplying the lateral ankle are the fibular artery (FA), the anterior tibial artery (ATA) and the medial calcaneal branches of the posterior tibial artery (MCBPTA). Sparing these arteries becomes even more paramount in the already fragile soft tissues of a bruised foot after a high energy trauma. In such cases iatrogenic arterial damage may easily result

in soft tissue ischemia leading to infection and necrosis of the lateral hindfoot. Especially in large surgical exposures, such as the extended lateral approach for the calcaneus, an optimal location of the skin incision is important to maintain adequate perfusion of soft tissue. Following open reduction and internal fixation of calcaneal fractures for instance, superficial necrosis has been reported to occur in up to 25%[10-12] of treated cases resulting in a high (permanent) morbidity rate.

First the anatomy of the sural nerve and the main arterial blood supply of the lateral ankle and hindfoot will be described. Then we will discuss the clinical implications to surgical approaches of the lateral ankle such as the extended lateral approach of the ankle (ELAC), the sinus tarsi approach (STA), and the minimally invasive longitudinal approach (MILA). Also implications to ankle arthroscopy, the lateral approach to the fifth metatarsal and the dorso-lateral approaches to the cuboid will be examined.

MATERIALS AND METHODS

The neurovascular anatomy of the lateral hindfoot was dissected in 10 embalmed and 10 fresh frozen unpaired lower legs from adult donors. None of the limbs showed macroscopic signs of disease or scarring. In the embalmed specimens the course of the sural nerve and its concurrent branches was dissected. These specimens had been flushed with AnubiFiX[13] to regain tissue and joint flexibility and were embalmed with a mixture of 6% formaldehyde and 5% phenol. In the fresh frozen specimens the arterial blood supply of the lateral ankle was dissected. After cannulation of the popliteal artery these specimens had been flushed with FillOpaQ[14]. FillOpaQ is a filling-agent having the viscosity close to that of water. It therefore is capable to even reach the smallest capillaries in the foot. Blue-green dye was added to the filler as it contrasts well to the color of fresh-frozen specimen. Once set, FilloPaQ stays slightly flexible (a rubber like rigidity is created) which allows for easy manipulation when dissecting. Dissection was performed using a magnifying glass (5 diopter) until nervous or arterial branches were too small for further dissection (<1mm).

Computer-Assisted Surgical Anatomy Mapping (CASAM)

The anatomy-mapping tool CASAM[1,15,16] was used to visualize and evaluate the complex and variable anatomy of each specimen and to visualize all dissected nerves and arteries in one image of a single ankle with average dimensions. First, each ankle was flexed in 90°, simulating the onset position for most lateral ankle

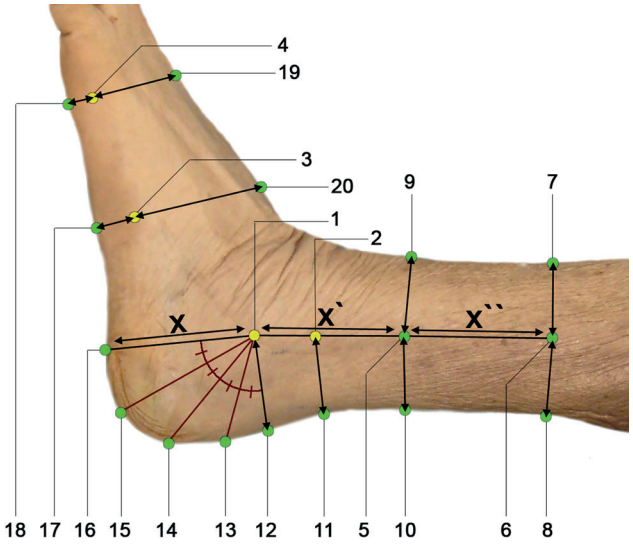

Figure 1. landmarks used for CASAM
Yellow: bony landmarks: The most distal (= malleolus tip; 1) and the most proximal part of the malleolus (malleolus top; 2), the tuberosity of the fifth metatarsal (3) and the fifth metatarsal head (4).
Green: non-bony landmarks: On the sole of the foot: The nearest point to the tip of the lateral malleolus (16), the nearest point to the tuberosity of the fifth metatarsal (17), the nearest point to the fifth metatarsal head (18). On the foot ridge: the nearest point to the fifth metatarsal head (19), the nearest point to the tuberosity of the fifth metatarsal (20). On the achilles tendon: the nearest point to the tip of the lateral malleolus (12), the nearest point to the top of the lateral malleolus (11).
The distance between landmark 1 and 16 (X) was used to create landmark 5 (X`) and 6 (X``) (in line with the tibia). Landmarks 7 and 8 are the nearest points on the posterior and anterior side of the leg to landmark 6. Landmarks 9 and 10 are the nearest points on the posterior and anterior side of the leg to landmark 5.
The angle between landmark 12 and 16 over landmark 1 was measured and divided into four segments (Red lines), thereby creating landmarks 13, 14 and 15 on the edge of the hindfoot.

surgeries. Then, osseous landmarks were identified and marked. Subsequently, non-osseous landmarks were deduced from the osseous landmarks to delineate the different shapes of the individual ankles (Figure 1). Each ankle was photographed, using a standardized protocol, with a Canon 350D camera (Canon USA, Lake Success, New York) with a Canon EF-S 18-55-mm lens (Canon USA). The average location of all osseous and nonosseous landmarks were calculated from each specimen. Then, with the use of Magic Morph 1.9510 software (EffectMatrix Software Studio)[17], each specimen in each original photograph was reshaped (warped) to match the calculated average shape. A thin plate spline was used as

a warping algorithm. Since all warped specimens have an identical calculated average shape, the relative position of the anatomical structures of interest could be mapped and visualized in one averagely shaped ankle. Photoshop CS4 (Adobe Systems, San Jose, California)[18] was used to highlight relevant anatomy and make renditions. The following renditions were made:

- The sural nerve and its branches
- arterial blood supply of the lateral foot
    - o Anterior tibial artery (ATA)
    - o Medial calcaneal branches of the posterior tibial artery (MCBPTA)
    - o Fibular artery (FA)

Watershed area

The main branches of each supplying artery were defined both in each specimen and in each photographed ankle. Arteries of distribution were located and assigned to either one of the three supplying arteries. An area of 25 pixels (=5 times the width of the smaller branches) surrounding each artery was selected and colored. Areas of distribution of each artery were colored and their opacity was set to 40% (Figure 5 A-E). Overlapping areas were again selected and colored, describing the estimated angiosomes of each of the three main arteries supplying the lateral foot. The area in which all three angiosomes overlap was colored green.

RESULTS

Sural nerve

The dissected sural nerves of 10 specimens are visualized in an ankle with average dimensions (Figure 2). The main branch of the sural nerve runs a fairly predictable course. In five specimens the main branch of the sural nerve is a continuation of the medial branch of the sural nerve (originating from the tibial nerve) whereas in the other five specimens the medial branch conjoins with the lateral branch of the sural nerve (originating from the common peroneal nerve) just distal to the posterior inferior tibiofibular ligament. Between the lateral malleolus and the Achilles tendon the posterior border of the main branch is located at 58% of the distance between landmark 1 and 12, and 90% of the distance between landmark 2 and 11. Also, the distal border of the main branch is located at 50% of the distance between landmark 1 and 16. Anteriorly, the border of the main branch variation is located at 60% of the distance between landmark 5 and 10, and 40% of the distance between landmark 2 and 11. The main branches of all specimens run anterior and proximal to the tuberosity of the fifth metatarsal. In

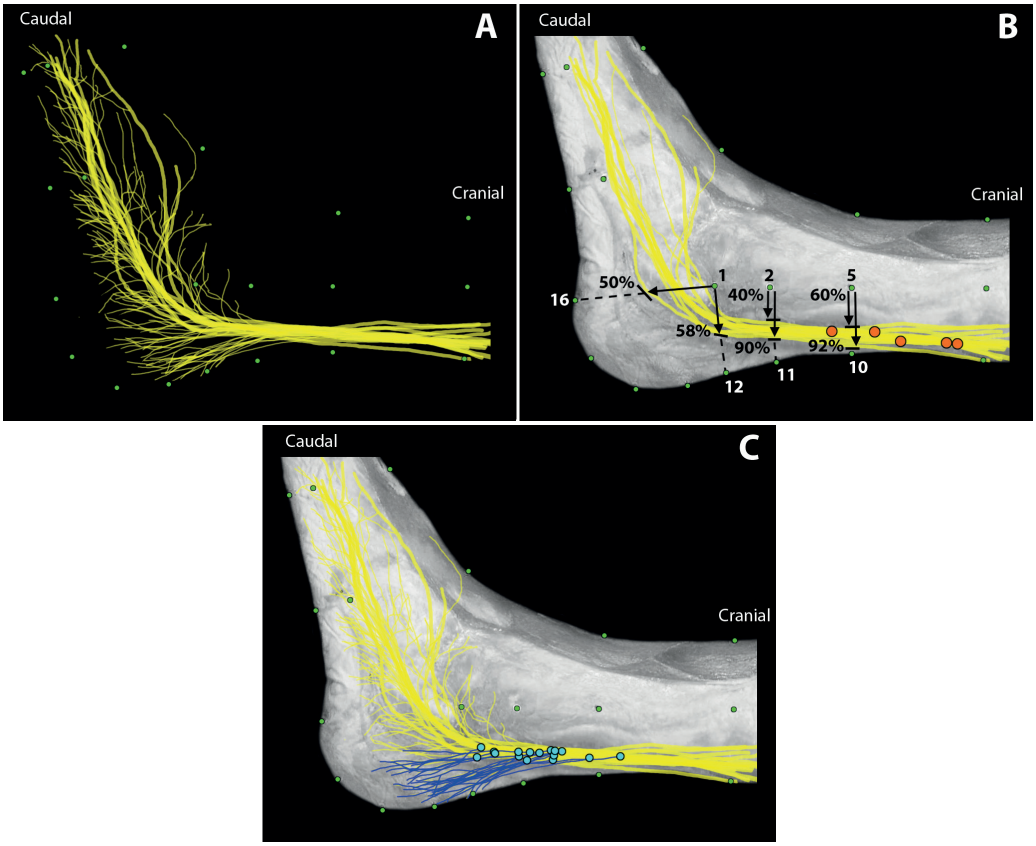

Figure 2. Anatomy of the sural nerve.
A. Variations of the ten dissected sural nerves. B. Orange dots: location where the lateral and medial branch of the sural nerve conjoin. Posterior edges of main branch variations: 92% (d 5-10), 90% (d 2-11), 58% (d1-12) and 50% (d 1-16). Anterior edges of main branch variations: 60% (d5-10) and 40% (d 2-11). All main branches of the sural nerve run anterior and proximal to the tuberosity of the fifth metatarsal. C. The calcaneal branch (blue) and the dorsal branch (purple).

six specimens the lateral calcaneal branch of the sural nerve (innervating the heel) consists of two separate branches and in three specimens only one branch is identified. Twelve of the sixteen origins of the lateral calcaneal branch originate proximal to the uppermost top of the lateral malleolus and in four specimens the origin of the lateral calcaneal branch is located posterior to the lateral malleolus. No origins are found more distal than the most distal tip of the lateral malleolus. In four specimens the sural nerve has a dorsal branch, splitting of the main branch just caudal to the lateral malleolus. This branch then runs to the dorsum of the

foot either conjoining with the intermediate cutaneous branch (of the peroneal nerve) or completely replacing it.

Arterial blood supply

Medial calcaneal branches of the posterior tibial artery

A total of 15 medial calcaneal branches of the posterior tibial artery (MCBPTA) are present in nine specimens. In one specimen the medial calcaneal branch is not present. Four specimens contain only one medial calcaneal branch, whereas in another four two individual branches are present. In one specimen three individual branches were present. All branches originate from the lateral plantar artery, distal to its bifurcation from the posterior tibial artery (PTA) (Figure 3 A). In the specimen with three medial calcaneal branches, the most proximal branch runs off directly from the posterior tibial artery. The superficial, terminal branches supply arterial blood to a large area of the plantar part of the lateral ankle, ranging from the heel to as far as the fifth metatarsal head (Figure 3 B).

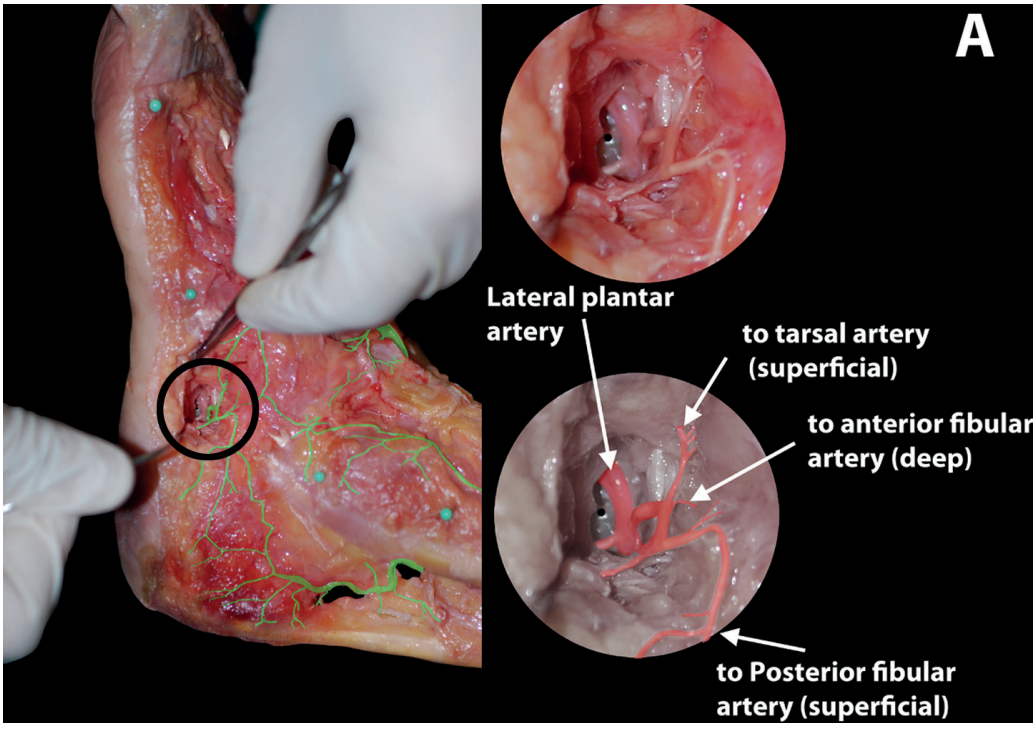

Figure 3 A. Medial calcaneal branch of the posterior tibial artery
A: Example of a dissected medial calcaneal branch of the posterior tibial artery, originating from the lateral plantar artery and connecting superficially with both the tarsal and posterior fibular artery. The connecting artery with the anterior fibular artery runs beneath the peroneal tendons.

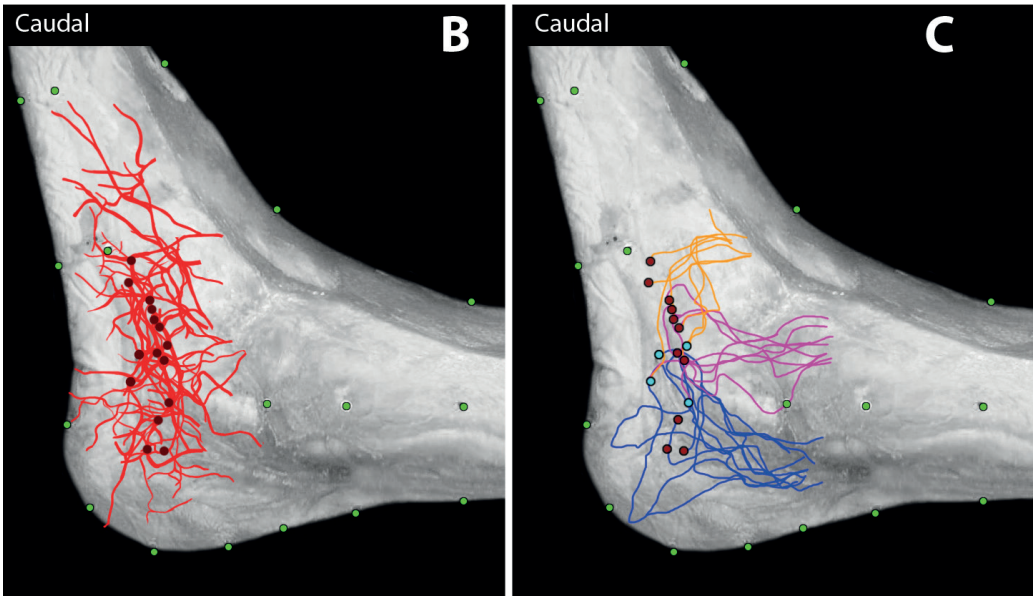

Figure 3B-C. Medial calcaneal branch of the posterior tibial artery
B: Terminal branches, highlighting the probable arterial supply area for the medial calcaneal branch. C: Blue dots: medial calcaneal branch, when only one branch is present. Red dots: medial calcaneal branch when more than one branch is present. Blue lines: connecting arteries that run superficially to the posterior fibular artery. Purple lines: connecting arteries that run posterior to the peroneal tendons to connect with the anterior fibular artery. Orange lines: superficial arteries connecting with the tarsal artery.

If only one medial calcaneal branch is present, it is located just anterior to the lateral process of the calcaneal tuberosity and it runs a transverse course close to the "roof" of the calcaneal bone (Figure 3 C, blue dots). If more than one medial calcaneal branch is present, the perforators are located along the lower ridge of the calcaneal bone and also run a transverse course close to the bone (Figure 3 C, red dots). The perforators then always communicate with each other superficially.

In seven specimens either one of the medial calcaneal branches communicates with the anterior fibular artery. The interlaying artery runs a deep course just beneath the tendons of peroneus longus and brevis muscles, and pierces the cruciate ligament just anterior to the lateral malleolus before it connects with the anterior fibular artery (Figure 3 C, purple lines). In seven specimens the medial calcaneal branch communicates with the posterior fibular artery through the superficial arteries running subcutaneous between the peroneal tendons and Achilles tendon (Figure 3 C, blue lines). In five specimens, either one of the medial calcaneal branches communicates superficially with the arteria tarsalis

or the arteria arcuata (both continuations of the arteria dorsalis pedis). The interlaying artery always runs a subcutaneous course posterior and proximal to the tuberosity of fifth the metatarsal (Figure 3 C, orange lines).

Fibular artery

In all but one specimen the fibular artery (FA) consists of two main branches. The posterior branch is always present and dominant. Its proximal course is deep and posterior to the fibula whilst at the level of the lateral malleolus it runs closer to the Achilles tendon. At this level horizontal anastomoses to the PTA exist that run a course flush on the Achilles tendon. The posterior branch has no clear branching pattern but in four specimens a distinct calcaneal branch is identified that runs a course close to the calcaneus in the direction of the outermost part of the heel. The anterior branch runs a very superficial course just anterior to the fibula. On average two anastomoses between the anterior and posterior branch exist located over or just caudal to the lateral malleolus. The fibular arterial system connects to the anterior tibial artery (ATA) in all 10 specimens (Figure 4 A, purple and orange dots). In specimens in which no anterior branch of the fibular artery was present, the anterior tibial artery consists of two instead of one branch and there are two connections between the fibular artery and the ATA located caudal to the lateral malleolus (Figure 4 A, orange dots).

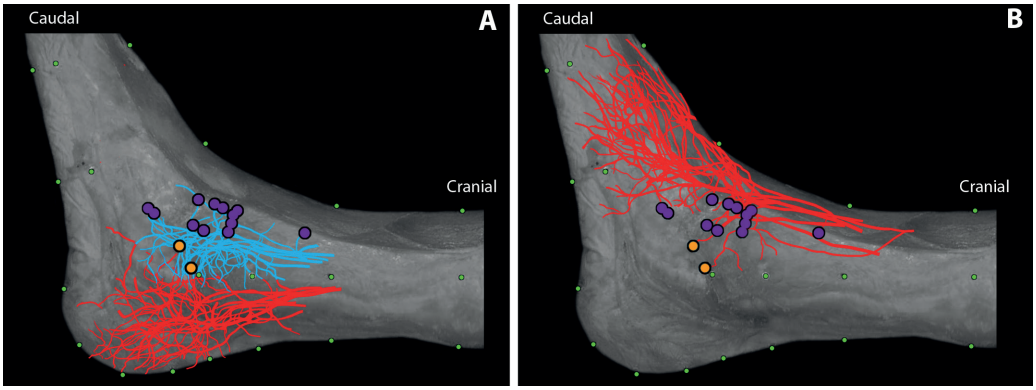

Figure 4. Fibular artery and anterior tibial artery
A: Fibular artery. Red: posterior branch. Blue: anterior branch. Purple dots: connections between the anterior branch and the ATA. Orange dots: connections between the posterior branch and the ATA (both in one specimen).
B: Anterior tibial artery. (a. dorsalis pedis).

Anterior tibial artery

The branches of the ATA mainly supply the dorsolateral side of the foot and the soft tissues caudal to the head of the fifth metatarsal (Figure 4 B). The ATA is the dominant branch and always runs a course anterior to the tibia. Most of the arterial branches are located deep to the extensor tendons, giving off multiple perforating superficial branches. Connections with the fibular artery are generally situated deep, close to the bone, whilst connections with the MCBPTA are found superficially, in the subcutaneous fat.

In one specimen in which the anterior branch of the fibular artery was not present, the ATA consists of two main branches of which one runs a course perpendicular to the fibula supplying the soft tissue caudal and anterior to the lateral malleolus, thus completely taking over the area of distribution of the anterior branch of the fibular artery.

Watershed area of the lateral foot

The areas of distribution between all three supplying arteries showed much overlap. Especially in the area inferior-anterior to the lateral malleolus many connections between either three of the supplying arteries exist. In previous classical texts such an area is suggested to be a watershed area, in which surgical approaches should be avoided as bloodflow, and thus optimal wound healing, cannot be guaranteed. In the present study, in which meticulous and specific dissection and mapping techniques were used, the anatomical data suggests that in fact no real or full watershed area exists. Instead a system of multiple small and sometimes deeply situated branches exists through which a patent blood flow can be guaranteed in case of damage to other branches of this system. In other words: a complex system of anastomoses exists which can compensate for (surgical) trauma if constituent main branches are spared.

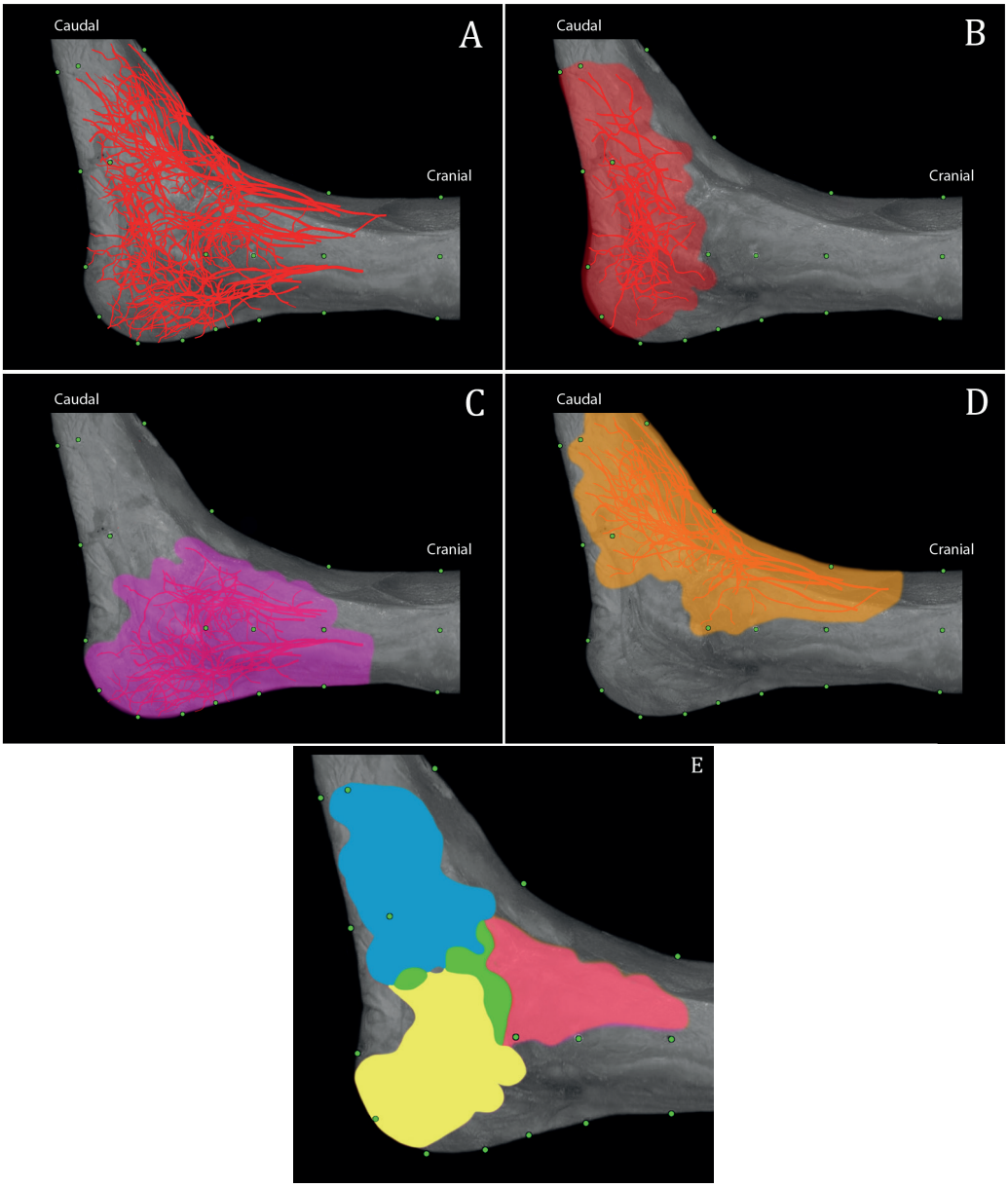

Figure 5. Angiosomes of the lateral foot
A: Dissected arteries (N=10) up to 1mm. B: Medial calcaneal artery of the posterior tibial artery. C: Fibular artery. D: Anterior tibial artery. E: Approximation of the watershed areas of the lateral hindfoot. Pink area: between ATA and fibular artery. Yellow area: between MCBPTA and the fibular artery. Blue area: between MCBPTA and the ATA. Green area: overlap between the angiosomes of all three arteries.

DISCUSSION AND CLINICAL IMPLICATIONS

Iatrogenic injury to branches of the neural and arterial structures of the lateral ankle is common. A detailed description of the relative course of these structures is important to redefine clinical guidelines and minimize the risk of iatrogenic damage.

Both the main trunk of the sural nerve as well as its two main branches, the calcaneal branch and the dorsal branch, show a relatively predictable course and distribution pattern. Our findings, although much more detailed and visualized in an average specimen, are in accordance to previous reports on sural nerve anatomy[5,19]. Although this study revealed that the exact location of arteries in the lateral hindfoot showed much variation, the general irrigation zones (angiosomes) and the anatomy of the three main supplying arteries are more or less uniform. The concept of angiosomes, dividing the body into three-dimensional blocks of tissue supplied by specific arterio-venous roots, has first been described by Taylor et al[20]. Attinger et al.[21,22] further developed this concept in relation to treatment algorithms for the diabetic foot and lower extremity artherosceloritic disease. In essence each angiosome is irrigated via one main arterio-venous bundle that perforates various anatomical layers and has tangential connections to neighbouring angiosomes either via reduced caliber "choke vessels" or normal sized true anastomoses.

In contrast to previous reports[20,21,22] this study shows that the role of subcalcaneal perforators of the PTA (MCBPA`s) are important for adequate perfusion of the lateral hindfoot. Previously described watershed areas (areas located between the angiosomes in which mostly small caliber "choke vessels" are located) proved to be located differently mainly because the MCBPA was not integrated in these models. Extensive surgical procedures through incisions in formerly defined watershed areas are prone for complications such as wound dehiscence, infection and necrosis. These incisions should be avoided as the vascular blood supply is easily compromised. Conversely, in the center of all three watershed areas, the area anterior and inferior to the lateral malleolus, our study identified a zone which is perfused by all three main supplying arteries in nine of the ten dissected specimens. Incisions in this area might be less prone to soft-tissue complications since soft tissues have multiple good caliber alternatives of perfusion.

Our anatomical observations can be applied to several standard surgical approaches to the laterale side of the ankle and hindfoot.

Extended lateral approach of the calcaneus (ELAC)

The classic exposure of the calcaneus is the angulated incision from the base of the 5th metatarsal, running parallel to the sole of the foot to the dorsal end of the calcaneus and sharply turning 80-90 degrees cranially. Depending on the exact location of the vertical part of the incision the sural nerve might be at risk[4,8,23,24], especially since skin and subcutis are mobilized as a thick soft-tissue flap in ELAC[23,25]. Sural nerve damage is seen in up to 10% of patients and an iatrogenic sural nerve lesion can lead to invalidating pain[8,9].

When an incision is drawn exactly conform the gold standard (Figure 6 A), the main branch of the sural nerve is at risk of transection in 10% of the dissected specimens. An incision line with the vertical limb running slightly posterior towards the Achilles tendon, as described by Eastwood and Atkins et al.[23], can reduce the risk of such iatrogenic sural nerve damage[5].

Especially in more extended approaches of the hindfoot complications such as necrosis are associated with the localization of the skin incision. Due to the high energetic etiology of calcaneal fractures, soft tissue is already damaged and extensively bruised and any further iatrogenic damage to arteries results in the high necrosis rates reported after calcaneal surgery. The PTA perforators are not only at a high risk for transection during the initial incision for an extended lateral approach, but especially when the full/thickness skin flap is dissected as the perforators run perpendicular to the dissection plane. Furthermore, since the perforators run almost flush to the roof of the calcaneus they are prone for injury during the initial trauma or osteosyntheses using the lateral side of the calcaneus. Figure 6 (B-D) shows an ELAC: Damage to MCBPTA`s and FA will compromise the arterial blood supply to the lateral calcaneus invariably (orange area in Figure 6 E). As a consequence the only remaining arterial inflow is through the very small arteries in subcutaneous tissue of the heel (Figure 6 D and E). In fresh calcaneus fractures flow in these subcutaneous arteries can be seriously compromised due to extensive swelling and soft tissue damage as a result of the high impact trauma and will be further compromised by a surgical exposure of the calcaneus. This study shows that it is beneficial to have the incision for an ELAC as close to the sole of the foot as possible to avoid damage to the MCBPTA`s (both during incision and dissection of the full-thickness flap) and to keep the subcutaneous flow to the heel as short as possible. Since no anastomoses exist anymore, postoperative pressure to the sole of the foot and heel should be avoided and swelling should be reduced as much as possible to prevent additional ischemia.

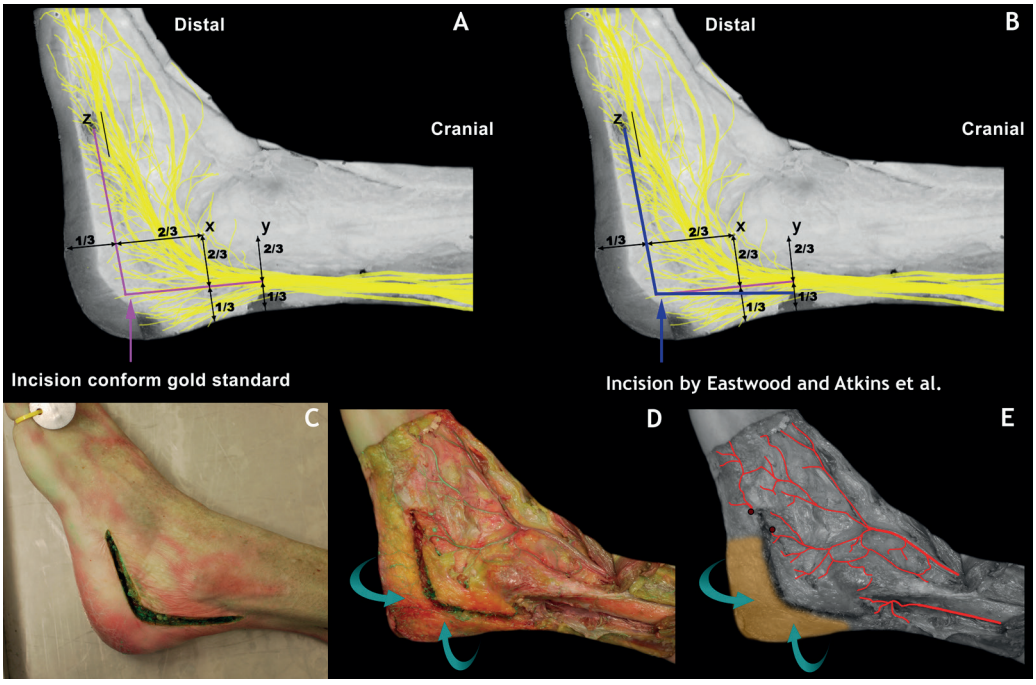

Figure 6. Gold standard Extended Lateral Approach of the Calcaneus (ELAC)
A) X: distal tip lateral malleolus. Y: top of lateral malleolus Z: tuberosity of the 5th metatarsal. Purple line: ELAC conform gold standard.
B) Blue line: an incision as described by Eastwood and Atkins et al. will reduce main branch sural nerve damage since the angle of the proximal incision is aimed at eh posterior Achilles tendon and the average angle between the proximal and distal incision is 120 degrees (instead of the conventional 80-90 degrees).
C), D) and E) Especially ELAC incisions that are placed further away from the sole of the foot will have a higher risk to damage the MCBPTA`s and FA, which further compromises the arterial blood supply to the lateral calcaneus (colored area in figure C) and consequently the only remaining arterial inflow is through the very small arteries in the subcutaneous tissue of the heel and sole of the foot (turquoise arrows in fig D and E).

Sinus tarsi approach (STA)

The sinus tarsi approach has recently gained popularity in calcaneus surgery since it provides a good surgical exposure and is more tissue sparing. Results of STA have shown to be similar or favorable when compared to the gold-standard and soft-tissue related complication rates after STA are lower when compared to ELAC and range from 0-15%[26]. In STA the dorsal branch of the SN, which is present in 40% of the specimen, needs to be transected (Figure 2 C). This may in theory lead to more neuroma formation in a generally sensitive area (the instep of the foot). The main branch of the SN should not be at risk in STA as long as the proximal incision starts just inferior from the distal tip of the malleolus and

then runs towards a point approximately 15 mm cranial to the tuberosity of the fifth metatarsal bone. The major part of the STA is located in a watershed area, in which is traditionally incisions should not be located. However this area of the lateral hindfoot is perfused by all three major supplying lower leg arteries (Figure 5.E, green area): PTA, ATA and FA in nine of the ten dissected specimens. The high amount of choke vessels in this area gives plenty of opportunity for alternative arterial perfusion of the soft tissues after surgery and might therefore contribute to lower rates of soft-tissue complications.

Minimally invasive longitudinal approach (MILA)

Zhang et al. first described MILA, a longitudinal incision located at the posterior calcaneus. First results of this approach of calcaneal fractures of Sanders type II and III show lower soft tissue related complication rates when compared to STA[27]. Besides the minimal invasive nature of this approach the low complication rates can be explained using the data of this anatomical study. The largest part of the incision is located outside of the posterior watershed area and the incision line runs perpendicular to branches of the FA. The posterior skin is perfused by anastomoses located just deep to the Achilles tendon and the superficial "choke vessels" are not those of the foot sole and therefore not injured by the initial trauma.

Other approaches

Ankle arthroscopy is frequently performed through stab incisions not exceeding 1 cm in length. The sural nerve is at risk of iatrogenic damage from such a stab incison to create the posterolateral portal. Damage to the main branch of the SN can be avoided if the skin is incised close to the Achilles tendon and immediately a deep course towards the postero-lateral ankle is followed. Damage to the calcaneal branch of the SN cannot be reduced by changing the incision location. However, a blunt dissection through a slightly larger incision can easily reduce the risk of damaging this branch. In the lateral approach to the 5th metatarsal an incision inferior to the MT5 (closer to the sole of the foot) minimizes the risk of damaging the main branch of the SN and avoid any chance of damaging the dorsal branches of the SN. A dorsolateral approach to the cuboid should follow the same guidelines as a sinus tarsi approach to the calcaneus; An incision on a virtual line between the inferior tip of the lateral malleolus to a point 15 mm dorsal to the tuberosity of the fifth metatarsal, can avoid damage to the main branch of the sural nerve. The dorsal branch of the SN, if present, will likely be damaged by a dorsolateral approach of the cuboid.

CONCLUSION

The neurovascular anatomy of the lateral hindfoot is relatively predictable and common soft tissue complications due to iatrogenic neurovascular damage following ankle and calcaneal surgery can be further minimized by using personalized ‘tailor made’ incisions, choosing the most fitting approach for each patient.

REFERENCES

1) Kerver AL, Leliveld MS, den Hartog D, Verhofstad MH, Kleinrensink GJ. The surgical anatomy of the infrapatellar branch of the saphenous nerve in relation to incisions for anteromedial knee surgery. J Bone Joint Surg Am. 2013 Dec 4;95(23):2119-25. doi: 10.2106/JBJS.L.01297. Review. PubMed PMID: 24306699.
2) Balcı Hİ, Polat G, Dikmen G, Atalar A, Kapıcıoğlu M, Aşık M. Safety of posterior ankle arthroscopy portals in different ankle positions: a cadaveric study. Knee Surg Sports Traumatol Arthrosc. 2016 Jul;24(7):2119-23. doi: 10.1007/s00167-014-3475-6. Epub 2014 Dec 13. PubMed PMID: 25502830.
3) Bai L, Han YN, Zhang WT, Huang W, Zhang HL. Natural history of sensory nerve recovery after cutaneous nerve injury following foot and ankle surgery. Neural Regen Res. 2015 Jan;10(1):99-103. doi: 10.4103/1673-5374.150713. PubMed PMID: 25788928; PubMed Central PMCID: PMC4357126.
4) Sanders R, Fortin P, DiPasquale T, Walling A. Operative treatment in 120 displaced intraarticular calcaneal fractures. Results using a prognostic computed tomography scan classification. Clin Orthop Relat Res. 1993 May;(290):87-95. PubMed PMID: 8472475.
5) Eastwood DM, Irgau I, Atkins RM. The distal course of the sural nerve and its significance for incisions around the lateral hindfoot. Foot Ankle. 1992 May;13(4):199-202. PubMed PMID: 1634152.
6) Baumhauer JF, O'Brien T. Surgical Considerations in the Treatment of Ankle Instability. J Athl Train. 2002 Dec;37(4):458-462. PubMed PMID: 12937567; PubMed Central PMCID: PMC164377.
7) Jowett AJ, Sheikh FT, Carare RO, Goodwin MI. Location of the sural nerve during posterolateral approach to the ankle. Foot Ankle Int. 2010 Oct;31(10):880-3. doi: 10.3113/FAI.2010.0880. PubMed PMID: 20964966.
8) Harvey EJ, Grujic L, Early JS, Benirschke SK, Sangeorzan BJ. Morbidity associated with ORIF of intra-articular calcaneus fractures using a lateral approach. Foot Ankle Int. 2001 Nov;22(11):868-73. PubMed PMID: 11722137.
9) Ebskov L, Rasmussen PB, Erichsen M. [Isolated lesions to the sural nerve. Causes, claims review procedure and compensation]. Ugeskr Laeger. 2008 Sep 8;170(37):2885-7. Danish. PubMed PMID: 18796285.
10) Rammelt S, Amlang M, Barthel S, Zwipp H. Minimally-invasive treatment of calcaneal fractures. Injury. 2004 Sep;35 Suppl 2:SB55-63. Review. PubMed PMID: 15315879.
11) Zwipp H, Rammelt S, Barthel S. Calcaneal fractures--open reduction and internal fixation (ORIF). Injury. 2004 Sep;35 Suppl 2:SB46-54. PubMed PMID: 15315878.
12) Folk JW, Starr AJ, Early JS. Early wound complications of operative treatment of calcaneus fractures: analysis of 190 fractures. J Orthop Trauma. 1999 Jun-Jul;13(5):369-72. PubMed PMID: 10406705.
13) http://www.anubifix.com/?action=pagina&id=310&title=Over%20AnubiFIX
14) http://www.anubifix.com/?id=311&id2=35
15) Kerver AL, Leliveld MS, den Hartog D, Verhofstad MH, Kleinrensink GJ. The surgical anatomy of the infrapatellar branch of the saphenous nerve in relation to incisions for anteromedial knee surgery. J Bone Joint Surg Am. 2013 Dec 4;95(23):2119-25. doi: 10.2106/JBJS.L.01297. Review. PubMed PMID: 24306699.
16) Kerver AL, Carati L, Eilers PH, Langezaal AC, Kleinrensink GJ, Walbeehm ET. An anatomical study of the ECRL and ECRB: feasibility of developing a preoperative test for evaluating the strength of the individual wrist

extensors. J Plast Reconstr Aesthet Surg. 2013 Apr;66(4):543-50. doi: 10.1016/j.bjps.2012.12.015. Epub 2013 Jan 29. PubMed PMID: 23369737.

17) EffectMatrix Software Studio. Magic Morph 1.95. "http://www.effectmatrix.com/morphing/".

18) Adobe Corp. Adobe Photoshop CS-4. 40) "http://www.adobe.com/nl/products/photoshop/photoshop/".

19) Geng X, Xu J, Ma X, Wang X, Huang J, Zhang C, Wang C, Muhammad H. Anatomy of the sural nerve with an emphasis on the incision for medial displacement calcaneal osteotomy. J Foot Ankle Surg. 2015 May-Jun;54(3):341-4. doi: 10.1053/j.jfas.2014.07.008. Epub 2014 Sep 8. PubMed PMID: 25201235.

20) Taylor GI, Palmer JH. The vascular territories (angiosomes) of the body: experimental study and clinical applications. Br J Plast Surg. 1987 Mar;40(2):113-41. PubMed PMID: 3567445.

21) Attinger CE, Evans KK, Bulan E, Blume P, Cooper P. Angiosomes of the foot and ankle and clinical implications for limb salvage: reconstruction, incisions, and revascularization. Plast Reconstr Surg. 2006 Jun;117(7 Suppl):261S-293S. Review. PubMed PMID: 16799395.

22) Taylor GI, Pan WR. Angiosomes of the leg: anatomic study and clinical implications. Plast Reconstr Surg. 1998 Sep;102(3):599-616; discussion 617-8. PubMed PMID: 9727424.

23) Eastwood DM, Langkamer VG, Atkins RM. Intra-articular fractures of the calcaneum. Part II: Open reduction and internal fixation by the extended lateral transcalcaneal approach. J Bone Joint Surg Br. 1993 Mar;75(2):189-95. PubMed PMID: 8444935.

24) Paley D, Hall H. Intra-articular fractures of the calcaneus. A critical analysis of results and prognostic factors. J Bone Joint Surg Am. 1993 Mar;75(3):342-54. PubMed PMID: 8444912.

25) Ishikawa K, Kyutoku S, Takeuchi E. Free lateral calcaneal flap. Ann Plast Surg. 1993 Feb;30(2):167-70. PubMed PMID: 8489183.

26) Schepers T. The sinus tarsi approach in displaced intra-articular calcaneal fractures: a systematic review. Int Orthop. 2011 May;35(5):697-703. doi: 10.1007/s00264-011-1223-9. Epub 2011 Feb 19. Review. PubMed PMID: 21336854; PubMed Central PMCID: PMC3080500.

27) Zhang T, Su Y, Chen W, Zhang Q, Wu Z, Zhang Y. Displaced intra-articular calcaneal fractures treated in a minimally invasive fashion: longitudinal approach versus sinus tarsi approach. J Bone Joint Surg Am. 2014 Feb 19;96(4):302-9. doi: 10.2106/JBJS.L.01215. PubMed PMID: 24553886.

01000011 01101000 01100001 01110000
01110100 01100101 01110010 00100000
00110010 00101110 00110100 00001010

Chapter 2.4

The surgical anatomy of the infrapatellar branch of the saphenous nerve in relation to incisions for anteromedial knee surgery.

Kerver ALA, Levliveld MS, den Hartog D, Verhofstad MH, Kleinrensink GJ.

J.Bone Joint Surg. Am. 2013 Dec 4.

ABSTRACT

Background: Iatrogenic injury to the infrapatellar branch of the saphenous nerve is a common complication of surgical approaches to the anteromedial side of the knee. A detailed description of the relative anatomic course of the nerve is important to define clinical guidelines and minimize iatrogenic damage during anterior knee surgery.

Methods: In twenty embalmed knees, the infrapatellar branch of the saphenous nerve was dissected. With use of a computer-assisted surgical anatomy mapping tool, safe and risk zones, as well as the location-dependent direction of the nerve, were calculated.

Results: The location of the infrapatellar branch of the saphenous nerve is highly variable, and no definite safe zone could be identified. The infrapatellar branch runs in neither a purely horizontal nor a vertical course. The course of the branch is location-dependent. Medially, it runs a nearly vertical course; medial to the patellar tendon, it has a –45° distal-lateral course; and on the patella and patellar tendon, it runs a close to horizontal-lateral course. Three low risk zones for iatrogenic nerve injury were identified: one is on the medial side of the knee, at the level of the tibial tuberosity, where a –45° oblique incision is least prone to damage the nerves, and two zones are located medial to the patellar apex (cranial and caudal), where close to horizontal incisions are least prone to damage the nerves.

Conclusions: The infrapatellar branch of the saphenous nerve is at risk for iatrogenic damage in anteromedial knee surgery, especially when longitudinal incisions are made. There are three low risk zones for a safer anterior approach to the knee. The direction of the infrapatellar branch of the saphenous nerve is location-dependent. To minimize iatrogenic damage to the nerve, the direction of incisions should be parallel to the direction of the nerve when technically possible.

Clinical Relevance: These findings suggest that iatrogenic damage of the infrapatellar branch of the saphenous nerve can be minimized in anteromedial knee surgery when both the location and the location-dependent direction of the nerve are considered when making the skin incision.

INTRODUCTION

The infrapatellar branch of the saphenous nerve is a sensory nerve innervating the anterior aspect of the knee, the anterolateral aspect of the proximal part of the lower leg, and the anteroinferior part of the knee joint capsule[1,2]. The infrapatellar branch of the saphenous nerve originates from the saphenous nerve and arizses distal to the adductor canal[3]. It pierces the sartorius muscle, after which it runs a superficial course and generally forms two branches[4,5]. Both branches cross the patellar tendon in a transverse way to form the infrapatellar plexus[1,6]. These small superficial branches are at risk for transection, especially when longitudinal surgical incisions are made.

Injury to the infrapatellar branch of the saphenous nerve usually results in numbness on the anterior aspect of the knee and the proximal lateral part of the lower leg. Neuropathic pain and symptomatic neuroma can develop even without noxious stimuli[7,8]. A relationship between damage to the infrapatellar branch of

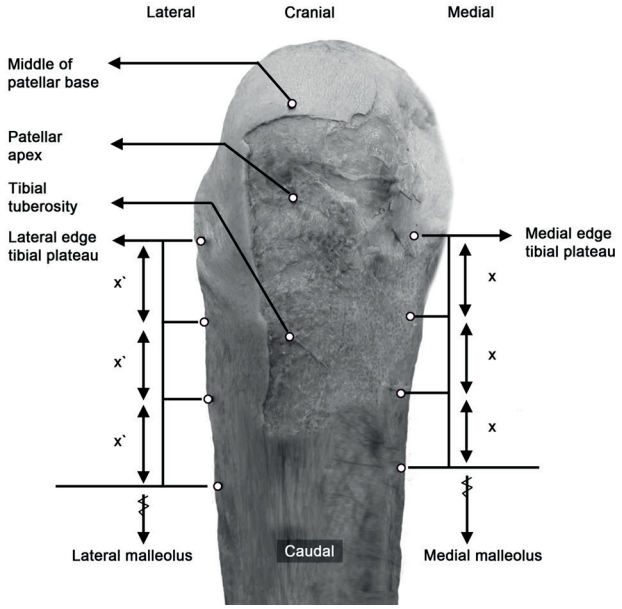

Figure 1. Anatomical landmarks. Osseous landmarks include the patellar apex, the highest, most prominent palpable point of the tibial tuberosity; the medial and lateral edge of the tibial plateau; and the medial and lateral malleoli. Nonosseous landmarks are placed at one-tenth of the distance between the tibial plateau and both the medial (X) and lateral (X`) malleoli. The cranial three landmarks on the medial and lateral side are used for CASAM (computer-assisted surgical anatomy mapping) calculations. Test-retest reproducibility of all landmarks was determined by two authors.

the saphenous nerve and reflex sympathetic dystrophy has been described[9-11]. Finally, as the infrapatellar branch of the saphenous nerve innervates the anterior medial ligaments of the knee, it is important for proprioception[12] and thus knee stability and balance. Impaired joint proprioception might in theory contribute toward osteoarthritis[13-15].

After total knee arthroplasty, numbness due to damage of the infrapatellar branch of the saphenous nerve has been reported in 55% to 100% of patients when a longitudinal incision was used[16,17]. Ojima et al. found significantly fewer subjectively and objectively assessed areas of hypoesthesia when a transverse incision was used. Furthermore, they found significantly more patients who were able to kneel and stated this might partially be due to less pain and numbness as the infrapatellar nerve remained intact[18].

Damage to the infrapatellar branch of the saphenous nerve has also been reported after surgical meniscectomy (up to 28% of patients report irritating paresthesia[19]), in arthroscopy[6,9,20], after anterior cruciate ligament reconstruction (anesthesia was found in 37% to 86% of patients[21,22]), and even in resections of the prepatellar bursa[23,24]. Although damage to the infrapatellar nerve in tibial nailing has been mentioned by only a few authors[25,26], it can be a causative factor for chronic anterior knee pain[27-29] and a frequent and invalidating complication in tibial nailing (10% to 86%)[30,31] and retrograde femoral nailing (26%)[25].

The clinical importance of damage to the infrapatellar branch of the saphenous nerve is amplified by the fact that recent studies on arthroplasty[32] and tibial nailing[29] have shown that patient satisfaction is inversely correlated to the presence of injury to the infrapatellar nerve.

Although the infrapatellar branch of the saphenous nerve is a known anatomic structure, its relevance in daily clinical practice is underestimated as of yet, since longitudinal incisions in the anteromedial region of the knee are still commonly used. Therefore, the purpose of this study was to further describe and visualize the relative anatomic course of the infrapatellar branch of the saphenous nerve in the flexed knee to provide the surgeon with a safe zone and clinical guidelines to minimize iatrogenic injury during anterior knee surgery.

METHODS

Materials

Twenty unpaired embalmed legs (ten left and ten right) from adult donors were dissected in the knee region to study the course of the infrapatellar branch of the saphenous nerve. The specimens had been flushed with AnubiFiX[33]

(Department of Neuroscience and Anatomy, Erasmus MC, University Medical Center Rotterdam, Rotterdam, The Netherlands) to regain joint flexibility and were embalmed with a mixture of 6% formaldehyde and 5% phenol. None of the limbs showed macroscopic signs of disease or scarring. The saphenous nerve and the main infrapatellar branch(es) of the nerve were localized by careful dissection and followed peripherally with a magnifying glass (5 dioptre) until branches were too small for further dissection (<1 mm). All knees were then flexed into a 90° angle, simulating the intraoperative position for most anteromedial knee surgical procedures. Osseous landmarks (Figure 1) were placed as a reference for measurements and calculations.

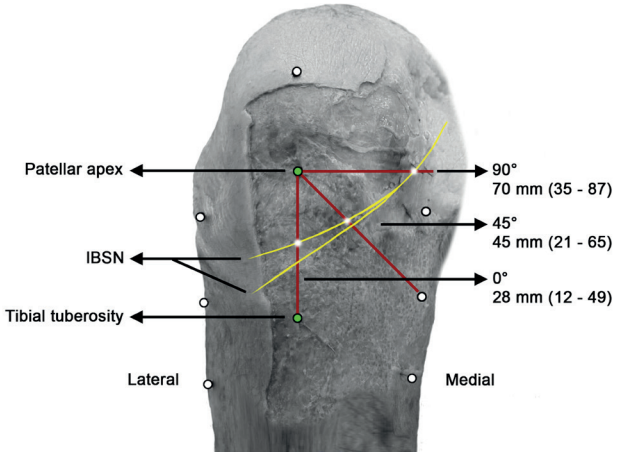

Figure 2. Measurements of the distance to the closest infrapatellar branch of the saphenous nerve (IBSN) over three reference lines are shown. The mean distance was 70 mm (range, 35 to 87 mm) over the 90° reference line, 45 mm (range, 21 to 65 mm) over the 45° reference line, and 28 mm (range, 12 to 49 mm) over the 0° reference line.

Measurements

The distance between the apex of the patella and the tibial tuberosity (the most distal part of the patellar apex and the palpatory center of the tuberosity) was measured. From the apex of the patella, three reference lines (at 90°, 45°, and 0° relative to the line between the apex of the patella and the tibial tuberosity) were projected over the knees for distance measurements to the closest branch of the infrapatellar nerve (Figure 2). At the intersection of an infrapatellar branch of the nerve with the projected lines, a pin was placed and the distance to the patellar apex was measured along the circumference of the limb. The position of the nerve was also related to the distance between the apex of the patella and the

tibial tuberosity. When the nerve was split into two or more branches, the closest branch to the reference point was used for calculations.

The angle of the nerve related to the midline of the patellar tendon was measured. When more than one branch crossed the patellar tendon, the angles were also noted.

Distances were measured using calipers, and angles were measured using a goniometer. Measurements were repeated, and the mean of both measurements was used for further analysis. Statistical tests were performed using SPSS software (version 17; SPSS, Chicago, Illinois). Nonparametrical tests were used if variables were not normally distributed.

Computer-Assisted Surgical Anatomy Mapping (CASAM)

The novel anatomy-mapping tool CASAM[34-37] was used to visualize and evaluate the complex and variable anatomy of multiple specimens and to visualize the dissected infrapatellar branch of the saphenous nerve in one image of a knee with average dimensions. First, the knees were photographed, using a standardized protocol, with a Canon 350D camera (Canon USA, Lake Success, New York) with a Canon EF-S 18-55-mm lens (Canon USA). Then, nonosseous landmarks were calculated from osseous landmarks to delineate the different shapes of the individual knees (Figure 1).

The average location of each landmark was calculated from all specimens. Then, with use of Magic Morph 1.9510 software (EffectMatrix Software Studio)[38], each specimen in each original photograph was reshaped (warped) to match the calculated average shape. A thin plate spline was used as a warping algorithm. As the warped specimens had the same calculated average shape, the anatomy of the infrapatellar branch of the saphenous nerve of all specimens could be mapped and visualized in one averagely shaped knee. Photoshop CS4 (Adobe Systems, San Jose, California)[39] was used to highlight relevant anatomy and make renditions. The following four renditions were made:

1. All dissected infrapatellar branches of the saphenous nerve were visualized in one image (Figures 3-A).
2. A risk zone of 5 mm was determined and colored in each specimen. All risk zones were then compiled into one image, and a gradient of risk zones was visualized (Figure 3-B).
3. Zones were identified in the anteromedial aspect of the knee in which a low density of infrapatellar branches of the saphenous nerve was found (Figure 4).

4. A grid of squares was placed over the computerized image depicting all infrapatellar branches of the saphenous nerve (Figure 3). Within each individual square, the direction of all branches was measured in relation to a horizontal line. Each square was given a color corresponding to the average direction of the branches within that square. The result is a grid of squares depicting the location-dependent direction of infrapatellar branches of the saphenous nerve (Figure 5).

Comparison with Published Literature

A PubMed/MEDLINE search was performed using the search terms "infrapatellar branch of the saphenous nerve" OR "infrapatellar branches of the saphenous nerve." This search revealed forty-nine titles. Abstracts were judged for relevance. In case of doubt, full articles were read and checked for cross-references. Three anatomical studies on the course of the infrapatellar branch of

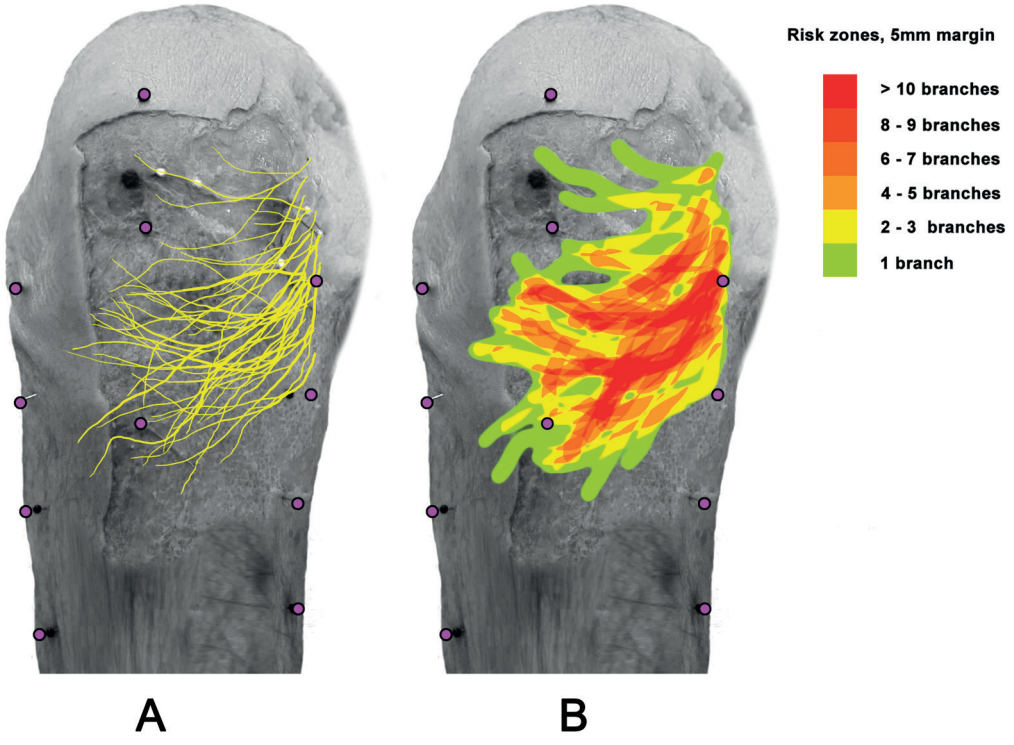

Figure 3. The location of the infrapatellar branch of the saphenous nerve with CASAM-generated photographs showing the anatomy of the infrapatellar branch of the saphenous nerve in a knee with average dimensions (n = 20). A Distribution of the infrapatellar branches. B A 5-mm margin around each dissected nerve.

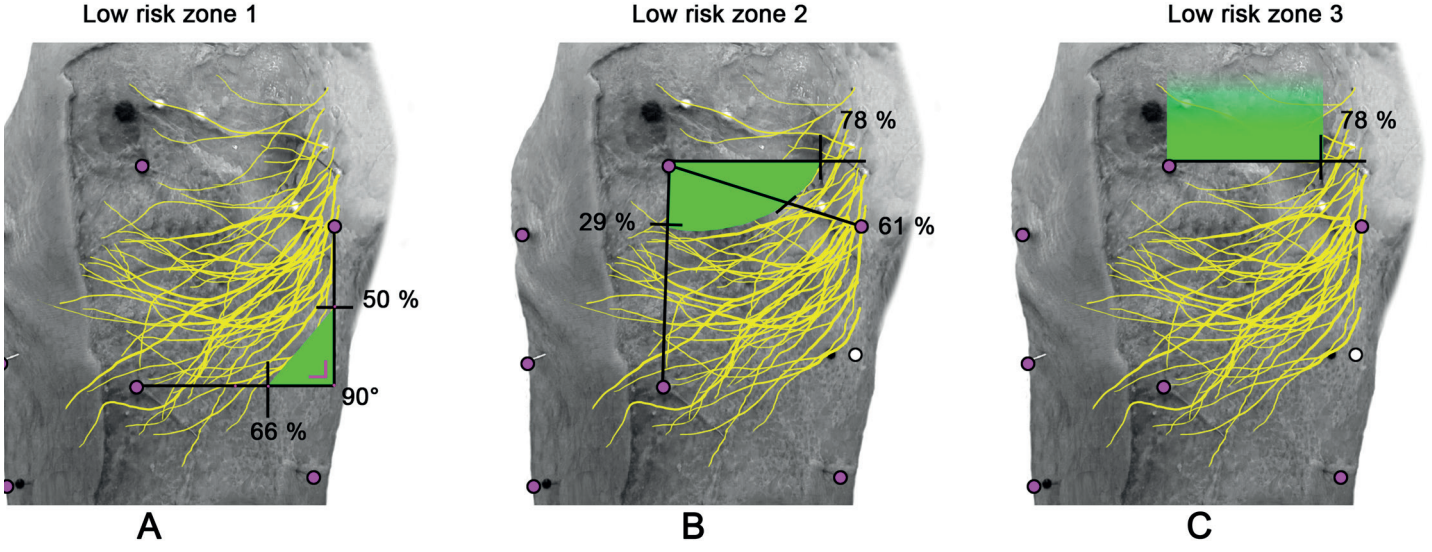

Figure 4.Suggested low risk zones.
A Low risk zone 1. A vertical line is projected downward from the medial edge of the tibial plateau and a horizontal line from the tibial tuberosity to the medial side of the knee. The zone is located distally from 50% of the vertical line and medially from 66% of the horizontal line.
B Low risk zone 2. The zone extends from the patellar apex up to 29% of the distance to the tibial tuberosity, up to 61% of the distance to the medial edge of the tibial plateau, and up to 78% of the distance to a projected vertical line from the medial edge of the tibial plateau.
C Low risk zone 3. Medially and cranially, the zone extends over a horizontally projected line to 78% of the distance between the patellar apex and the level of the medial edge of the tibial plateau.

the saphenous nerve were selected. The anatomic risk and/or safe zones described by Tifford et al[20] (twenty flexed fresh-frozen knees), Mochida and Kikuchi[6] (129 extended, embalmed knees), and Ebraheim and Mekhail[1] (twenty-eight flexed knees) were delineated in three new embalmed specimens. The knees were then photographed (flexed in 90°), and data were mapped with CASAM and compared with the location of the dissected infrapatellar branch of the saphenous nerve (Figures 3 and 6).

RESULTS

Topographic Anatomy

The median distance between the apex of the patella and the tibial tuberosity was 64 mm (range, 46 to 78 mm).

The infrapatellar branch of the saphenous nerve consisted of one branch in two specimens, of two branches in twelve specimens, and of three branches in six specimens. The distance between the apex of the patella and the points along the course of the uppermost infrapatellar branch of the saphenous nerve is demonstrated in Figure 2. In all twenty specimens, the infrapatellar branch of the saphenous nerve crossed the 90° reference line at a mean distance of 70 mm (range, 35 to 87 mm). In nineteen specimens, the infrapatellar branch crossed the 45° reference line at a mean distance of 45 mm (range, 21 to 65). In sixteen specimens, the infrapatellar branch crossed the 0° reference line at a mean distance of 28 mm (range, 12 to 49). There was no significant difference between left and right knees for these distances ($p = 0.256$, $p = 0.870$, and $p = 0.447$, respectively). Sixteen proximal branches cross the patellar tendon, and four of them are located on the proximal third; ten, on the middle third; and two, on the distal third of the patellar tendon.

A total of twenty-four branches (in sixteen knees) crossed the sagittal plane of the center of the patellar tendon. On average, these branches run a nearly horizontal course in a −4° downward-lateral direction (range, +28° upward-lateral direction and −58° downward-lateral direction). There was no significant difference between left and right knees for these angles ($p = 0.052$).

Computer-Assisted Surgical Anatomy Mapping

The dissected infrapatellar branches of the saphenous nerve of all twenty specimens were visualized in a knee with average dimensions (Figure 3-A). The location of the branches demonstrates much variation. The main trunks are located at the medial side of the knee, near the medial edge of the tibial plateau.

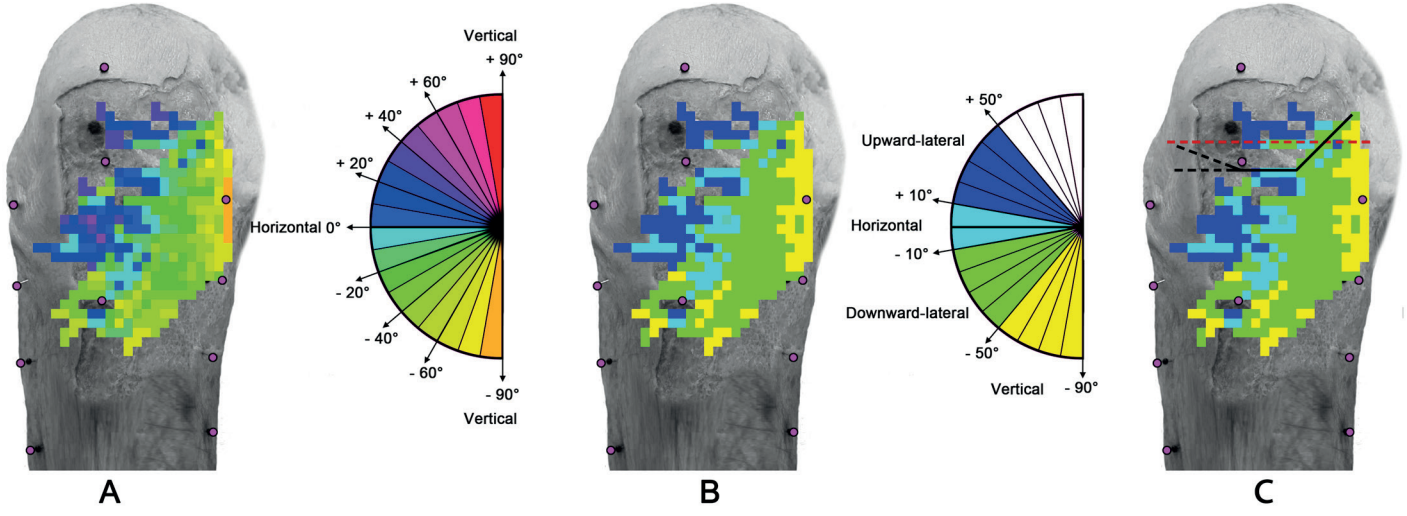

Figure 5. The location-dependent direction of the infrapatellar branch of the saphenous nerve.
A The location-dependent direction of the nerve, divided in 10° increments.
B The location-dependent direction of the nerve, divided in vertical (–90° to approximately –50°), downward-lateral (–50° to approximately –10°), horizontal (–10° to approximately +10°), and upward-lateral (+10° to approximately +50°) directions.
C The red dashed line indicates the transverse incision as proposed by Ojima et al.[18]: "A transverse incision was made at a 90° knee flexion at the level of the lower end of the patella, along the skin crease." The black line shows an adaptation to the incision line proposed by Ojima et al. To make the incision mostly run perpendicular to the infrapatellar branch of the saphenous nerve, the medial part runs in a 45° downward direction. The middle, horizontal part of this incision is located in safe zone 2. The lateral part either runs horizontally or in an upward 20° angle.

Branching mostly occurs on the medial side of the knee at a midpatellar tendon level. Branches then follow a more horizontal course toward the patellar tendon.

When the 5-mm margins around all twenty dissected infrapatellar branches of the saphenous nerve were combined, possible safe zones as well as risk zones (with a higher density of branches) could be identified (Figure 3-B). The location of infrapatellar branches of the saphenous nerve is extremely variable, and there is no definite or unique safe zone in which iatrogenic nerve damage can be prevented completely. However, there are three distinct areas with a low (or lower) density of infrapatellar branches of the saphenous nerve (Figure 4).

The first area is located on the medial side of the knee at the level of the tibial tuberosity (Figure 4-A). The boundaries are formed by a virtual vertical line downward from the medial edge of the tibial plateau and a horizontal line from the tibial tuberosity to the medial side of the knee. This zone is located distally from 50% of the vertical line and medially from 66% of the horizontal line.

The second zone is located medial and distal to the patellar apex (Figure 4-B). Distally, it extends to 29% of the distance between the patellar apex and the tibial tuberosity. Then it extends to 61% of the distance between the patellar apex and the medial edge of the tibial plateau. Medially, it extends over a horizontally projected line to 78% of the distance between the patellar apex and the level of the medial edge of the tibial plateau.

The third zone is located medial and proximal to the patellar apex (Figure 4-C). Medially, it extends over a horizontally projected line to 78% of the distance between the patellar apex and the level of the medial edge of the tibial plateau.

The location-dependent direction of the infrapatellar branches of the saphenous nerve is shown in Figure 5. At the medial edge of the knee, the main trunks of the infrapatellar branches of the saphenous nerve run a close to vertical course. Most branches then continue to follow a curved course, and medial to the patellar tendon, branches run, on average, in a distal-lateral direction. At the medial edge of the patellar tendon, the branches run a close to horizontal course. Then, over the patellar tendon, infrapatellar branches of the saphenous nerve curve to proximal and mostly run a proximal-lateral course. However, branches located near the tibial tuberosity do not run a curved course and continue to run in a distal-lateral direction. The average direction of the infrapatellar branches was −45° in low risk zone 1, −8° in low risk zone 2, and +8° in low risk zone 3 (Figure 4).

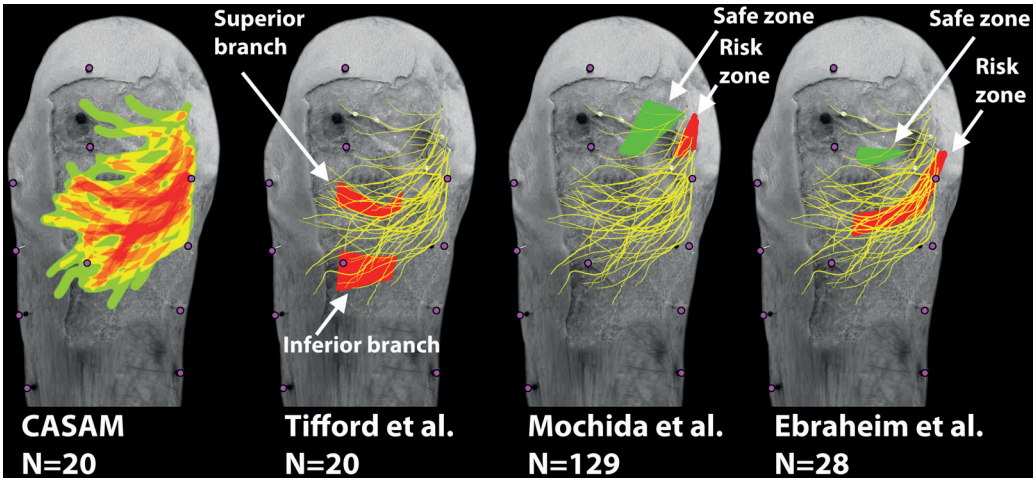

Figure 6. Comparison with reports in the literature. The first image of the infrapatellar branch of the saphenous nerve (left) was made with CASAM visualization and a 5-mm margin and shows the gradient of low risk and high risk zones. The second image shows the findings of Tifford et al.[20], with red indicating risk zones for both the superior and inferior branch of the nerve. The third image shows the findings in the study by Mochida and Kikuchi[6], with red indicating the risk zone and green, the safe zone. The fourth image (right) shows the findings of Ebraheim and Mekhail[1], with red indicating the risk zone and green, the safe zone.

Comparison with the Literature

Risk and/or safe zones described by Tifford et al.[20], Mochida and Kikuchi[6], and Ebraheim and Mekhail[1] are shown in Figure 6. The location of the superior branch of the infrapatellar nerve described by Tifford et al. corresponds well to the superior part of the high risk zone depicted in Figure 3-B. However, they found the inferior branch to be located more distal than most infrapatellar branches dissected in our study. The safe zones situated medial to the patella, as described by Mochida and Kikuchi and by Ebraheim and Mekhail, mostly overlap the low risk zones 2 and 3, described in Figure 4. The high risk zone that Mochida and Kikuchi described is located medial to our low risk zone 3 (Figure 4) and overlaps the most cranial medial part of the high risk zone described in Figure 3-B. The high risk zone described by Ebraheim and Mekhail overlaps most of the high risk zone depicted in Figure 3, but does not extend to the middle of the patellar tendon.

DISCUSSION

In accordance with previous anatomical studies[1,4,6], the present study shows that variation in the topographic anatomy of the infrapatellar branch of the

saphenous nerve is high. Therefore, no safe zones were defined, and the nerve is at risk for transection at the initial surgical incision.

However, three low risk zones were identified; in these zones, fewer infrapatellar branches of the saphenous nerve were located, and incorporation of these zones into daily clinical practice may reduce complications related to the nerve. Low risk zones 1 and 3 are relatively rare sites for anteromedial approaches of the knee. Zone 1, however, provides a safer entry site in open meniscectomy and tendon-harvesting. In addition, medial portal placement during arthroscopy might be possible via this area, but the technical feasibility needs further research as it is located distal to the conventional site. Low risk zone 2 can be used as an entry site for a prepatellar bursectomy. Similarly, low risk zones 2 and 3 provide for a safer approach in tibial nailing and retrograde nailing of the femur. In total knee arthroplasty, when the medial edges of low risk zones 2 and 3 are taken into account, the transverse approach described by Ojima et al.[18] may be even more beneficial regarding complications related to the infrapatellar branch of the saphenous nerve. Furthermore, when the location-dependent direction of the infrapatellar branch of the saphenous nerve is taken into account, a cranial deviation of the lateral and medial part of the incision, resulting in a horizontal "smile" incision just distal to the patella, might further reduce iatrogenic damage to the nerve as the incision then mostly runs perpendicular to the infrapatellar nerve (Figure 5-C). The proposed incision may be used, if technically feasible, in total knee arthroplasty. The medial and middle part of the proposed incision can be used in retrograde femoral nailing, tibial nailing, bursectomy, and unicompartmental arthroplasty.

The safe and risk zones described in Figures 3 and 4 correspond with reports in the literature[1,6,20], except for the location of the inferior branch as described by Tifford et al. Apart from the infrapatellar branch of the saphenous nerve, other superficial nerves such as the saphenous nerve, the sartorial branch of the saphenous nerve, the superficial femoral nerve, and the medial retinacular nerve were not dissected.

In accordance with the literature, we hypothesized that horizontal incisions lead to less iatrogenic damage and fewer subsequent postoperative complications than do longitudinal incisions[1,6,18,20,29,40]. Two recent studies have investigated the possibility of transverse or horizontal incisions for various surgical procedures on the anteromedial aspect of the knee[18,41]. A disadvantage of nonlongitudinal incisions in routine surgery on the anteromedial part of the knee is that subsequent total or partial knee replacement is mostly performed using a longitudinal incision, and the patient would have two perpendicular and crossing incisions. However,

Ojima et al. showed that total knee arthroplasty using a transverse incision is technically feasible[18]. Conversely, horizontal incisions cannot be extended and are limited in both length and direction. Therefore, when further exposure for additional surgery, such as quadricepsplasty, is needed, horizontal incisions might be restrictive. Also, the medial retinacular nerve and medial cutaneous femoral nerve[42] might be at risk for transection in a horizontal skin incision.

Since no clear safe zone is identified, the direction of the infrapatellar branches of the saphenous nerve becomes more important; incisions parallel to the nerves exert less risk of damage. Although multiple studies have suggested that horizontal incisions should be made in the anteromedial aspect of the knee, the infrapatellar branch only runs a horizontal course just medial to the patellar tendon. Anteromedially, the infrapatellar branch mostly runs in a downward-lateral angle of −30°, favoring oblique over horizontal incisions. At the medial border of the knee, the infrapatellar nerve, on average, runs a close to vertical course, and longitudinal incisions should be favored. However, in this area, there is a high risk of damage to the infrapatellar branch of the saphenous nerve. On the proximal two-thirds of the patellar tendon and on the patella, the infrapatellar branch mostly runs in an upward-lateral direction of +20°.

In low risk zone 1, the infrapatellar branch of the saphenous nerve runs in a −45° downward-lateral direction, and a parallel oblique incision would be optimal in this area. In low risk zones 2 and 3, a close to horizontal incision would minimize the risk of iatrogenic damage to the infrapatellar branch.

In contrast to previous anatomic studies, the complete course of the infrapatellar branch of the saphenous nerve over the anteromedial side of the knee was mapped and measured using CASAM and was also compared with reports in the current literature. Data gathered with CASAM can be made available via a web-based version, potentially allowing the surgeon to upload a photograph and/or radiographs of a patient. Then, the dissected infrapatellar branch of the saphenous nerve, low risk zones, and location-dependent direction can be displayed over the photograph of the patient's knee.

Conclusion

In conclusion, the infrapatellar branch of the saphenous nerve is at risk for iatrogenic damage in any surgery on the anteromedial aspect of the knee, especially when longitudinal incisions are used. Three low risk zones for iatrogenic nerve injury were identified: one is located on the medial side of the knee, at the level of the tibial tuberosity, in which a −45° oblique incision is least prone to damage the infrapatellar branch, and two zones are located medial to the

patellar apex (cranial and caudal), in both of which nearly horizontal incisions are least prone to damage the infrapatellar branch. To minimize iatrogenic damage to the infrapatellar branch of the saphenous nerve, the direction of incisions should be parallel to the direction of the nerve when technically possible.

ACKNOWLEDGMENTS

The authors thank A.R. Poublon, who contributed to this research. They also thank Yvonne Steinvoort and Berend-Jan Kompanje for embalming and looking after the specimens used in this study.

REFERENCES

1) Ebraheim NA, Mekhail AO. The infrapatellar branch of the saphenous nerve: an anatomic study. J Orthop Trauma. 1997;11(3):195-9.
2) Arthornthurasook A, Gaew-Im K. Study of the infrapatellar nerve. Am J Sports Med. 1988;16(1):57-9.
3) Netter FH. Atlas of the Human Anatomy. Book; Ciba-Geigy 1997. ISBN-10: 0914168819
4) Kartus J, Ejerhed L, Eriksson BI, Karlsson J. The localization of the infrapatellar nerves in the anterior knee region with special emphasis on central third patellar tendon harvest: a dissection study on cadaver and amputated specimens. Arthroscopy. 1999;15(6):577-86.
5) Ramasastry SS, Dick GO, Futrell JW. Anatomy of the saphenous nerve: relevance to saphenous vein stripping. Am Surg. 1987;53(5):274-7.
6) Mochida H, Kikuchi S. Injury to infrapatellar branch of saphenous nerve in arthroscopic knee surgery. Clin Orthop Relat Res. 1995;(320):88-94.
7) Dellon AL, Mont MA, Mullick T, Hungerford DS. Partial denervation for persistent neuroma pain around the knee. Clin Orthop Relat Res. 1996;(329):216-22.
8) Berg P, Mjöberg B. A lateral skin incision reduces peripatellar dysaesthesia after knee surgery. J Bone Joint Surg Br. 1991;73(3):374-6.
9) Poehling GG, Pollock FE Jr, Koman LA. Reflex sympathetic dystrophy of the knee after sensory nerve injury. Arthroscopy. 1988;4(1):31-5.
10) Cooper DE, DeLee JC, Ramamurthy S. Reflex sympathetic dystrophy of the knee. Treatment using continuous epidural anesthesia. J Bone Joint Surg Am. 1989;71(3):365-9.
11) Katz MM, Hungerford DS. Reflex sympathetic dystrophy affecting the knee. J Bone Joint Surg Br. 1987;69(5):797-803.
12) J ohnson DH, Pedowitz RA (Editors), Practical Orthopaedic Sports Medicine and Arthroscopy. Book; Lippincott Williams & Wilkins 2006. ISBN-10: 0781758122
13) Brandt KD. Neuromuscular aspects of osteoarthritis: a perspective. Novartis Found Symp. 2004;260:49-58; discussion 58-63, 100-4, 277-9.

14) Sharma L, Pai YC. Impaired proprioception and osteoarthritis. Curr Opin Rheumatol. 1997;9(3):253-8.
15) Barrett DS, Cobb AG, Bentley G. Joint proprioception in normal, osteoarthritic and replaced knees. J Bone Joint Surg Br. 1991;73(1):53-6.
16) Sundaram RO, Ramakrishnan M, Harvey RA, Parkinson RW. Comparison of scars and resulting hypoaesthesia between the medial parapatellar and midline skin incisions in total knee arthroplasty. Knee. 2007;14(5):375-8.
17) Borley NR, Edwards D, Villar RN. Lateral skin flap numbness after total knee arthroplasty. J Arthroplasty. 1995;10(1):13-4.
18) Ojima T, Yoshimura M, Katsuo S, Mizuno K, Yamakado K, Hayashi S, Tsuchiya H. Transverse incision advantages for total knee arthroplasty. J Orthop Sci. 2011;16(5):524-30.
19) Johnson RJ, Kettelkamp DB, Clark W, Leaverton P. Factors effecting late results after meniscectomy. J Bone Joint Surg Am. 1974;56(4):719-29.
20) Tifford CD, Spero L, Luke T, Plancher KD. The relationship of the infrapatellar branches of the saphenous nerve to arthroscopy portals and incisions for anterior cruciate ligament surgery. An anatomic study. Am J Sports Med. 2000;28(4):562-7.
21) Sgaglione NA, Warren RF, Wickiewicz TL, Gold DA, Panariello RA. Primary repair with semitendinosus tendon augmentation of acute anterior cruciate ligament injuries. Am J Sports Med. 1990;18(1):64-73.
22) Spicer DD, Blagg SE, Unwin AJ, Allum RL. Anterior knee symptoms after four-strand hamstring tendon anterior cruciate ligament reconstruction. Knee Surg Sports Traumatol Arthrosc. 2000;8(5):286-9.
23) Quayle JB, Robinson MP. An operation for chronic prepatellar bursitis. J Bone Joint Surg Br. 1976;58-B(4):504-6.
24) Ogilvie-Harris DJ, Gilbart M. Endoscopic bursal resection: the olecranon bursa and prepatellar bursa. Arthroscopy. 2000;16(3):249-53.
25) Lefaivre KA, Guy P, Chan H, Blachut PA. Long-term follow-up of tibial shaft fractures treated with intramedullary nailing. J Orthop Trauma. 2008;22(8):525-9.
26) Robinson CM, McLauchlan GJ, McLean IP, Court-Brown CM. Distal metaphyseal fractures of the tibia with minimal involvement of the ankle. Classification and treatment by locked intramedullary nailing. J Bone Joint Surg Br. 1995;77(5):781-7.
27) Katsoulis E, Court-Brown C, Giannoudis PV. Incidence and aetiology of anterior knee pain after intramedullary nailing of the femur and tibia. J Bone Joint Surg Br. 2006;88(5):576-80.
28) Karladani AH, Styf J. Percutaneous intramedullary nailing of tibial shaft fractures: a new approach for prevention of anterior knee pain. Injury. 2001;32(9):736-9.
29) Leliveld MS, Verhofstad MH. Injury to the infrapatellar branch of the saphenous nerve, a possible cause for anterior knee pain after tibial nailing? Injury. 2012;43(6):779-83.
30) Karachalios T, Babis G, Tsarouchas J, Sapkas G, Pantazopoulos T. The clinical performance of a small diameter tibial nailing system with a mechanical distal aiming device. Injury. 2000;31(6):451-9.
31) Toivanen JA, Väistö O, Kannus P, Latvala K, Honkonen SE, Järvinen MJ. Anterior knee pain after intramedullary nailing of fractures of the tibial shaft. A prospective, randomized study comparing two different nail-insertion techniques. J Bone Joint Surg Am. 2002;84-A(4):580-5.

32) Laffosse JM, Potapov A, Malo M, Lavigne M, Vendittoli PA. Hypesthesia after anterolateral versus midline skin incision in TKA: a randomized study. Clin Orthop Relat Res. 2011;469(11):3154-63.

33) AnubifixTM. “http://anubifix.com/English.html”

34) Kerver AL, van der Ham AC, Theeuwes HP, Eilers PH, Poublon AR, Kerver AJ, Kleinrensink GJ. The surgical anatomy of the small saphenous vein and adjacent nerves in relation to endovenous thermal ablation. J Vasc Surg. 2012;56(1):181-8.

35) Kerver AL, Carati L, Eilers PH, Langezaal AC, Kleinrensink GJ, Walbeehm ET. An anatomical study of the ECRL and ECRB: Feasibility of developing a preoperative test for evaluating the strength of the individual wrist extensors. J Plast Reconstr Aesthet Surg. 2013; in press.

36) van der Graaf T, Verhagen PC, Kerver AL, Kleinrensink GJ. Surgical anatomy of the 10th and 11th intercostal, and subcostal nerves: prevention of damage during lumbotomy. J Urol. 2011;186(2):579-83.

37) Ten Berge MG, Yo TI, Kerver A, de Smet AA, Kleinrensink GJ. Perforating veins: an anatomical approach to arteriovenous fistula performance in the forearm. Eur J Vasc Endovasc Surg. 2011;42(1):103-6

38) EffectMatrix Software Studio. Magic Morph 1.95. 38) “http://www.effectmatrix.com/morphing/”.

39) Adobe Corp. Adobe Photoshop CS-4. 40) “http://www.adobe.com/nl/products/photoshop/photoshop/”.

40) Tennent TD, Birch NC, Holmes MJ, Birch R, Goddard NJ. Knee pain and the infrapatellar branch of the saphenous nerve. J R Soc Med. 1998;91(11):573-5.

41) Papastergiou SG, Voulgaropoulos H, Mikalef P, Ziogas E, Pappis G, Giannakopoulos I. Injuries to the infrapatellar branch(es) of the saphenous nerve in anterior cruciate ligament reconstruction with four-strand hamstring tendon autograft: vertical versus horizontal incision for harvest. Knee Surg Sports Traumatol Arthrosc. 2006;14(8):789-93.

42) Horner G, Dellon AL. Innervation of the human knee joint and implications for surgery. Clin Orthop Relat Res. 1994 Apr;(301):221-6.

01000011 01101000 01100001 01110000
01110100 01100101 01110010 00100000
00110010 00101110 00110101 00001010

Chapter 2.5

The anatomical relationship of the superficial radial nerve and the lateral antebrachial cutaneous nerve: A possible factor in persistent neuropathic pain.

A.R. Poublon, E.T. Walbeehm, L.S. Duraku, P.H.C. Eilers, A.L.A. Kerver, G.J. Kleinrensink, J.H. Coert.

J Plast Reconstr Aesthet Surg. 2014 Oct 16.

ABSTRACT

Background: The superficial branch of the radial nerve (SBRN) is known for developing neuropathic pain syndromes after trauma. These pain syndromes can be hard to treat due to the involvement of other nerves in the forearm. When a nerve is cut, the Schwann cells, and also other cells in the distal segment of the transected nerve, produce the nerve growth factor (NGF) in the entire distal segment. If two nerves overlap anatomically, similar to the lateral antebrachial cutaneous nerve (LACN) and SBRN, the increase in secretion of NGF, which is mediated by the injured nerve, results in binding to the high-affinity NGF receptor, tyrosine kinase A (TrkA). This in turn leads to possible sprouting and morphological changes of uninjured fibers, which ultimately causes neuropathic pain. The aim of this study was to map the level of overlap between the SBRN and LACN.

Methods: Twenty arms (five left and 15 right) were thoroughly dissected. Using a new analysis tool called CASAM (Computer Assisted Surgical Anatomy Mapping), the course of the SBRN and LACN could be compared visually. The distance between both nerves was measured at 5-mm increments, and the number of times they intersected was documented.

Results: In 81% of measurements, the distance between the nerves was >10 mm, and in 49% the distance was even <5 mm. In 95% of the dissected arms, the SBRN and LACN intersected. On average, they intersected 2.25 times.

Conclusions: The close (anatomical) relationship between the LACN and the SBRN can be seen as a factor in the explanation of persistent neuropathic pain in patients with traumatic or iatrogenic lesion of the SBRN or the LACN.

INTRODUCTION

In 1984, Dellon and Mackinnon[1] stated that surgery on the radial side of the wrist is notorious for the development of neuropathic pain. Their explanation was that in 80% of cases the cause of this complication was stretching or compression of the superficial branch of the radial nerve (SBRN).

Mackinnon and Dellon[2] also presumed that the persisting symptoms in some patients might be caused by the fact that the course of the lateral antebrachial cutaneous nerve (LACN) for a large part overlaps with the course of the SBRN. Thus, when the SBRN is lacerated, the LACN almost certainly also is cut. Therefore, they postulated that in these patients the pain was caused by the LACN and not the SBRN.

By performing a diagnostic nerve block to the LACN using a local anesthetic (1% lignocaine), pain can be temporarily reduced in some patients[3] This shows that there is at least a relation between pain caused by lesion of the radial superficial nerve (SBRN) and the LACN. However, it remains unclear at which level the actual problem is localized: the distal segment, the dorsal root ganglion (DRG), or even central parts of the nervous system.[4]

It has been postulated that the nerve growth factor (NGF) plays a role in neuropathic pain,[5-8] although the exact mechanisms remain elusive.[9,10] When a nerve is transected, Schwann cells, but also other cells, in the entire distal segment of this transected nerve produce NGF[11,12] This production is initiated by axonal degeneration and Schwann cell upregulation, also known as Wallerian degeneration. If the branches of two nerves overlap anatomically (e.g., in the case of the LACN and SBRN), the produced NGF in the distal part of one nerve stimulates the other nerve, causing pain. Therefore, our interest is to demonstrate the areas of overlap between the LACN and SRBN more precisely. This is hard to describe by standard anatomical techniques and, therefore, a system called Computer Assisted Surgical Anatomy Mapping (CASAM) was used. CASAM is a system created in the Erasmus MC Anatomy laboratory[13,14] that can create an average of all used dissections (i.e., a virtual “average arm”) and subsequently create a visual representation of the “average” course of the SBRN and the LACN (see the CASAM section below).

The goals of the study were twofold: to describe the variation in the anatomy of the LACN and the SBRN, and to quantify the amount of overlap between the LACN and the SBRN by creating a visual model using CASAM.

METHODS

Materials

Twenty arms (nine male and 11 female; mean age 79.35 years (range 61–90); 15 right and five left) were embalmed with a solution containing 4% formalin preceded by flushing the specimen with Anubifix™. All dissections were performed using a 2.5× magnifying loupe.

To ensure comparable exposures, the dissection and imaging method were standardized.[14] Incisions were made from 5 cm below the caput humeri up to 5 cm above the elbow exposing the biceps. At the ends of the incision lines, two perpendicular incisions were made, creating two skin flaps that could be removed laterally and medially. Once the biceps brachi muscle was exposed, the fascia surrounding the muscle was incised and via blunt preparation the biceps was released from the underlying muscle tissue. Right behind the biceps, the musculocutaneous nerve, being the origin of the LACN, could be identified and the biceps was cut at the insertion and removed proximally. The LACN was dissected along its course distally down to the metacarpal region. Along the way, the nerve was marked using colored pins. Once the distal one-third of the arm was reached, the brachioradialis (BR) muscle was identified and bluntly dissected from the underlying tissue, while keeping the LACN intact.

In step 2, the SBRN was identified deep to the BR muscle. Once identified, the nerve was followed to the insertion of the BR where it continued to run a more superficial course. This spot was also marked with a colored pin. The SBRN was also dissected distally down to the metacarpal joint level.

Measurements

To quantify our findings, necessary to operate CASAM, the following measurements were taken:

1) The distance between both the epicondyles and the point where the SBRN emerges
2) The distance to both epicondyles and the first branch of the SBRN (the same procedure was performed with regard to the LACN)
3) The distance between both epicondyles and the location of crossings between the SBRN and LACN

Furthermore, along the course of both nerves, every 5 mm, the smallest distance between the SBRN and the LACN was measured using digital calipers (IP67 waterproof digital caliper, Hogetex, Varsseveld, the Netherlands).

Every arm was photographed with a digital camera (Nikon D 60 with Sigma 50 mm 1:2,8 DG MACRO lens). The camera was placed perpendicular to the specimen at a distance of 100 cm on a tripod. The pictures were loaded onto Photoshop CS4, and the measurements performed on each arm were stored digitally.

Computer-Assisted Surgical Anatomy Mapping (CASAM)

As human arms vary in size, anatomical comparison can be difficult. Therefore, a program called CASAM was used. In CASAM, it is possible to morph the digital image of each individual arm to the average size of all arms.

CASAM is based on the fact that "bony landmarks" (BLs), such as Lister's tubercle, lie in the same place relative to every arm. Besides BLs, the so-called shape-defining landmarks (SDLs) were created, to mark the outline of the arm, by dividing the space between two BLs into equal parts. We take these BLs and SDLs and mark them in the program. The picture can now be warped around these bony landmarks using active shape modeling (ASM) creating an average arm. All arms are then warped to the dimensions of the average arm, making it possible to compare all the arms directly. The "scaled" course of the SBRN and the LACN of all individual arms can now be compared directly.

The "bony" landmarks were used at: the lateral and medial epicondyle, the caput ulnae, Lister's tubercle, the lateral and the medial side of the metacarpophalangeal (MCP) and interphalangeal (IP) joints of the thumb, the caput phalanx I of the index finger, and the caput phalanx I of the third finger (Figure 1, green marks). These BLs were used, because their relative position in each arm is the same. The distance between the epicondyles and caput ulnae was divided into four equal parts, thus forming the three SDLs at the dorsal site of the arm. At the ventral side of the arm, the distance between the medial epicondyle and MCP I was divided into four equal parts, forming the ventral SDLs. The last two SDLs were defined as follows: halfway between the medial and lateral epicondyle and halfway between the caput ulnae and caput phalanx I (Figure 1, blue marks.)

The image created by CASAM shows a template of the individual course of the SBRN and the LACN, scaled to the average dimension of all 20 arms. The mean distance between a line through the lateral and medial epicondyle and Lister's tubercle was 239.15 mm (range 209–281 mm). This distance was used as the reference length of the arm.

Photoshop CS4 was used to trace the SBRN and the LACN in all pictures of the specimen. Then all morphed pictures could be compiled into one picture for further reference.

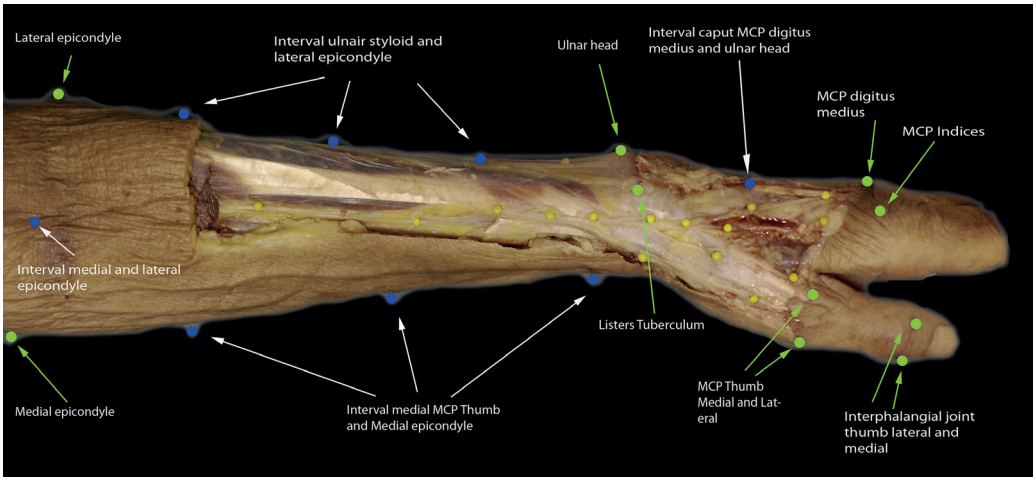

Figure 1. Landmarks used to outline the arm.

RESULTS

Topographic Anatomy

The LACN runs a course from a point under the biceps on the lateral side of the tendon in the elbow. It can be found in the subcutaneous fatty tissue on the radial side of the arm over the complete length of the forearm. It was noted that in 25% (n = 5) of cases the LACN branched early into two main branches continuing on both sides of the cephalic vein. In 70% (n = 14) of cases, the main branch of the LACN was localized volar to the cephalic vein. In 5% (n = 1) of cases, the LACN lay dorsal to the cephalic vein.

The radial nerve divides into the posterior interosseous nerve (PIN) and the SBRN emerging from a point deep to the BR muscle at an average distance of 159.6 mm (14.07) from the lateral epicondyle representing two-thirds of the length of the arm. On average, the SBRN showed 5.75 (five to seven) branches. Two branches reached the thumb, two reached the index finger, and one is localized in the direction of the middle finger. The SBRN was present in the subcutaneous fat tissue in the distal one-third of the arm.

In five arms, the SBRN and the LACN showed a total overlap, and in 14 arms partial overlap was observed. One arm showed no overlap (Table 1).

Nr	Left/ right	Gender	length of arm	SBRN branches	LACN branches	Crossings	overlap	LACN conjoins with WBRN
1	R	F	306	5	4	2	Yes	No
2	R	M	378	7	2	2	Yes	No
3	R	F	294	5	2	5	Yes	No
4	R	F	327	6	3	2	Yes	No
5	R	M	362	5	2	2	Yes	No
6	L	M	361	6	3	3	Yes	No
7	L	F	327	6	3	2	Yes	No
8	L	M	307	5	2	2	Yes	No
9	L	F	311	5	3	3	Yes	No
10	l	F	328	6	2	3	Yes	Yes
11	R	M	330	7	1	2	Yes	Yes
12	R	F	340	6	3	3	Yes	No
13	R	M	395	6	4	3	Yes	No
14	R	F	320	5	2	2	Yes	No
15	R	F	337	5	2	0	No	No
16	R	M	374	6	4	2	Yes	No
17	R	F	300	5	2	2	Yes	Yes
18	R	M	369	5	3	3	Yes	No
19	R	M	352	5	2	1	Yes	No
20	R	M	307	6	3	1	Yes	No

Table 1. Results of 20 arms.

In all cases, the main branch of the LACN runs volar to the point where the SBRN emerges. In the distal third of the arm where the two nerves overlap, the LACN crossed the SBRN with a mean of 2.25 times; these crossings (n = 45) occurred between 148.12 and 256.04 mm (corrected for length of the arm) distal to the lateral epicondyle. In 95% of the arms (n = 19), the LACN intersected with the SBRN at the point where the SBRN emerged from under the BR (Figure 2). A Pearson correlation of 0.820 with a significance of 0.00 (two-tailed) was found.

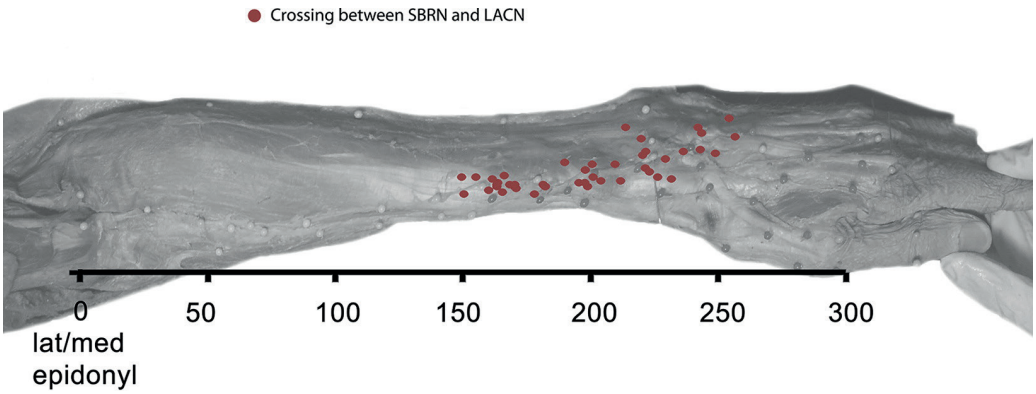

Figure 2. Spread of the intersection of the SBRN and LACN (corrected for length of the forearm).

Corrected for the length of the arm, the correlation coefficient dropped to 0.034, suggesting that there is an absolute distance between the two measurements. The distance between the first intersection and the site where the SBRN emerged from under the BR is 8.8 mm (standard deviation (SD) 12 mm). The distance between the nerves was measured in 5-mm intervals resulting in an average of 30 data points per arm. In 81% of the measurements, the distance between the two nerves was >10 mm and in 49% even lesser than 5 mm. In addition, the data show that the closest proximity can be found just after the SBRN emerges from under the deep fascia (Figure 3).

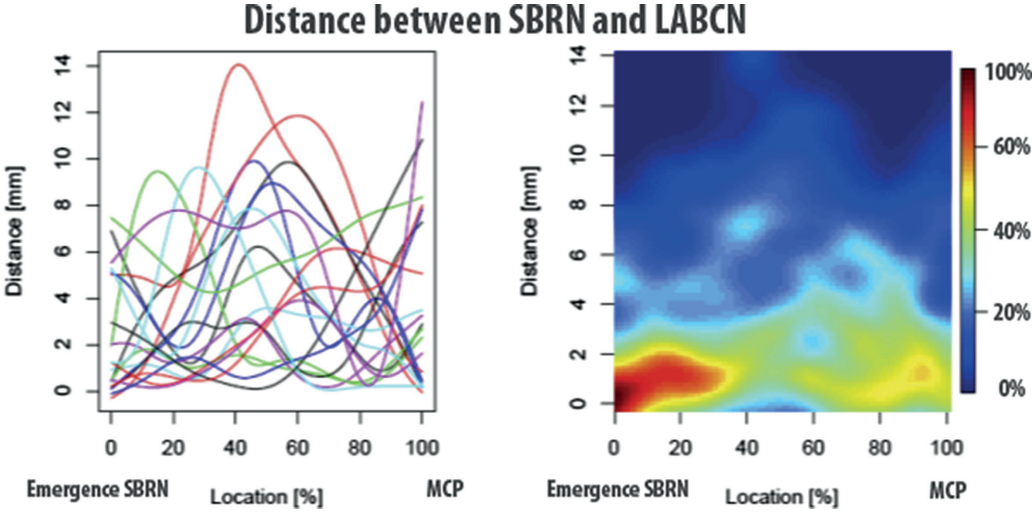

Figure 3. Left: distance of SBRN to LABCN in each individual arm. Right: Rendering in which the color indicates the percentage of arms with the distance between the SBRN and LABCN being the same. Dark red 100%, dark blue 0%.

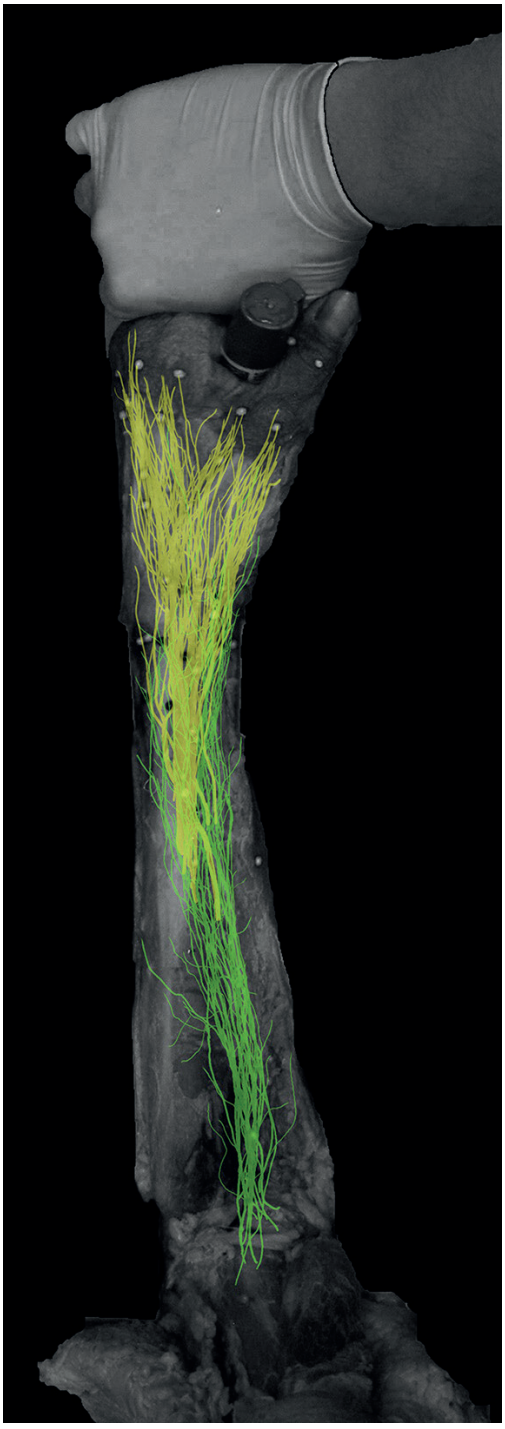

Figure 4. Course of 20 SBRN (yellow) and 20 LACN (green).

In two cases, the most volar branch of the SBRN merged with the LACN continuing along the radial side of the thumb.

In three cases, the LACN merged with the SBRN to innervate the radial aspect of the thumb.

In the images created in CASAM, the close distance between the courses of the two nerves is clearly visible. The image shows that there actually is no real safe zone concerning surgical trauma to LACN and SBRN in the radial part of the wrist (Figure 4).

DISCUSSION

Surgery to the radial aspect of the wrist is known for its pain-related complications.[16-18] There are many hypotheses to explain the susceptibility of the wrist to neuropathic pain. One of the explanations is based on the intimate anatomical relationship between the end branches of the two nerves. The purpose of this study was to map the course of the LACN and the SBRN and especially the close relation between both nerves at some point resulting in actual, topographical intersections of these two nerves.

In this study, a close relation between the SBRN and the LACN was demonstrated. In all but one arm, the nerves overlapped and intersected on average 2.25 times. The point where the SBRN emerges from a deep point to the BR is also closely related to the first intersection with the LACN. The correlation between the two measurements was high and not dependent on the length of the arm. In 50% of cases, the first crossing was within 18 mm from the point where the SBRN pierces the fascia.

Mackinnon and Dellon[2] showed that in 75% of cases there is an overlap of the terminal branches of the LACN and SBRN. They concluded that, if the SBRN is damaged, the LACN also has a high probability of being damaged. This lesion of the LACN explains why excision of a neuroma in the SBRN sometimes does not relieve the sensation of pain in patients with neuropathic pain.

Beldner[19] showed that, in several cases, the LACN flanks the cephalic vein on both sides. This study also found a close relation between the cephalic vein and the LACN. This flanking pattern was found in 15% of cases. The fact that the LACN and the cephalic vein are closely related makes it much easier to identify the nerve.

The n demonstrated that the neurosomes of an injured nerve are populated by collateral sprouting fibers from adjacent uninjured nerves.[20] These uninjured nerve fibers may change functionally as a consequence of a peripheral nerve lesion.

Due to Wallerian degeneration of the distal segment of the injured nerve, intact nerve fibers are in close proximity of activated Schwann cells, macrophages, and other inflammatory cells, which secrete high levels of neurotrophic factors like NGF. These neurotrophic factors are known to influence excitability, enhance sensory transmission, and/or induce ongoing activity in uninjured peripheral nerve fibers. In addition, in the DRG, signaling from injured DRG cells could infer uninjured DRGs either directly or via nonneuronal cells. The consequences could be changes of excitability and/or ectopic activity in the cell bodies.

Another postulated mechanism for neuropathic pain at the site of the injured nerves is the expression of novel sodium channels that have ongoing and evoked ectopic excitability.

Therefore, it is possible that, if the LACN is sectioned iatrogenically, the SBRN might be responsible for the pain and vice versa. This also explains why, if pain remains after treatment of an SBRN neuroma, it is often diminished on denervation of the LACN, without finding a treatable neuroma in the LACN, as described by LLuch. However, this does not explain the role of the PIN in persistent neuropathic pain on the radial side of the wrist, as this nerve does not have a neurosome in the skin, and yet denervation of the PIN to treat radial-sided pain of the wrist does sometimes reduce pain.

Clinically, when patients present with pain in the area of the SBRN or LACN, diagnostic blockades are performed with 1% lidocaine of SBRN, LACN, PIN, and the palmar cutaneous branch of the median nerve (PCBMN). To determine the efficiencies of such blocks, they are performed in sequential order, with minimally half an hour in between blocks. The next step consists of denervation of the nerve causing pain.

In conclusion, the close (anatomical) relationship between the LACN and the SBRN can be seen as a factor in the explanation of persistent neuropathic pain in patients with traumatic or iatrogenic lesion of the SBRN or the LACN.

ACKNOWLEDGMENTS

The authors would like to thank Y. Steinvoort for her help in providing a room for the dissections. The authors would also like to thank A. Vossen for his help in dissecting and data collection.

REFERENCES

1) A.L. Dellon, S.E. Mackinnon. Susceptibility of the superficial sensory branch of the radial nerve to form painful neuromas. J Hand Surg Br, 9 (1984), pp. 42–45
2) S.E. Mackinnon, A.L. Dellon. The overlap pattern of the lateral antebrachial cutaneous nerve and the superficial branch of the radial nerve. J Hand Surg Am, 10 (1985), pp. 522–526
3) S.E. Mackinnon, A.L. Dellon. Results of treatment of recurrent dorsoradial wrist neuromas. Ann Plast Surg, 19 (1987), pp. 54–61
4) A. Truini, G. Cruccu. Pathophysiological mechanisms of neuropathic pain. Neurol Sci, 27 (Suppl. 2) (2006), pp. S179–S182
5) X.Q. Shu, L.M. Mendell. Neurotrophins and hyperalgesia. Proc Natl Acad Sci U S A, 96 (1999), pp. 7693–7696
6) P. Anand. Neurotrophic factors and their receptors in human sensory neuropathies. Prog Brain Res, 146 (2004), pp. 477–492
7) K. Obata, K. Noguchi. BDNF in sensory neurons and chronic pain. Neurosci Res, 55 (2006), pp. 1–10
8) W. Marcol, K. Kotulska, M. Larysz-Brysz, J.L. Kowalik. BDNF contributes to animal model neuropathic pain after peripheral nerve transection. Neurosurg Rev, 30 (2007), pp. 235–243 [discussion 43]
9) D. Siniscalco, F. Rossi, S. Maione. Molecular approaches for neuropathic pain treatment. Curr Med Chem, 14 (2007), pp. 1783–1787
10) D. Siniscalco, C. Giordano, F. Rossi, S. Maione, V. de Novellis. Role of neurotrophins in neuropathic pain. Curr Neuropharmacol, 9 (2011), pp. 523–529
11) M. Theodosiou, R.A. Rush, X.F. Zhou, et al. Hyperalgesia due to nerve damage: role of nerve growth factor. Pain, 81 (1999), pp. 245–255
12) R. Heumann, S. Korsching, C. Bandtlow, H. Thoenen. Changes of nerve growth factor synthesis in nonneuronal cells in response to sciatic nerve transection. J Cell Biol, 104 (1987), pp. 1623–1631
13) A.L. Kerver, L. Carati, P.H. Eilers, et al.. An anatomical study of the ECRL and ECRB: feasibility of developing a preoperative test for evaluating the strength of the individual wrist extensors. J Plast Reconstr Aesthet Surg, 66 (2013), pp. 543–550
14) A.L. Kerver, A.C. van der Ham, H.P. Theeuwes, et al.. The surgical anatomy of the small saphenous vein and adjacent nerves in relation to endovenous thermal ablation. J Vasc Surg, 56 (2012), pp. 181–188
15) P.H. Eilers, J.J. Goeman. Enhancing scatterplots with smoothed densities. Bioinformatics, 20 (2004), pp. 623–628
16) M.S. Arons. de Quervain's release in working women: a report of failures, complications, and associated diagnoses. J Hand Surg Am, 12 (1987), pp. 540–544
17) R. Birch, G. Bonney, J. Dowell, J. Hollingdale. Iatrogenic injuries of peripheral nerves. J Bone Jt Surg Br, 73 (1991), pp. 280–282
18) R.M. McAllister, S.E. Gilbert, J.S. Calder, P.J. Smith. The epidemiology and management of upper limb peripheral nerve injuries in modern practice. J Hand Surg Br, 21 (1996), pp. 4–13

19) S. Beldner, D.A. Zlotolow, C.P. Melone Jr., A.M. Agnes, M.H. Jones. Anatomy of the lateral antebrachial cutaneous and superficial radial nerves in the forearm: a cadaveric and clinical study. J Hand Surg Am, 30 (2005), pp. 1226–1230

20) L.S. Duraku, M. Hossaini, B.N. Schuttenhelm, et al.. Re-innervation patterns by peptidergic substance-P, non-peptidergic P2X3, and myelinated NF-200 nerve fibers in epidermis and dermis of rats with neuropathic pain. Exp Neurol, 241 (2013), pp. 13–24

01000011 01101000 01100001 01110000
01110100 01100101 01110010 00100000
00110010 00101110 00110110 00001010

Chapter 2.6

The surgical anatomy of the small saphenous vein and adjacent nerves in relation to endovenous thermal ablation.

Kerver, A.L.A., Van Der Ham, A.C., Theeuwes, H.P., Eilers, P.H.C., Poublon, A.R., Kerver, A.J.H., Kleinrensink, G.-J.

J Vasc Surg. 2012 Apr 12.

ABSTRACT

Background: Thermal damage to peripheral nerves is a known complication of endovenous thermal ablation (EVA) of the small saphenous vein (SSV). Therefore, the main objective of this anatomic study was to define a safe zone in the lower leg where EVA of the SSV can be performed safely.

Methods: The anatomy of the SSV and adjacent nerves was studied in 20 embalmed human specimens. The absolute distances between the SSV and the sural nerve (SN) (closest/nearest branch) were measured over the complete length of the leg (>120 data points per leg), and the presence of the interlaying deep fascia was mapped. The distance between the SSV and the tibial nerve (TN) and the common peroneal nerve was assessed. A new analysis method, computer-assisted surgical anatomy mapping, was used to visualize the gathered data.

Results: The distance between the SSV and the SN was highly variable. In the proximal one-third of the lower leg, the distance between the vein and the nerve was <5 mm in 70% of the legs. In 95%, the deep fascia was present between the SSV and the SN. In the distal two-thirds of the lower leg, the distance between the vein and the nerve was <5 mm in 90% of the legs. The deep fascia was present between both structures in 15%. In 19 legs, the SN partially ran beneath the deep fascia. In the saphenopopliteal region, the average shortest distance between the SSV and the TN was 4.4 mm. In 20%, the distance was <1 mm. The average, shortest distance between the SSV and the common peroneal nerve was 14.2 mm. The distance was <1 mm in one leg.

Conclusions: At the saphenopopliteal region, the TN is at risk during EVA. In the distal two-thirds of the lower leg, the SN is at risk for (thermal) damage due to the small distance to the SSV and the absence of the deep fascia between both structures. The proximal one-third of the lower leg is the optimal region for EVA of the SSV to avoid nerve damage; the fascia between the SSV and the SN is a natural barrier in this region that could preclude (thermal) damage to the nerve.

INTRODUCTION

Clinical Relevance

Iatrogenic damage to peripheral nerves is a known, incapacitating complication of endovenous thermal ablation (EVA) of the small saphenous vein (SSV). Although EVA is quickly replacing conventional surgery as the treatment of choice for saphenous ablation, no consensus has been reached regarding the surgical landmarks for a safe EVA of the SSV. This study describes and visualizes the anatomic limits in relation to the sural nerve and deep crural fascia, the tibial nerve, and the common peroneal nerve using a new anatomy mapping tool, computer-assisted surgical anatomy mapping. The results offer the surgeon a better understanding of the complex anatomy of the SSV and thereby provide surgical guidelines to reduce complications of EVA of the SSV.

General introduction

Thermal damage to peripheral nerves is a known complication of endovenous thermal ablation (EVA) of the small saphenous vein (SSV). Therefore, the main objective of this anatomic study is defining a safe zone in the lower leg where EVA of the SSV can be performed safely. Although surgical stripping is still considered the gold standard for saphenous vein ablation,[1] EVA, such as endovenous laser therapy and radiofrequency ablation, has become a more recognized alternative in common practice.[1,2] Therefore, the need for thorough research on complications, recurrence rates, and relevant anatomy becomes greater. Many publications have established the role of EVA for ablation of the great saphenous vein,[3-5] but studies on EVA of the SSV are still scarce. Short-term and midterm results are promising and show low recurrence rates and fewer complications with EVA than with conventional surgery.[6-9] Nevertheless, no consensus has been reached regarding the surgical anatomic landmarks for a safe approach of the SSV.

Many complications of surgical stripping of the SSV have been described, along with damage to the sural nerve (SN), the tibial nerve (TN), and the common peroneal nerve (CPN).[10,11] The anatomic course of these nerves is important because of new, extra risks caused by EVA coagulation temperatures and the insertion of a needle when injecting tumescent anesthesia around the vein.

The SSV mainly runs a course between the superficial (saphenous) and the deep crural (muscular) fascia of the lower leg.[12] The proximal part of the SN, however, courses under the deep fascia; therefore, it could well function as a natural barrier to prevent the SN from excessive heat during EVA. The deep fascia could also prove to be a good barrier between the nerve and vein during

the injection of tumescent anesthesia. The fluid being entrapped within the fascial "tube" could perform its function longer. Consequently, the main question to be answered is: Is there an anatomic zone in the leg where EVA of the SSV can be performed safely?

METHODS

Materials

This study used 20 legs (nine left, 11 right) from 20 embalmed human bodies. The bodies were embalmed at room temperature and perfused at low pressure with a mixture of 6% formaldehyde and 5% phenol to minimize shrinkage. None of the limbs demonstrated shrinkage artefacts, (external) macroscopic signs of venous disease, or scarring. The SN and the SSV were dissected. Measurements were taken using flexible scale bars. Owing to postmortem rigidity and fixation in 19 legs, the Achilles tendon was cut to flex the ankle 90°.

Computer-Assisted Surgical Anatomy Mapping (CASAM)

Computer-assisted surgical anatomy mapping (CASAM) is a new anatomic method developed by two of the authors (A.K., G.K.) to map and visualize surgical anatomic details relevant for safe surgical approaches.[13] All dissected legs were photographed using a Canon 350D with a Canon EF-S (Canon USA, Inc, San Jose, Calif) 18- to 55-mm lens. The camera was positioned perpendicular to the leg at a distance of 95 cm. Landmarks 1 and 3 were used to horizontally position each leg in line with the camera, and landmark 9 was used to center each leg (Figure 1). Each picture was then processed using the CASAM method, which consists of three phases.

1. Magic Morph 1.9510 software[14] was used to define the shape and size of each leg using landmarks (Figure 1), followed by a calculation of the average shape and size of all legs.
2. The 20 legs in all 20 pictures were warped (reshaped) to exactly match the shape and size of the created and calculated average leg. As a result, all 20 legs in all 20 pictures now had the exact same shape and size. Magic Morph uses a thin plate spline transformation as a warping algorithm.[14]

3 Photoshop CS-4 (Adobe Inc, San Jose, Calif)[15] was used to compile all warped pictures in one image, renditions of which were generated to highlight the relevant anatomic structures and landmarks.
No measurements were made using Photoshop CS-4.

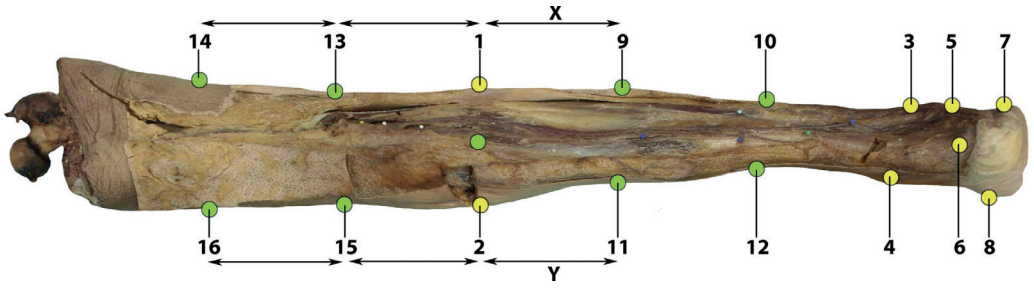

Figure 1. Bony and nonbony landmarks used for computer-assisted surgical anatomy mapping (CASAM). Bony ultrasound landmarks commonly used in endovenous thermal ablation (EVA) of the small saphenous vein (SSV): the tibia plateau (1) and (2) and the lateral malleolus (3) and (5). Yellow: bony landmarks; the most lateral (1) and most medial (2) part of the tibia plateau, the proximal (3) and distal (5) border of the lateral malleolus, the proximal border of the medial malleolus (4), the insertion of the Achilles tendon (6), the tuberosity of the fifth metatarsal (7), and the tuberosity of the first metatarsal (8). Green: nonbony landmarks, halfway between landmarks 1 and 2, at one-third (9) and two-thirds (10) between landmarks 1 and 3, and at one-third (11) and two-thirds (12) between landmarks 2 and 4. Distance X was used to create the upper lateral landmarks (13, 14). Distance Y was used to create the upper medial landmarks (15, 16). Distance X = one-third of the distance between landmark 1 and 3. Distance Y = one-third of the distance between landmark 2 and 4.

General Assessments

The distance between the tibia plateau and the proximal lateral malleolus was measured to define the length of each lower leg. Bony landmarks were used as reference points for intrinsic measurements and the CASAM assessment (Figures 1 and 2). To map the relevant anatomy with CASAM, eight nonbony or soft tissue landmarks were created in addition to the bony landmarks (Figure 1).

Basic Anatomy

SSV: CASAM was used to map and warp the course of each individual SSV. The courses of the 20 SSVs were compiled into one area of distribution. The most distal saphenopopliteal junction (SPJ) in each leg was identified and marked. The area in which each SSV ran above the superficial fascia was colored blue with 5% opacity. The following distances were manually measured in each specimen:

1 The length of the SSV from its most distal SPJ to the proximal tip of the lateral malleolus.

2 The most distal SPJ to the nearest part of the dermis (depth of the SPJ).

3 The distances from the tibia plateau to the most distal SPJ, the entrance of the SSV into the superficial fascia, and the entrance of the SSV into the deep fascia.

SN: CASAM was used to map and warp the course of each individual SN. Each SN was categorized, and the medial sural cutaneous nerve (MSCN), the lateral sural cutaneous nerve (LSCN), and combined sural nerve (CSN) were identified. The courses of the 20 SNs were compiled into one area of distribution. The area in which each SN ran under the deep fascia was colored green with 5% opacity. The distances from the tibia plateau to the entrance of the SN into the superficial fascia and into the deep fascia were manually measured in each specimen.

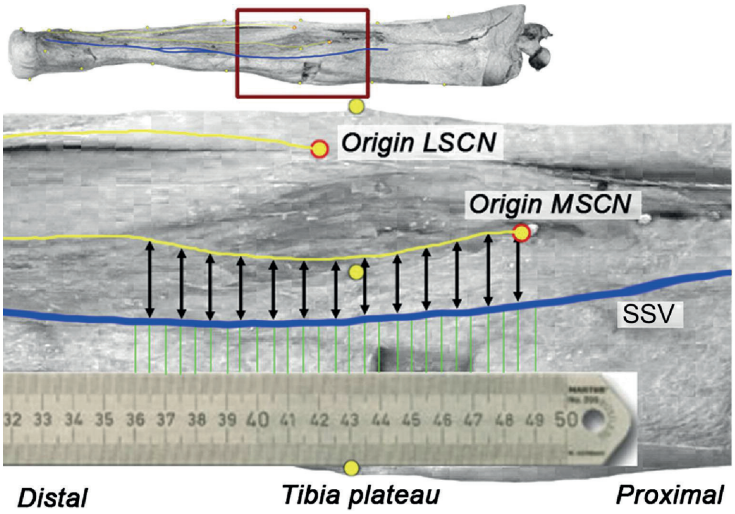

Figure 2. Measurements.
Yellow line: lateral and medial sural cutaneous nerve sural nerve (LSCN, MSCN). Blue line: small saphenous vein (SSV). Black arrows: measurements taken with a 5-mm interval from the most distal saphenopopliteal junction (SPJ) to the most proximal part of the lateral malleolus: the absolute distance between the SSV and the closest branch of the sural nerve (MSCN, LSCN, or combined sural nerve [CSN]); the presence of a fascia layer between the SSV and the SN.

Relative anatomy

SSV in relation to the SN and deep crural fascia: The areas of distribution of the SSV and the SN were overlaid and compared using CASAM. The following

manual measurements were performed with a 5-mm interval from the most distal SPJ to the most proximal part of the lateral malleolus (Figure 2):

1 The absolute distance between the SSV and the SN (MSCN, LSCN, CSN).
2 The presence of a fascia layer between the SSV and the SN.

SSV in relation to the TN: The distance between the SSV to the nearest point on the TN was measured, and the presence of a fascia layer between both structures was noted.

SSV in relation to the CPN: The distance between the SSV to the nearest point on the CPN was measured.

RESULTS

The mean distance between the tibia plateau and the most proximal part of the lateral malleolus was 404.2 mm (range, 345-471 mm).

Basic Anatomy

SSV: The course of the SSV is highly variable (Figure 3, A). The area of distribution is therefore large. It is mainly located in the axial part of the calf and runs a course just lateral to the Achilles tendon. Near the lateral malleolus, it curves toward the lateral side of the foot. The most distal SPJ is also highly variable (Figure 3, A) and, on average, located at 92 mm (range, 18-248 mm) proximal of the tibia plateau. In one leg, the most distal SPJ is situated distal (−18 mm) to the tibia plateau. The depth of the SPJ in relation to the upper part of the skin is 34.1 mm (range, 15-67 mm).

The SSV penetrates the superficial fascia in all 20 legs. The SSV runs under the superficial fascia until 330 mm distal from the tibia plateau (range, 254-404 mm distal from the tibia plateau) (Figure 4, A). In two specimens, the SSVs penetrate the deep fascia layer, respectively, at 91 and 105 mm proximal to the tibia plateau.

SN: The course of the SN is highly variable (Figure 3, B) and has a large area of distribution located both in the middle part of the calf (mainly the MSCN) as well as in the lateral part of the calf (mainly the LSCN). Although the anatomy is highly variable, the SN in most cases consists of two branches: the MSCN and the LSCN. The MSCN originates from the TN and the LSCN originates from the CPN. Both branches conjoin in the calf to form the CSN. In seven specimens, the

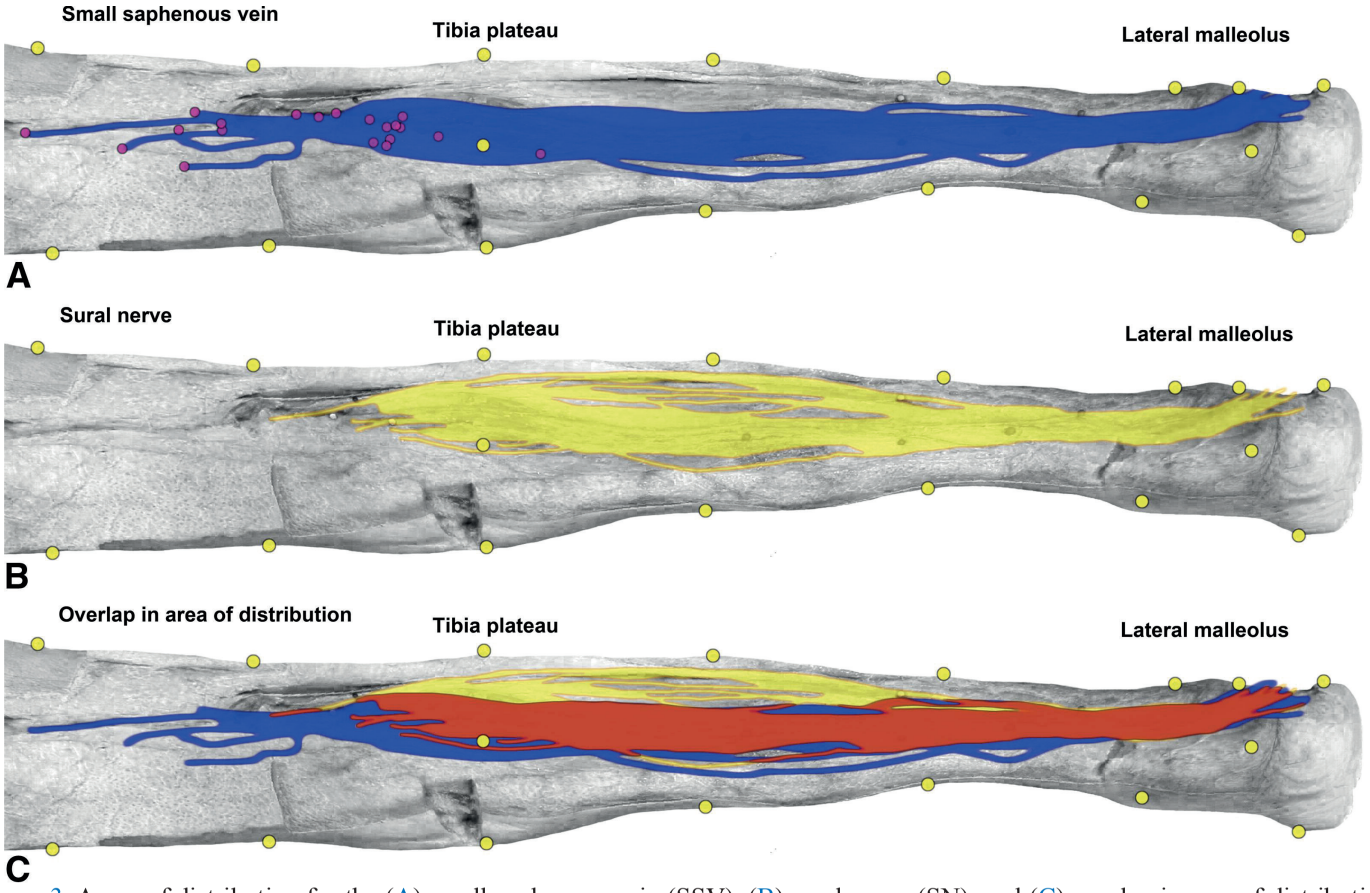

Figure 3. Areas of distribution for the (A) small saphenous vein (SSV), (B) sural nerve (SN), and (C) overlap in area of distribution shown on a computer-assisted surgical anatomy mapping (CASAM)-generated image depicting an average leg in which the SSV and the SN of all 20 legs were warped. Yellow dots: landmarks used for CASAM. A,Purple dots: most distal saphenopopliteal junction (SPJ) of each specimen. Blue: area of distribution of the SSV. Yellow: area of distribution of the SN. Orange: overlap between both distribution areas.

branches never join and each either runs a highly variable course to the lateral side of the foot (n = 5) or the MSCN or the LSCN have not been formed (n = 2).

The SN penetrates the superficial fascia in all 20 legs at the same point as the SSV (Figure 4, A), 331 mm distal from the tibia plateau (range, 254-404 mm). In 19 legs (95%), the SN partially runs under the deep fascia (Figure 4, B), 233 mm distal from the tibia plateau (range, 139-399 mm; Figure 5). In one specific leg without a fascia layer between the SSV and the SN, only an LSCN and no MSCN are present. The distance between the SSV and LSCN is >5 mm until a point 220 mm distal from the tibia plateau.

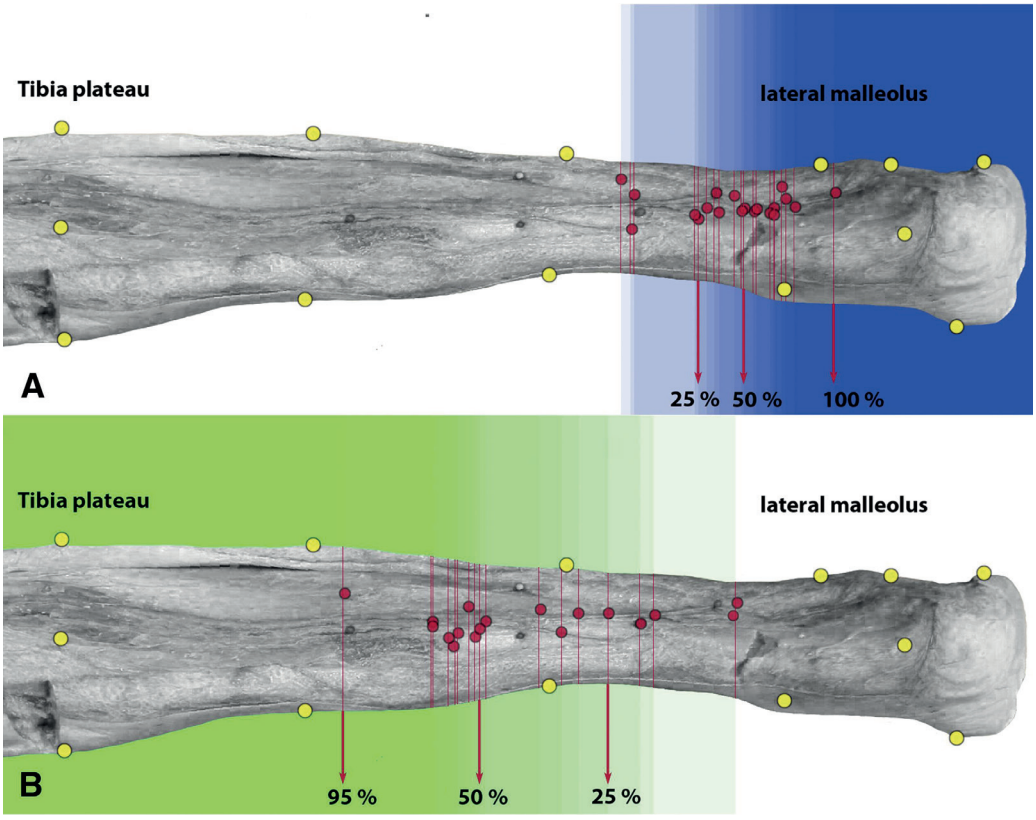

Figure 4. Small saphenous vein (SSV) and sural nerve (SN) are shown in relation to the fascia layers, with computer-assisted surgical anatomy mapping (CASAM)-generated image depicting an average leg in which relevant areas regarding the deep (crural) and superficial fascia (of all 20 legs) were warped. A, Area in which both the SSV and SN run superficial. B, Area in which the SN runs beneath the deep (crural) fascia. Yellow dots: landmarks used for CASAM. Blue area: progressive percentage of legs in which both the SSV and SN run superficial. Green area: digressive percentage of legs in which the SN runs beneath the deep crural fascia.

Relative Anatomy

SSV in relation to the SN: The areas of distribution of the SSV and the SN show much overlap: 63% of the distribution area of the SSV is covered by the distribution area of the SN (Figure 3, C). Up to 71% of the SN distribution area is covered by the distribution area of the SSV. Most LSCN trunks, however, have no overlap with any of the variations of the SSV, whereas almost all MSCN trunks show overlap with multiple SSV variations. The manually measured distance between the SSV and the closest part of the SN ranges from 19 to <1 mm (Figure 5).

At the level of the tibia plateau, the distance between the SSV and the closest trunk of the SN is <5 mm in 60% of the legs. At 100 mm distal of the tibia plateau, the distance between the SSV and the SN is <5 mm in 70% of the legs. From 200 mm distal of the tibia plateau to the lateral malleolus, the distance between the SSV and the SN is <5 mm in all legs (Figure 5).

All measurements have also been corrected for the length of the SSV (measured from the most distal SPJ to the most proximal part of the lateral malleolus). At the SPJ in 35% of the legs, the distance between the SSV and the closest trunk of the SN is <5 mm. At the proximal one-third of the length of the SSV in 65% of the legs, the distance between the SSV and the SN is <5 mm. At the distal two-third of the length of the SSV in 85% of the legs, the distance between the SSV and the SN is <5 mm. At the lateral malleolus, the distance between the SSV and the SN is <5 mm in 95% (Figure 6).

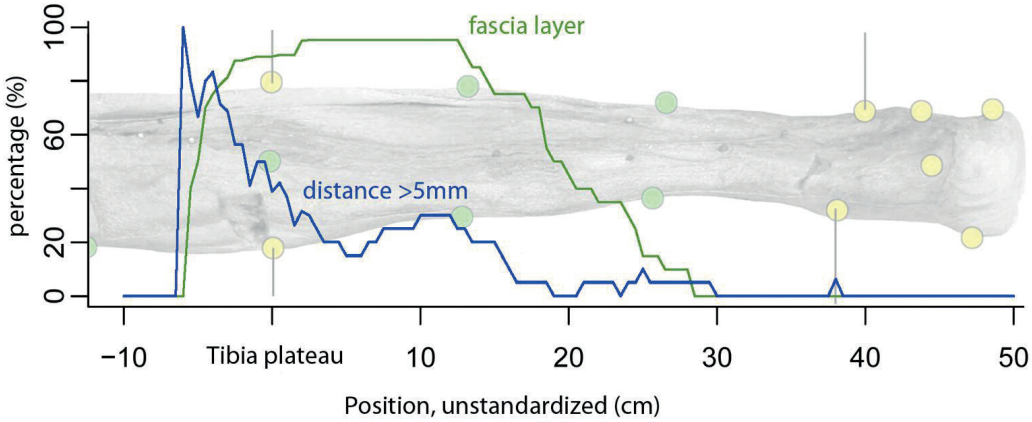

Figure 5. Standardized distance between small saphenous vein (SSV) and sural nerve (SN) and interlaying fascia. X axis: 0.0 = start measurements, 1.0 = stop measurements (proximal part of the lateral malleolus) standardized for the length of the SSV. Y axis: percentage of legs; blue line: percentage of legs in which the distance between the SSV and the SN is more than 5 mm; green line: percentage of legs with a fascia present between the SSV and the SN.

SSV and SN in relation to the deep crural fascia: At the level of the tibia plateau in 90% of the legs, a fascia layer is present between the SSV and the closest part of the SN. At 100 mm distal to the tibia plateau, a fascia layer between the SSV and the closest part of the SN is present in 95% of the legs. At 200 mm distal to the tibia plateau, a fascia layer between the SSV and the SN is present in 50% of the legs. From 300 mm distal of the tibia plateau to the lateral malleolus, a fascia layer between the SSV and the SN is present in 0% of the legs (Figure 5).

All measurements have been corrected for the length of the SSV. At the SPJ in 85% of the legs, a fascia layer is present between the SSV and the SN. At the proximal one-third of the length of the SSV in 95% of the legs, a fascia layer is present between the SSV and the SN. In the distal two-third of the length of the SSV in 15% of the legs, a fascia layer is present between the SSV and the SN. At the lateral malleolus in none of the legs, a fascia is present between the SSV and the SN (Figure 6).

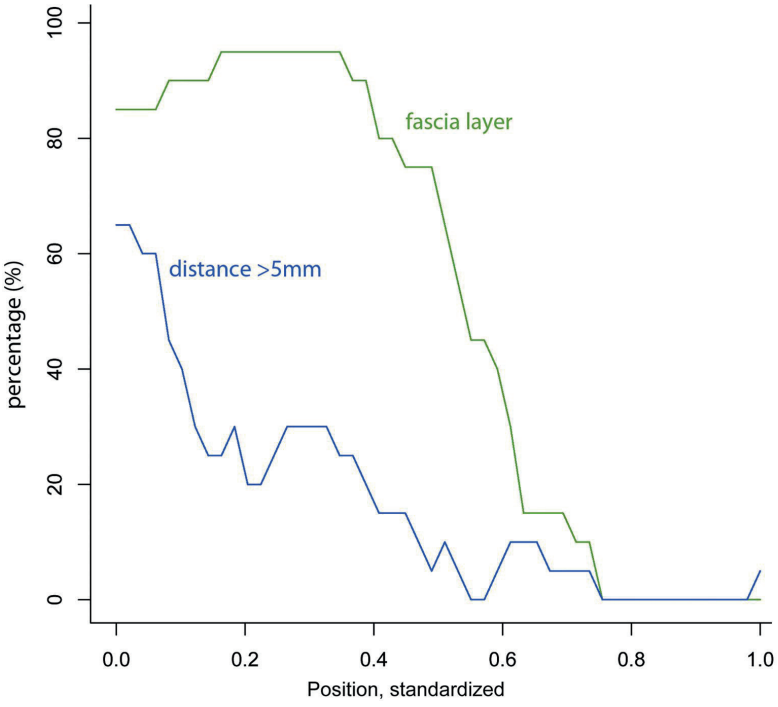

Figure 6. Distance between the small saphenous vein (SSV) and sural nerve (SN) and the interlaying fascia. The X axis: 10 = 100 mm proximal to the tibia plateau, 0.0 = tibia plateau, and 50 = 500 mm distal from the tibial plateau. Y axis: percentage of legs. Blue line: percentage of legs in which the distance between the SSV and the SN is >5 mm. Green line: percentage of legs with a fascia present between the SSV and the SN.

To summarize the data schematically: in the proximal part of the lower leg, the SSV runs an interfascial course, whereas the SN (mainly the MSCN) runs a course under the deep crural fascia and above the gastrocnemius muscle (Figure 7,A). More distal, the SN penetrates the deep crural fascia and the SSV and SN both run an interfascial course between the superficial and deep fascia (Figure 7, B). In the distal part of the lower leg, the SSV and the SN have penetrated the superficial fascia and run a superficial course above the superficial fascia (Figure 7, C).

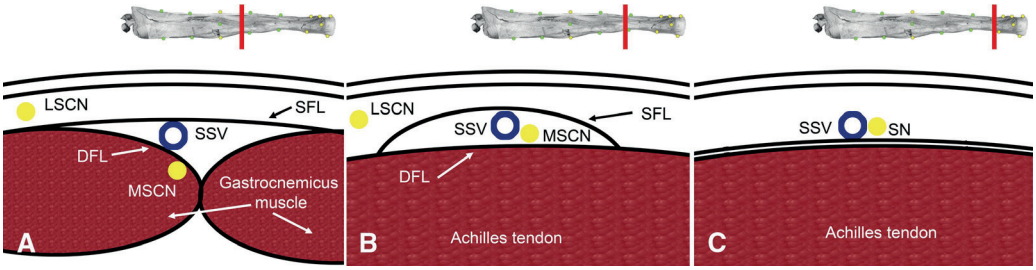

Figure 7. Schematic transverse drawing of the general course of the small saphenous vein (SSV) and the sural nerve (SN) in relation to the fascia layers. A, Proximal part of the lower leg until the saphenopopliteal junction (SPJ). The SSV runs an interfascial course. The medial sural cutaneous nerve (MSCN) runs under the deep fascia layer (DFL) above the medial or lateral gastrocnemius muscle. The lateral sural cutaneous nerve (LSCN) runs a superficial course. B, The SSV and the MSCN both run an interfascial course under the superficial fascia layer (SFL) and above the DFL. The LSCN runs a superficial course. C, In the distal part of the lower leg, the SSV and the SN both run a superficial course.

SSV in relation to the TN: The average distance between the SSV and the TN is 4.4 mm (range, 1-12 mm). In 55% of the legs, the distance between the SSV and the TN is <5 mm, and in 20%, it was even ≤1 mm (Figure 8). In 85% of the legs, a clear and thick epineurium is present around the TN; however, no clearly visible epineurium is observed in 15%.

SSV in relation to the CPN: The average distance between the SSV and the CPN is 14.3 mm (range, 1-26 mm) as measured in 19 legs. In three legs, the distance between the SSV and the CPN was <5 mm.

DISCUSSION

The purpose of this study is to clearly define and describe the three-dimensional relation between the SSV and surrounding nerves in order to define a zone in which EVA can be performed safely.

Regarding the SN: Three variables are prominent in our data: the distance between the SSV and the SN, the presence of a fascia between the SSV, and the SN, and the highly variable SPJ.

1 The distance between the SSV and the closest part of the SN is highly variable.

2 The presence of a fascia between the SSV and the SN is less variable. In 95% of the legs, a fascia between the SN and the SSV is present in a zone from the tibia plateau until a point 130 mm distal to the tibia plateau. In one leg, no fascia is present between the SSV and the SN, but in this case, no MSCN is present (only an LSCN, which was located far more than 5 mm laterally from the SSV). Proximal to the tibia plateau, the percentage of legs that have a deep fascia between the SSV and the SN drops from 90% to 0%, but the percentage of legs

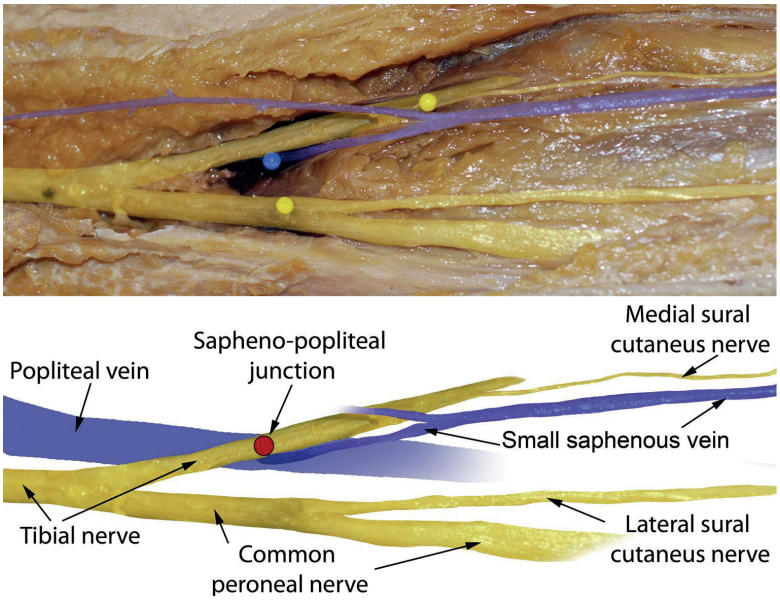

Figure 8. An original photograph was enhanced with Photoshop CS-4 to highlight the relevant anatomy of the saphenopopliteal fossa. The small saphenous vein (SSV) actually curls under the tibial nerve (TN) to conjoin in the popliteal vein.

that have a distance between the SSV and the SN of >5 mm increases from 50% to 100% (Figures 5 and 6). This suggests that although a fascia layer is not always present between the SSV and the SN, the area proximal to the tibia plateau is still relatively "safe" for EVA.

When these measurements are combined, the new safe zone for EVA of the SSV can be defined as a zone in which:

- Either the distance between the SSV and surrounding nerves is such that it is safe to use heat-generating therapy,
- Or a fascia layer is present between the SSV and the SN.

3 Because the location of the SPJ shows no correlation with the tibia plateau, all measurements are corrected for the length of the SSV instead of the length of the lower leg. Defining a safe zone proves to be more reliable when the most distal SPJ is used as a defining landmark rather than the tibia plateau (Figures 5 and 6).

Regarding the deep fascia and the use of tumescent anesthesia: Local tumescent anesthesia is known to protect surrounding tissue from high coagulation temperatures.[16] When the distance between the SSV and SN is <1 mm, the SN runs immediately next to or partly under the SSV. Insertion of tumescent anesthesia exactly between the SSV and the SN might therefore be difficult, if not impossible. Because the deep fascia layer is a natural barrier between the SSV and the SN, it can be seen as a very effective separation between the SSV and the SN.

Regarding the TN and the CPN: Surprisingly, the distance between the SSV and the TN is extremely small. Because permanent TN damage after EVA has not been reported, we can only assume that the fascia between the SSV and the TN or the admission of tumescent anesthesia provides enough protection against high coagulation temperatures. However, the SSV was observed to curl around the TN to conjoin with the popliteal vein, as described by Tuveri M et al,[17] thereby making it impossible to completely surround the SSV with tumescent anesthesia. Also, the CPN runs surprisingly close to the SSV. These data suggest that extra care should be taken when performing EVA at the saphenopopliteal area.

The risk of damaging the TN and CPN might be reduced by placing the catheter tip at the portion of the SSV where it begins its dive into the popliteal fossa. During dissection, however, it was observed that at this point, especially in

thinner legs, the TN could still be close to the SSV. Also, in SSVs that had a more lateral course, the shortest distance between the SSV and the CPN was measured just distal from its dive into the popliteal fossa. Finally, this would also leave important tributaries near the SPJ untreated, and consequently, recurrence rates might rise. In our opinion, special emphasis must instead be placed on prudent tumescent anesthesia (cooling) near the SPJ.

Comparison of data with known literature and future research: In the literature, the SSV is also not considered to be a superficial vein.[18-22] However, we found that the dissected SSV penetrated the superficial fascia in the distal part of the lower leg; this contrasts with the findings of Caggiati et al[18] and Cavezzi et al[20] and is in accordance to the findings of Schweighofer et al.[21] Caggiati[23] argued that this might be due to the use of embalmed specimen. The wide variability of the course of the SSV and the location of the SPJ has been well described.[18-22] In accordance with the literature,[21, 22] multiple SPJs per specimen were observed in 20% of the specimens, and the SPJ was not the end of the SSV in most cases.

The relation between the SSV and the SN has been mentioned[2, 18, 21] as well as the presence of the deep fascia layer[18, 22] but neither had been quantified. The proximity of the SSV to the CPN[2] and the TN[18, 21, 22] was mentioned but as yet has also not clearly been quantified. The proximity of the SSV to surrounding nerves may have its origin in embryology, as the genesis of the SSV is induced by angioguiding nerves of the embryo.[22]

The use of the suggested safe zones in the clinic could increase the recurrence rate of EVA because this would necessarily leave many tributaries untreated. Therefore, presently a more detailed study is being performed on the anatomy of the SSV regarding the SPJ, tributaries, and duplications. Consequently, the traditional open surgical ligation should still be considered as the gold standard for SSV ablation.[1]

Regarding CASAM: Because the CASAM method relies on image adjustments and computer calculations, it is not 100% accurate. However, the CASAM method proved to be a great asset to visualize the complex anatomy and can be used in addition to conventional means of documenting anatomic data for surgical purposes. Furthermore, data acquired with CASAM were comparable to data gathered in a conventional way.

CONCLUSION

To define a safe zone for EVA of the SSV, the distance between the SSV and surrounding nerves as well as the presence of a fascia layer between the SSV and SN should be taken into account. Defining a safe zone proves to be more reliable when the most distal SPJ is used as a reference point rather than the tibia plateau.

The distal two-third of the SSV is a dangerous zone for EVA: the distance between the SSV and the SN is ≤1 mm in many legs, and no fascia layer is present between the SSV and the SN. The proximal one-third of the SSV is the best zone for EVA; the deep fascia layer between the SSV and the SN provides a natural barrier.

The region around the SPJ should be handled with extra care, because of many variations and the proximity to the TN and the CPN, it is a dangerous location for EVA of the SSV.

A protocol, based on these results would then be:

1. Locate the most distal SPJ (duplex scan).
2. Measure the distance to the lateral malleolus.
3. Introduce ablation device only in the proximal one-third of the latter distance. Take extra care in the saphenopopliteal area or follow the superficial part of the SSV instead of coagulating until the SPJ.

ACKNOWLEDGEMENTS

We acknowledge the work of Jorn de Vlieger who also contributed to this research. We also thank Yvonne Steinvoort for embalming and looking after the specimens used in this study.

REFERENCES

1) Enzler, M.A., van den Bos, R.R. A New Gold Standard for Varicose Vein Treatment? (2010) European Journal of Vascular and Endovascular Surgery, 39 (1), pp. 97-98.
2) McBride, K.D. Changing to endovenous treatment for varicose veins: How much more evidence is needed (2011) Surgeon, 9 (3), pp. 150-159.
3) Nordon, I.M., Hinchliffe, R.J., Brar, R., Moxey, P., Black, S.A., Thompson, M.M., Loftus, I.M. A prospective double-blind randomized controlled trial of radiofrequency versus laser treatment of the great saphenous vein in patients with varicose veins (2011) Annals of Surgery, 254 (6), pp. 876-881.
4) Nesbitt, C., Eifell, R.K., Coyne, P., Badri, H., Bhattacharya, V., Stansby, G. Endovenous ablation (radiofrequency and laser) and foam sclerotherapy versus conventional surgery for great saphenous vein varices (2011) Cochrane Database Syst Rev, 10 (10), pp. CD005624.
5) Rasmussen, L.H., Lawaetz, M., Bjoern, L., Vennits, B., Blemings, A., Eklof, B. Randomized clinical trial comparing endovenous laser ablation, radiofrequency ablation, foam sclerotherapy and surgical stripping for great saphenous varicose veins (2011) British Journal of Surgery, 98 (8), pp. 1079-1087.
6) Kontothanassis, D., Di Mitri, R., Ferrari Ruffino, S., Zambrini, E., Camporese, G., Gerard, J.L., Labropoulos, N. Endovenous laser treatment of the small saphenous vein (2009) Journal of Vascular Surgery, 49 (4), pp. 973-979.e1.
7) Park, S.J., Yim, S.B., Cha, D.W., Kim, S.C., Lee, S.H. Endovenous laser treatment of the small saphenous vein with a 980-nm diode laser: Early results (2008) Dermatologic Surgery, 34 (4), pp. 517-524.
8) Agus, G.B., Mancini, S., Magi, G., Santuari, D., Mondani, P., Brambilla, S., Mancini, S., Botta, G., Spartera, C., Mastromarino, A., Magi, G., Antonelli, P., Nardoiani, V., D'Amico, D., Kontothanassis, D., Scuro, A., Spreafico, G., Baccaglini, U., Salfi, R., Monaca, V., Vinciguerra, D., Amicucci, G., De Donato, G., Plati, S., Farina, M., Pignatelli, F. The first 1000 cases of Italian Endovenous-laser Working Group (IEWG). Rationale, and long-term outcomes for the 1999-2003 period (2006) International Angiology, 25 (2), pp. 209-215.
9) Gibson, K.D., Ferris, B.L., Pepper, D. Endovenous Laser Treatment of Varicose Veins (2007) Surgical Clinics of North America, 87 (5), pp. 1253-1265.
10) Atkin, G.K., Round, T., Vattipally, V.R., Das, S.K.Common peroneal nerve injury as a complication of short saphenous vein surgery (2007) Phlebology, 22 (1), pp. 3-7.

11) Van Groenendael, L., Flinkenflögel, L., Van Der Vliet, J.A., Roovers, E.A., Van Sterkenburg, S.M.M., Reijnen, M.M.P.J. Conventional surgery and endovenous laser ablation of recurrent varicose veins of the small saphenous vein: A retrospective clinical comparison and assessment of patient satisfaction (2010) Phlebology, 25 (3), pp. 151-157.
12) Caggiati, A., Bergan, J.J., Gloviczki, P., Jantet, G., Wendell-Smith, C.P., Partsch, H. Nomenclature of the veins of the lower limbs: An international interdisciplinary consensus statement (2002) Journal of Vascular Surgery, 36 (2), pp. 416-422.
13) Kerver, A.L.A., Kleinrensink, G.J., Smit, N.N., Rabbelier, S., Sedee, B.M.W., Botha, C.P. Web-based 'computer assisted surgical anatomy mapping' (2010) Proceedings from the Webist 2010: Sixth International Conference on Web Information Systems and Technologies.
14) EffectMatrix Software Studio Magic Morph 1.95. http://www.effectmatrix.com/morphing/
15) Adobe Photoshop CS5. Cited 3 times. http://www.adobe.com/nl/products/photoshop/photoshop/
16) Beale, R.J., Mavor, A.I.D., Gough, M.J. Heat dissipation during endovenous laser treatment of varicose veins - Is there a risk of nerve injury? (2006) Phlebology, 21 (1), pp. 32-35.
17) Tuveri, M., Borsezio, V., Argiolas, R., Medas, F., Tuveri, A. Ultrasonographic venous anatomy at the popliteal fossa in relation to tibial nerve course in normal and varicose limbs. (2009) Chirurgia italiana, 61 (2), pp. 171-177.
18) Caggiati, A. Fascial relationships of the short saphenous vein (2001) Journal of Vascular Surgery, 34 (2), pp. 241-246.
19) Warwick, R., Williams, P.L. (1973) Gray's Anatomy, p. 705.
20) Cavezzi, A., Labropoulos, N., Partsch, H., Ricci, S., Caggiati, A., Myers, K., Nicolaides, A., Smith, P.C. Duplex ultrasound investigation of the veins in chronic venous disease of the lower limbs - UIP consensus document. Part II. Anatomy (2006) European Journal of Vascular and Endovascular Surgery, 31 (3), pp. 288-299.
21) Schweighofer, G., Mühlberger, D., Brenner, E. The anatomy of the small saphenous vein: Fascial and neural relations, saphenofemoral junction, and valves (2010) Journal of Vascular Surgery, 51 (4), pp. 982-989.
22) Uhl, J.-F., Gillot, C. Embryology and three-dimensional anatomy of the superficial venous system of the lower limbs (2007) Phlebology, 22 (5), pp. 194-206.
23) Caggiati, A. Regarding "the anatomy of the small saphenous vein: Fascial and neural relations, saphenofemoral junction, and valves" (2010) Journal of Vascular Surgery, 52 (5), pp. 1428-1429.

01000011 01101000 01100001 01110000
01110100 01100101 01110010 00100000
00110010 00101110 00110110 00001010

Chapter 2.7

An anatomical study of the ECRL and ECRB: Feasibility of developing a preoperative test for evaluating the strength of the individual wrist extensors.

Kerver, A.L.A., Carati, L., Eilers, P.H.C., Langezaal, A.C., Kleinrensink, G.J., Walbeehm, E.T.

J Plas Reconstr Aesthet Surg. 2013 Jan 29.

ABSTRACT

Background: Tendon transfers are essential for reconstruction of hand function in tetraplegic patients. To transfer the extensor carpi radialis longus (ECRL), the extensor carpi radialis brevis (ECRB) has to be sufficiently strong. However, there is currently no reliable clinical test to individually analyse both muscles. In order to develop a reliable preoperative clinical test, the anatomy of the muscle (innervation) areas of ECRB, ECRL and brachio-radialis (BR) was examined.

Methods: In 20 arms, the ECRB, ECRL and BR were dissected and localised. Subsequently, muscle-innervation points were mapped and categorised. A novel method, computer-assisted surgical anatomy mapping (CASAM), was used to visualise muscle areas and innervation points in a computed arm with average dimensions.

Results: For both ECRL and ECRB a 100% area could be identified, a specific area in the computed average arm in which the muscle was present for all 20 arms. For the ECRL, this area was situated at 16% of the distance between the lateral epicondyle and the deltoid muscle insertion. The ECRB 100% area was 5 times bigger than that of the ECRL and was located at 40% of the distance between the lateral epicondyle and the radial styloid process. The ECRL and BR showed one to three innervation points, the ECRB one to four. In 47% of the cases, there was a combined nerve branch innervating both the ECRL and the ECRB.

Conclusions: It is feasible to develop a preoperative test; the 100% areas can be used for needle electromyography (EMG) or local anaesthetic muscle injections.

INTRODUCTION

Damage to the cervical spinal cord represents 60% of all spinal cord injuries.[1] Tetraplegic patients become dependent on external help for daily activities and both productivity and quality of life are lowered significantly.[2,3] The loss of upper limb function can be partially restored with tendon transfers, especially in C4–C6 lesions.[2-4] In these patients, an extensor carpi radialis brevis (ECRB) with motor strength M4 allows for an extensor carpi radialis longus (ECRL) tendon transfer to regain active finger flexion for cylinder grip or to restore thumb opposition.[4,5] However, if the ECRL is transferred without a sufficiently strong remaining ECRB the transferred ECRL will overcome the weaker ECRB and force the wrist in flexion on gripping, decreasing the strength of the grip.

The International Classification for Surgery of the Hand in Tetraplegia (ICSHT) was developed to identify the number of muscles below the elbow with an M4 motor grade or more. In complete spinal cord lesions, it is possible to conclude that if the pronator teres muscle is M4, the ECRB should be M4 also. However, if the pronator teres muscle is not strong enough it is difficult to clinically predict the individual strength of ECRB as both ECRL and ECRB have the same function in wrist movement.

In incomplete spinal cord lesions, muscle function does not follow a specific pattern and it usually is difficult to assign an ICSHT level to these patients.[6,7] Therefore, it is particularly important to evaluate the to-be-transferred ECRL. Moreover, in these patients functional outcome after tendon transfer is unpredictable; if the ECRL muscle shows evidence of abnormal regeneration during needle electromyography (EMG), it will probably perform poorly if transferred.[6]

Previously, several tests have been proposed to individually evaluate the function of ECRL and ECRB but these tests were either invasive (Moberg and House[8, 9]) or unreliable (Mohammed and Rothwell[4]).

In order to develop such a reliable test, knowledge of the anatomical relationship of the individual muscles in the forearm and their motor-innervation points is the first step. Although described in mainstream anatomy textbooks,[5,10] the present study provides a new way of visualising data of multiple specimens in one combined image using computer assisted surgical anatomy mapping (CASAM).[11-13]

METHODS

General

In this study 20 arms (11 left and 9 right) from 20 embalmed human bodies, flushed with Anubifix,[14] were used. The borders of the ECRB, ECRL and brachioradialis (BR) were dissected and marked with pins.

'Bony' landmarks were assessed and used as a reference for measurements. In order to define the dimensions of each arm, 'non-bony' or 'shape-defining' landmarks were calculated from bony landmarks and positioned on the outer contour of each arm (Figure 1). Reproducibility of the landmarks was tested and the landmarks were assessed by two authors.

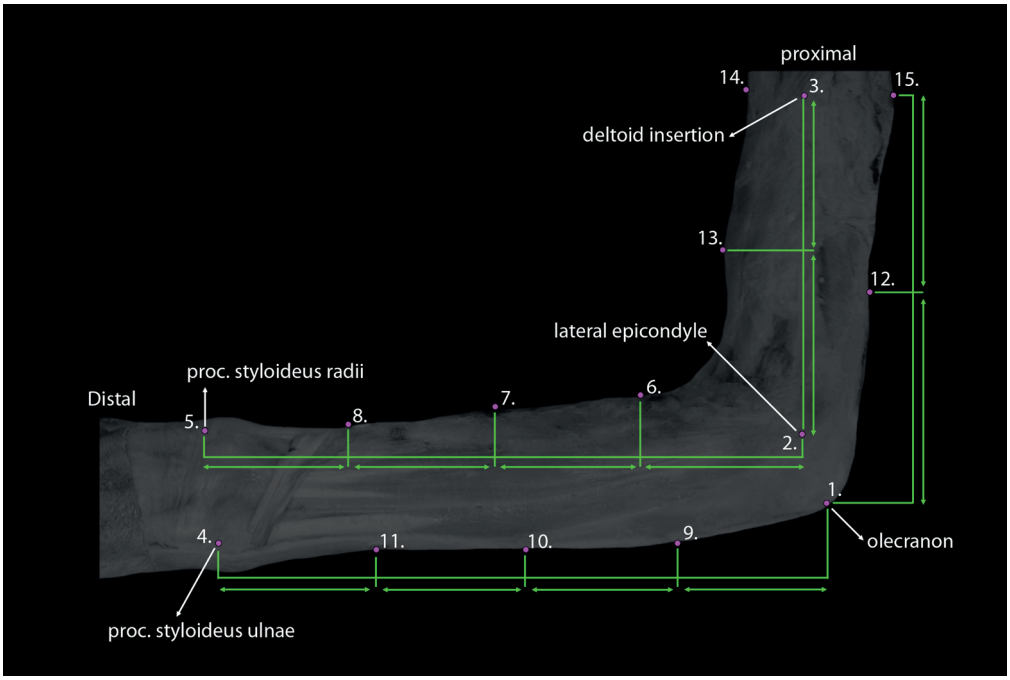

Figure 1. Landmarks.
Bony landmarks: the most lateral and proximal part of the olecranon (1), the lateral epicondyle (2), the deltoid muscle insertion on the humerus (3), the ulnar styloid process (4) and the radial styloid process (5). Non-bony or shape defining landmarks: at one fourth (6), halfway (7) and three fourth (8) between landmark 2 and 5. At one fourth (9), halfway (10) and three fourth (11) between landmark 1 and 4. Halfway between landmark 1 and 3 (12) and halfway between landmark 2 and 3 (13). Two landmarks were placed on the most medial (14) and the most lateral (15) edge of the upper arm at the level of landmark 3.

Each arm was photographed using a Nikon D60 with a Sigma 50 mm 1:2.6 DG macro lens. The arm was positioned in 90° flexion. A 100-mm reference ruler was placed next to the arm. Raw images were loaded into Photoshop CS-4.[15] Digital measurements were taken using the 'ruler tool' and calibrated with the ruler.

General assessments: The distance between the lateral epicondyle and the radial styloid process was measured to define the length of the forearm.

Computer-Assisted Surgical Anatomy Mapping (CASAM)

CASAM[11] is a new method to compare and evaluate the anatomy of multiple specimens. First, using the landmarks (Figure 1) the shape of each photographed specimen is defined and an average shape is calculated from all 20 specimens. With MagicMorph,[16] each specimen in each original picture is reshaped/warped to match the calculated average shape. MagicMorph uses a thin plate spline transformation as a warping algorithm. Then, as all reshaped specimens have the same average shape, the anatomy can be compared. In Photoshop CS-4, the reshaped photographs can be loaded into stack and the relevant anatomy can be highlighted. Finally, renditions can be made to simultaneously visualise the anatomy of multiple specimen in one picture (e.g., the location of the ECRL of 20 specimens shown in one computed averagely shaped arm).

In all 20 warped specimens, the ECRB, ECRL and BR were highlighted and data on the muscle locations of all 20 specimens were compiled into one image. To visualise the variance in anatomy three zones were computed:

1) 100% area. In this area of the average arm the muscle is present in all 20 specimens. Thus, in each individual specimen, the muscle can be found within the 100% area.
2) 50% area. In this area the muscle is present in 10–19 of the 20 specimens. Thus, in a specific specimen, there is a 50–95% chance that the muscle can be found in the 50% area.
3) General area of distribution. In this area the muscle was present in one to nine of the 20 specimens.

Description on the course of the ECRB, ECRL and BR

CASAM is a novel method of anatomy mapping and therefore the data needed to be evaluated in a more conventional way. Measurements were taken every 10 mm from a virtual line between the lateral epicondyle and the radial styloid process (Figures 2 and 3).

Statistical Package for Social Sciences (SPSS) 17 was used to perform basic statistical analysis of the data and to produce graphs:

1) Tables were standardised on the x-axis for the length of the forearm and on the y-axis for the length of the arm (deltoid muscle insertion and the lateral epicondyle).
2) The x- and y-axes were divided into a grid of small squares. To squares inside the region where a muscle is located, the number 1 is added for each specimen. The result is a grid of counts, each showing how many of the individual muscles cover the corresponding squares.
3) A smoothing procedure was applied to the histogram to reduce the influence of sampling variation.17

The statistical procedure is described for one way of standardisation. The principle is the same for the width of the muscles, except no standardisation on the y-axis was applied.

Innervation

The innervating nerves of the ECRB, ECRL and BR were dissected. The radial nerve was localised and the muscular branches, the superficial radial branch and the posterior interosseous nerves were dissected. The (extramuscular-) motor-innervation points of each muscle were marked with pins, digitally mapped and projected on the computed, average-sized arm using CASAM. Finally, the branches innervating the muscles were categorised.

RESULTS

General measurements

Collective intrinsic measurements and locations computed with CASAM were expressed as a percentage of either the length of the (upper-) arm or the forearm. The arm is defined as a scale ranging from the lateral epicondyle (0%) towards the deltoid muscle insertion (100%). The forearm is defined as a scale ranging from the lateral epicondyle (0%) towards the radial styloid process (100%).

The mean distance between the lateral epicondyle and the radial styloid process is 24.92 cm (range 21.5–27.5 cm).

Measurements on the course of the ECRB, ECRL and BR

The anatomical localisation of the ECRB, ECRL and BR is highly variable (Figures 2 and 4).

Brachio-radialis

In the CASAM assessment, there is no area in which all BR muscles of all 20 specimens are present. The 50% area and the general area of distribution show much overlap distally with the ECRL. The main direction of variation is in the width of the muscle (Figure 4). Further, in the SPSS assessment the BR shows the most variation in anatomical localisation (Figure 2.2). In a maximum of 80% of the arms, the muscle is present at the same location. This area is located near

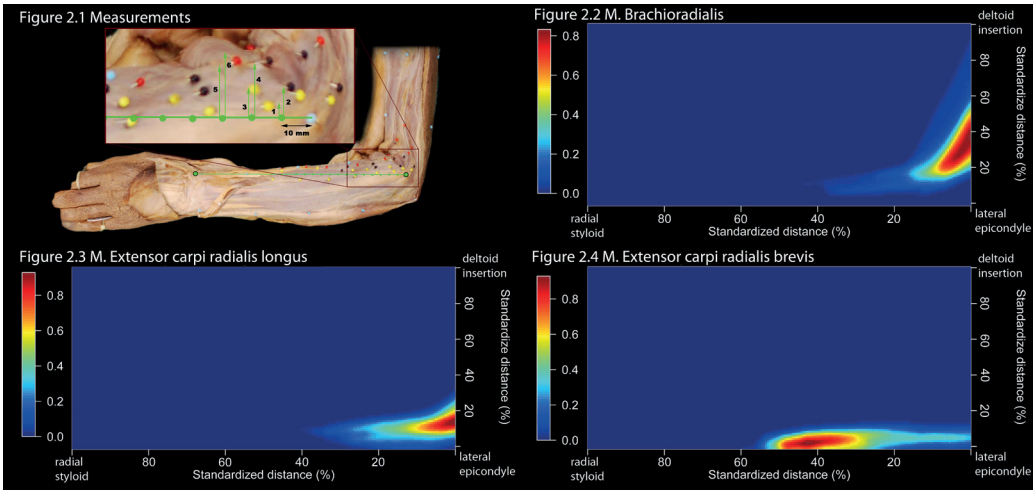

Figure 1. The location of the BR, ECRL and ECRB.
2.1 Measurements taken. Landmarks and axes used. Red pins: borders of the BR. Red pins: borders of the ECRL. Yellow pins: borders of the ECRB. 1: to the nearest part of the ECRB. 2: to the furthest part of the ECRB. 3: to the nearest part of the ECRL. 4: to the furthest part of the ECRL. 5: to the nearest part of the BR. 6: to the furthest part of the BR. 2.2 the location of the BR in all 20 arms. Dark red depicts the location in which the BR was present in 80% of the arms. Dark blue depicts the location in which the muscle was not present. 2.3 the location of the ECRL. Dark red depicts the location in which the ECRL was present in 100% of the arms. Dark blue depicts the location in which the muscle was not present. 2.4 the location of the ECRB. Dark red depicts the location in which the ECRB was present in 100% of the arms. Dark blue depicts the location in which the muscle was not present. Figures 2.2, 2.3 and 2.4 were standardised on the x-axis for the length of the lower arm and on the y-axis for the length of the upper arm. X-axis: the distance between the lateral epicondyle (0) and the radial styloid process (100). Y-axis: the distance between the lateral epicondyle (0) and the m. deltoid insertion on the humerus (100).

the origin of the BR at a level of 45% of the length of the arm. In all 20 arms, the width of the BR is 2.0–8.2 cm. The BR is widest near its origin (Figure 3.2).

Extensor carpi radialis longus

In the CASAM assessment the ECRL only has a small area in which the muscle is always present, the 100% area (Figure 4). This area is situated at a level of 16% of the arm, close to the origin of the muscle (Figure 5). The 50% area is larger but proximally shows much overlap with the general area of distribution of the BR. Distally the 50% area shows overlap with the general area of distribution of the ECRB (Figure 4). In the SPSS assessment the ECRL is also relatively variable (Figure 2.3). An area can be identified in which the muscle is present in all 20 arms. This 100% area is located near the origin of the ECRL at a level of 17% of the arm. The main direction of variation is in the length of the ECRL. In all 20 arms the muscle is 1.1–4.0 cm wide. The ECRL is widest near its origin (Figure 3.3).

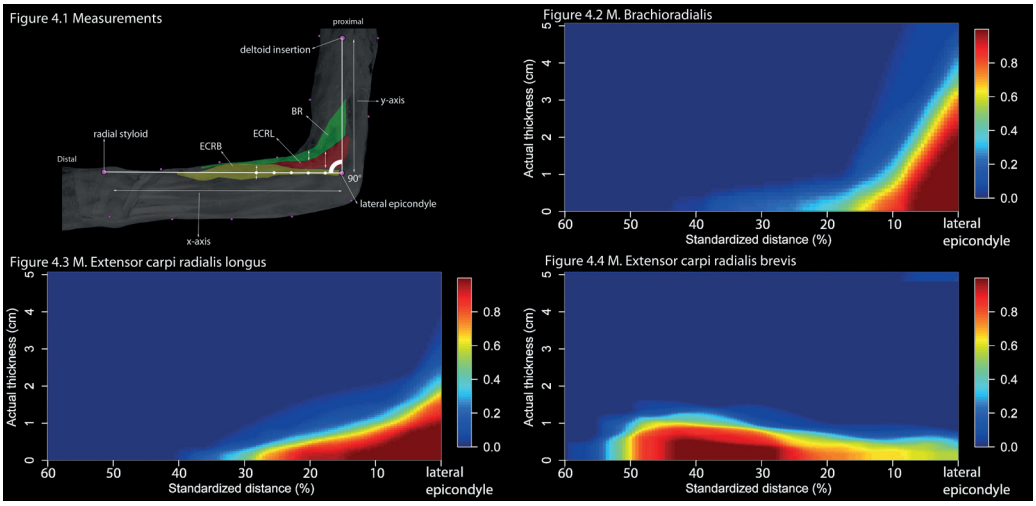

Figure 3.The width of the BR, ECRL and ECRB.
3.1, measurements taken, landmarks used for both x-axis and y-axis. 3.2, the width of the BR. 3.3 the width of the ECRL. 3.4, the width of the ECRB. X-axis: the distance between the lateral epicondyle (0) and the radial styloid process (100). Y-axis: the actual thickness of the muscles. Dark red depicts 80% (in 3.2) or 100% (in 3.3 and 3.4) of all muscles. Dark blue depicts 0% of all muscles.

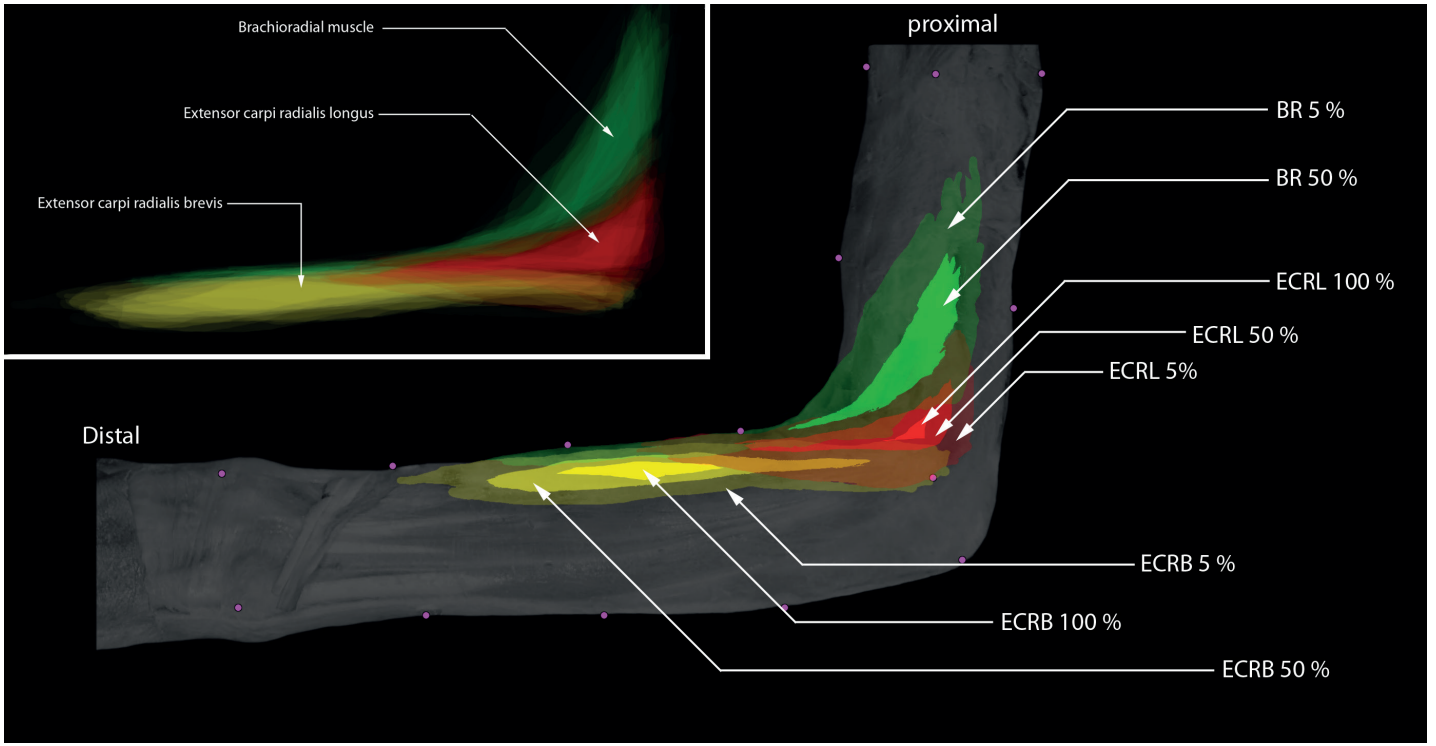

Figure 4. Spreading of the BR, ECRL and ECRB.
Original overlay of all muscles (top left) and subsequent renditions of the 5%, 50% and 100% area of spreading of the BR, ECRL and ECRB (N = 20). Purple dots: landmarks used for warping.

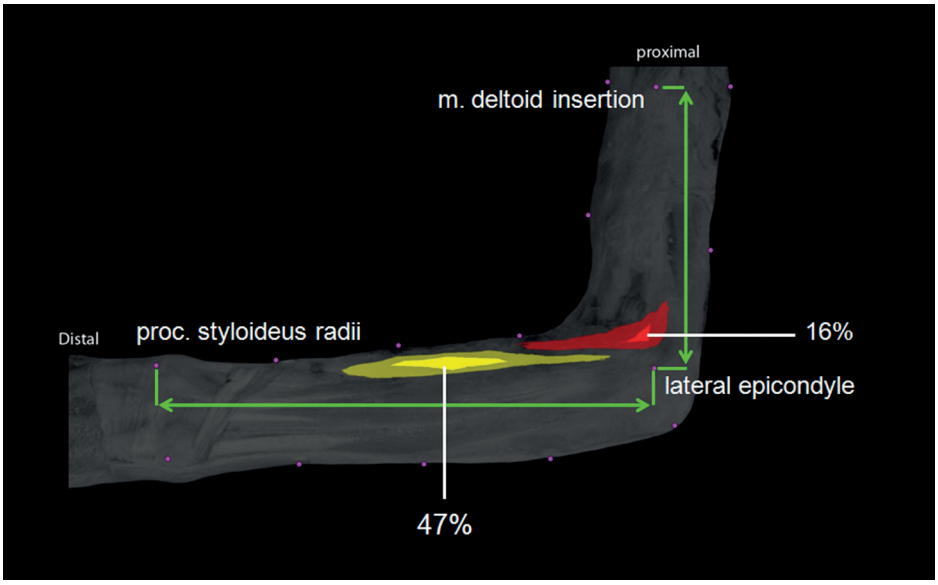

Figure 5.The 100% and 50% area of spreading of the ECRL and ECRB.
Purple dots: landmarks. Red: extensor carpi radialis longus. Yellow: extensor carpi radialis brevis.

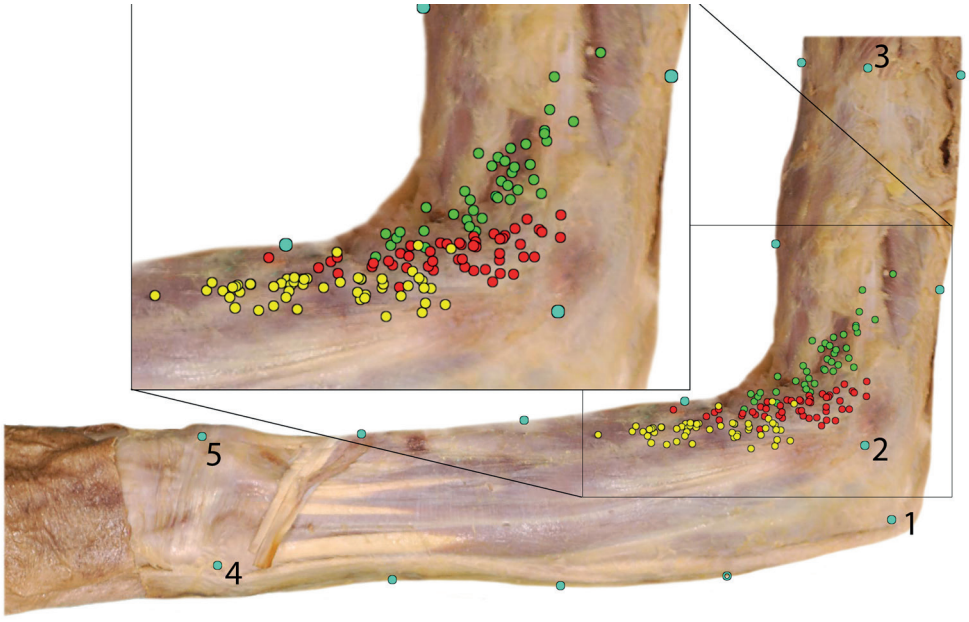

Figure 6. Spreading of the innervations of the BR, ECRL and ECRB.
Blue dots: landmarks. Green dots: motor innervations of the BR (N = 40). Red dots: motor innervations of the ECRL (N = 49). Yellow dots: motor innervations of the ECRB (N = 49).

Extensor carpi radialis brevis

In the CASAM assessment, the general variation in the localisation of the ECRB origin is relatively low. The 20 dissected muscles show a large area in which the muscle is always present, the 100% area (Figure 4). This area is situated at a level of 47% of the forearm. The 100% area of the ECRB is 4.8 times bigger than the 100% area of the ECRL. The area in which the muscle is present in 50% is not much larger than the 100% area, but proximally it shows an overlap with the general area of distribution of the ECRL (Figure 4). With SPSS, the ECRB also is the least variable and an area can be identified in which the muscle is located in all 20 specimens (Figure 2.4). This area is found at a level of 45% of the forearm and is substantially larger than the 100% area of the ECRL (Figure 2). The main direction of variation is in the length of the muscle. The widest part of the muscle is located at a level of 45% of the forearm. The ECRB shows the least variation in width, with a range of 0.6–1.6 cm at the widest part of the muscle (Figure 3.4).

Innervation

The BR on average had 2.0 (range 1–3) extra-muscular motor-innervation points, which were consistently located close to the 50% area of the BR. The ECRL had 2.5 (range 2–3) motor-innervation points, which were located distal to the 100% area of the ECRL. The ECRB had 2.45 (range 2–4) motor-innervation points, which were located proximal to the 100% area of the ECRB.

The highest density of motor-innervation points for ECRL and ECRB together is located at a level of 16% of the forearm. The average level of motor-innervation points for the ECRB is located at a level of 24% of the forearm and for the ECRL at a level of 10% of the forearm (Figure 6). The motor-innervation points were categorised in two main variations (Figure 7):

1) Variations with a combined branch which innervates both the ECRL and the ECRB (N = 9). The combined branch originates from the deep branch of the radial nerve (RN), or the posterior interosseous nerve (PIN) or the superficial radial nerve (SRN).
2) Variations without a combined branch (N = 10).

The BR has one or two direct innervations originating from the RN and in addition to a possible combined branch, the ECRL has one or two direct innervations from the RN.

If a combined branch originates from the RN or SRN, the ECRB is additionally innervated by one or two branches from the SRN. If the combined branch originates from the PIN, the ECRB is additionally innervated by one, two or three branches from the PIN. If no combined branch is present, the ECRB is in innervated by both the SRN and PIN (N = 8) or only by the SRN (N = 2).

One arm could not be categorised as the origin of one of the branches to the ECRL could not be located.

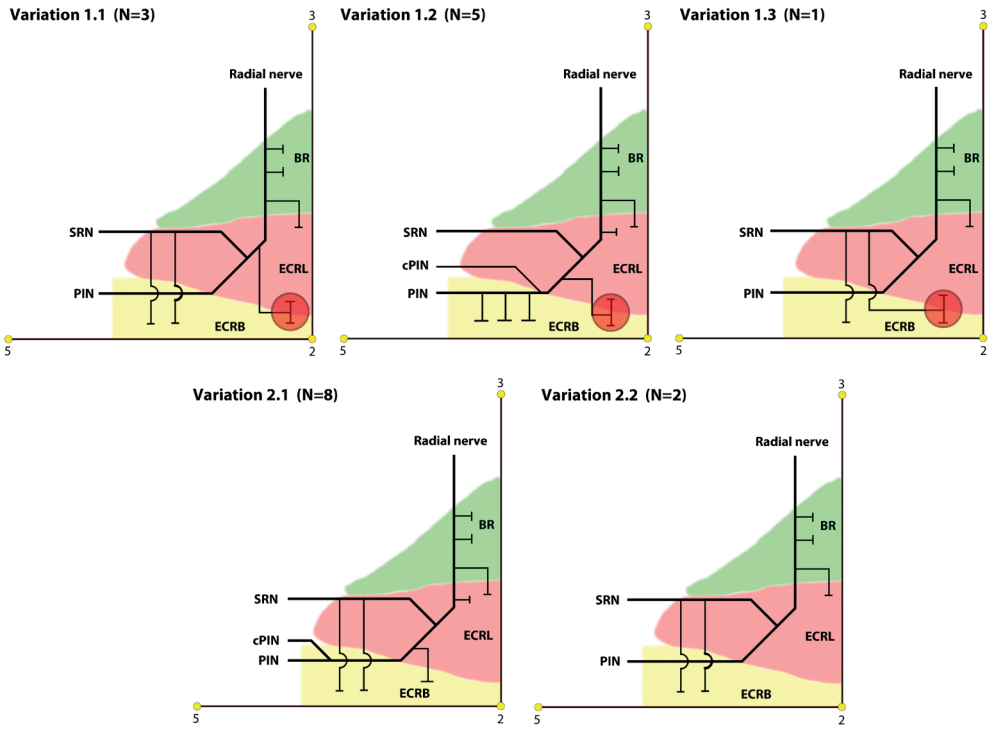

Figure 7. Categorisation of innervations of the BR, ECRL and ECRB.
Yellow dots: landmarks used, 2 = lateral epicondyle, 3 = deltoid muscle insertion, 5 = radial styloid process. SRN: superficial radial nerve, PIN: posterior interosseous nerve. cPIN: concomitant posterior interosseous nerve. Variation 1 (N = 9): combined branch: innverating both the ECRL and ECRB. It originates either from the deep branch of the radial nerve (1.1), the posterior interosseous nerve (1.2) or the superficial radial nerve (1.3). ECRB: one or two direct innervations from the superior radial nerve (1.1, 1.3) or one to three innervations from the posterior interosseous nerve (1.2). Variation 2 (N = 10): No combined branch to the ECRL and ECRB is present. ECRB: one or two direct innervations from the posterior interosseous nerve and two or three direct innervations from the superficial radial nerve (2.1) or only two or three direct innervations from the superficial radial nerve (2.2).

DISCUSSION

For a successful ECRL tendon transfer, both the ECRL and the ECRB need to be sufficiently strong (M4–M5). At present, no reliable clinical test is available to independently test the function of the ECRB and ECRL. Knowledge of the anatomical relationship of the individual muscles is a first step in the development of a reliable clinical test.

Location of muscles

As described in the literature,[10, 18-20] considerable variation is found in the anatomy of the radial wrist extensors. The ECRB, ECRL and BR of all 20 specimens show much overlap. Therefore, non-invasive identification of muscle bellies is difficult and complicates the development of a clinical test. Nevertheless, two distinct 100% areas are identified for the ECRB and ECRL. In such an area, the respective muscle is found at that location in all 20 specimens (100%) and has no overlap with any other muscles. For the ECRB, this 100% area is situated at a level of 47% of the forearm (Figure 5). This corresponds to the needle-insertion location for individual EMG of the ECRB proposed by Riek et al. (47.58% of forearm length).[21]

Similarly, for the ECRL the 100% area is located near its origin at a level of 16% of the arm (Figure 5). This area does not correspond to needle-insertion locations found in the literature.[21, 22]

Further, both ECRB and ECRL are widest near their respective 100% areas. Clinically, these findings allow for non-invasive identification and use in the clinical testing of both muscles.

The 100% area of the ECRB is 4.8 times bigger when compared to the 100% area of the ECRL. In theory, it would be easier to identify the ECRB and use it for a clinical test. However, a drawback of this study is that healthy, non-tetraplegic arms were used. This poses two problems for extrapolation to clinical practice. Afflicted muscles of tetraplegic patients are likely to be atrophic upon clinical presentation and their anatomy might consequently differ from the anatomy described. As the 100% area of the ECRL is much closer to its origin than the 100% area of the ECRB, there will be less variation in the 100% area of the ECRL between healthy and atrophic muscles.

The small width of the ECRB (0.6–1.6 cm) and ECRL (1.1–4.0 cm) does not allow for surface EMG, especially since surface EMG is prone to have crosstalk from more distant sources.[23, 24] Further, the amount of overlap between the ECRB and ECRL could cause considerable crosstalk and therefore lead to inaccurate

test results. Calder et al.[25] however showed that surface EMG results of the radial wrist extensors are more reliable than needle EMG though they did not distinguish between ECRB and ECRL.

Motor-innervation points

The number of (extramuscular) motor-innervation points for ECRB and ECRL varies widely in the literature. We found that the ECRL had two or three motor-innervation points, in contrast to one or two[26] or on average 3.8 motor innvervations.[27] The ECRB had two to four motor-innervation points; this contrasts with findings of Nayak et al. (one motor innervation)[5] and is more in accordance with El-Din Safwat et al. (two to five motor innervations)[28] and Abrams et al. (on average 3.4 motor innervations).[27]

The wide variability of the origin of ECRB branches has been well described. In accordance with current literature,[5, 26, 27] we found that the ECRB can be innervated by the RN, PIN and/or SRN.

However, we also found a singular combined branch innervating both ECRB and ECRL, present in 45% of the specimens. This combined branch might affect test results when the ECRL is injected with a local anaesthetic; due to diffusion of the local anaesthetic the entire combined branch, and therefore also the (proximal) branch innervating the ECRB, might be affected. Succeeding wrist function tests might therefore give lower results in 45% of patients. In local anaesthetic nerve block of the ECRL branch,[29] the combined branch might be missed resulting in incomplete paralysis of the ECRL, or if the combined branch is effectively paralysed part of the ECRB will be paralysed also.

The highest density of motor-innervation points for ECRL and ECRB together is located at a level of 16% of the forearm, which correlates to the site most used for needle EMG of the radial wrist extensors: 4 cm distal to the lateral epicondyle = 16% of the average forearm length.[22]

The location of motor innervations of ECRB and ECRL showed overlap. This overlap might provoke crosstalk in surface EMG measurements. Further in local anaesthetic ECRL nerve blocks,[29] some branches to the ECRB might be affect ed.

Motor innervations of the ECRB were located proximal to the 100% area, whilst those of the ECRL were located distally to its respective 100% area. Although still controversial, functional electrical stimulation has been used to enhance recovery in central nerve lesions. Popovic et al. stated that the efficiency of intramuscular electrical stimulation is reduced when electrodes are placed further away from the motor-innervation points of the muscle.[30] As most motor-innervation points of the ECRB and ECRL are not located near their respective

100% areas, the 100% areas should not be used for electrode placement. Instead, the electrodes should be placed at the level of 24% and 10% of the length of the forearm for the ECRB and the ECRL, respectively.

CONCLUSION

Local anaesthetic muscle injection: analogous to the preoperative testing with Marcaïne of brachialis and BR muscles in biceps to triceps transfers. [31, 32] Both ECRB and ECRL have a 100% area that can be used for local anaesthetic muscle injection. As the tendon of the ECRL is usually transferred, the individual function of the ECRB determines the postoperation wrist extension. After injecting the ECRL, the individual function of the ECRB can be tested. However, the combined branch should be taken into account as the local anaesthetic might diffuse to the ECRB branch and affect succeeding test results.

Local anaesthetic nerve block of the ECRL branch: as proposed by Genet et al. [29] Both the combined branch present in 45% of the specimens and the overlap between motor-innervation points of ECRB and ECRL will influence the outcome of succeeding function tests of the ECRB.

Surface EMG: analogous to the muscle activity assessment of the vastus intermedius.[33, 34] Anatomically, it is not feasible to individually assess motor function of ECRB and ECRL using surface EMG.

Needle EMG: Most literature on needle EMG indicates that it is not possible to differentiate between ECRB and ECRL.[25, 35] However, the distinct 100% areas for the ECRB (47% of the length of the forearm) and ECRL (16% of the length of the (upper-) arm) found in this study suggest it is. These areas allow for accurate needle placement in the intended muscle and thus the individual function of ECRB and ECRL can be examined directly.

ACKNOWLEDGEMENTS

The authors would like to thank Alex Poublon and Robert Dijkman who contributed to this study.

REFERENCES

1) Lamb, D.W., Chan, K.M. Surgical reconstruction of the upper limb in traumatic tetraplegia. A review of 41 patients (1983) Journal of Bone and Joint Surgery - Series B, 65 (3), pp. 291-298.
2) Cizmar, I., Zalesak, B., Pilny, J., Drac, P., Fialova, J. Possible restorations of the upper extremity motion in tetraplegic patients - 5-year clinical experience. (2006) Biomedical papers of the Medical Faculty of the University Palacký, Olomouc, Czechoslovakia, 150 (2), pp. 313-319.
3) Freehafer, A.A. Gaining independence in tetraplegia: Cleveland technique (1998) Clinical Orthopaedics and Related Research, (355), pp. 282-289.
4) Mohammed, K.D., Rothwell, A.G., Sinclair, S.W., Willems, S.M., Bean, A.R. Upper-limb surgery for tetraplegia (1992) Journal of Bone and Joint Surgery - Series B, 74 (6), pp. 873-879.
5) Nayak, S.R., Krishnamurthy, A., Prabhu, L.V., Rai, R., Ranade, A.V., Madhyastha, S. Anatomical variation of radial wrist extensor muscles: A study in cadavers (2008) Clinics, 63 (1), pp. 85-90.
6) Hentz, V.R., Leclercq, C. The Management of the Upper Limb in Incomplete Lesions of the Cervical Spinal Cord (2008) Hand Clinics, 24 (2), pp. 175-184.
7) Ditunno Jr., J.F., Cohen, M.E., Hauck, W.W., Jackson, A.B., Sipski, M.L. Recovery of upper-extremity strength in complete and incomplete tetraplegia: A multicenter study (2000) Archives of Physical Medicine and Rehabilitation, 81 (4), pp. 389-393.
8) Moberg, E. Surgical rehabilitation of the upper limb in tetraplegia (1990) Paraplegia, 28 (5), pp. 330-334.
9) Moberg, E. Surgical treatment for absent single hand grip and elbow extension in quadriplegia: principles and preliminary experience (1975) Journal of Bone and Joint Surgery - Series A, 57 (2), pp. 196-206.
10) William, P.L., Warwich, R., Dyson, M., Bannister, L.H. (1989) The Muscles of the Forearm. Gray's Anatomy, p. 622.
11) Kerver, A.L.A., Van Der Ham, A.C., Theeuwes, H.P., Eilers, P.H.C., Poublon, A.R., Kerver, A.J.H., Kleinrensink, G.-J. The surgical anatomy of the small saphenous vein and adjacent nerves in relation to endovenous thermal ablation (2012) Journal of Vascular Surgery, 56 (1), pp. 181-188.
12) Van Der Graaf, T., Verhagen, P.C.M.S., Kerver, A.L.A., Kleinrensink, G.-J. Surgical anatomy of the 10th and 11th intercostal, and subcostal nerves: Prevention of damage during Lumbotomy (2011) Journal of Urology, 186 (2), pp. 579-583.
13) Ten Berge, M.G., Yo, T.I., Kerver, A., De Smet, A.A.E.A., Kleinrensink, G.-J. Perforating veins: An anatomical approach to arteriovenous fistula performance in the forearm (2011) European Journal of Vascular and Endovascular Surgery, 42 (1), pp. 103-106.

14) http://anubifix.com/English.html
15) Adobe Corp. Adobe Photoshop CS-4
http://www.adobe.com/nl/products/photoshop/photoshop/
16) EffectMatrix Software Studio. Cited 1 time. Magic Morph 1.95
http://www.effectmatrix.com/morphing/
17) Eilers, P.H.C., Goeman, J.J. Enhancing scatterplots with smoothed densities (2004) Bioinformatics, 20 (5), pp. 623-628.
18) Caetano, F.M., Albertoni, M.W., Caetano, B.E., Perez, M.R. Anatomical study of insertions of the extensor carpi radialis longus and brevis (2004) Int J Morphol, 22, pp. 245-251.
19) Albright, J.A., Linburg, R.M. Common variations of the radial wrist extensors (1978) Journal of Hand Surgery, 3 (2), pp. 134-138.
20) MacAlister, A. Additional observations on muscular anomalies in human anatomy with a catalogue of the principal muscular variations hitherto published (third series) (1871) Trans Ir Acad Dublin, 25, pp. 101-102.
21) Riek, S., Carson, R.G., Wright, A. A new technique for the selective recording of extensor carpi radialis longus and brevis EMG (2000) Journal of Electromyography and Kinesiology, 10 (4), pp. 249-253.
22) Misra, U.K., Kalita, J. (1999) Clinical Neurophysiology.
23) Gerdle, B., Karlsson, S., Day, S., Djupsjöbacka, M. (1999) Acquisition, Processing and Analysis of the Surface Electromyogram. Modern Techniques in Neuroscience. Chapter 26, pp. 705-755.
24) Farina, D., Merletti, R., Indino, B., Graven-Nielsen, T. Surface EMG Crosstalk Evaluated from Experimental Recordings and Simulated Signals: Reflections on Crosstalk Interpretation, Quantification and Reduction (2004) Methods of Information in Medicine, 43 (1), pp. 30-35.
25) Perotto, A.O. (1994) Anatomical Guide for the Electromyographer: The Limbs and Trunk.
26) Ravichandiran, M., Ravichandiran, N., Ravichandiran, K., McKee, N.H., Richardson, D., Oliver, M., Agur, A.M. Neuromuscular partitioning in the extensor carpi radialis longus and brevis based on intramuscular nerve distribution patterns: A three-dimensional modeling study (2012) Clinical Anatomy, 25 (3), pp. 366-372.
27) Abrams, R.A., Ziets, R.J., Lieber, R.L., Botte, M.J. Anatomy of the radial nerve motor branches in the forearm (1997) Journal of Hand Surgery, 22 (2), pp. 232-237.
28) Safwat, M.D.E.-D., Abdel-Meguid, E.M. Distribution of terminal nerve entry points to the flexor and extensor groups of forearm muscles: An anatomical study (2007) Folia Morphologica, 66 (2), pp. 83-93.
29) Genet, F., Autret, K., Schnitzler, A., Lautridou, C., Bernuz, B., Denormandie, P., Allieu, Y., Parratte, B. Motor branch of extensor carpi radialis longus: Anatomic localization (2012) Archives of Physical Medicine and Rehabilitation, 93 (12), pp. 2309-2312.
30) Popovic, D., Gordon, T., Rafuse, V.F., Prochazka, A. Properties of implanted electrodes for functional electrical stimulation (1991) Annals of Biomedical Engineering, 19 (3), pp. 303-316.
31) Kozin, S.H., D'Addesi, L., Chafetz, R.S., Ashworth, S., Mulcahey, M.J. Biceps-to-Triceps Transfer for Elbow Extension in Persons With Tetraplegia (2010) Journal of Hand Surgery, 35 (6), pp. 968-975.

32) Endress, R.D., Hentz, V.R. Biceps-to-triceps transfer technique (2011) Journal of Hand Surgery, 36 (4), pp. 716-721.

33) Watanabe, K., Akima, H. Validity of surface electromyography for vastus intermedius muscle assessed by needle electromyography (2011) Journal of Neuroscience Methods, 198 (2), pp. 332-335.

34) Watanabe, K., Akima, H. Cross-talk from adjacent muscle has a negligible effect on surface electromyographic activity of vastus intermedius muscle during isometric contraction (2009) Journal of Electromyography and Kinesiology, 19 (4), pp. e280-e289.

35) Riek, S., Bawa, P. Recruitment of motor units in human forearm extensors (1992) Journal of Neurophysiology, 68 (1), pp. 100-108.

01000011 01101000 01100001 01110000
01110100 01100101 01110010 00100000
00110010 00101110 00110111 00001010

Chapter 2.8

Innervation mapping of the hind paw of the rat using Evans Blue extravasation, Optical Surface Mapping and CASAM.

S. Kambiz, M. Baas, L.S. Duraku, A.L. Kerver, A.H.J. Koning, E.T. Walbeehm, T.J.H. Ruigrok.

J Neurosci Methods. 2014 Apr 8.

ABSTRACT

Background: Although numerous studies investigate sensory regeneration and reinnervation of the hind paw of the rat after nerve damage, no comprehensive overview of its normal innervation is present in literature. The Evans Blue extravasation technique is a well-known technique to study patterns of skin innervation. This technique has been performed differently by various groups but was never used to study the entire skin innervation in rats' hind paw including all three branches of the sciatic nerve and the saphenous nerve in detail.

Methods: In this paper, we have used the Evans Blue extravasation technique to chart the skin areas innervated by the sural, peroneal, tibial and/or saphenous nerves, which together innervate the entire hind paw of the rat, and use a new technique to analyze the distribution, overlap and variability of the results. The technique is based on analysis of whole hind paws using Optical Surface Mapping (OSM) in combination with the Computer Assisted Surgical Anatomy Mapping (CASAM) technology.

Results: While the plantar hind paw is mainly innervated by the tibial nerve, the dorsal hind paw is supplied by the sural, peroneal and the saphenous nerve.

Comparison with existint methods: Although our results basically concur with the general nerve-specific innervation of the rat hind paw, they show considerable detail in their areas of overlap as well as in the amount of variability between animals.

Conclusions: These results will be invaluable to study and evaluate patterns of innervation and reinnervation of intact and damaged nerve fibers.

INTRODUCTION

The past decade has seen an increased interest in the patterns of skin innervation by individual nerves in both naïve and pathological situations, such as neuropathic pain and itch in humans as well as in animal models. The reason for this growing interest is the possibility to analyze different classes of sensory skin fibers for diagnostic purposes.[1, 2] The glabrous skin of rat's hind paw has become a commonly used tissue to investigate the pathological changes of sensory skin fibers, especially when examining sensory denervation and reinnervation after peripheral nerve injury [3-6].

In order to properly evaluate these studies it is crucial to understand the pattern of innervation by individual nerves and the areas of overlap found between separate nerves as well as to the intra-individual variability in these patterns, as they might vary in different pathological conditions.

Previous studies have mapped the innervation of rats' hind paw by a recognized technique called 'Evans Blue extravasation' [7-20]. After intravenous injection of the Evans Blue dye the peripheral nerve of interest is electrically stimulated to cause plasma extravasation, which will be visible as blue staining on the skin. Since plasma extravasation is caused by sympathetic nerve fibers, namely C-fibers [21, 22], this technique offers a valuable approach to study the innervation areas of C-fiber afferents in the skin. Indeed, both in normal and pathologic conditions the areas with extravasated dye have been shown to correspond with the cutaneous innervation area of the investigated nerve[23]. Although plasma extravasation has been used in multiple studies, it is mostly evaluated by either a translation of the staining pattern to a diagram or extraction of the dye from the skin sample. The translating technique is sufficient for a general localization of the extravasation, but as size and anatomy varies between rats and interpretations may vary between individuals, the translation to a diagram is always based on subjective interpretation, which may cause high variability in results[8, 13, 16]. Extracting the Evans Blue dye for photospectrometry is used when studying quantity of the dye[10, 12]. However, apart from increased vascular permeability, electric stimulation eventually may also cause vasodilatation, which enhances the blood flow and thereby increases the Evans Blue extravasation in the skin after electrical stimulation. Therefore, the results of innervation areas by extracting the dye could be overestimated. Moreover, when extracting the dye from the skin the localization of the dye is lost. This prevents a description of the overlap between extravasation areas or to provide an overview of the entire pattern of extravasation areas. Yet, although the Evans Blue extravasation is known to be

a valid method for visualizing skin innervation areas, there is no comprehensive study describing and quantifying the detailed innervation areas, overlap areas and variability of innervation patterns by the nerves that innervate the rat's hind paw.

The aim of the present study is to use a novel technique to describe and analyze the cutaneous region of the hind paw that is innervated by a particular nerve. This technique enables a merging of measures of localization, quantity, and overlap. This is accomplished by combining a standardized Evans Blue extravasation technique, Optical Surface Mapping (OSM) and computer-assisted surgical anatomy mapping (CASAM) technologies[24-26].

METHODS

Animals and anaesthesia

Experiments were performed on adult female Lewis rats (n=37). All experiments were approved by the Dutch Ethical Committee at Erasmus MC Rotterdam on Animal Welfare (DEC) and all procedures adhered to the European guidelines for the care and use of laboratory animals (Council Directive 86/6009/EEC). During the experiments 3 animals were excluded due to lack of extravasation after 10 minutes of stimulation. Possible reasons for the lack of extravasation could have been a potential break of the anodal or cathodal wire of the stimulation cuff. The final experimental group contained 28 rats, which were subjected to stimulation of either the tibial (n=7), sural (n=7), peroneal (n=7) or saphenous nerve (n=7). Six additional animals were used in a control study.

The animals were anesthetized with 3% isoflurane, weighted and subsequently the paw was depilated using depilatory-crème 'Veet' to acquire a clear image of the skin.

Surgical procedure

An incision was made on the lateral or medial side of the hind limb depending on the choice of nerve to be investigated. The sciatic branches were approached by a 4 cm incision over the intramuscular septum between the vastus lateralis and the biceps femoris muscles, whereas the saphenous nerve was exposed by a 5 cm incision over the inner thigh. Subsequently, the nerve of interest was microsurgically dissected from its environment and crushed proximal to the stimulation site in order to prevent central propagation of the stimulus[11, 16]. The surgical procedure and placement of the stimulation cuffs were performed under microscopic guidance (Zeiss OP-MI 6-SD; Carl Zeiss, Goettingen, Germany) to prevent damage to the nerve of interest and adjacent tissue.

Evans blue extravasation procedure

The nerve was inserted into a handmade silicone stimulation cuff (diam. 3 mm, length 6 mm) in which the anodal and cathodal electrode were embedded (Figure 1). These cuffs were developed to restrict stimulation of surrounding tissue. A solution of Evans Blue (2% EB solved in 0.9% saline, 4ml/kg body mass) was injected slowly into the tongue vein of the rat. Because of discrepancies noted in literature[11, 16, 20], we determined the optimal EB concentration in several trial experiments using subjective evaluation of the extravasation contrast.

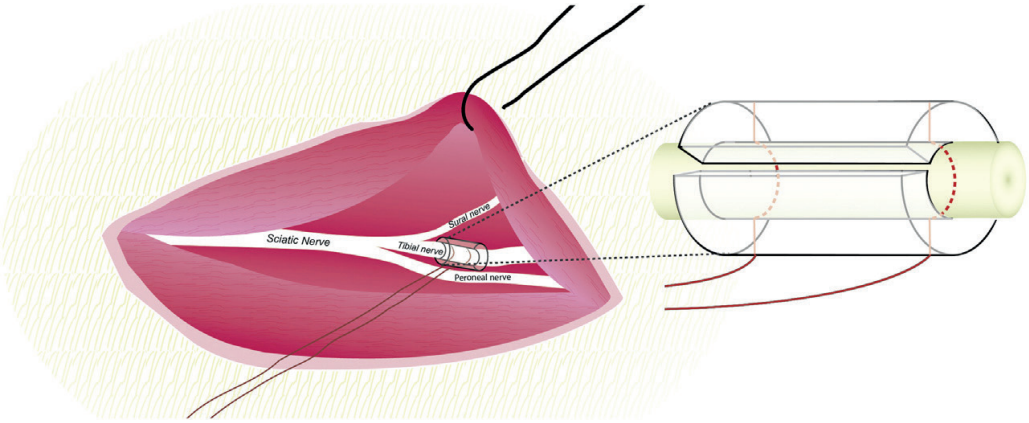

Figure 1. Cuff stimulation of nerves.
The stimulation cuff is placed over the nerve of interest (n. peroneous in this figure). Proximal to this site a crush lesion is made to avoid central transmission of the stimulation. The cuff is made of a silicone tube with both anodal (+) and cathodal (-) wires (visible in red) placed in it. The wire's insulation is removed in the cuff but remains intact outside the cuff to avoid stimulation of the surrounding structures.

Stimulation of the nerves started 5 minutes after the Evans Blue injection and lasted for 10 minutes using a continuous 10Hz, 0,5ms pulse width and 12mA current stimulation (Viking stimulator, Nicolet Biomedical IES405-2). Parameters were chosen based on trials and resembled those in literature[11, 12, 14]. During stimulation a slow blue coloring of a part of the hind paw was observed which was attributed to extravasation of the dye. Often, additional extravasation was seen for several minutes after terminating the stimulation[12]. Therefore, a 6-minute interval in which the animals were not handled was incorporated before sacrificing the animals by an overdose of pentobarbital (100mg/kg ip). Subsequently, the hind paws of all animals were cut at the level of the heel joint. Then the hind paws were fixed in an identical position using insect needles. Both

the tendons and the skin was pulled back to obtain a neutral hind paw position in animals; without flexion of the toes and enough web space between the toes for further imaging of the paw.

Control experiments

In three additional rats the correlation between the Evans Blue extravasation in the skin and the epidermal innervation was verified. In this animal the sciatic nerve was transected and ligated proximally to prevent regeneration of this nerve. Five weeks later, to ensure complete degeneration of the sciatic nerve, the Evans Blue experiment (see section 2.3) was performed by stimulation of the unaffected saphenous nerve, which resulted in extravasation of the medial side of the paw. After sacrificing the animal the paw was photographed. Using microscopical guidance, a superficial epidermal cut was made with a scalpel at the border of the extravasated and non-extravasated skin. A subsequent large skin biopsy of the transition area was taken, fixated in 2% paraformaldehyde-lysin-periodate (PLP) for 24 hours at 4˚C. The skin was embedded in 10% gelatine, hardened and sectioned at 40 µm with a freezing microtome. Sections were processed to visualize nerve fibers using PGP9.5 immunohistochemistry according to Duraku et al.[4, 5] Briefly, free-floating sections were rinsed in phosphate-buffered saline (PBS), pre-treated with hydrogen peroxide to reduce background, heated to 80˚C in citrate buffer (pH 8.75) to unmask immunoreactivity, incubated in rabbit anti-PGP9.5 (48 h at 4˚C in PBS with 0.5% Triton X-100; dilution 1/10.000: Enzo). After subsequent incubations with biotinylated goat-anti rabbit (1.5h at room temperature, RT; dilution 1/200: Biotine) and Vectastain ABC-Elite™ (1.5h at RT: Vector, Burlingame, CA) followed by additional signal amplification using biotin tyramide 27 for 12 minutes, the antigenic sites were revealed by diaminobenzidine (DAB) histochemistry. Sections were counterstained with thionine, which faded the epidermis blue as a result clear border between epidermis and dermis was visible. Finally, the slides were dehydrated and coverslipped with Permount (Fisher, Hampton, NH). The labelled nerve fiber terminals within the epidermial region of 64 mm² (400µm x 160µm) at the level of the epidermal cut were quantified using an Olympus BH microscope equipped with a Lucivid™ miniature monitor and Neurolucida™ software (MicroBrightField, Inc., Colchester, VT) with a 20x objective.

OSM and CASAM

An optical projection tomography (OPT) scanner [28, 29], which is a commonly used technique for investigating small specimens to visualize aspects of anatomy

and gene expression, was used to produce a 3D image of the surface of rats' hind paw in a novel procedure called Optical Surface Mapping (OSM). This method allows an accurate quantification of the paw in which even the areas between the toes can be taken in consideration in contrast to a mere 2D-analysis. Furthermore, we have developed a systematic way of recording and quantifying extravasation making use of a 360° view of the paw by combining the UV sensitive quality of the Evans Blue dye and the UV Filter in the Bioptics OPT scanner For determining statistical differences of the surface areas, the one way-ANOVA with a Tukey post hoc test was used for intergroup comparisons to calculate the average staining in each group. Errors in variations were determined as standard error of the mean (SEM), and $p < 0.05$ was taken as significant.

In the CASAM analysis single pixels within the circumference of the landmarks were either assigned the label "stained" or "non-stained". Pixels with identical incidences (ranging from stained in 1 animal to stained in all 7 cases) were grouped and two way t-test with a Tukey post hoc test was used to determine the threshold for significance ($p<0.05$) between groups. Subsequently overlap was divined as groups of individual significantly "stained" pixels with no significant difference between the compared nerves. [28, 29] Subsequently, the variability in nerve innervations patterns between various individuals was assessed by applying the CASAM technology[30], which is a new anatomy mapping tool used in clinic to improve description of the variability of complex anatomical regions. Using the combination of Evans Blue extravasation, OSM and CASAM allows us to present, for the first time, an anatomically correct impression of the average innervations pattern and indication of intra-animal variability as well as assessment of the areas of overlap between the innervation territories of different nerves.

Analysis

The Bioptronics OSM Scanner 3001 was set up as described in the manual. However, the scan medium was changed from benzyl alcohol benzyl benzoate to demineralised water to avoid unwanted interaction with the specimen or the dye. The scans were made using UV light and a Cys3 filter (Cys3 fluorescence, 545nm/30nm exciter, 610/75nm emitter)[31, 32]. In our experiments bright-field images were used. Every specimen was scanned using a 1.8° angle increase per frame, resulting in 200 frames per scan. Every paw was recorded in two series because their sizes exceeded the 21 mm frame of the OSM scanner in the vertical position. Both series were merged whilst overlap between recordings was digitally excluded using based on the vertical position of the specimen in the scanner.

Quantification of the extravasation was performed using a custom-developed labVIEW™ (NationalInstruments) application. The percentage of staining per view was calculated using different thresholds to distinguish between background, unstained skin and stained skin. The thresholds were adjusted every 18° (10 frames) to compensate for the varying lightning due to the irregular surface of the paw. The 0°point was determined as the largest surface area (as measured by the total number of stained plus unstained pixels containing skin) on the plantar side of the paw.

The extent of extravasated skin area and the overlap between areas innervated by different nerves were determined using the CASAM technology[30]. Four frames in total, at 0° (plantar view), 90° (lateral view), 180° (dorsal view) and 270° (medial view) were selected to show the average extravasation, intra-animal variability of extravasation per nerve and overlap of extravasation for the studied nerves. Matching frames were selected from every scan and characteristic landmarks such as on each toe and at the base of the paw were placed, resulting in 30 to 50 landmarks per frame depending on the shape and variability of the paws for that specific frame. From these landmarks an average size and shape of the hind paw was computed and all paws were morphed to match this average. Subsequently, the area of extravasation for each animal was manually selected onto these average paws. Merging and comparing the resulting images in Adobe Photoshop enabled determination and quantification of both intra-animal variability of extravasation area per nerve as well as of the areas of overlap between two nerves.

Statistical analysis

For determining statistical differences of the surface areas, the one way-ANOVA with a Tukey post hoc test was used for intergroup comparisons to calculate the average staining in each group. Errors in variations were determined as standard error of the mean (SEM), and $p < 0.05$ was taken as significant.

In the CASAM analysis single pixels within the circumference of the landmarks were either assigned the label “stained” or “non-stained”. Pixels with identical incidences (ranging from stained in 1 animal to stained in all 7 cases) were grouped and two way t-test with a Tukey post hoc test was used to determine the threshold for significance ($p<0.05$) between groups. Subsequently overlap was divined as groups of individual significantly “stained” pixels with no significant difference between the compared nerves.

RESULTS

All nerve stimulations resulted in a blue coloring of a part of the skin of the hind paw. Several controls were conducted to verify that Evans Blue extravasation was positively correlated with the innervation of the skin innervated by the stimulated nerve. First, lesion of the nerve distal to stimulation site 10 weeks prior to the Evans Blue experiment failed to result in blue coloring of any part of the skin (not shown). In addition, in three rats a lesion of the sciatic nerve was performed five week previous to stimulation of the saphenous nerve which resulted in a blue colored extravasation of the medial part of the paw (Figure 2). The transition area was indicated by a shallow epidermal cut which was subsequently excised and processed for PGP9.5 immuohistochemistry. Although the Evans Blue coloring disappeared during the immunohistochemical procedure, the results clearly demonstrate that at the formerly extravasated side of the transition line (i.e. medial of the cut) PGP9.5-positive fibers of the stimulated saphenous nerve are present (Figure 2C), which could not be discerned at the formerly non-extravasated area (Figure 2D), lateral of the cut, which had been denervated by the sciatic lesion. Quantification of the epidermal nerve fibers was performed in all three animals. Average of 980 ± 16 PGP9.5 positive epidermal nerve fibers per mm² were counted on the formerly extravasated side. The few (28 ± 7 per mm²) remaining fibers, which are mainly present in the upper dermis, at the non-extravasated area are very thin (arrows in Figure 2D) and could reflect sprouting fibers.

These results exclude any possible blue staining of the skin due to diffusion of the dye and show a positive correlation between the extravasation by Evans Blue and the innervation of the epidermis.

Finally, two control animals were transcardially perfused with saline followed by 4% paraformaldehyde in order to determine if the wash-out of Evans Blue from the blood vessels interfered with the OSM measurements. Because no difference was observed between the perfused and non-perfused animals we chose to standardly use non-perfused animals in the current study

Evans Blue extravasation areas of the individual nerves

Stimulation of the four selected nerves resulted invariably in characteristic patterns of extravasation as evidenced by a dark blue staining of the skin. Stained areas always formed a consistent and continuous region with well-defined borders. Remarkably, no staining was observed on the footpads while less staining was seen on the callosities of the toes in all cases (Figure 3 and supplementary material S1). The extravasation of the innervated areas by individual nerves were

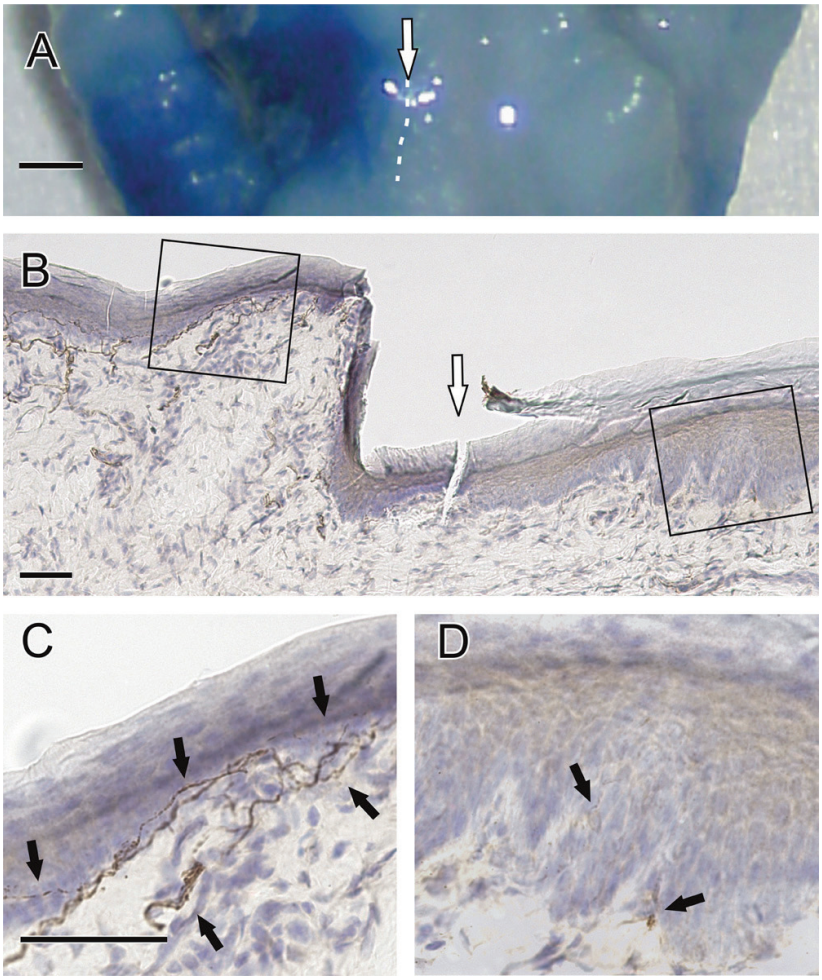

Figure 2. Correlation between Evans Blue extravasation and the innervation of the skin.
A) View of a part of the left plantar hind paw of the rat. After ligation of the sciatic nerve, stimulation of the healthy saphenous nerve showed blue coloring of the medial part of the plantar hind paw. The border between the extravasated and non-extravasated skin was indicated by a scalpel incision visible as white dotted line (white arrow).
B) PGP9.5 staining of the glabrous skin of rats' hind paw, in which an epidermal cut (white arrow) is made to localize the border between extravasated (left) side and non-extravasated (right) side. PGP9.5-positive nerve fibers are observed in the extravasated area medial to the incision.
C) Magnification of the Evans Blue extravasated side of the skin. The black arrows show the brown PGP9.5 positive nerve fibers.
D) Magnification of the non-extravasated side of the skin. The black arrows show some light staining in the upper dermis of the skin. These thin fiber-like structures could reflect sprouting fibers. Scale bar A) 1mm B-D) 50µm. E = epidermis, UD = upper dermis.

quantified and are represented by different colours (i.e. tibial nerve pink, sural nerve red, peroneal nerve green and saphenous nerve blue) (Figure3). In addition, different shadings of the colours pink, red, green and blue from bright to dark were used to represents the incidence (i.e. one to seven) of extravasation resulting from the stimulation of a particular nerve in the group of 7 animals (Figure 3).

In order to obtain accurate quantification of the extravasation areas in the paw, a 3D movie of the staining was acquired using the 200 frames (supplementary material S1). In addition, the percentage of staining per individual case was calculated from these 200 views in which the unstained hind paw from the most proximal footpad until the tip of the toes (including the footpads and the callosities) was automatically determined as 100% of the area that was analyzed by labVIEW. Subsequently, the average overall staining of the hind paw for the individual nerves and in each view of the 360° rotation was calculated over all 7 cases in each group (Figure 4). A general description of the 3D staining pattern and the average percentage staining for the individual nerves is given below.

Tibial nerve

Stimulation of the tibial nerve typically caused staining of the glabrous skin, extending to both the lateral and the medial sides of the paw (Figure 3). Maximal coverage of the paw with extravasated skin (up to 66,7% ± 5.0) after tibial nerve stimulation was seen on the plantar side of the hind paw at 0-45° and 315-360° (Figure 4A and S1). Note that the cycle starts with the full plantar view. Since the footpads, that do not show extravasation, are included in this view a lower than maximal percentage of extravasation was obtained. The dorsal view also shows some extravasation due to the innervation of the skin areas between the toes (Figure 4A and S1). The average overall extravasation area of the skin of the rats' hind paw after tibial nerve stimulation is 44.4% (±2,3) (Figure 4E).

Sural nerve

Stimulation of the sural nerve resulted in a dark blue staining on the lateral side of the paw, extending to the 4th and 5th digit on the dorsal side and partially the 5th digit on the plantar side (Figure 3). Although the sural nerve extravasation area is narrow proximally, it becomes wider towards the toes (Figure 3). This typical narrow elongated band of staining on the lateral part of the hind paw is represented by the low rather narrow peak that was present around 100° reaching 71.3% ± 6.3 (Figure 4B and S1). Lowest coverage (7.1%± 0.1) is seen in the medioplantar view of the paw between 270° and 315° (Fig. 4B and S1). Stimulation of the sural nerve caused an overall extravasation of 28.8% (±2.7) in

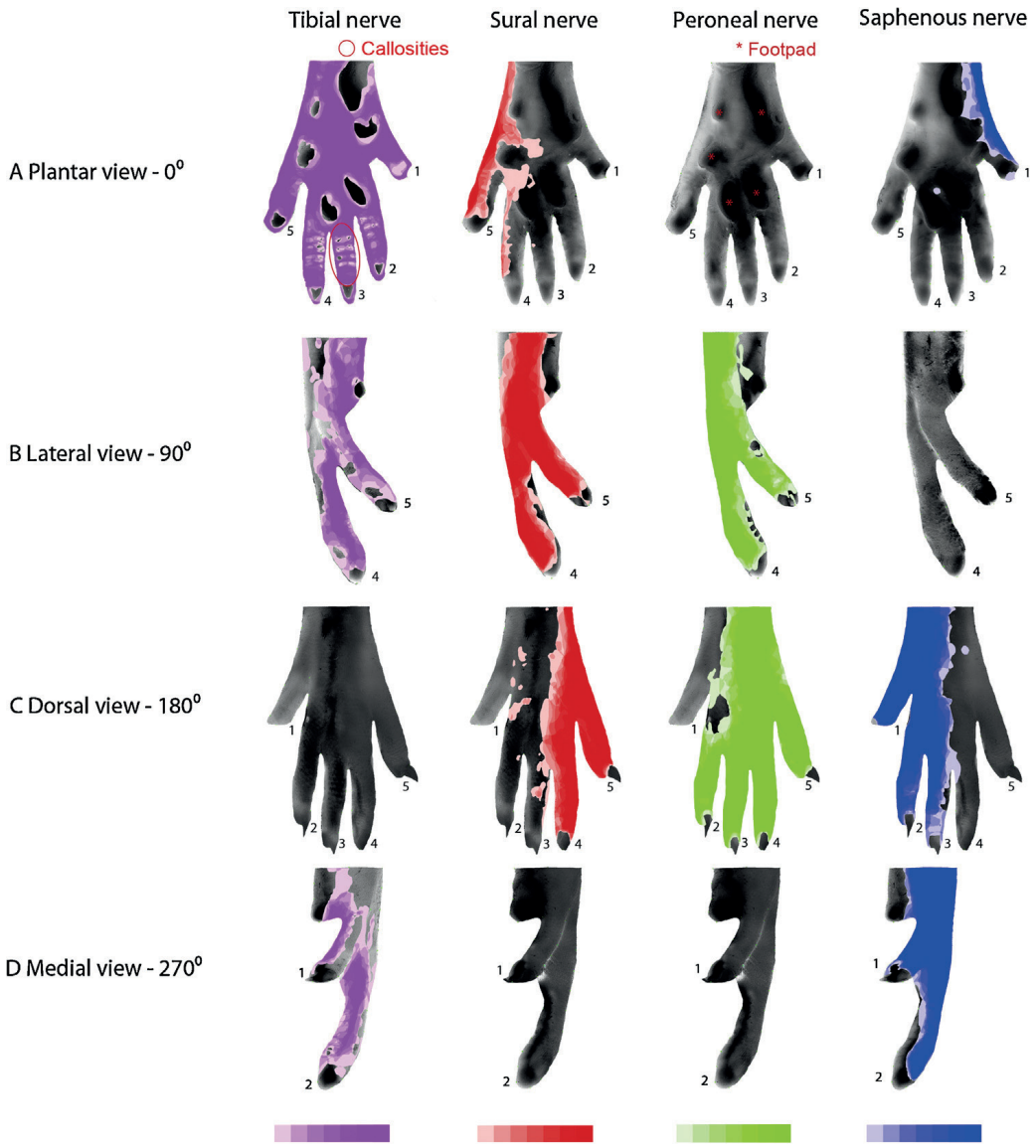

Figure 3. Intra-animal variability in nerve specific extravasation patterns.
The figure shows examples of the nerve specific extravasation pattern results from CASAM protocol after stimulation of the tibial, sural, peroneal and saphenous nerve in four views: A) 0̊ for the plantar view, B) 90̊ for the lateral view, C) 180̊ for the dorsal view and D) 270̊ for the medial view. All grey blank hind paws represent the views without extravasation. The pink (tibial nerve), red (sural nerve), green (peroneal nerve) and blue (saphenous nerve) colours indicate nerve specific extravasation ranging in incidence from light (1 animal) to dark (all 7 animals) as shown in the colour legend at the bottom of the figure. A) Footpads are visible as red asterisks and callosities as red circles.

rats' hind paw, which represents the lowest overall Evans Blue extravasation of the four nerves supplying the hind paw (Figure 4E).

Peroneal nerve

The skin area coloured by peroneal nerve stimulation shows remarkable correspondence with the proximal part of the area of extravasation by sural nerve stimulation. However, peroneal nerve-induced extravasation extends far wider distally than the sural nerve and covers all digits except digit 1 (Figure 3) with a wide high peak of 88.0% (± 3.3) in the dorsolateral view of the paw at 131° (Fig. 4C and S1). Note that both slopes of the peroneal nerve and the sural nerve are initially very much alike (Figure 4B,C and S1). Like the sural nerve, the least amount of extravasation after peroneal nerve stimulation was found in the medioplantar view of the paw between 270° and 315° reaching a minimum of 11,4% (±1.5) (Figure 4 and S1). The average extravasation after peroneal nerve stimulation is 40,9% (±1.3) (Figure 4E).

Saphenous nerve

Saphenous nerve stimulation typically resulted in extravasation of the medial-most side of the paw, covering the best part of the 1st, 2nd and 3rd digit and extending till the medial footpads on the plantar side of the paw (Figure 3). Similar to the stimulation of the peroneal nerve, the saphenous nerve has a broad extravasation area causing a high wide peak covering 78.6% (±3.0) of the dorsomedial paw at 225° (Figure 4D and S1). Minimal extravasation (9.7% ± 1.2) was found on the plantar view of the paw. Overall, stimulation of the sapheneous nerve caused 36.6% (±1.7) of the skin to demonstrate extravasation (Figure 4E).

In summary, the average extravasation area of the skin in rats' hind paw after tibial nerve stimulation is 44.4% (±2.3), whereas the sural nerve shows 28.8% (±2.7) extravasation, the peroneal nerve 40.9% (±1.3) and the saphenous nerve 36.6% (±1.7) extravasation (Figure 4e). From this first analysis, which is based on the summed projections of individual frames, it is determined that the sum of all averaged extravasation areas in the skin of rats' hind paw contributed to 150.7% (±16.0), which indicates a considerable overlap of the extravasation areas induced by stimulation of the individual nerves.

Analysis of variability and overlap

Although stimulation of a particular nerve generally resulted in extravasation of a specific part of the skin, small differences were observed between animals. As these differences may reflect intra-animal variability in the extent of the areas

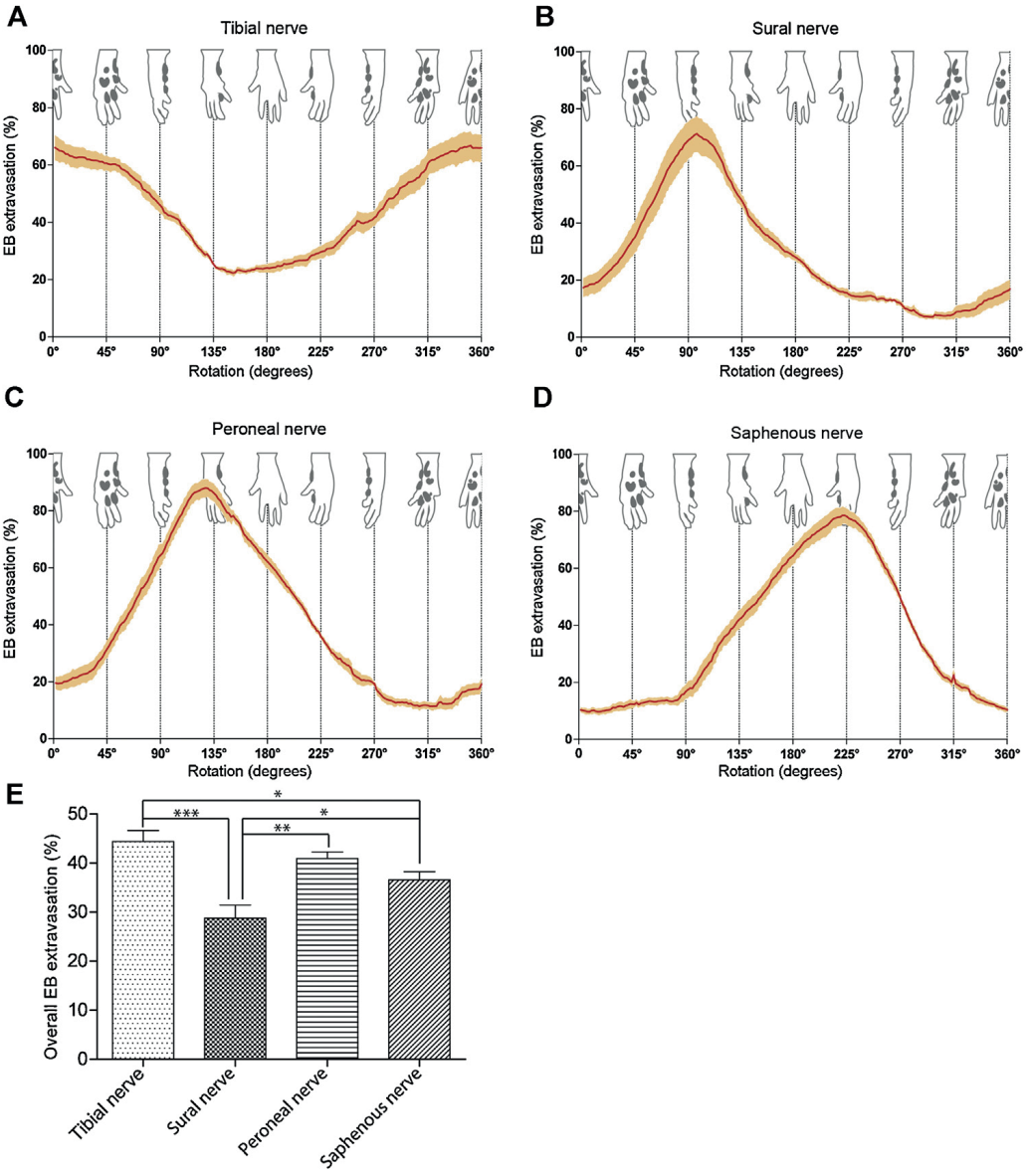

Figure 4. Percentage average extravasation per nerve.
A-D) show the average extravasation as a function of rotation after stimulation of the tibial nerve, the sural nerve, the peroneal nerve and the saphenous nerve subsequently. The yellow band around the red line indicates SEM's in figures. E) shows the average extravasation calculated for tibial, sural, peroneal and saphenous nerve over all 200 frames made by the OSM-scanner. In this figure the location is not taken into consideration. Note the significant differences in average percentage extravasation between the different nerves and that these percentages add up to 155%. Analysis by two-tailed t-test. * ($p<0.05$) ** ($p<0.01$) *** ($p<0.001$).

innervated by a single nerve, we have analyzed the intra-animal variability further using the CASAM technique 24, which entails superimposing the extravasated areas on an averaged hind paw (Figure 3). In addition, the staining areas of two adjacent nerves were merged to gain a better understanding of the location of the considerable overlap areas as found in our previous average staining calculations (Figure 5,6,7,8 and 9). The intra-animal variability within the four groups of seven animals has been taken into account by using different shades of the colour that represents the specific cutaneous nerve extravasation ranging from bright to dark as described previously. After merging the stained areas for two nerves, it was possible to create a new 49 (7x7) grid of colour combinations that represents the incidence that a particular surface area is extravasated by stimulation of either or both of the nerves (Figure 5B, 6B, 7B, 8B). Subsequently, the areas that showed significant overlap in extravasation by both nerves (i.e. at least four of the seven animals showed extravasation in this area in both groups) were extracted (Figure 5C, 6C, 7C, 8C). Using this analysis we can now describe which skin areas show systematic overlap in extravasation due to stimulation of different nerves.

Plantar View

As shown in figure 3A and visible in figure 5, parts of the plantar aspect of the paw are extravasated by the saphenous, tibial and sural nerves. The plantar skin of the paw shows most consistent staining after stimulation of the tibial nerve (Figure5A). Colour coding indicates the consistency of the results. Dark pink indicates that all seven studied animals showed extravasation of the tibial nerve in the same region whereas bright pink to white regions depict areas with extravasation in only one of the rats. Note that in all animals the footpads appear as black islands since they never show extravasation of the skin (Figure 5). Variety in shape and position of footpads caused some lower densities around the footpad areas. The callosities on the plantar side of the toes also demonstrate a lower incidence of coloring.

Both the sural and the saphenous nerves have a minimal area of extravasation in the plantar view as compared to the dorsal view. Moreover, these small plantar areas also show some variability as indicated by the amount of bright colours (i.e. bright red in case of the sural nerve in figure 5A.3). Intra-animal variability in the extent of extravasation area for the saphenous nerve is further represented by the white shade proximal to the first digit next to the first proximal footpad (Figure 5A.1).

In addition, Figure 5C shows the consistency in areas of overlap between the tibial and saphenous nerve (Figure 5C-1.2) and between the tibial and sural nerves

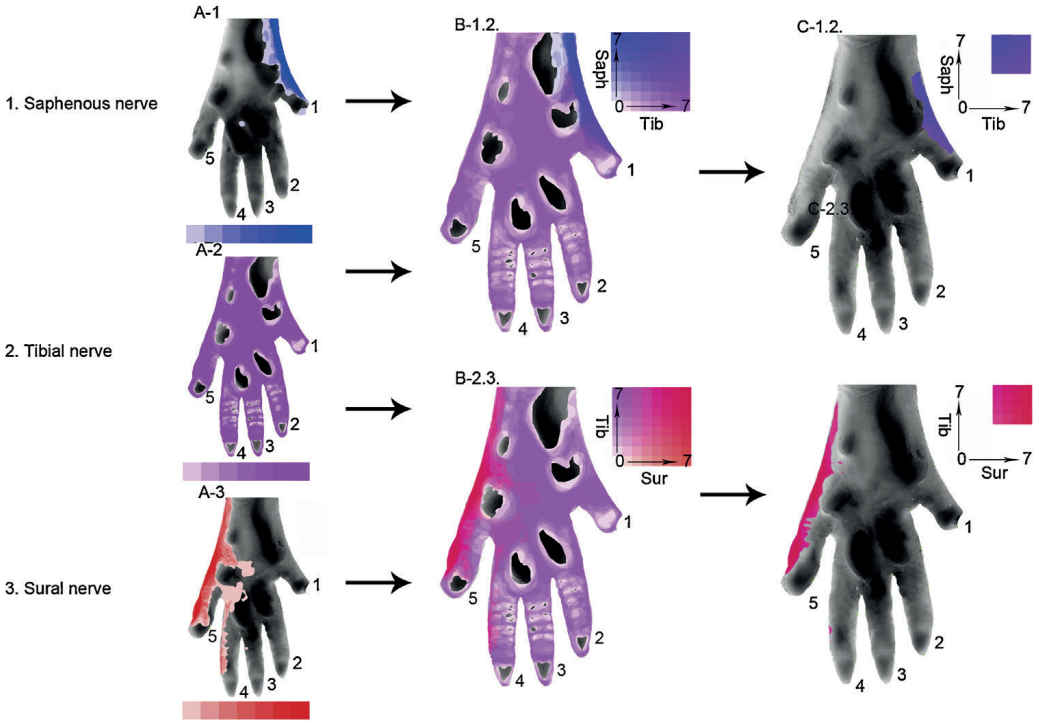

Figure 5. Plantar overlap analysis.
A) The intra-animal variability of the extravasation is shown individually for saphenous (blue), tibial (pink) and sural (red) nerve on the plantar side of the paw ranging in incidence from light (1 animal) to dark (all 7 animals). Note the lack of extravasation by the peroneal nerve on the plantar view as shown in the colour legend below the hind paw. B) Combined extravasation areas showing overlap. The combined figures of the saphenous and the tibial nerve (B-1.2) as well as the combined figures of tibial and the sural nerve (B-2.3) showed a small blue area on the medial and red area on the lateral part of the paw showing overlap with tibial nerve extravasation. C) Extraction of significant overlap areas between the n. saphenous and the n. tibialis (C-1.2) shows a small area of overlap on the medioproximal part of the plantar side while the overlap between n. tibialis and n. suralis (C-2.3) is seen on the lateral part of the paw. B) The 7x7 grid of colour combinations is represented to show the incidence that a particular surface area is extravasated by stimulation of either or both of the nerves as given in the x and the y axis. C) 4x4 grid of colour in overlap areas of two nerves in at least four of the seven animals in each group. Saph= saphenous nerve, Tib= tibial nerve, Sur = sural nerve.

(Figure 5C-2.3). Indeed, small regions of consistent overlap in extravasation by these nerves are noted. The overlap region of the saphenous nerve and the tibial nerve starts at the medial base of the proximal-most footpad and ends on the 1st digit (Figure 5C-1.2). Lack of overlap at the base of the first digit next to the most proximal footpad, visible as a white curve surrounding the medial side of the footpads, can be observed (Figure 5C-1.2). This is related to absence of extravasation by tibial nerve stimulation on this part of the glabrous skin (Figure 5A-2).

The overlap between the saphenous and tibial nerves at the medial edge of the plantar view is mimicked laterally by the overlap between the tibial and the sural nerves (Figure 5C-1.2, 5C-2.3). The area of overlap covers almost the entire lateral edge of the paw including the 4th digit (Figure 5C-2.3: fuchsia area). However, it should be noted that this overlap region is more consistently involved after tibial nerve stimulation as compared to sural nerve stimulation.

Lateral view

The lateral view of the hind paw incorporates a view of both the 4th and 5th digit and the separation of dorsal and glabrous skin on the lateral side of the paw (Figure 3B). The saphenous nerve is the only nerve that does not contribute to the extravasation of this view while the sural nerve provided the most consistent extravasation (Figure 3B). Peroneal and tibial nerves, to varying degrees, also contribute to the extravasation of the lateral aspect, both resulting in considerable overlap with the territory of the sural nerve (Figure 6A, B). However, note that, in contrast to the tibial nerve, both sural and peroneal nerve stimulation predominantly resulted in extravasation of the dorsal edge of the paw.

Although, the extravasation area by the peroneal nerve shows overlap with extravasation areas of tibial as well as sural nerves, more prominent interaction was seen with the latter. This is illustrated by figure 6C-1.2 where the large dark red/dark green areas indicate consistency of overlap in the extravasation areas between the peroneal and sural nerve without any dominance for either nerve in this area. Less overlap was seen between the sural and tibial nerves (fuchsia area in Figure 6C-2.3), which were mostly restricted to the border between the glabrous skin and non-glabrous skin at the lateral view. However, least overlap was found between the peroneal and tibial nerve (Figure 6-C3.4).

Dorsal view

All animals showed extravasation of at least some parts of the skin at the dorsal aspect of the paw after stimulation of either the saphenous, peroneal or

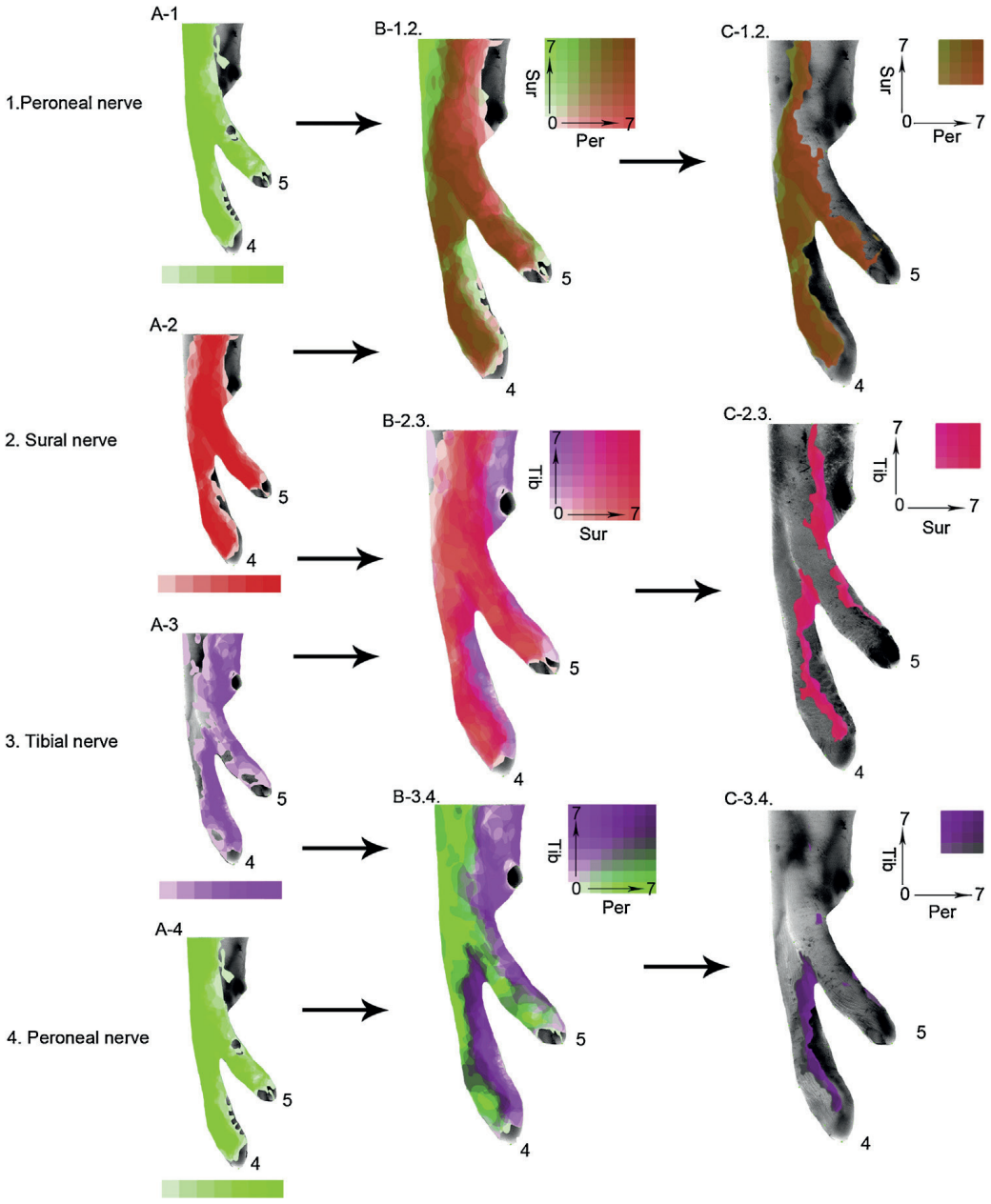
1.Peroneal nerve
2. Sural nerve
3. Tibial nerve
4. Peroneal nerve
A-1
A-2
A-3
A-4
B-1.2.
B-2.3.
B-3.4.
C-1.2.
C-2.3.
C-3.4.
Sur
Per
Tib
0
7
4
5

Figure 6. (left page) Lateral overlap analysis.
A) The intra-animal variability of the extravasation is shown individually for the peroneal (green), sural (red) en tibial (pink) nerves on the lateral side of the paw ranging in incidence from light (1 animal) to dark (all 7 animals) as shown in the colour legend below the hind paw. In the lateral view there is overlap between three nerves, therefore in (A) the peroneal nerve was displayed twice. B) Combined extravasation figures show comparable extravasation areas while after correction for anatomical variety three different overlapping areas are seen (C). Relatively large significant overlap was seen between the peroneal and sural nerve (C-1.2), whereas the tibial and the sural nerves show typically overlap in a vertical line on the lateral border between the glabrous and hairy skin (C-2.3). The peroneal and the tibial nerve present overlap mostly on the 4th digit of the lateral hind paw (C-3.4). B) The 7x7 grid of colour combinations is represented to show the incidence that a particular surface area is extravasated by stimulation of either or both of the nerves as given in the x and the y axis. C) 4x4 grid of colour in overlap areas of two nerves in at least four of the seven animals in each group. Sur = sural nerve, Per= peroneal, Tib= tibial nerve.

sural nerves. Tibial nerve stimulation resulted only in some animals in some spots of extravasation between the digits (S1). Since these spots did not represent a significant overlap they were excluded in the analysis of overlap with other nerves.

Stimulation of the sural nerve caused extravasation of the dorsolateral part of the paw, covering the 5th and the 4th digit and in 3 out of 7 cases some spots were noticeable on the 3rd digit as well (Figure 3C, 7A). Saphenous stimulation, on the other hand, resulted in coloring of the dorsomedial aspect of the paw, usually including the 3rd digit. Peroneal-induced extravasation is located centrolaterally at the dorsal view of the paw and incorporating the 2nd -5th digits in all 7 cases. As such, some overlap with both the sural nerve laterally and the saphenous nerve medially exists (Figure 3C, 7A).

From the dorsal extravasation figures it can be appreciated that the territories extravasated by the saphenous and peroneal nerve stimulation cover almost the entire dorsal aspect of the paw (Figure 7B-2.3). Both areas meet each other proximally in the centre of the hind paw and generally demonstrated a shared extravasation of the skin of the 2nd and 3rd digits. Comparing the extravasation representations of the peroneal and sural nerve in the lateral view indicates that the sural nerve area is systematically and almost completely overlapped by that of the peroneal nerve. The overlap area is mostly dark red showing an even administration of the extravasation with a dark green line at the centre of the hind paw due to dominance of the peroneal nerve in this overlap area (Figure7C-1.2).

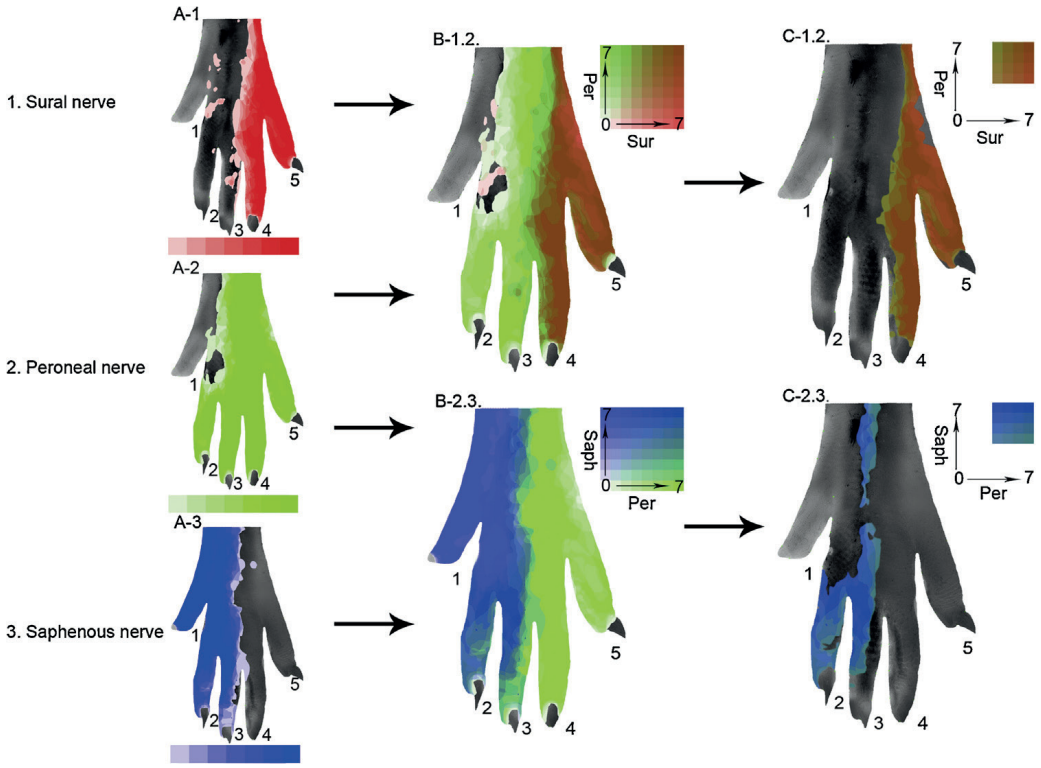

Figure 7. Dorsal overlap analysis.
A) The intra-animal variability of the extravasation is shown individually for the sural (red), peroneal (green) and saphenous (blue) nerves on the dorsal side of the paw ranging in incidence from light (1 animal) to dark (all 7 animals) as shown in the colour legend below the hind paw. B) Combined extravasation areas showing overlap (B-1.2.) Note that the area of combined overlap of the peroneal and the sural nerve is very alike the extravasation figure of peroneal nerve (A-2) (B-2.3) The combined extravasation areas of the saphenous and the peroneal nerve show a complete innervation of the dorsal skin of the hind paw. C) The significant overlap between the saphenous and the peroneal nerve (C-1.2) and between the peroneal and sural nerve (C-2.3) are shown. B) The 7x7 grid of colour combinations is represented to show the incidence that a particular surface area is extravasated by stimulation of either or both of the nerves as given in the x and the y axis. C) 4x4 grid of colour in overlap areas of two nerves in at least four of the seven animals in each group. Per= peroneal, Sur = sural nerve, Saph= saphenous nerve.

Medial view

The medial view specifically incorporated the 1st and 2nd digits and the separation of dorsal and glabrous skin at the medial side of the paw (Figure 3D, 8A). The saphenous nerve caused extravasation of almost the entire medial view of the paw while extravasation by the tibial nerve was observed at the medioplantar side of the paw (Figure 8A). Stimulation of the tibial nerve resulted in coloring of more selective and rather variable spots while extravasation by

the saphenous nerve showed more consistent and elaborate staining. Note again that also in this view no extravasation of the footpads was noted (Figure 8). Furthermore, the saphenous nerve (blue) dominates the mediodorsal side, while the tibial nerve (pink) dominates the medioplantar side (Figure 3D, 8A). Similar to the lateral view of overlap (Figure 6C-2.3), the overlap at the medial aspect is mostly restricted to the border between the glabrous skin and non-glabrous skin at the medial view (Figure 8C-1.2).

All significant extravasation areas by individual nerves and all significant overlap areas are summarized in the four views shown in Figure 9. This Figure clearly illustrates the dominant appearance of the tibial nerve at the plantar side of the paw, whereas the dorsal side is covered by saphenous, peroneal and sural nerves and demonstrates the significant overlap in innervation areas of these nerves.

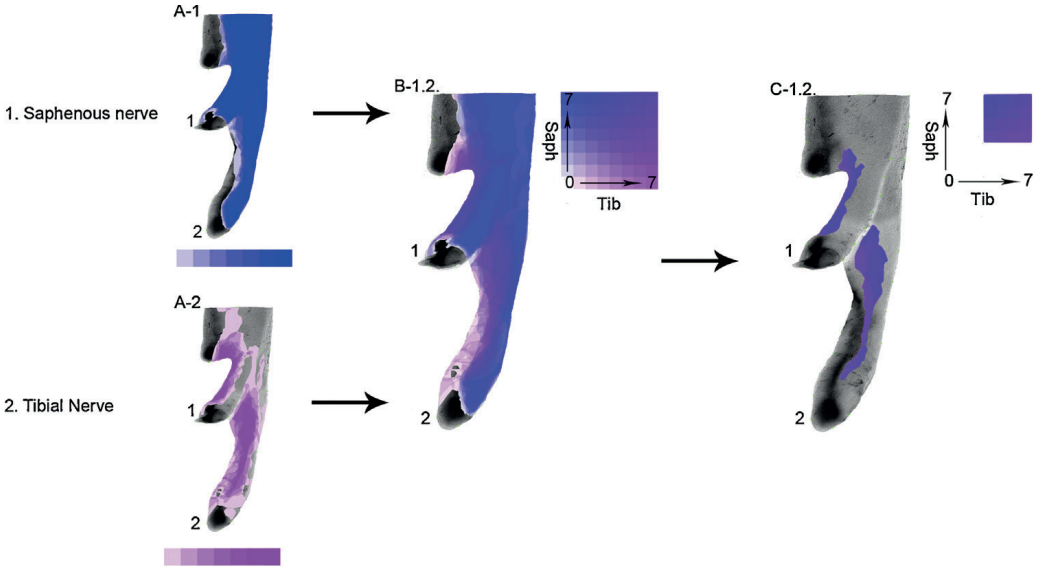

Figure 8. Medial overlap analysis.
A) The intra-animal variability of the extravasation is shown individually for the saphenous and tibial nerves on the medial side of the paw ranging in incidence from light (1 animal) to dark (all 7 animals) as shown in the colour legend below the hind paw. B) The combined extravasation areas of the saphenous and tibial nerves shows extravasation of all skin areas of the medial view except the footpads. This area consist mostly of the colours blue (saphenous nerve) on the dorsal side and and pink (tibial nerve) on the plantar side of the medial view, suggesting little overlap. C) Indeed the overlap figure shows a small area of significant overlap between saphenous and tibial nerve. B) The 7x7 grid of colour combinations is represented to show the incidence that a particular surface area is extravasated by stimulation of either or both of the nerves as given in the x and the y axis. C) 4x4 grid of colour in overlap areas of two nerves in at least four of the seven animals in each group. Saph= saphenous nerve, Tib= tibial nerve.

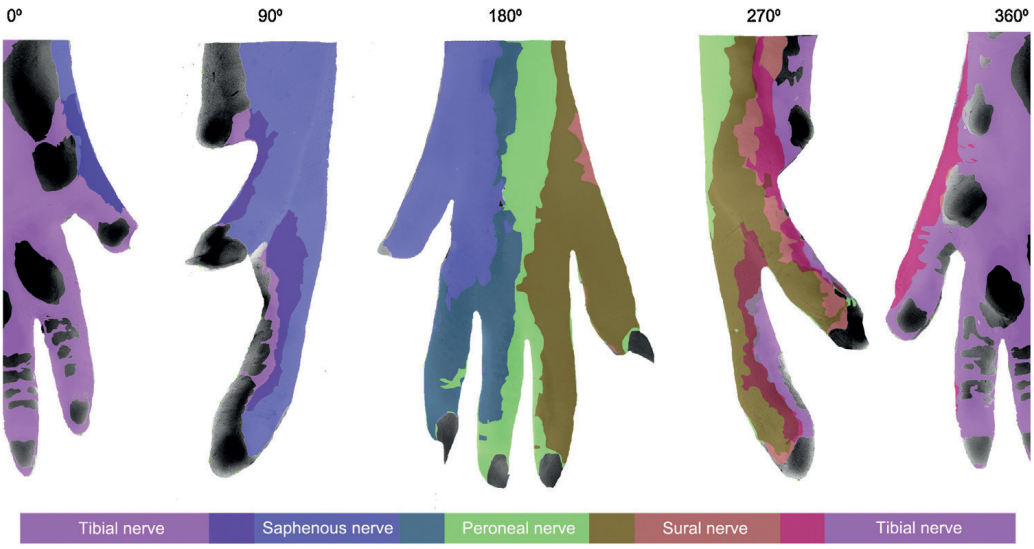

Figure 9. Complete extravasation areas of rats' hind paw.
All extravasation areas of rats' hind paw are shown in plantar (0º), lateral (90º), dorsal (180º) and medial (270º) view by tibial (pink), saphenous (blue), peroneal (green) and sural (orange) nerve. Each significant overlap area between the two nerves is indicated by different coulours: overlap between tibial and saphenous nerve is dark purple, between saphenous and peroneal nerve dark green, between peroneal and sural nerve brown and between sural and tibial nerve fuchsia. This figure serves as a summary of both individual extravasation as well as overlap in extravasation areas of rats' hind paw.

DISCUSSION

Methodological considerations combining Evans Blue extravasation, OSM scanner and CASAM technology

Sensory nerve fibers are important in perception of the environmental stimuli in order to allow interaction but also to avoid traumatic forces and extreme thermal exposure[33]. Individual fibers are characterized by well-defined receptive fields, which may partly overlap with that of other fibers. Many studies have been devoted to the analysis of changes in sensory skin fibers after peripheral nerve injury. The hind paw of the rat has become a commonly used model in studying these changes resulting from different kinds of trauma[3, 5].

In order to better evaluate and understand the various processes that take place during degeneration and regeneration of cutaneous nerves we have noted that a more precise description of the innervation areas of the hind paw would be invaluable. Although several studies have used the well-known technique based

on vascular labeling in order to examine the cutaneous regions of innervation by particular nerves,[7-20], their results are prone to subjective interpretations or are very cumbersome to obtain; i.e. subjective translation of staining patterns and extraction of dye from skin samples, respectively . The OSM scanning technique enabled a new and objective analysis of the area of extravasation by using a full 360° circle of views. Furthermore, it should be noted that the results of extraction studies are based on the assumption that the extracted amount of the extravasated dye is proportional to the number of nerve endings present in the skin[10]. However, this assumption seems less reliable since studies indicated that the extent of plasma extravasation depends on stimulation parameters such as frequency and time[11, 12]. These parameters have been used differently in literature, which makes comparison of evaluated dye extraction between studies difficult.

The stimulation parameters used in the present study were chosen with utmost care. Our stimulation frequency of 10 Hz was based on that of earlier results from which it could be deduced that changing stimulation frequency from 4 to 8 Hz (for 10 min) resulted in a more prominent plasma extravasation in the event of 8 Hz[11, 12, 14]. Furthermore, a trial study was performed from which the stimulation parameters were determined to ensure an optimal plasma extravasation without loss of information. Although some studies have used guanethidine (a vasodilator), at varying concentrations in order to enhance both blood flow and extravasation[12, 13, 16], this was not deemed necessary in the present study , as we have used isoflurane as an anesthetic, which has been demonstrated to also have a vasodilatory action[34].

After Evans Blue experiment the hind paw was morphed to an average size using CASAM technology. However, the heel was excluded in these calculations since no anatomic landmarks, which are required to morph the hind paw, are present in the heel. In addition, the heel is partly innervated by the gastrocnemius nerve, which is not included in this manuscript[35]. Therefore, the hind paw from the most proximal footpad until the tip of the toes was chosen as the area of interest to maintain consistent and accurate CASAM measurements for each paw and to show the innervation areas of the four (tibial, sural, peroneal, and saphenous) nerves supplying this area of the hind paw. The glabrous skin containing footpads is an important area in nerve regeneration and neuropathic pain studies in animals; behavioral studies to determine mechanical sensitivity using von Frey filaments is performed between the footpads[36-38], while thermal sensitivity (cold- and hot plate)[39, 40] is measured in the footpads. Furthermore, the four nerves that supply this area are stained in immunohistochemical studies, in which the sensory nerves in the footpads and/or in between the footpads are visualized and quantified[3, 41, 42].

Although accurate and exact results were obtained by combining the Evans Blue extravasation technique and the 360° imaging using OSM scanning technique, it was not possible to determine the overlap between the extravasation areas of different nerves within the same animal. Knowledge about the extent of overlap of innervation areas is crucial when studying the short and long-term effects of peripheral nerve injury. In addition, collateral sprouting of undamaged fibers following nerve injury may induce or enlarge areas of overlap in innervation area, which may be important when evaluating the behavior of regenerating nerves.

By using extravasation of two different dyes (Evans Blue and colloid silver) Dux et al.[20] already used the plasma extravasation technique in order to study the overlap areas of cutaneous innervation. Staining of the skin by both dyes visualized skin areas with Evans Blue, areas with colloid silver and areas with both Evans Blue and colloid silver staining that indicates for the overlap territory. However, these authors used an interval of 60 minutes between the stimulation of the two nerves in the same specimen to exclude any skin staining by the previous dye and waited another 30 minutes after the last nerve stimulation. It is known that Evans Blue is a fluorescent dye[43], which faded in time in our trial study (data not shown). In our view, this may have caused an underrepresentation of the Evans Blue extravasation areas in the study by Dux et al.[20], which could explain the smaller overlap in extravasation areas in comparison to our results. Moreover, the intra-animal variability of the individual extravasation areas was not taken in consideration in their translation studies. As the CASAM technology employed in our study uses many landmarks in order to determine an average hind paw, an accurate representation and subsequent comparison of the individual extravasation areas was possible[24]. Subsequently, the individual representations were marked and an overlay was made to quantify the area of overlap between two adjacent extravasation areas. It is important to note that in order to prevent dispersion in average paw size calculation, all animals had to be from the same strain, sex and of a comparable body weight. Although the hind paws were scanned and analyzed in 200 frames to cover 360° to determine the extravasation and overlap areas, only four views are shown in the present study as they cover the complete hind paw (apart from the 3rd inter-digital space).

Results of extravasation in comparison with previous studies

Previously it has been shown that antidromic stimulation of the autonomic nervous system can lead to an increase in skin blood flow due to activation of Aδ-fibers[21], whereas the C-fiber activation causes both vasodilatation and plasma extravasation of Evans Blue by release of neuropeptides[22]. Therefore,

the interpretation of the results from Evans Blue extravasation is based on the assumption that the stained skin corresponds with the afferent C-fiber innervation area of the stimulated nerve, as could be verified with electrophysiological techniques[23]. Consistent with this evidence, preliminary results from our laboratory using the pan-neuronal marker PGP9.5 confirmed that the extravasation areas correspond exactly to the innervation area of the stimulated nerve (see control study). From these findings we can conclude that the Evans Blue extravasation results in an indirect but accurate representation of C-fiber innervated skin regions of a particular nerve.

Swett and Woolf were one of the first to describe the size and location of cutaneous innervation of rats' hind paw by electrophysiological recording techniques and labeling[44]. Consistent with our findings, they show that the plantar side of the paw is mainly innervated by the tibial nerve (Figures 5, 9). Moreover, the boundaries between the sural and saphenous nerves with the tibial nerve corresponded closely with the hair line margin of the plantar skin, which is similar to our results (Figures 5B). Interestingly, over time different groups studying nerve regeneration have been referring to the classic work of Swett and Woolf when considering the plantar innervation area of rats' hind paw[45, 46]. It seems however that these studies described the plantar innervation of the hind paw differently: in three equal parts in which the medial part (including the entire 1st and parts of the 2nd digit) would be innervated by the saphenous nerve, the central part by tibial nerve and the lateral part (including parts of the 4th digit and the entire 5th digit) by sural nerve. In the light of the present findings and the initial paper of Swett and Woolf we think that this representation is incorrect and should be interpreted attentively and with caution.

The results from this study indicated that the intra-animal variability in extravasation areas for individual nerves is rather low (Figure 3). This is visible by small areas of bright-discolored (low incidence) hind paw (Figure 3) and small SEM values for average extravasation calculation (Figure 4). Hence, the stained areas were consistent and continuous in all animals showing characteristic patterns of extravasation. As described by other studies, the skin of the footpads never show any sign of extravasation (Figures.3 and S1)[13, 18]. Moreover, we found that the callosities also show less extravasation in several cases (Figures.3 and S1), while it is shown that the footpads are innervated[47]. These findings are previously ascribed to the thickening of the skin in the footpads . However, recent studies in our lab by Duraku et al.[4], showed that the density of peptidergic nerve fibers in the epidermis of the footpads was considerably lower in comparison to the surrounding non-footpad area of rats' hind paw. After stimulation of the

nerve, peptidergic neuropeptides are excreted and cause the extravasation of the dye[12, 48]. Moreover, the epidermis of the footpads is almost three times as thick as the surrounding skin. Taken together, these properties, at least partly, could explain the generally poor extravasation results of the foot pads.

Although our extravasation areas are highly consistent, they are generally somewhat larger than those observed in in other studies[8, 9, 18] . A control experiment was performed to exclude that possible diffusion of the Evans Blue dye could cause the larger extravasation area. The results of this control experiment showed a positive correlation between the Evans Blue extravasation and the innervation of the skin by PGP9.6 positive nerve fibers (Figure 2). In our view the larger extravasation area can be ascribed to the usage of the hook electrodes that could keep the nerve under tension and may cause damage to the nerve. Although mineral oil and liquid paraffin was used, relatively long stimulation time (ranging from 5 to 90 minutes) might have caused drying of the nerve[8, 9, 18].

Furthermore, some studies have mapped the innervation of the hind paw of the rat in which both hind paws (ipsi- and contralateral) were simultaneously stimulated. Although comparable stimulation intensity as in the recent study was applied, these studies showed smaller extravasation areas that could be assigned to bilateral stimulation of the nerve[9, 10]. This assumption is confirmed by a study in which subsequently two nerves are stimulated to show overlap areas: when saphenous nerve is stimulated first followed by the peroneal nerve the dorsal 5th digit, which is stained completely in the recent study due to peroneal nerve stimulation (Figure 7A-2), does not show any extravasation. However, when the condition is reversed and the peroneal nerve is stimulated first almost the entire 5th digit shows extravasation[18]. From these findings we can conclude that bilateral or subsequent stimulation of two or more nerves shows less plasma extravasation, which, apparently, may result in incomplete extravasation areas. In addition, it seems possible that by allowing central transmission, stimulation of a nerve also influence extravasation not only of the contralateral paw but potentially in the ipsilateral paw as well. Therefore, in the present study unilateral stimulation was performed with a crush lesion proximal from the stimulation site to obtain a complete and detailed extravasation.

One of the most remarkable findings from this study is the dorsal innervation of the paw by the peroneal and saphenous nerve. These nerves intersect at the center of the dorsal hind paw causing a complete extravasation of the skin with a small area of overlap (Figure 7B-2.3). In contrast, the combination of the sural and peroneal nerve extravasation areas showed exclusively overlap of the entire area of the sural nerve on the dorsal view (Figure 7B-2.3). Moreover, it is

interesting to note that larger areas of overlap were seen on the dorsal part of the paw, whereas the overlap on the plantar side was minimal[18]. In our view these differences in overlap between the dorsal and the plantar surface could have implications for regeneration processes of the relevant nerves.

Results from this study could be used as control to compare the denervation and reinnervation areas of specific nerves in the skin after nerve injury. Since sprouting plays a major role once denervation takes place, it is important to acknowledge the correct and detailed innervation areas and the amount of overlap in healthy skin when studying nerve regeneration. In our view the use of the Evans Blue technology in combination with OSM and CASAM analysis represents an excellent tool to examine the origin of the nerves that sprout and contribute to the hypersensitivity in neuropathic pain animals. This could help answering the question why and where neuropathic pain syndromes occur.

ACKNOWLEDGEMENTS

The authors would like to express their gratitude to Ineke Hekking-Weijma for the surgery, anesthesia and practical suggestions and Dr. L.W.J. Bosman for his help with the Labview software.

REFERENCES

1. Narayanaswamy H, Facer P, Misra VP, et al. A longitudinal study of sensory biomarkers of progression in patients with diabetic peripheral neuropathy using skin biopsies. J Clin Neurosci. 2012;19: 1490-1496.
2. McCarthy BG, Hsieh ST, Stocks A, et al. Cutaneous innervation in sensory neuropathies: evaluation by skin biopsy. Neurology. 1995;45: 1848-1855.
3. Peleshok JC, Ribeiro-da-Silva A. Delayed reinnervation by nonpeptidergic nociceptive afferents of the glabrous skin of the rat hindpaw in a neuropathic pain model. J Comp Neurol. 2011;519: 49-63.
4. Duraku LS, Hossaini M, Hoendervangers S, et al. Spatiotemporal dynamics of re-innervation and hyperinnervation patterns by uninjured CGRP fibers in the rat foot sole epidermis after nerve injury. Mol Pain. 2012;8: 61.
5. Duraku LS, Hossaini M, Schuttenhelm BN, et al. Re-innervation patterns by peptidergic Substance-P, non-peptidergic P2X3, and myelinated NF-200 nerve fibers in epidermis and dermis of rats with neuropathic pain. Exp Neurol. 2013;241: 13-24.
6. Hsieh CH, Jeng SF, Lu TH, et al. Correlation between skin biopsy with quantification of intraepidermal nerve fiber and the severity of sciatic nerve traction injury in rats. J Trauma. 2009;66: 737-742.
7. Baranowski AP, Priestley JV, McMahon S. Substance P in cutaneous primary sensory neurons--a comparison of models of nerve injury that allow varying degrees of regeneration. Neuroscience. 1993;55: 1025-1036.
8. Bester H, Allchorne AJ, Woolf CJ. Recovery of C-fiber-induced extravasation following peripheral nerve injury in the rat. Exp Neurol. 1998;154: 628-636.
9. Brenan A. Collateral reinnervation of skin by C-fibres following nerve injury in the rat. Brain Res. 1986;385: 152-155.
10. Brenan A, Jones L, Owain NR. The demonstration of the cutaneous distribution of saphenous nerve C-fibres using a plasma extravasation technique in the normal rat and following nerve injury. J Anat. 1988;157: 57-66.
11. Carmichael NM, Dostrovsky JO, Charlton MP. Enhanced vascular permeability in rat skin induced by sensory nerve stimulation: evaluation of the time course and appropriate stimulation parameters. Neuroscience. 2008;153: 832-841.
12. Gonzalez HL, Carmichael N, Dostrovsky JO, Charlton MP. Evaluation of the time course of plasma extravasation in the skin by digital image analysis. J Pain. 2005;6: 681-688.
13. Hansson T, Povlsen B. Functional regeneration of C-fibres inside a silicone tube after sciatic neurotomy in rats. Scand J Plast Reconstr Surg Hand Surg. 1997;31: 7-11.
14. Jancso N, Jancso-Gabor A, Szolcsanyi J. Direct evidence for neurogenic inflammation and its prevention by denervation and by pretreatment with capsaicin. Br J Pharmacol Chemother. 1967;31: 138-151.

15. Kingery WS, Guo TZ, Poree LR, Maze M. Colchicine treatment of the sciatic nerve reduces neurogenic extravasation, but does not affect nociceptive thresholds or collateral sprouting in neuropathic or normal rats. Pain. 1998;74: 11-20.
16. Povlsen B, Hildebrand C, Stankovic N. Functional projection of sensory lateral plantar and superficial peroneal nerve axons to glabrous and hairy skin of the rat hindfoot after sciatic nerve lesions. Exp Neurol. 1994;128: 129-135.
17. Povlsen B, Hildebrand C, Wiesenfeld-Hallin Z, Stankovic N. Functional projection of regenerated rat sural nerve axons to the hindpaw skin after sciatic nerve lesions. Exp Neurol. 1993;119: 99-106.
18. Wiesenfeld-Hallin Z. Partially overlapping territories of nerves to hindlimb foot skin demonstrated by plasma extravasation to antidromic C-fiber stimulation in the rat. Neurosci Lett. 1988;84: 261-265.
19. Wiesenfeld-Hallin Z, Kinnman E, Aldskogius H. Expansion of innervation territory by afferents involved in plasma extravasation after nerve regeneration in adult and neonatal rats. Exp Brain Res. 1989;76: 88-96.
20. Dux M, Jancso G. A new technique for the direct demonstration of overlapping cutaneous innervation territories of peptidergic C-fibre afferents of rat hindlimb nerves. J Neurosci Methods. 1994;55: 47-52.
21. Janig W, Lisney SJ. Small diameter myelinated afferents produce vasodilatation but not plasma extravasation in rat skin. J Physiol. 1989;415: 477-486.
22. Gee MD, Lynn B, Cotsell B. The relationship between cutaneous C fibre type and antidromic vasodilatation in the rabbit and the rat. J Physiol. 1997;503 (Pt 1): 31-44.
23. Pertovaara A. Collateral sprouting of nociceptive C-fibers after cut or capsaicin treatment of the sciatic nerve in adult rats. Neurosci Lett. 1988;90: 248-253.
24. Kerver AL, van der Ham AC, Theeuwes HP, et al. The surgical anatomy of the small saphenous vein and adjacent nerves in relation to endovenous thermal ablation. J Vasc Surg. 2012;56: 181-188.
25. Kerver AL, Carati L, Eilers PH, Langezaal AC, Kleinrensink GJ, Walbeehm ET. An anatomical study of the ECRL and ECRB: feasibility of developing a preoperative test for evaluating the strength of the individual wrist extensors. J Plast Reconstr Aesthet Surg. 2013;66: 543-550.
26. van der Graaf T, Verhagen PC, Kerver AL, Kleinrensink GJ. Surgical anatomy of the 10th and 11th intercostal, and subcostal nerves: prevention of damage during lumbotomy. J Urol. 2011;186: 579-583.
27. Hopman AH, Ramaekers FC, Speel EJ. Rapid synthesis of biotin-, digoxigenin-, trinitrophenyl-, and fluorochrome-labeled tyramides and their application for In situ hybridization using CARD amplification. J Histochem Cytochem. 1998;46: 771-777.
28. Sharpe J, Ahlgren U, Perry P, et al. Optical projection tomography as a tool for 3D microscopy and gene expression studies. Science. 2002;296: 541-545.
29. Sharpe J. Optical projection tomography as a new tool for studying embryo anatomy. J Anat. 2003;202: 175-181.
30. Kerver AL, van der Ham AC, Theeuwes HP, et al. The surgical anatomy of the small saphenous vein and adjacent nerves in relation to endovenous thermal ablation. J Vasc Surg. 2012.

31. Rossner W, Tempel K. [Quantitative determination of the permeability of the so-called blood-brain barrier of Evans blue (T 1824)] Quantitative Bestimmung der Permeabilitat der sogenannten Blut-Hirnschranke fur Evans-Blau (T 1824). Med Pharmacol Exp Int J Exp Med. 1966;14: 169-182.
32. Hed J, Dahlgren C, Rundquist I. A simple fluorescence technique to stain the plasma membrane of human neutrophils. Histochemistry. 1983;79: 105-110.
33. Weddell G, Miller S. Cutaneous sensibility. Annu Rev Physiol. 1962;24: 199-222.
34. Kirstetter P, Lagneau F, Le Corre F, et al. Vascular properties of isoflurane: comparison between normal and cirrhotic rats. Br J Anaesth. 1998;81: 968-969.
35. Apps R, Garwicz M. Anatomical and physiological foundations of cerebellar information processing. Nat Rev Neurosci. 2005;6: 297-311.
36. Chaplan SR, Bach FW, Pogrel JW, Chung JM, Yaksh TL. Quantitative assessment of tactile allodynia in the rat paw. J Neurosci Methods. 1994;53: 55-63.
37. Smits ES, Duraku LS, Niehof SP, et al. Cold-induced vasodilatation in cold-intolerant rats after nerve injury. Journal of Plastic Reconstructive and Aesthetic Surgery. 2013;66: 1279-1286.
38. Castel A, Helie P, Beaudry F, Vachon P. Bilateral central pain sensitization in rats following a unilateral thalamic lesion may be treated with high doses of ketamine. BMC Vet Res. 2013;9: 59.
39. Carter RB. Differentiating analgesic and non-analgesic drug activities on rat hot plate: effect of behavioral endpoint. Pain. 1991;47: 211-220.
40. Jasmin L, Kohan L, Franssen M, Janni G, Goff JR. The cold plate as a test of nociceptive behaviors: description and application to the study of chronic neuropathic and inflammatory pain models. Pain. 1998;75: 367-382.
41. Oaklander AL, Brown JM. Unilateral nerve injury produces bilateral loss of distal innervation. Ann Neurol. 2004;55: 639-644.
42. Yen LD, Bennett GJ, Ribeiro-da-Silva A. Sympathetic sprouting and changes in nociceptive sensory innervation in the glabrous skin of the rat hind paw following partial peripheral nerve injury. J Comp Neurol. 2006;495: 679-690.
43. Saria A, Lundberg JM. Evans blue fluorescence: quantitative and morphological evaluation of vascular permeability in animal tissues. J Neurosci Methods. 1983;8: 41-49.
44. Swett JE, Woolf CJ. The somatotopic organization of primary afferent terminals in the superficial laminae of the dorsal horn of the rat spinal cord. J Comp Neurol. 1985;231: 66-77.
45. Decosterd I, Woolf CJ. Spared nerve injury: an animal model of persistent peripheral neuropathic pain. Pain. 2000;87: 149-158.
46. Smits ES, Duraku LS, Niehof SP, et al. Cold-induced vasodilatation in cold-intolerant rats after nerve injury. J Plast Reconstr Aesthet Surg. 2013.
47. Lauria G, Lombardi R, Borgna M, et al. Intraepidermal nerve fiber density in rat foot pad: neuropathologic-neurophysiologic correlation. J Peripher Nerv Syst. 2005;10: 202-208.
48. Louis SM, Jamieson A, Russell NJ, Dockray GJ. The role of substance P and calcitonin gene-related peptide in neurogenic plasma extravasation and vasodilatation in the rat. Neuroscience. 1989;32: 581-586.

01000011 01101000 01100001 01110000
01110100 01100101 01110010 00001010
00110011 00101110 00110011 00101110
00110001 00001010

Chapter 3.1

WEB-BASED ‘COMPUTER ASSISTED SURGICAL ANATOMY MAPPING’

A.L.A. Kerver, G-J. Kleinrensink, N.N. Smit, S. Rabbelier, B.M.W. Sedee, C.P. Botha

6th i.c. on Web Information Systems and Technology

ABSTRACT

In surgery one of the major problems is a safe approach of the operation site. For surgeons it is paramount to know the location of surgically relevant nerves and vessels. Especially in surgery of the lateral (outside) foot, the anatomy is not always completely clear since the location of nerves and vessels is highly variable.

Therefore **CASAM** is developed by students in Delft and Rotterdam (Netherlands). This web-application is based on the Django-framework and is a useful tool for three usergroups:

1) Researchers: After photographing dissected specimen a Thin Plate Spline transformation is used to compute an average foot and the pictures of individual specimen are warped to match this reference, average-foot. Renditions can be made to depict relevant surgical anatomy. Finally the researchers can define a zone in the lateral foot in which it is safe to approach the operation site.

2) Surgeons: Relevant anatomy (gathered by the researcher) can be warped over the picture of the patient. This pre-operative planning using CASAM assists the surgeon in determining a 'tailor made' safe-zone for each patient.

3) Students: For educational purposes, a drawn incision line can be compared to the computed location of nerves and vessels, thus providing personal feedback.

INTRODUCTION

In surgery one of the major problems is the safe approach of the operation site. Exposure of this operation site is the most important aspect but tissue sparing is just as important. In order to make a good evaluation between exposure and tissue sparing the knowledge of the related human anatomy is of paramount importance. For surgeons though, it is impossible to exactly know the anatomy of the complete human body mainly because:

1) There is an enormous inter- and intra-individual variety in human anatomy. The location of nerves, arteries and veins differs between each patient.
2) Since the dimensions of each specimen are different (shape, size, length width, etc) it is impossible to compare the anatomy of different specimen.
3) As new techniques are being developed to lessen complications the surgical procedures themselves often become more complex.
4) Some surgical procedures are very rare and a surgeon only does three or four of them per year.

Iatrogenic damage to nerves and vessels and hence postoperative pain and poor wound healing are a very common complication in surgery. To avoid damage of nerves and vessels it is imperative for a surgeon to know the exact location of important anatomical structures.

In order to overcome (some of) these problems, researchers at the Erasmus Medical Centre in Rotterdam began to map the human anatomy related to the 25 most current surgical procedures. In cooperation with the Delft Technical University: Faculty of Electrical Engineering, Mathematics and Computer Science; dept. of medical and data visualisation (head: Dr. C. Botha/ Dr. F.H. Post), a web-based tool was developed. The main focus of the tool was to be able to compare the anatomy of different specimen and relate it to a specific patient. Also, the application needed to be fast, user friendly and scientifically verifiable. Finally it needed to be easily accessible for our three main focus groups: researchers, surgeons, and surgical residents.

Many surgeons have dreamed of a preoperatively, real time available and easily accessible database to compare their patients to. The current web-based system tries to make a step forward in having this kind of database.

APPLICATION

One of the surgical procedures that illustrates these problems is the lateral (outside) approach of the calcaneus (heel bone) for fractured ankles. Up to 15% post-operative pain due to damage of the nerves and up to 10% wound necrosis due to damage of the arteries is reported[1]. As a fracture of the calcaneus is rare [2] surgeons on average only perform four of these surgical procedures per year.

User groups

This application can benefit three user-groups:

1) Researchers

A Thin Plate Spline transformation is used to project each picture of each individual specimen to match a reference, average-foot. Renditions can then be made to depict the relevant surgical anatomy (Figure 1). As an additional feature, the Point Distribution Model can display variations within anatomical structures.

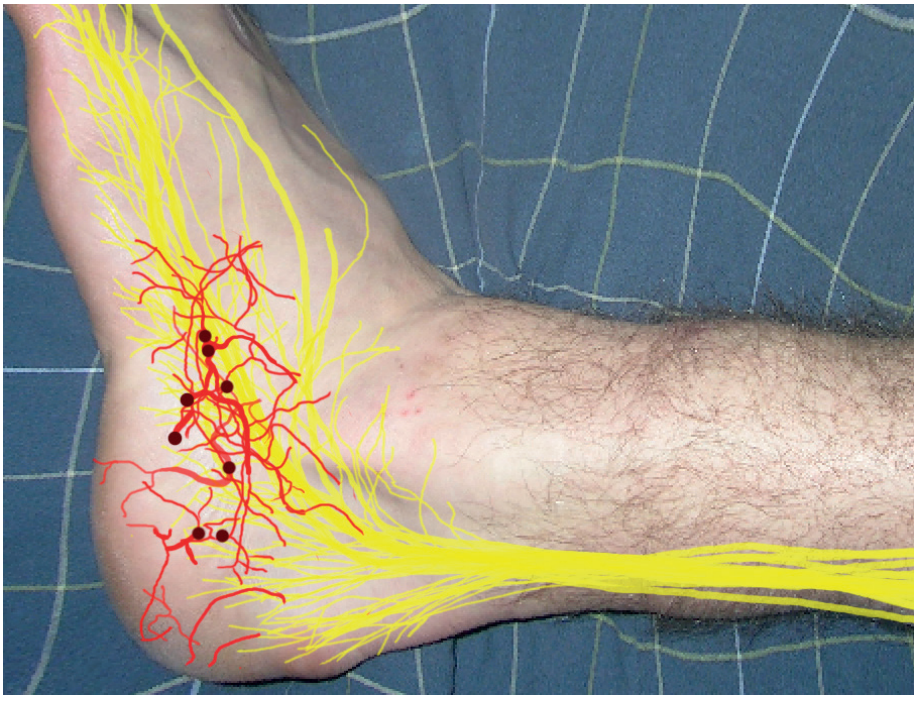

Figure 1. A patients lateral ankle depicting the surgically relevant anatomy of ten dissected sural nerves and six posterior tibial arteries.

Using these tools the members of our CASAM research project group can define a zone in the lateral foot in which it is safe to approach the operation site.

2) Surgeons

A simplified intuitive version of the web-application allows the surgeon to upload a picture of the ankle of his specific patient, after which he can warp the relevant anatomy (provided by the CASAM research group) over the picture of his patient (Figure 1). In this way the surgeon has an easily accessible database at his disposal to optimise his pre-operative planning and determine a 'tailor made' safe zone in each patient.

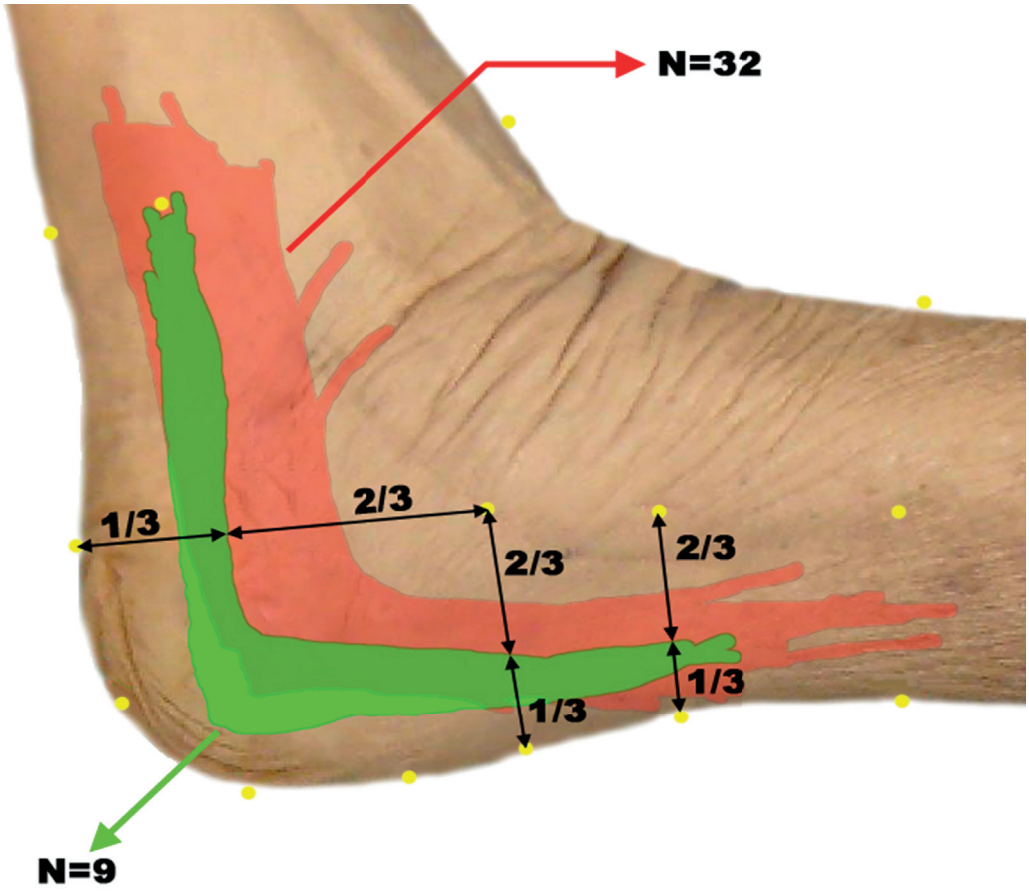

Figure 2 . CASAM-generated image, depicting an average leg in which 43 incisions drawn by 23 surgeons were evaluated. Red area: Incisions that were marked as 'wrong' (N=32). Green area: Incisions that were marked as 'good' (N=9).

3) Surgical Residents

Another version of the web-application allows the resident/student to upload a reference picture (for example real time, during an anatomy course) of a drawn incision line. Then, for educational purposes, this incision line can be compared to the gold standard or the computed location of nerves and vessels, thus providing personal feedback and hence making his /her learning curve steeper (Figure 1 and Figure 2).

Within each of these groups rights can be assigned to different users, to allow access to specific projects for specified users only. Also it is possible to differentiate between 'read-write' and 'read-only' access. A time-out for inactivity prevents unauthorized use of the data.

Features

Our software enables users to do their work in an efficient and intuitive manner. After log-in the user is presented with available projects (Figure 3).

Figure 3. The project selection screen in the web interface.

After selecting a project the main work area is shown where the user can view and edit (only when permitted) existing data or add new data (Figure 4). Implemented features include:

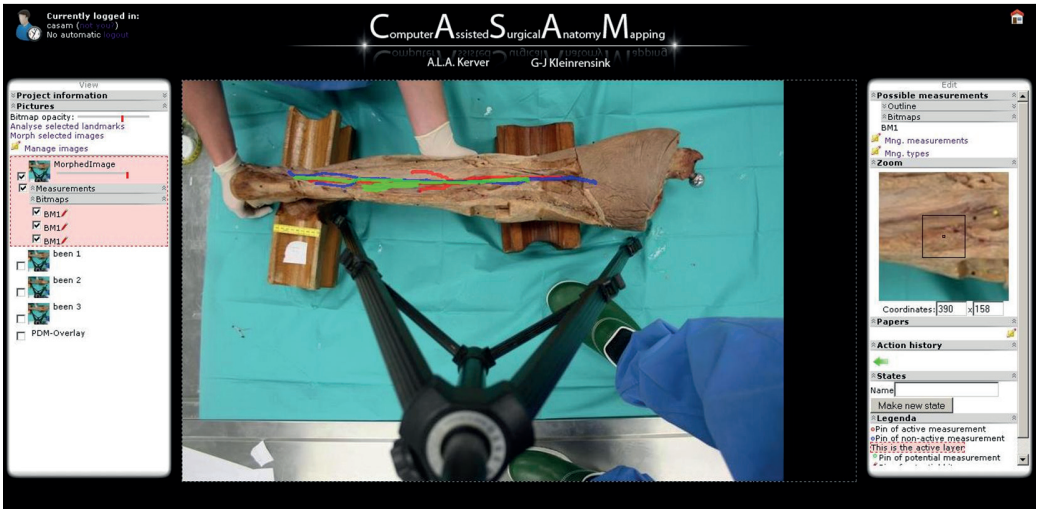

Figure 4. The web-interface work-area for researchers. Adding tags to projects for easy project reference;

- Adding tags to projects for easy project reference;
- Adding relevant scientific papers and URLs to projects;
- Fast adding and editing of shape-defining and anatomical landmarks;
- Accurate landmark-placement with the zoom-function;
- Transparency sliders for layered viewing and comparing of multiple images and overlays;
- Drawing bitmap overlays in any color to highlight structures of interest;
- Saving compositions of images, landmarks and bitmaps as states;
- Exporting project data to a zip- or CSV-file.

IMPLEMENTATION

Technologies

At the heart of this project Python, the Visualization Toolkit (VTK) and Python Imaging Library (PIL) were used for the required image processing techniques.

Also the Web framework Django was used. Its Object-relational mapper allowed to define our datamodels in Python and allow for dynamic database-access. The built-in automatic admin interface saved a lot of work. The present application also uses JavaScript and two JavaScript frameworks: Scriptaculous for some visual effects and Prototype for easy class-driven development and Ajax. For the webpage itself HTML and CSS was used. For the drawing application Flash was used.

Django was extensively used, especially its database and templating capabilities. This allowed for testing using a simple SQLite Database, whilst MySQL was used when deploying the system on a server. Another advantage of Django's database features is that no SQL queries had to be written, since Django handles these. This made it possible to write expressive queries, whose purpose is clear from looking at them. Django's templating system made it easy to separate the HTML code from the Python code. This results in a separation between logic and presentation, which is considered to be good coding practice.

The use of JavaScript makes our system highly interactive. Prototype allowed for creating a number of different classes within this system, so that users could be allowed to easily drag-and-drop the different landmarks, change the order of the different images, and even undo the (re)placement of the landmarks. Prototype also allows for easy access to Ajax-calls, so that most changes can be stored in the database, through the use of Django's mapper, without the users noticing it.

Image Processing

The first feature is a calculation of the Point Distribution Model (PDM), as developed by Tim Cootes, given a set of landmarks. This is a part of the Active Shape Model Cootes developed[3]. This model gives an overview of the average positions of the landmarks and local variations.

The second feature is an improvement of the original morphing technique. By defining several shape defining landmarks (for example, bony landmarks: anatomical landmarks that are palpable) per specimen all the drawn overlays can be morphed to the selected specimen, which serves as a 'gold standard specimen'. The morphing is done using a Thin Plate Spline[4] transformation. The end result is an image of the target specimen and the drawn overlays of other specimens morphed to the target specimen.

Exporting Data

Lastly, an export feature is provided, which makes it possible to export all data from the system into an archive. This archive can then be backed up to disk, and restored later in the event of a disk failure or similar. These imports can also be restored on another system, allowing for an easy way to exchange data between different researchers. Additionally, a method is provided to export landmarks as a comma separated value (CSV) file, which enables other researchers such as statisticians to work with the data.

DISCUSSION

All variations of a nerve or vessel cannot be mapped, as this would require an immense number of human specimen. Therefore CASAM cannot provide a definitive safe-zone. It can however make the range for safe approach to the surgical area more precise and hence decrease the occurrence of postoperative pain and wound management problems due to unintended iatrogenic lesions of nerves and vessels

As the CASAM method relies on extended image adjustments and computer calculations it is not 100% accurate. However, the CASAM method proved to be a great asset to visualize the complex anatomy and can be used in addition to conventional means of anatomy data gathering.

In this paper, the surgically relevant anatomy of the lateral (outside) foot and the surgical approach to the calcaneus were used as an example of the successful use of the application. The CASAM method, however, can be very useful for any 2D anatomy research.

At the moment the website with the CASAM database is improved to be more user-friendly and easily accessible to surgeons and residents around the world. Currently, several projects are performed to extend CASAM to a tool used for 3-D anatomy mapping .

CONCLUSION

The web-based CASAM method can prove to be a great asset to visualize the complex anatomy of the human body and can be used in addition to conventional means of anatomy data gathering. The gathered data is also more applicable for surgeons than the current situation. The data can easily be related to an individual

patient and 'tailor made' safe zones and advised incision lines might prove to lessen surgical complications. Students might benefit from more accurate safe zones and personal feedback on drawn incision lines might reduce the learning curve of modern complex surgeries.

Future work

Several improvements are planned for the web-application. Features we are still working on include:

- Compatibility with file formats other than JPEG;
- Use of multiple colors in one image in the drawing application;
- Replacing the Flash drawing application with a canvas implementation;
- Storing statistical data with landmarks;
- Measuring distances within images;
- Creating new graphical user interfaces for surgeons and students;
- Multi-level zooming.
- Verification of all anatomical data in embalmed specimen.
- Determine the clinical significance and functionality of the CASAM system

REFERENCES

1) Poeze M, Verbruggen JP, Brink PR. The relationship between the outcome of operatively treated calcaneal fractures and institutional fracture load. A systematic review of the literature. J Bone Joint Surg Am. 2008 May;90(5):1013-21.
2) Barei, D.P., 2000. Fractures of the calcaneus. Orthopedic Clinics of North America 2000
3) Cootes, T., 2000. An introduction to active shape models. In Image Processing and Analysis. Oxford University Press.
4) Bookstein, F.L., 1989. Principal warps: Thin-plate splines and the decomposition of deformations. In IEEE Transactions on pattern analysis and machine intelligence 11-6.

01000011 01101000 01100001 01110000
01110100 01100101 01110010 00001010
00110011 00101110 00110011 00101110
00110010 00001010

Chapter 3.2

‘COMPUTER ASSISTED SURGICAL ANATOMY MAPPING’
Advanced description of the web-based version

S.E.F. van Berkel, B. Bijl. J.Y.T. den Hollander, S. Rabbelier, B.M.W. Sedee, N.N. Smit.

Bachelor project nr. IN3405. Supervisors: A.L.A. Kerver, C.P. Botha, G.J. Kleinrensink, M. Sepers.

INTRODUCTION

The benefits of a web-based version of CASAM are numerous. Most importantly it gives the researcher full control over the algorithms used for averaging and warping. When commercial software, such as MagicMorph is used the exact algorithms and computations cannot be legally looked at directly and the final renditions can only be verified using conventional anatomy research. Furthermore, when all steps of CASAM are included in the web-site it provides a fully integrated system that allows for quick computations and rendition making without the need for any commercial software such as Photoshop and MagicMorph. This means that all aspects of CASAM are fully controlled by algorithms chosen by the developers and/or researchers.

A further obvious benefit of a web-based application is that it is accessible from anywhere. Working on your anatomy research from the comforts of your home whilst not needing a high-end computer would be possible since all calculations are done server-side. Also, all data is saved encrypted and backed-up server-side. A globally accessible anatomy database, with standardized ways for adding new data, would in theory be the necessary basis for international collaboration between anatomy labs.

Therefore the aim of this Bachelor project is to integrate each step necessary for CASAM into one web-based application, using only open-access libraries and algorithms. The principle idea is that the user can create a clinically relevant anatomy project. After dissecting and photographing multiple specimens in the dissection room he can add the images to that project. When the images are uploaded the user is guided through the different steps of CASAM; averaging, warping and making renditions.

IMPLEMENTATION.

The system was build using so called “spike solutions”(quick and simple solutions to subproblems) to build the different basic functions such as uploading images and placing landmarks on images using drag & drop. Spike solutions were also written for more specific functions such as the warping of photos and visualizing a point distribution model. Well-working spike solutions were then added to the existing system and basic functions.

Interface.

The design of the interface is of great importance as it mainly facilitates the interaction with the users; A well designed interface enhances the user`s

productivity. JavaScript and its libraries are mainly used for the interface. This allowed for easy implementation of visual effects such as drag & drop, fade, and the use of sliders. By using JavaScript it is also possible to use AJaX techonologies, allowing server request and page updates to be send without actual user input.

The main interface entails a left and right menu and centrally there is an area which contains the images (Figure 1). Both menu`s are divided into specific areas in which different tabs are loaded. Since most of the tabs are not used simultaneously the tabs are foldable.

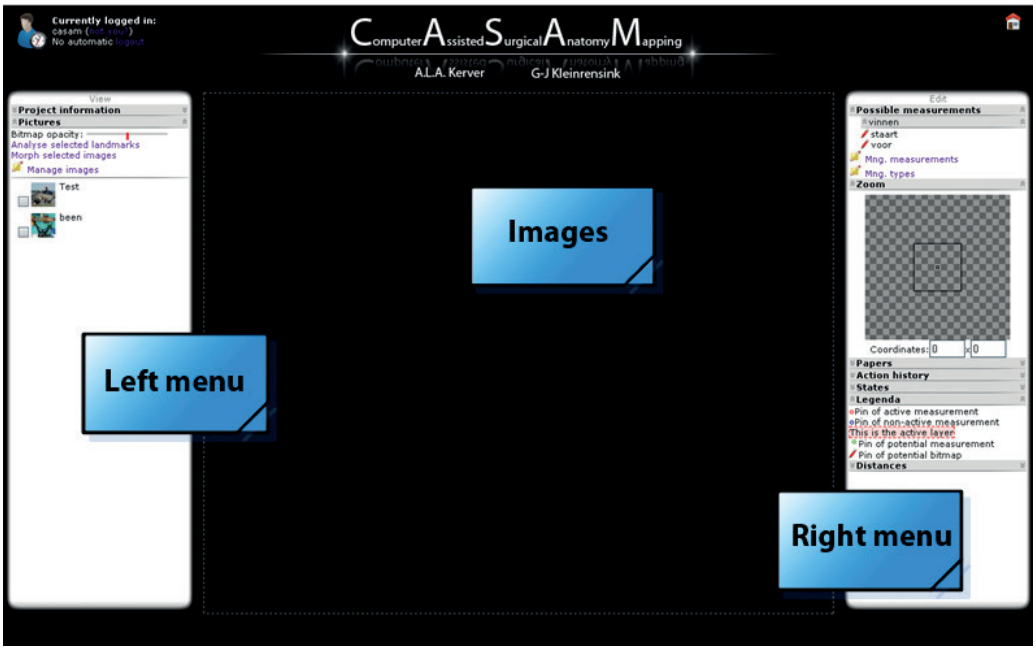

Figure 1. main interface design

The left menu shows project related settings and a list of project linked images with accompanying bitmaps and landmarks. The right menu shows tools for adjusting the images that are loaded in the left menu. The upper right tab contains measurements that can be applied to the currently active image. The next tab shows a magnified part of the active image, allowing for accurate landmark placement and measurements. Then there are tabs such as “action history” to undo changes and tabs for “relevant papers”, “States”, “Legend” and “Distances”.

The interface also provides several popups in which certain objects are managed. One window allows for adding and deleting images. There also are

popup windows for “Measurements” and “Classifying Measurements”. Popup windows need to be closed before work in the original window can be continued.

Visual effects were added to the interface for a fluid workflow. The effects provided by Scriptaculous are used for effects such as slide down tabs and fade-in popups. Also, in the left menu, added landmarks are briefly colored yellow to show that they have been added.

To manage different projects a project selection page was made (Figure 2) in which current projects can be selected and new projects can be added. Small thumbnails are shown for each project which change every few seconds, giving a slideshow of all images of the project.

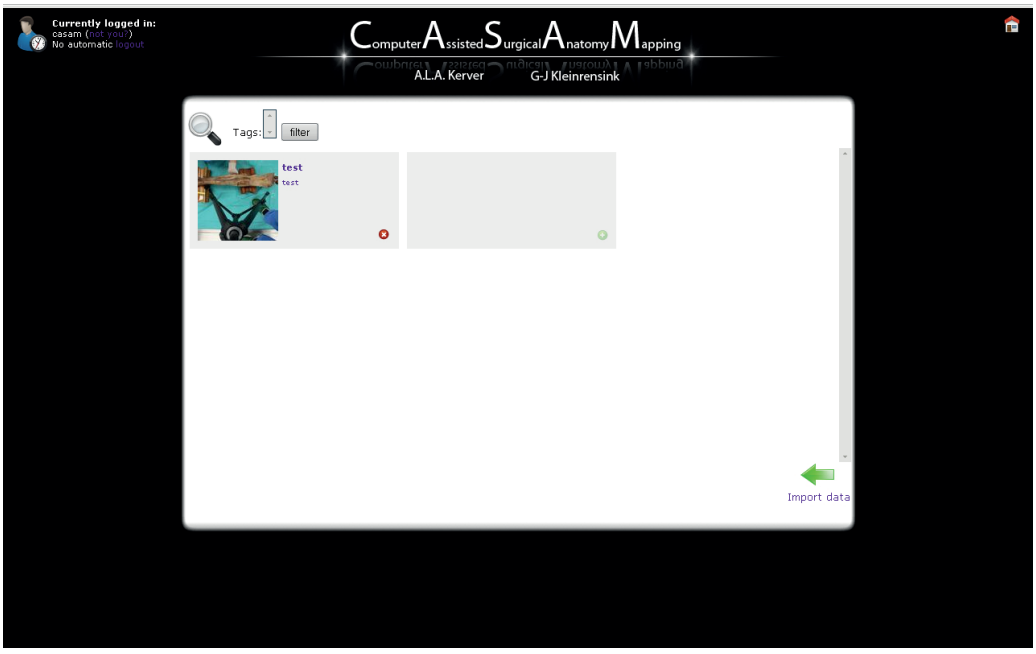

Figure 2. Project Selection page.

DATABASE SYSTEMS

First the database model needed to be made (Figure 3). Since CASAM needs to be an easy to implement web-application and Python libraries are needed for image processing Django was chosen as the framework for this application. Django is a python framework that can be used to built websites and web applications. It is a Model View Controller designed language, which means that the datamodel and functionality regarding this datamodel are separated from the user-interface and functionality regarding the user interface. Django also has a clear abstraction layer for the database component, the Object-Relational Database Mapping. This allows for object-oriented programming with a direct mapping of created objects to a relational structure. As created objects are mapped to the relational database, implementation of these objects is simplified significantly. The class diagram of the database system is shown in figure 3.

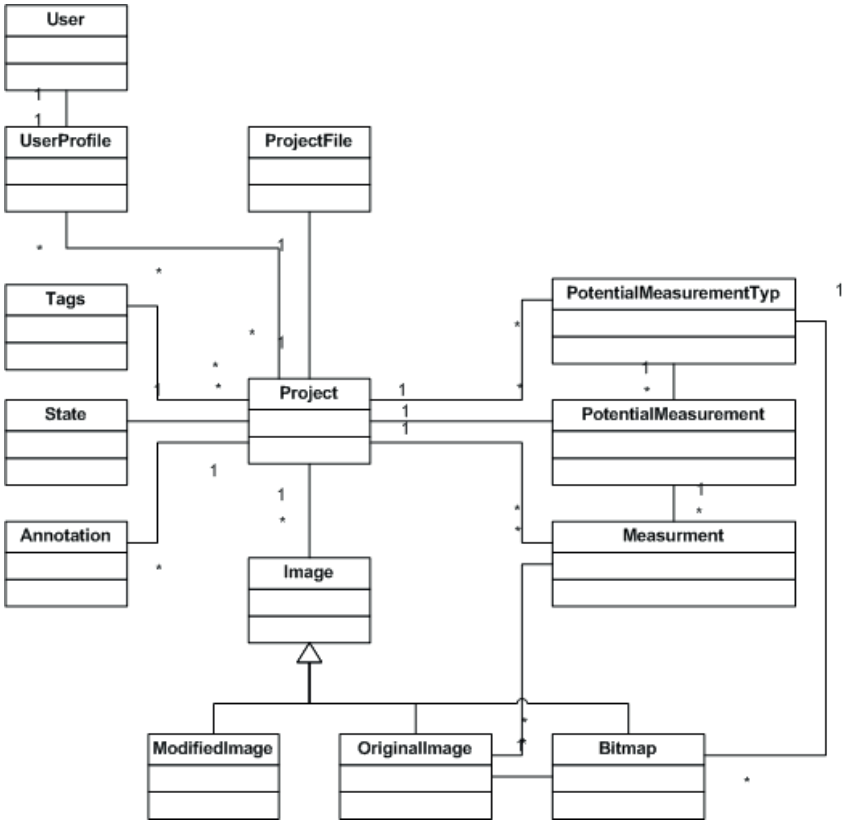

Figure 3. Class diagram of the database

ASPECTS OF THE DATABASE SYSTEM

Show multiple transparent images simultaneously

To show different highlighted renditions of anatomy it is imperative that multiple images, showcasing these renditions can be visualized simultaneously. The user needs to be able to change the order of images and their transparency individually. Therefore a slider is created for each image in each project. However the slider only loads when the image is made visible by the user. The user can then, using the slider, change the transparency of the corresponding image. The slider is derived from the Scriptaculous library. To change the order of images, a Sorttable was created in the left frame of the interface. The order of images can be changed by drag & drop of each individual image. The order of the images is automatically updated when a new image is added to the list. The image on top of the list also automatically is the "active image", meaning that computations are done on this image.

Landmarks

Landmarks are stored separately on another model in the database. This model is linked to three parts of the database: "potential measurements", the image the landmarks is part of and the project the image itself is part of. To save a landmark it fist needs to be created. When an image is loaded a listener is linked to it by JavaScript. The listener itself is removed when a new image is loaded and thus becomes the "active image".

The listener is activated when the image is clicked on (to create a landmark) and a popup window shows information on the landmark. In this popup window a PotentialMeasurement needs to be chosen to which that landmark belongs to, and an invisible ID of the image is added. When the landmark is saved (click on Save) the JavaScript code is checked for that specific landmark. If the landmark already exists a 'repositioning'-change is made in which the new coordinates are saved. Then an AJaX call is made to the server checking if that specific landmark of that specific image already exists. If it does exist it is retrieved and changed. If it does not exist, the landmark is added. In both cases the landmark is given back to JavaScript using a JSON-string. When the landmark is saved to the server the change is also saved in JavaScript. Finally, for an existing landmark, the position of the landmark is adjusted and a new "measurement" is created and placed on the correct new coordinates of the image.

Highlighting relevant parts of an image; Bitmaps

The flash-application is used to draw bitmaps over existing images to highlight relevant anatomy and anatomical areas. Figure 4 shows the sequence diagram of the flash application.

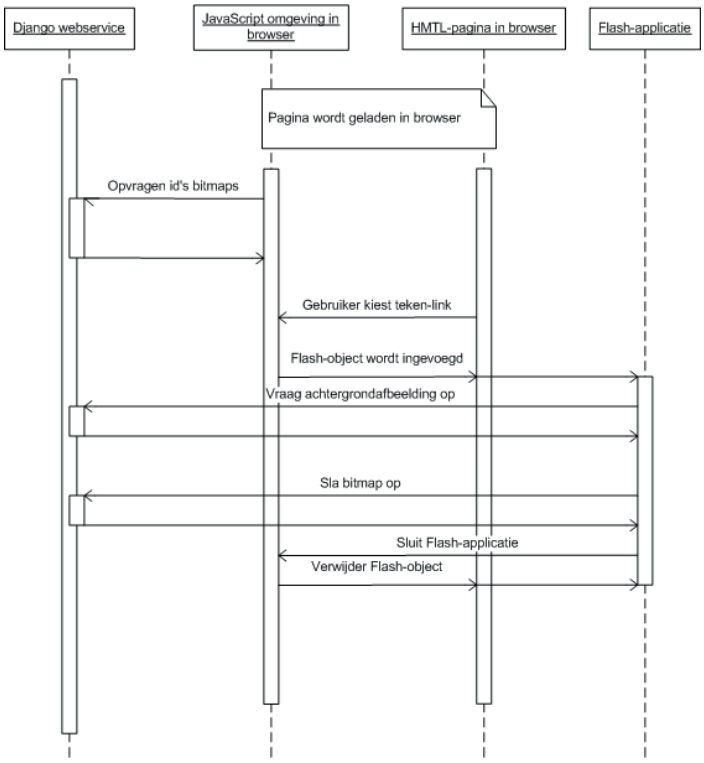

Figure 4. Sequence diagram of flash application.
The first part of the diagram shows how existing bitmaps are loaded in the JavaScript-environment. The rest of the diagram shows how the system reacts when the user chooses to either draw or adjusts a bitmap.

First, in the HTML-page, an object is added in which the flash application is loaded. Then the flash-application loads the image upon which is to be drawn. Both the size of the brush (the drawing tool) and the color can be adjusted. This allows not only for accurate highlighting of relevant anatomy such as nerves and arteries but also complete areas of for instance muscles can be colored.

When the user chooses to save the bitmap, the drawing is send to the server (Figure 5). If the drawing is successfully saved the Flash-application is given a confirmation and asks the JavaScript-environment to close the Flash-application.

Figure 5. Bitmaps drawn using the Flash application.

Adding relevant papers and websites

Papers and websites relevant to each specific project are saved in a separate model of the database. Papers can be stored locally and the link to a website consists of an URL. All relevant background can be accessed by the user under the "paper" tab.

Adding relevant Tags to a project

In order to categorize projects, Tags or Keywords need to be added. Especially in larger databases with numerous projects tags or keywords help users to access specific information. Also, by using tags, relations between different projects can be identified; If multiple projects for instance focus on a specific nerve the projects can be merged. When a new project is created the user can choose from a selection of existing tags. New tags can only be added to the project when the project is already created and open. This entices users to apply existing tags, thus promoting uniform tags that help link multiple projects.

Static states

States are a way of saving certain interesting sets of images, landmarks, measurements or bitmaps. A researcher can create a state, showing the nerves and arteries of 20 dissected specimen. A surgeon can then for example instantly load this state over the ankle of his patient; this makes data easily accessible to certain groups of users (surgeons/course participants) whilst other users (researchers) determine what exactly is shown. Currently when requested by the user, a part of

the HTML structure is saved as a state. This static state can then be opened as a pop-up.

Export datasets

As projects need to be interchangeable between different research departments (and databases) created objects are saved with Universal Unique ID`s. Since each object now has a unique ID it is possible to exchange datasets between multiple databases with a minimal chance of conflict. Administrators of databases are able to export and import these datasets. Datasets are exported to Zip-files and can either be imported automatically using the web-application or manually, using the script in the ZIP-package.

IMAGE PROCESSING

With CASAM variations of multiple specimens can be compared by warping individual specimen to match the average shape. One of the biggest aspects of the project therefore is Image Processing. The required techniques for a web-based version of CASAM could be implemented in multiple ways; Numpy[1], or bigger libraries such as Insight Segmentation and Registration ToolKit (ITK)[2] or the Visualization ToolKit (VTK)[3]. Also Python Imaging Library (PIL)[4] could be used for simple image processing. To combine the best of both worlds PIL was used in combination with the VTK library. The authors decided that to warp anatomical structures in a mathematically sound manner using part of the method for Active Shape Modelling[5,6], namely Point Distribution Models, in combination with Thin Plate Spline transformations[7].

Point distribution model

The goal of a point distribution model is to create an average and show the two main modes of variation, from a certain set of points. The user can select landmarks for each specimen (=image) and give each landmark a specific number and type. When all landmarks are selected for all specimen the user can click “Analyse selected landmarks” and the point distribution model of the selected landmarks is computed (Figure 7). JavaScript verifies which images and landmarks are selected and the ID`s of each image and all landmarks are passed on through an AJaX request. Using these ID`s the associated objects are then retrieved from the database. Then it is analysed if landmarks are suitable for a

point distribution model. Points are not suitable for a point distribution model if not enough points are selected or if points are of a different landmark type.

When the correct landmarks are selected a vtkUnstructuredGrid is made using the coordinates of the landmarks in each image. The vertices (a special kind of point that describes the corners or intersections of geometric shapes) represent the landmarks selected by the user. Then a Generalized Procrustes Analysis (a statistical analysis that compares the shapes of objects) is conducted using the vtkProcustesAlignmentFilter. By using the RigidBody mode, only rigid transformations (Chapter 2, translation, rotation, reflection) are used for the alignment of landmarks between each image.

The aligned grids are then put through a Principal Component Analysis (PCA) using the vtkPCAAnalysisFilter. This analysis reduces the variation of multiple landmarks into both an average point and linearly uncorrelated variables called principle components (Figure 6).

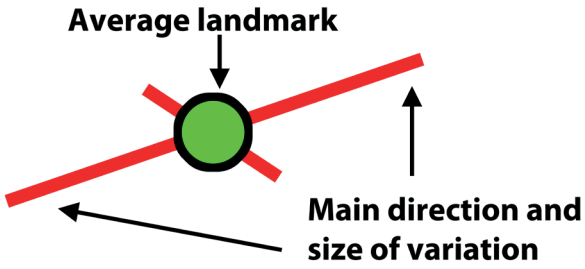

Figure 6. Point distribution model.
Average landmark and both the first and second principal component.

The first principal component has the largest possible variance and accounts for as much of the data variability as possible. The second principle component in turn has the highest variance possible as long as it is uncorrelated with previous components. In other words the green point represents the average of all landmarks of that type (for instance the lateral malleolus of 20 specimen) and the largest line represents both the direction and size of the largest (principle) variance (Figure 6 and 7). To compute these principal components the GetParameterisedShape is calculated (= three standard deviations from the mean). Visualisation of the computed data is done in PIL. Using the dimensions of the original image and the computed coordinates an ellipse is drawn. Then a line is drawn between the extremes of the ellipse, representing the two main modes of variation (principle components). The drawn lines and average landmarks are then projected on a

transparent background so they can be visualized over one of the original images (Figure 7).

Figure 7. Point distribution model of all landmarks of three different specimen.
Green dots: average landmark. red lines: first and second principle component (first and second direction and value of variation).

Thin plate spline transformation.

Similarly to the Point Distribution Model landmarks are loaded and read from the interface. Besides the normal landmarks checks as described for a PDM, for a warp all selected landmarks need to be shape-defining (ie. not measurement landmarks, or landmarks representing specific anatomical locations not used for warping). The shapedefining landmarks can be either bony or non-bony. The images and the accompanying coordinates of the landmarks are instantly transformed to vtkPoints objects. First al images and landmarks need to be aligned;l The vtkPoints are used in the vtkLandmarkTransform. vtkLandmarksTransform distinguishes between “source”and “target”. The “source”are the original coordinates of the landmarks of each image. The “target” can either be an average shape (created by the point distribution model) or a specific image (of a patient for example). Using vtkImageReslice the actual transformation is computed. To keep the quality of drawn structures the Nearest Neighbor method is chosen as the interpolation-mode. Similar to the Point Distribution model RigidBody mode is selected, so that images are aligned using only rigid transformations. The resulting grids are then used for the actual warp. The warp is implemented using

vtkThinPlateSplineTransform and the "source" are the images and landmarks that have been aligned previously. Again the "target" can either be an average shape (created by the point distribution model) or a specific image (of a patient for example). The end-result is shown using vtkImageReslice: all images, drawn bitmaps and landmarks are warped to match the "target" (Figure 8).

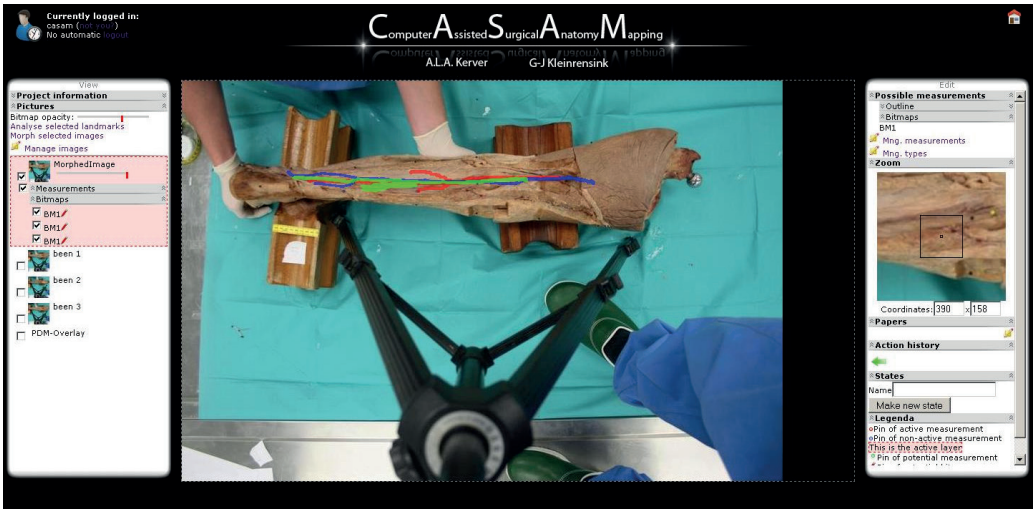

Figure 8. Warping.
"Morphed image" shows the warped bitmaps of three different specimen to match the shape of the first specimen. (the course of the short saphenous vein of three specimen is visualized over specimen nr.1)

CONCLUSION

With the web-based version of CASAM it is currently possible to perform all the necessary steps for CASAM online, using just your internet-browser; The images of multiple, photographed and dissected specimen are uploaded into a certain project. Then predefined landmarks can be placed which are either used for measurements or the warping process. Relevant anatomy can be highlighted in each individual specimen using the flash drawing application. An average shape of all the specimen can be computed using the Point Distribution Model. All drawn bitmaps, representing highlighted and relevant anatomy, can be warped to either match the average shape or the shape of a specific specimen (such as a patient). The technologies used in the web-based version of CASAM are summarized in figure 9.

Computations are done server-side, meaning that users with low-end computers will still be able to use CASAM and no commercial software is needed. If necessary, researchers from all over the world can be allowed to access and contribute to a project and the Export function allows for streamlined export and import of datasets between different databases.

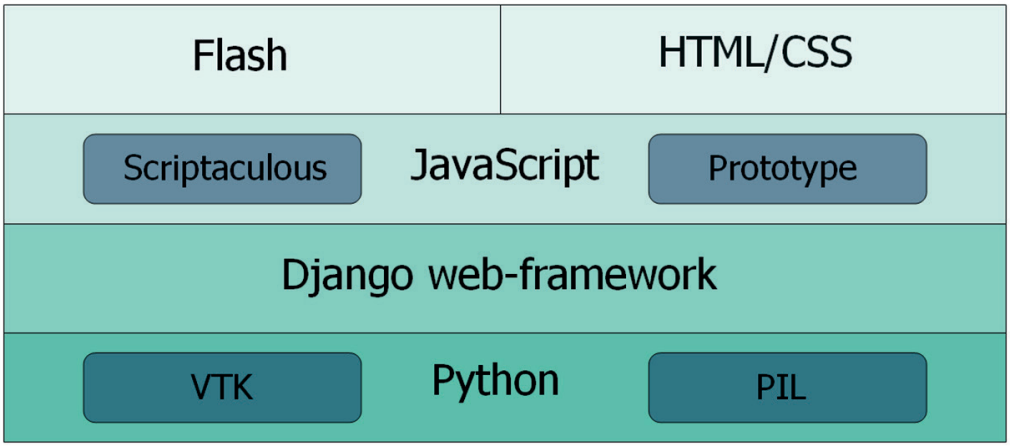

Figure 9. Technologies used for the web-based version of CASAM.
VTK: Visualization ToolKit[3] . PIL: Python Imaging Library[4].

APPLICATION IN PERSONALISED TEACHING

The web-based version of CASAM is especially well suited for an application in one of the main Pillars of modern surgery ; Personalized teaching. It is currently used in Anatomy and dissection programs at the Erasmus MC department of Anatomy and Neuroscience and benefits both residents and experienced surgeons. Using the web-based version of CASAM over the original CASAM means that whole process is much faster and the end-result is obtained quickly. Participants of a course on calcaneus (heel-bone) fractures for instance draw an incision line for a lateral approach of the ankle. The incision is either drawn using a skin-marker or made using a scalpel on an actual specimen of an ankle . The ankles with all drawn incision lines are then quickly photographed and loaded into the web-based version of CASAM. Since the dissected relevant anatomy of nerves and arteries is already loaded into the project their anatomy can be easily related

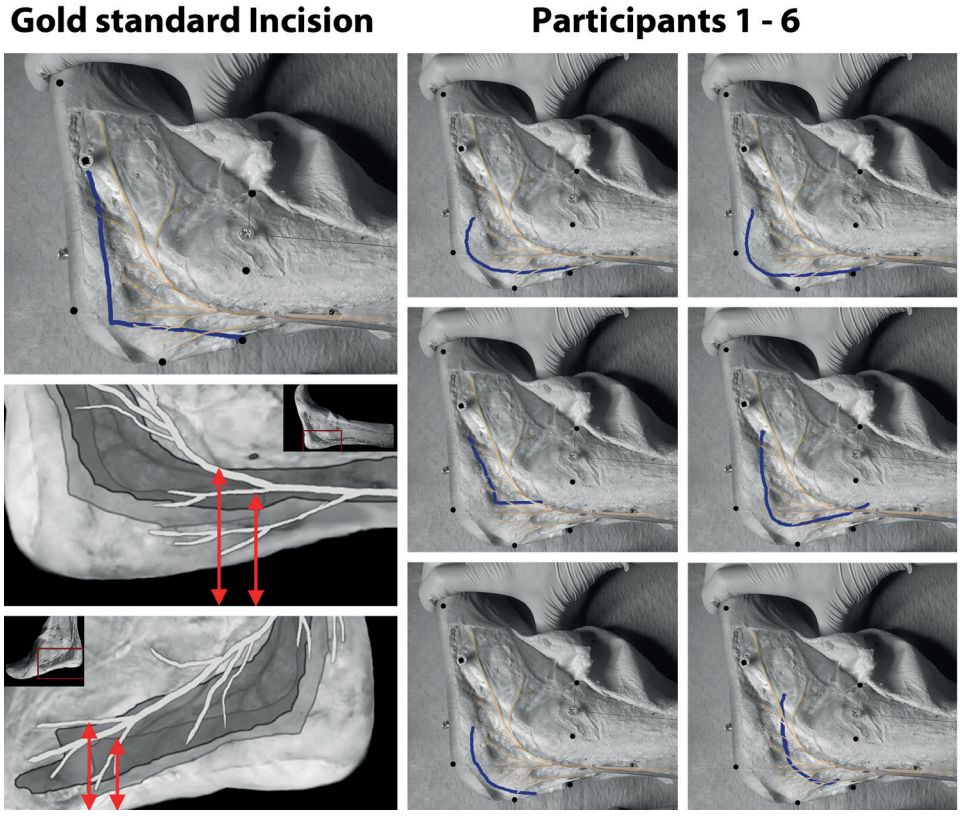

Figure 10. Incision lines of 6 participants related to the “gold standard”.

to each individually drawn incision line. Within an hour (and in the future within minutes) each individual course-participant has personal feedback on the incision line he drew himself on an actual ankle. The feedback can not only consist of the "gold standard incision line" (Figure 10) but also the location of 20 dissected nerves and or 20 dissected arteries (Figure 11).

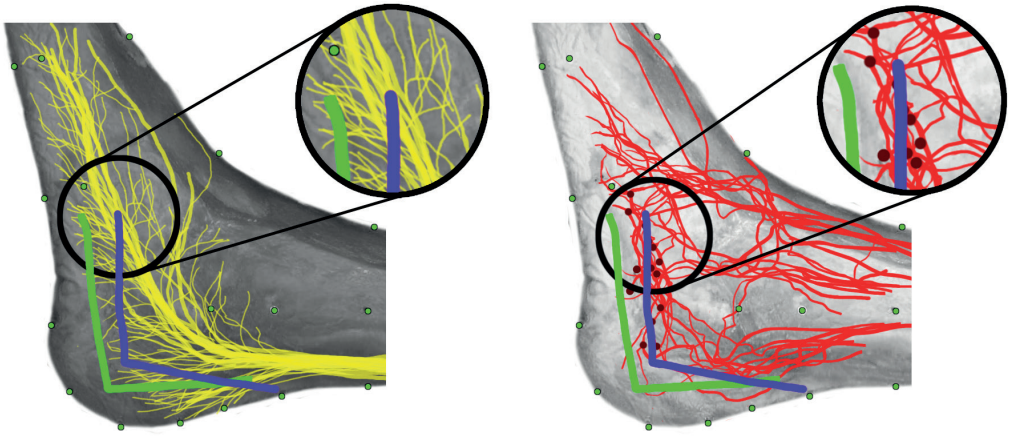

Figure 11. Examples of personalized feedback.
incisions of two participants in relation to the sural nerver (yellow) and main arterial blood supply of the lateral ankle (red). participant 1: good incision line (green). participant 2, bad incision line (purple). Notice how the incision line of participant two has more probability of damaging the sural nerve or the perforating artery (dark red dots).

REFERENCES

1) Numpy, 2009. http://numby.xcipy.org/ [Online; accessed 15-april-2009]
2) Itk insight toolkit, 2009. http://www.itk.org/ [Online; accessed 15-april-2009]
3) Vtk Visualization Toolkit, 2009. http://www.vtk.org/ [Online; accessed 15-april-2009]
4) Python imaging library (pil), 2009. http://www.pythonware.com/products/pil/ [Online; accessed 15-april-2009]
5) Tim Cootes. Statistical shape models. http://personalpages.manchester.ac.uk/staff/timothy.f.cootes/Models/pdms.html [Online; accessed 07-june-2009]
6) Tim Cootes. An introduction to active shape models. In Image Processing and Analysis, pages 223-248. Oxford University Press, 2000.
7) Bookstein, F.L., 1989. Principal warps: Thin-plate splines and the decomposition of deformations. In IEEE Transactions on pattern analysis and machine intelligence 11-6.

01000011 01101000 01100001 01110000
01110100 01100101 01110010 00001010
00110011 00101110 00110011 00101110
00110011 00001010

Chapter 3.3

Inter-surgeon variation in skin incisions for tibial nailing in relation to the infrapatellar nerve

A.L.A. Kerver, M. Leliveld, H.P. Theeuwes, M.H.J. Verhofstad, G.J. Kleinrensink.

Injury extra. 2010 Oct 26.

INTRODUCTION

Intramedullary nailing of the tibia has become the standard therapy for tibial shaft fractures. One of the most common complaints after this procedure is chronic anterior knee pain. This phenomenon is not yet elucidated, but might be associated with iatrogenic injury to the infrapatellar nerve. Damage of this nerve causes sensory disturbances in its area of distribution and also neuroma formation has been described. Although various surgical approaches of the entry point in the proximal tibia have been proposed, no consensus exists regarding the surgical-anatomical landmarks for a safe approach of the medullary canal.

Objective

To visualize the inter-surgeon variation in skin incisions for tibial nailing and to map the surgical anatomy of the infrapatellar nerve.

MATERIALS AND METHODS

Dutch trauma surgeons and residents (n=16) were asked to draw an incision for tibial nailing on different embalmed human knees. Incision placement was expressed in relation to these anatomical landmarks: the upper and lower edge of the patella, the tibial tubercle and the medial and lateral edge of the proximal tibia (Figures 1 and 2). Finally, the infrapatellar nerves of ten different cadaver knees were dissected and marked. All knees were digitally photographed and analysed using Computer Assisted Surgical Anatomy Mapping(CASAM),a new software tool that is able to depict all drawn incisions and all dissected infrapatellar nerves on real cadaver legs into one computed leg with standard dimensions.

RESULTS

On average trauma surgeons performed 5 (0–15) tibial nailing procedures per year and had 4.7 (0–16) years of experience. Form and place of the incisions were highly variable. Surgeons that performed five or more procedures per year mainly made a central incision whilst surgeons that performed less than five approaches per year showed more variation in incision placement (Figure 1). The variation in the topographic anatomy of the infrapatellar nerve was high, but it was mainly located medial of the patella and patellar tendon. Branching of the

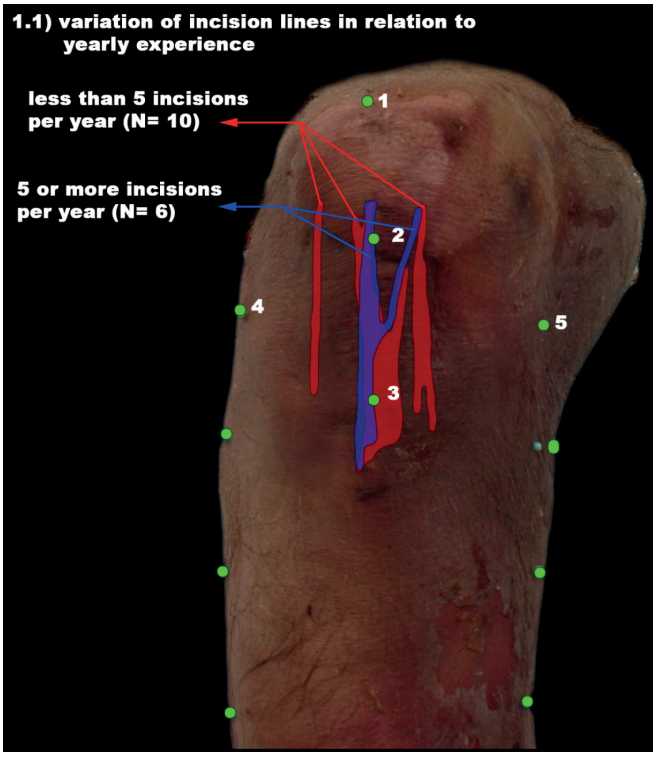

Figure 1. Variation of incision lines in relation to yearly experience.
With CASAM computed right knee with average dimensions; 1=patella top, 2= patella tip (distal), 3= tibial tuberosity, 4= lateral tibia plateau, 5= medial tibia plateau.

nerve occurred caudal to the patella and far most branches crossed the patellar tendon. Of 16 incisions drawn, only the lateral incision (n=1) would not have damaged an infrapatellar nerve branch. In the central incisions (n=10) and mainly in the medial incisions (n=5) the dissected infrapatellar nerves would have been at risk for transsection (Figure 2).

CONCLUSIONS

The variation between surgeons of the skin incision for tibial nailing appears highly variable. The infrapatellar nerve is at risk for iatrogenic damage in all vertical incisions except if performed lateral to the patella tendon. Oblique or horizontal approaches seem good alternatives to prevent iatrogenic nerve injury.

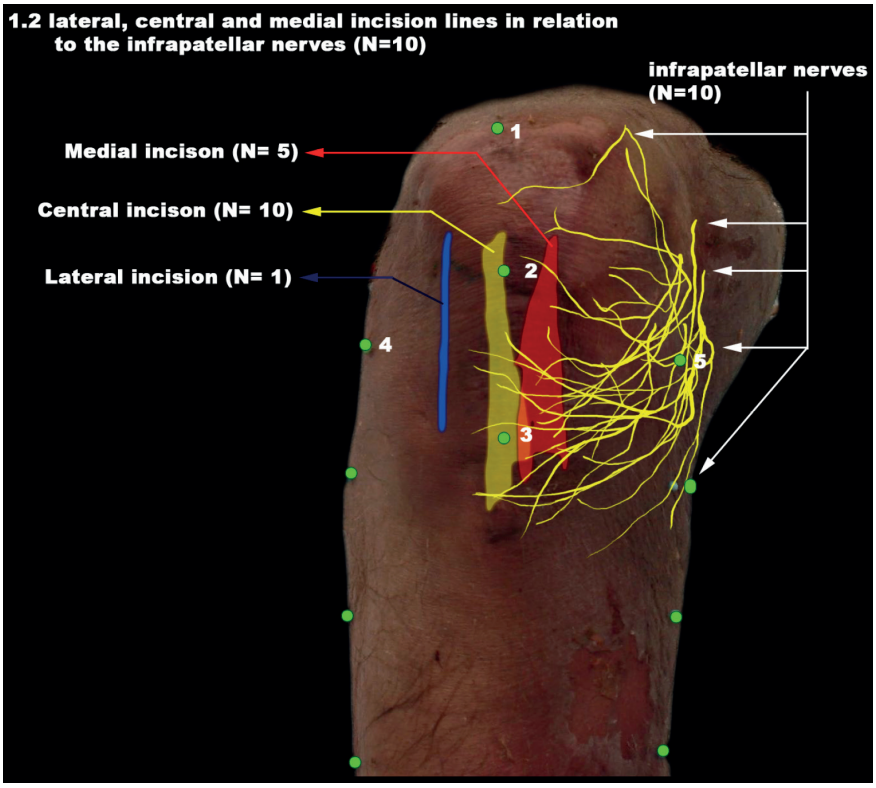

Figure 2. Lateral, central and medial incision lines in relation to the infrapatellar nerves (N=10) With CASAM computed right knee with average dimensions; 1=patella top, 2= patella tip (distal), 3= tibial tuberosity, 4= lateral tibia plateau, 5= medial tibia plateau.

01000011 01101000 01100001
01110000 01110100 01100101
01110010 00100000 00110011
00101110 00110100 00001010

Chapter 3.4

A CASAM study on the intra- and inter-surgeon variation of incision lines in the lateral approach of the calcaneus in surgical fracture treatment.

A.L.A.Kerver, K.W.J. Klop, W.E. Tuinebreijer, D. den Hartog, G.-J. Kleinrensink

Submitted 2017

ABSTRACT

Background: For intra-articular calcaneal fractures there is no real consensus on the treatment of choice and complication rates of surgical management are high. Surgeons are confronted with the basic dilemma between exposure and soft-tissue sparing. Our objective was to assess inter- and intra-surgeon variation in the extended lateral approach (ELA).

Methods: Dutch surgeons (N=23) were asked to draw two incisions for an ELA on embalmed ankles. Incisions were categorised, mapped and both inter- and intra-surgeon variation were quantified. Incisions were compared to the ELA gold standard and ten dissected sural nerves. Results were related to the surgeon`s experience in ELA surgery. Computer Assisted Surgical Anatomy Mapping (CASAM) was used to visualise data.

Results: Inter-surgeon variation was large, drawn incisions covered the entire lateral foot. Intra-surgeon variation was substantial, the second incision drawn varied over 6% of the dimensions of the foot. Based on four criteria of the gold standard nine incisions (22%) were accurate and 32 incisions (78%) demonstrated at least one aberration. The number of aberrations was not correlated to the surgeon`s experience. L-shaped incisions demonstrated less aberrations than J-shaped incisions. The main branch of at least one of ten sural nerves was at risk for transection in 35 of 41 incisions. In an incision following the gold standard the sural nerve would still be at risk in 10% of the specimen.

Conclusions: Even though ELA surgery is mainly performed by surgeons with many years of experience, inter- and intra surgeon variation was high. Only 22% of incisions followed the criteria of the gold standard. The main branch of the sural nerve is at risk in almost all incisions, even in an incision conform the gold standard. Consistent incision placement conform the gold standard seems teacher-based, not experience-based.

Clinical relevance: These findings suggest there is a need for an anatomy based teaching model for ELA aimed at both novice and expert surgeons in an attempt to lower current complication rates for intra-articular calcaneal fractures.

INTRODUCTION

Fractures of the calcaneus predominantly occur in young, active men. They represent one to two percent of all fractures in adults[1,2] and approximately 75% of fractures affecting the hindfoot[3]. No universal treatment or surgical approach exists that can be applied to treat all fractures of the calcaneus. Even though extensive research has been done on treatment, complications and diagnosis, no consensus has yet been reached on the treatment of choice. As many factors influence the surgeon`s treatment of choice[4] careful patient selection is important for good outcome[3, 5-7]. The lack of consensus may partially be due to the lack of a uniform classification and outcome-scoring system[1, 8]. However most surgeons consider Open Reduction and Internal Fixation (ORIF) to be the approach of first choice[9], 10. ORIF is not a uniform procedure. Many variants of ORIF have been described but the extended lateral approach (ELA) has been used most frequently[11, 12], as it provides the surgeon with good exposure for fracture management[13].

Complication rates for ORIF vary. Infection rates for a lateral approach vary between 1.3 to 21% [10, 14-16] and the rates for subtalar arthrodesis vary between zero and 15.4%[14]. Poeze et al. demonstrated that these complications were inversely correlated to institution's fracture load and the number of calcaneus fractures a surgeon operates per year[14]. Furthermore Sanders et al. stated that calcaneal surgery has a substantial learning curve as it is technically challenging[17].

Also, the skin incision is an important issue because this represents the basic surgical dilemma of creating a good exposure versus (nerve and vessel) sparing soft tissue. Arterial damage may result in necrosis of the wound or lateral hindfoot if the incision is not placed considering the angiosomes in the lateral hindfoot. Superficial necrosis is seen in 0.4 to 14% [15, 18]. Depending on the location of the incision the sural nerve might be at risk[17, 19-22] especially since the skin and soft tissue are usually mobilized as a thick soft-tissue flap[19, 23]. Sural nerve damage is seen in up to 10% of patients[22]. Iatrogenic sural nerve lesion can lead to different levels of post operative pain varying from numbness to sharp invalidating or even causalgic pain[22, 24].

The aim of the current study therefore is to explore whether:

1) there is any inter- and/or intra- surgeon variation in the skin incision when a surgeon is asked to draw an incision line for ELA and how these incisions compare to the ELA gold standard or the location of the sural nerve.

2) the results of these research questions are related to the surgeons years of experience and/or the number of ELA procedures he or she performs per year.

MATERIALS AND METHODS

Twenty three surgeons were asked to each draw an incision line, proposed for the ELA, on two different embalmed anatomic specimens. The specialty of each surgeon (trauma-, orthopaedic- or general surgery) was noted as well as his/her years of experience in ELA and the estimated number of ELA procedures performed last year. Then bony landmarks (Figure 1) and a ruler were placed. The ankles were photographed using a Canon 350D with a Canon EF-S 18-55 mm lens via a standardized protocol. Photographs were loaded into stack in Photoshop CS-4[25]. Non-bony landmarks were calculated from bony landmarks

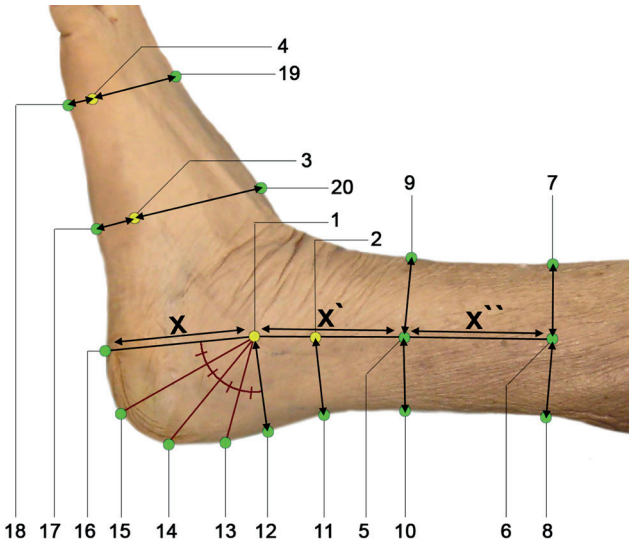

Figure 1. landmarks used for CASAM
Yellow: bony landmarks: The most distal (= malleolus tip; 1) and the most proximal part of the malleolus (malleolus top; 2), the tuberosity of the fifth metatarsal (3) and the fifth metatarsal head (4).
Green: non-bony landmarks: On the sole of the foot: The nearest point to the tip of the lateral malleolus (16), the nearest point to the tuberosity of the fifth metatarsal (17), the nearest point to the fifth metatarsal head (18). On the foot ridge: the nearest point to the fifth metatarsal head (19), the nearest point to the tuberosity of the fifth metatarsal (20). On the achilles tendon: the nearest point to the tip of the lateral malleolus (12), the nearest point to the top of the lateral malleolus (11).
The distance between landmark 1 and 16 (X) was used to create landmark 5 (X`) and 6 (X``) (in line with the tibia). Landmarks 7 and 8 are the nearest points on the posterior and anterior side of the leg to landmark 6. Landmarks 9 and 10 are the nearest points on the posterior and anterior side of the leg to landmark 5.
The angle between landmark 12 and 16 over landmark 1 was measured and divided into four segments (Red lines), thereby creating landmarks 13, 14 and 15 on the edge of the hindfoot.

to delineate the different shapes of the ankles (Figure 1). All landmarks were assessed independently by two authors and test-retest reproducibility of the landmarks was determined.

The photographed ruler was used as a reference for measurements taken with the "Ruler tool" in Photoshop. The accuracy of digital measurements had been verified in four specimens.

Statistical analysis was performed in SPSS version 17.0.

Computer Assisted Surgical Anatomy Mapping (CASAM)

CASAM[26-28] is a new method to evaluate the anatomy of multiple specimens. For this method MagicMorph 1.951029 is used to compute an average size of all specimen to which each photographed ankle is resized. As the dimensions of all ankles were the same, the individual incision lines and the relative anatomy could be compared.

Inter-surgeon variation

Incision lines were categorised as J- or L-shaped. The location of each incision was measured in relation to the landmarks (Figure 1). However, as the shape of each ankle differed, the location of drawn incisions could not be compared when expressed in absolute numbers (mm). Therefore the location of an incision was also expressed as a relative ratio related to four of the shape defining measurements (Figure 2, Table 1).

Furthermore the angle between the proximal (vertical) and the distal (horizontal) part of the incision lines was measured (Figure 2)

CASAM: Incisions were visualized in one ankle with average shape and size. An area of spreading was defined in which all drawn incision lines were located.

Statistics: The mean years of experience, number of ELA surgeries per year and angle of incision lines were calculated for J- and L-shaped incisions and the comparison was tested.

Intra-surgeon variation

In order to determine a surgeon`s consistency, the relative location of both incisions was compared (Table 1, ratio 1 - 4). The mean intra-surgeon variation was quantified as the mean difference in the relative location of both drawn incisions over all four ratios. Also the difference between the angles (Figure 2) of both incision lines drawn by the same surgeon was calculated.

Statistics: The mean intra-surgeon variation and difference in incision angle was calculated for J- and L-shaped incisions and the comparison was tested.

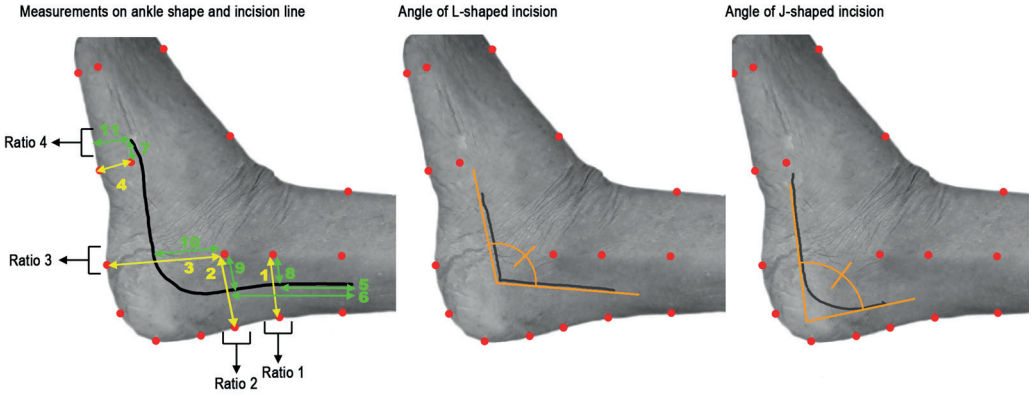

Figure 2. Measurements taken in original pictures
Black line: incision line drawn by a surgeon. Red dots: landmarks

Yellow lines/numbers: general measurements concerning the shape and size of the ankle.
Green lines/numbers: measurements regarding the location of the incision line.
orange lines: measurements regarding the angle of incision lines

Relative location of incision lines:
Ratio 1: (incision measurement 8 as a ratio of shape defining measurement 1)
Ratio 2: (incision measurement 9 as a ratio of shape defining measurement 2)
Ratio 3: (incision measurement 10 as a ratio of shape defining measurement 3)
Ratio 4: (incision measurement 11 as a ratio of shape defining measurement 3)

The correlation coefficient between intra-surgeon variation and a surgeon`s experience was calculated.

Comparison to the gold standard

Based on an ELA incision exactly conform gold standard (Figure 6)[30, 31,] ratios one to three (Table 1) had to be more than 66% for an incision to be conform gold standard. Also the distal part of an incision could not be located more than 5 mm superior to landmark three. Thus, a surgeon could make four aberrations per incision line (based on ratio 1-3 and the 5mm rule). An incision was marked as "accurate" if no aberrations were made.

CASAM: Incisions reshaped with CASAM were assessed equally. Two new areas of spreading were computed, one representing all accurate incisions and one representing all incisions with at least one aberration when compared to the gold standard.

Statistics: The median number of aberrations per surgical specialty and per J-or L-shaped incisions was calculated and the comparison was tested. The

Table 1, Measurements	Measurement Nr. (fig2)	from	to	Mean (mm)	Range from	to
defining the shape of each ankle (fig. 2, yellow)	(1)	landmark 2	achilles tendon	35.54	24.55	48.19
	(2)	landmark 1	achilles tendon	41.39	29.65	54.85
	(3)	landmark 1	sole of foot	65.08	49.89	82.49
	(4)	landmark 3	sole of foot	15.96	8.48	25.78
Proximal and distal endpoint of incision line (fig. 2, green)	(5)	proximal end of incision	the level of landmark 2	14.90 *	0.00	40.18
	(6)	proximal end of incision	the level of landmark 1	26.67 **	1.43	29.21
	(7)	distal end of incision	landmark 3	14.35 ***	0.00	43.71
Incision location (fig. 2, green)	(8)	landmark 2	incision (proximal)	23.97 *	12.35	41.17
	(9)	landmark 1	incision (proximal)	25.54 **	13.1	14.8
	(10)	landmark 1	incision (distal)	37.90	22.1	58.77
	(11)	incision (distal)	sole of foot	22.76	10.57	44.31
	Ratio	**Description**		**Mean (%)**	from	to
Relative location incision	ratio 1	(8) as a ratio of (1)		66 **	43	93
	ratio 2	(9) as a ratio of (2)		61 *	39	77
	ratio 3	(10) as a ratio of (3)		58	36	75
	ratio 4	(11) as a ratio of (3)		35	17	75
Intra surgeon variation	ratio 1	incision 1 - incision 2		9	2	20
	ratio 2	incision 1 - incision 2		8	0	23
	ratio 3	incision 1 - incision 2		4	0	9
	ratio 4	incision 1 - incision 2		6	0	18

Table 1.
* N=40. In one of the cases the incision was not extended proximal of the tip of the lateral malleolus, this case was excluded from the above calculation. The incision ended 4.5 mm distal of the tip of the lateral malleolus.
** N=22. In 19 cases where the incision was not extended proximally past the top of the malleolus, the average deficit was 15.97 mm (N=19, range 1.43-29.21 mm).
*** N=15 In cases where the incision was not extended distally past the tuberosity, the average deficit was 10.67 mm (N=26, range 1.59-34.79 mm).

correlation coefficient between the average number of aberrations a surgeon made and his experience was calculated. Finally correlation coefficients between the mean number of aberrations and intra-surgeon variation in both incision location and incision angle were calculated.

The incision in relation to the sural nerve

The sural nerves of ten additional specimens were dissected and photographed. Photographed specimens were reshaped with CASAM to match the computed average ankle. Thereby the incisions could be compared to the computed location of ten sural nerves.

Also, an ELA incision was drawn exactly according to the gold standard and it was compared to the location of the sural nerves.

RESULTS

Of 46 drawn incisions, five were discarded due to insufficient visibility of the incision or landmarks. Of 23 participating surgeons five were orthopaedic-, 12 trauma- and six were general surgeons. On average they had 13 years of experience (range 0-27) and performed 5 calcaneal surgeries per year (range 0-20). There was a strong correlation between the years of experience a surgeon had in ELA and the number of calcaneal surgeries performed per year. (Pearson`s ρ=0.621, p=0.002, N=22, one outlier removed[32]). Correlation coefficients of either one of these variables were therefore corrected for the latter and tested for multicollinearity[33].

Inter-surgeon variation

Of 41 incision lines drawn, 56% (N=23) incisions were J-shaped and 44% (N=18) incisions were L-shaped. Measurements regarding the location of the incision lines drawn are shown in Table 1. The proximal part of 22 incisions extended proximal of the lateral malleolus top at a mean distance of 14.9 mm, 19 incisions extended proximal of the lateral malleolus tip but not the lateral malleolus top and one was not extended beyond the lateral malleolus tip.

The distal part of 15 incisions extended beyond the tuberosity of the fifth metatarsal bone at a mean distance of 14.4 mm. In 26 cases the incisions stopped at a mean distance of 10.7 mm proximal to the tuberosity of the fifth metatarsal bone.

The average distance in height between the tuberosity of the fifth metatarsal bone and the incision was 6.1 mm (range -7.2 – 25.8 mm).

The relative location of the proximal part of incision lines was located at 66% (range 43 – 93%) of measurement one and at 61% (range 39 – 77%) of measurement two. The distal part of incision lines was located at 58% (range 36 – 75%) of measurement three. The distal end of incision lines was located at a level of 35% (range 17 – 75%) of measurement three.

CASAM: The drawn incisions demonstrated a wide variety in both location and shape. The computed area of spreading almost covered the entire lateral side of the foot (Figure 3).

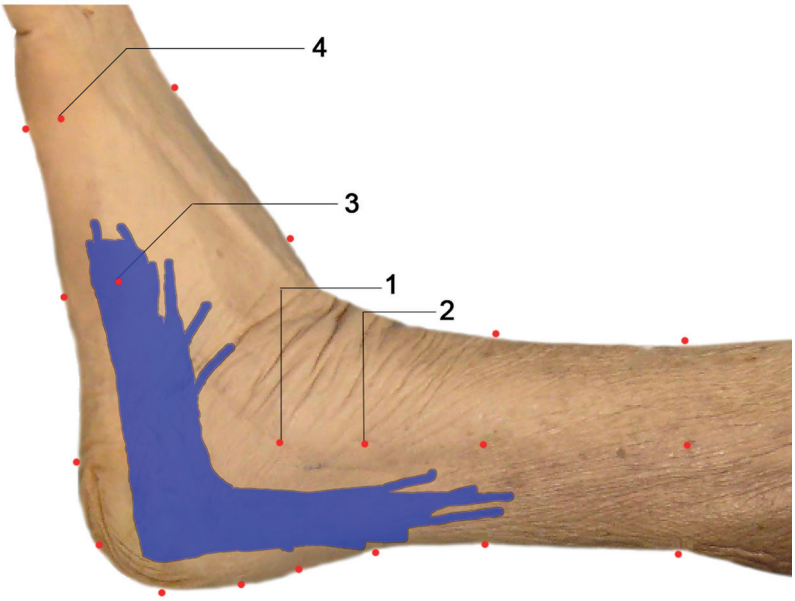

Figure 3. Spreading of all incision lines
With CASAM generated image depicting an average ankle in which all incision lines were warped.
Red dots: used landmarks.
Blue area: spreading of all drawn incision lines (n=41)

Statistics: Surgeons who drew a J-shaped incision on average had 13.5 years of experience (range 0-25) and performed 4.4 lateral calcaneal surgeries last year (range 0-10). Surgeons who drew a L-shaped incision on average had 12 years of experience (range 2 – 23) and performed 2.8 lateral calcaneal procedures last year (range 1.5 - 5). There was no statistical difference between J- and L-shaped incisions when related to years of experience (p=0.706, Mann-Whitney) or ELA`s performed per year (p=0.782, Mann-Whitney).

The mean angle of incision differed significantly (p=0.015, Mann-Whitney) between J-shaped (91.2° ± 12.1°) and L-shaped (99.3° ± 6.6°) incisions.

Intra-surgeon variation

The relative location (Table 1, ratio 1- 4) of both incisions drawn by the same surgeon varied.

Proximally the difference was 9% (range 2 - 20%) over ratio 1 and 8% (range 0 - 23%) over ratio 2. Distally the difference was 4% (range 0 – 9%) over ratio 3 and 6% (range 0 – 18%) over ratio 4. The average intra-surgeon variation over all four ratios was 6.3% (range 1.0 – 11.0%). Thus the intra-surgeon variation in incision line placement was on average 6.3% of the corresponding shape defining measurements (Figure 2, ratio 1- 4).

The mean intra-surgeon variation of the angle between the proximal and distal part of the incisions was 7.4° degrees (range 0.6°-17.6°).

Statistics: The mean intra-surgeon variation between two drawn incisions did not differ (p= 0.171 Mann-Whitney) between J-shaped (7.2% ± 2.1%) and L-shaped (5.4% ± 3.0%) incisions. The mean difference in incision line angle did not differ (p=0.216 Mann-Whitney) between J-shaped (8.7° ± 5.9°) and L-shaped (5.4° ± 3.9°). Intra-surgeon variation was not correlated to the number of ELA`s a surgeon performed per year (p=0.109, Pearson) or the years of experience a surgeon had in ELA surgeries (p=0.736, Pearson). Intra-surgeon variation in incision location was significantly correlated to the mean difference in angle between both incisions (Pearson ρ=0.596, p=0.012). Correlation coefficients of either one of these variables were therefore corrected for the latter and tested for multicollinearity.

Comparison to the gold standard

When the relative location of an incision and the height of an incision relative to landmark 3 were compared to values of the gold standard only nine incisions (22%) were considered “accurate”. The other 32 incisions (78%) were aberrant on one or more of the four criteria for an incision conform the gold standard (based on ratio 1 - 3 and the 5mm rule). Nine incisions demonstrated one aberration (22 %), ten incisions demonstrated two (24 %), eight incisions demonstrated three (20 %) and five incisions demonstrated four aberrations (12 %).

CASAM: Results computed with CASAM were identical; nine “accurate” and 32 “aberrant” incisions (Figure 4). Most aberrations were located on the proximal side of the incision, as incisions were drawn too close to the lateral malleolus.

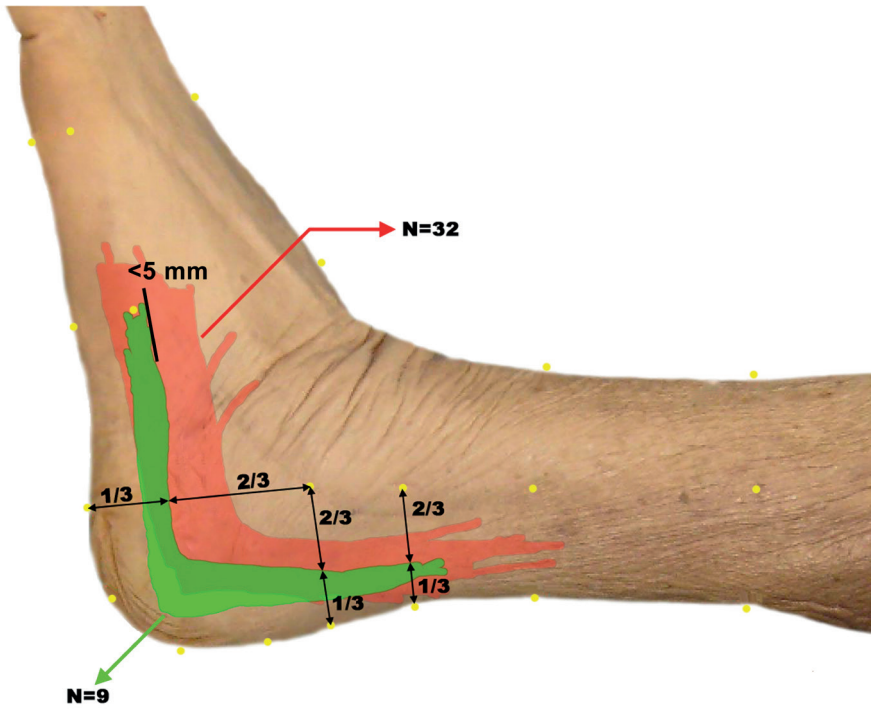

Figure 4. Comparison to the gold standard
With CASAM generated image, depicting an average leg in which all incision lines were warped
Yellow dots: Landmarks used
Red area: spreading of all incision lines with one or more aberrations (N=32)
Green area: spreading of all incision lines in accordance with the gold standard (N=9)

Statistics: The median number of aberrations was one (IQR=2) for orthopaedic surgeons, two (IQR=2) for trauma surgeons and two (IQR=3) for general surgeons (p=0.181, Kruskal-Wallis). There was a significant difference (p=0.018, linear chi-square34) in the number of aberrations in L-shaped incisions (median=1, IQR=2) and J-shaped incisions (median=2, IQR=2). In comparison to L-shaped incisions, J-shaped incision were 4.3 times more likely to have 3 or 4 aberrations instead of 0-2 aberrations (p=0.13 chi-square). The mean number of aberrations a surgeon made in both incisions was not correlated to the number of ELAs a surgeon performed per year (p=0.139, Pearson) or to the years of experience a surgeon had in ELA (p=0.148, Pearson). The mean number of aberrations per surgeon was not correlated to intra-surgeon variation in incision location (p=0.407 Pearson), but was correlated to the mean difference in angle between both incisions (Pearson`s ρ=0.661, p=0.005).

Comparison to the sural nerve

The distribution on the location of the main branch of the dissected sural nerves was small. Of 41 drawn incisions, 35 incisions (85 %) overlapped at least one main branch of the ten sural nerves. Six incision lines had no overlap with any main branch (Figure 5).

An incision line drawn exactly conform the gold standard would have damaged the main branch of one (10%) of the ten dissected sural nerves (Figure 6).

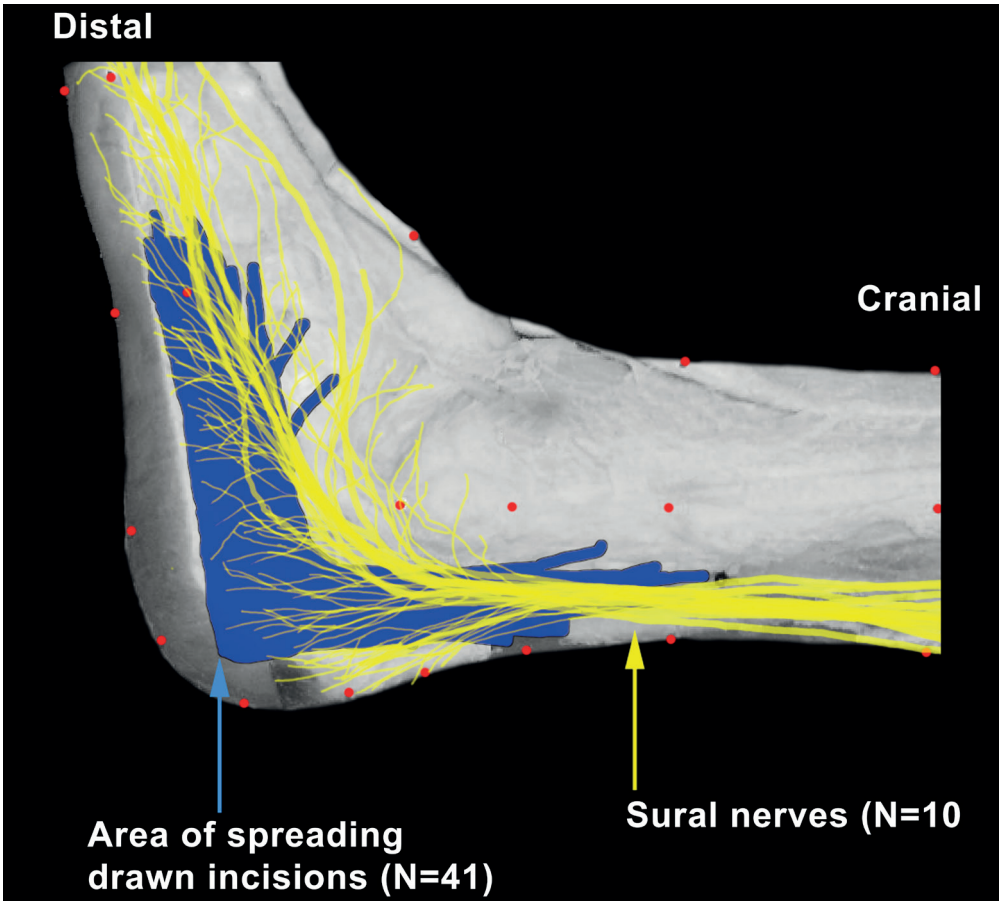

Figure 5. Spreading of incision lines and sural nerves

Lateral view of ten dissected sural nerves. With CASAM the original pictures were warped to match the average ankle size and renditions were made to depict the ten dissected sural nerves in one image
blue area: area of spreading of incision lines (N=41).
yellow lines: Sural nerves (N=10).

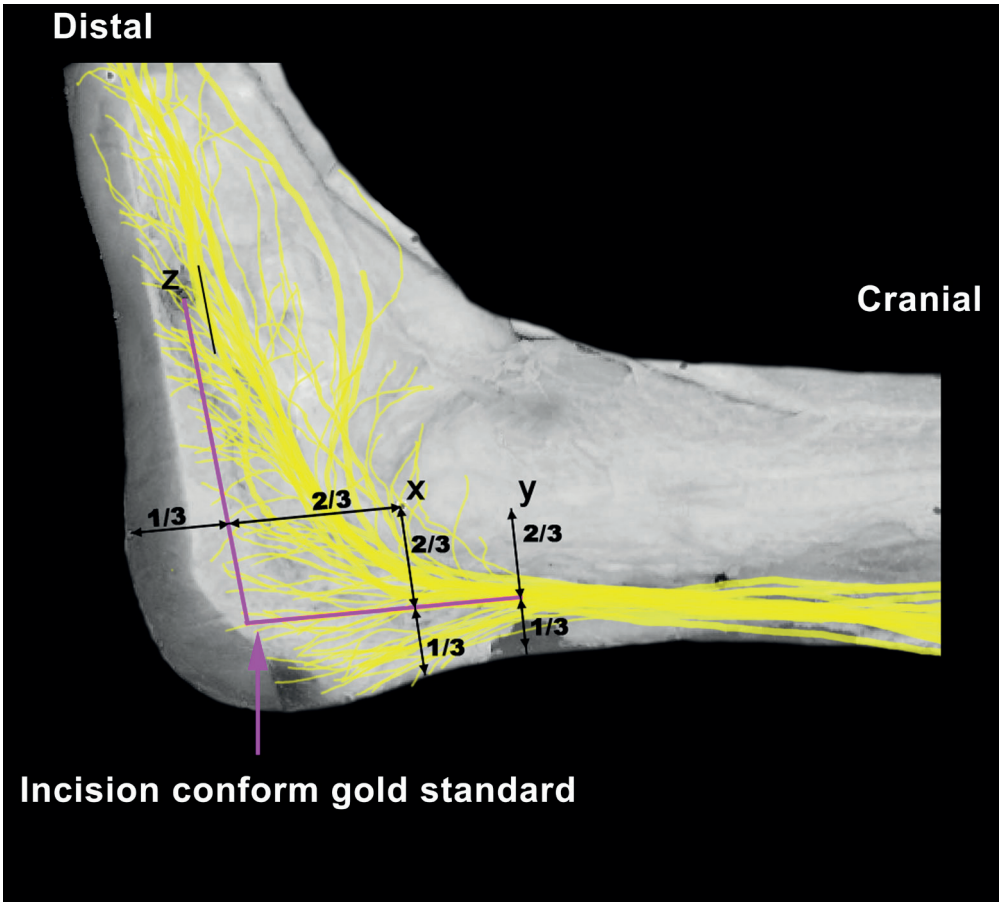

Figure 6. Incision line conform gold standard compared to the sural nerves

Purple line: proposed incision line exactly in accordance with the gold standard
yellow lines: Sural nerves (N=10).

DISCUSSION

Fractures of the calcaneus predominantly occur in young active men and are known for their varying clinical outcome and complications. Still no consensus has been reached on the best method of treatment nor on the optimal surgical treatment regarding the right approach and technique.

Inter-surgeon variation

There was a strong correlation between the years of experience a surgeon had in ELA surgery and the number of ELA surgeries he performs per year. As calcaneal surgery is considered to be technically demanding and it is possible that these surgical procedures are performed by surgeons with many years of experience. Sanders et al. already stated that calcaneal surgery has a substantial learning curve, mainly due to the complicated fracture management[17].

This study demonstrated a wide variety in the location and shape of ELA incisions. The surgeon's personal preference determined the location, shape and length of the incision. In some cases the proximal incision started superior to the lateral malleolus and was extended past the base of the fifth metatarsal, in other cases the incision was much shorter.

Half of the surgeons had drawn an L-shaped incision. The shape of the incision (J or L) was not correlated to the years of experience a surgeon had, nor how many ELA procedures he performed per year. The mean angle of all L-shaped incisions was wider when compared to J-shaped incisions. This either implies that surgeons that have been taught to make an L-shaped incision have also been taught to make a bigger angle or that it is easier to judge the incision angle when a L-shaped incision is made.

Intra-surgeon variation

The mean difference in ratios between the two drawn incision lines by each surgeon is a measure for intra-surgeon variation. The mean intra-surgeon variation for all four incision locating measurements was 6.3%. This means that the difference between the first and second incision drawn by the same surgeon on average is 6.3% of the related shape defining measurements (Figure 2, ratio 1-4), such as the distance between the lateral malleolus and the Achilles tendon. Surprisingly, the intra surgeon variation was not correlated to the surgeon`s years of experience or the number of ELA surgeries he performed per year. This implies that surgical consistency in incision placement is not based on experience, but might be teacher-based.

Comparison to the gold standard

Of 41 incision lines only nine were according to the gold standard. This implies that the gold standard for ELA is not applied by the majority of Dutch surgeons. This finding is amplified by the fact that only two surgeons drew both their incision lines conform gold standard, meaning that the other five "accurate" incisions were drawn by surgeons that were not consequent in their incision placement.

As with intra-surgeon variation, no significant correlation was found between a surgeon`s personal experience (years of experience in ELA surgery and ELA procedures performed per year) and the number of aberrations when incisions were compared to the gold standard. Therefore, incision-related complications such as sural nerve damage and wound or tissue necrosis might not be related to the experience of a surgeon but more related to persisting in the method learned from a supervisor. This in contrast to complications such as subtalar arthrodesis and wound infection which are inversely correlated to the number of calcaneus fractures a surgeon operates per year[14]. Interestingly, surgeons that were consistent in incision line angle made fewer aberrations when compared to the gold standard. Also, L-shaped incisions demonstrated fewer aberrations than J-shaped incisions, most likely because surgeons are more able to determine the angle of incision lines.

Comparison to the sural nerve

Not only were most incisions aberrant when compared to the theoretical gold standard but they also demonstrated much overlap to the highly clinically relevant computed location of the dissected sural nerves. The main branch of at least one of the ten sural nerves would have been at risk for transection in 35 of 41 drawn incision lines.

This is amplified by the fact that when an incision is drawn exactly conform the gold standard the sural nerve would still be at risk of transection in 10% of the specimen. An incision line, as described by Eastwood et al[19], can reduce such iatrogenic sural nerve damage[20].

CONCLUSION

- ELA surgery is mainly performed by surgeons with many years of experience.

- This study shows that there is a large inter- surgeon variation in incision line placement for an ELA and a substantial intra-surgeon variation.

- The location of drawn incision lines is not correlated to a surgeon`s years of experience or the number of ELA surgeries he/she performs per year. This indicates that the incision placement is teacher-based rather than experience-based.

- The dissected sural nerves would have been at risk for transection in almost all drawn incision lines.

- The sural nerve is still at risk in an incision line exactly conform gold standard.

These conclusions suggest that there is a need for an anatomy based teaching model aimed at both novice and expert surgeons. A web-based version of CASAM might be beneficial in two ways;

1) Pre-operative planning using CASAM, can assist the surgeon in determining a 'tailor made' safe zone in each patient.
2) For educational purposes CASAM is able to compare a surgeon`s incision with the gold standard or the computed location of nerve and arteries, thus providing personal feedback.

REFERENCES

1) Barei DP, Bellabarba C, Sangeorzan BJ, Benirschke SK. Fractures of the calcaneus. Orthop Clin North Am. 2002 Jan;33(1):263-85, x.
2) Potter MQ, Nunley JA. Long-term functional outcomes after operative treatment for intra-articular fractures of the calcaneus. J Bone Joint Surg Am. 2009 Aug;91(8):1854-60.
3) Basile A. Subjective results after surgical treatment for displaced intra-articular calcaneal fractures. J Foot Ankle Surg. 2012 Mar-Apr;51(2):182-6. Epub 2011 Dec 7.
4) Magnuson PB, Stinchfield F. Fracture of the os calcis. The American Journal of Surgery, Volume 42, Issue 3, December 1938, Pages 685-692
5) Maskill JD, Bohay DR, Anderson JG. Calcaneus fractures: a review article. Foot Ankle Clin. 2005 Sep;10(3):463-89, vi.
6. Mcbride DJ, Ramamurthy C, Laing P. The hindfoot: Calcaneal and talar fractures and dislocations—Part I: Fractures of the calcaneum. Current Orthopaedics, Volume 19, Issue 2, April 2005, Pages 94-100
7) Gaskill T, Schweitzer K, Nunley J. Comparison of surgical outcomes of intra-articular calcaneal fractures by age. J Bone Joint Surg Am. 2010 Dec 15;92(18):2884-9.
8) Gougoulias N, Khanna A, McBride DJ, Maffulli N. Management of calcaneal fractures: systematic review of randomized trials. Br Med Bull. 2009;92:153-67.
9) Schepers T, van Lieshout EM, van Ginhoven TM, Heetveld MJ, Patka P. Current concepts in the treatment of intra-articular calcaneal fractures: results of a nationwide survey. Int Orthop. 2008 Oct;32(5):711-5.
10) Sanders R. Displaced intra-articular fractures of the calcaneus. J Bone Joint Surg Am. 2000 Feb;82(2):225-50.
11) Buckley R, Tough S, McCormack R, Pate G, Leighton R, Petrie D, Galpin R. Operative compared with nonoperative treatment of displaced intra-articular calcaneal fractures: a prospective, randomized, controlled multicenter trial. J Bone Joint Surg Am. 2002 Oct;84-A(10):1733-44.
12) Benirschke SK, Sangeorzan BJ. Extensive intraarticular fractures of the foot. Surgical management of calcaneal fractures. Clin Orthop Relat Res. 1993 Jul;(292):128-34.
13) Thordarson DB, Latteier M.Open reduction and internal fixation of calcaneal fractures with a low profile titanium calcaneal perimeter plate. Foot Ankle Int. 2003 Mar;24(3):217-21.
14) Poeze M, Verbruggen JP, Brink PR. The relationship between the outcome of operatively treated calcaneal fractures and institutional fracture load. A systematic review of the literature. J Bone Joint Surg Am. 2008 May;90(5):1013-21.
15) Rammelt S, Amlang M, Barthel S, Zwipp H. Minimally-invasive treatment of calcaneal fractures. Injury. 2004 Sep;35 Suppl 2:SB55-63.
16) DeWall M, Henderson CE, McKinley TO, Phelps T, Dolan L, Marsh JL. Percutaneousreduction and fixation of displaced intra-articular calcaneus fractures. J Orthop Trauma. 2010 Aug;24(8):466-72.
17). Sanders R, Fortin P, DiPasquale T, Walling A. Operative treatment in 120 displaced intraarticular calcaneal fractures. Results using a prognostic computed tomography scan classification. Clin Orthop Relat Res. 1993 May;(290):87-95.

18) Zwipp H, Rammelt S, Barthel S. Calcaneal fractures--open reduction and internal fixation (ORIF). Injury. 2004 Sep;35 Suppl 2:SB46-54.
19) Eastwood DM, Langkamer VG, Atkins RM. Intra-articular fractures of the calcaneum. Part II: Open reduction and internal fixation by the extended lateral transcalcaneal approach. J Bone Joint Surg Br. 1993 Mar;75(2):189-95.
20) Eastwood DM, Irgau I, Atkins RM. The distal course of the sural nerve and its significance for incisions around the lateral hindfoot. Foot Ankle. 1992 May;13(4):199-202.
21) Paley D, Hall H. Intra-articular fractures of the calcaneus. A critical analysis of results and prognostic factors. J Bone Joint Surg Am. 1993 Mar;75(3):342-54.
22) Harvey EJ, Grujic L, Early JS, Benirschke SK, Sangeorzan BJ. Morbidity associated with ORIF of intra-articular calcaneus fractures using a lateral approach. Foot Ankle Int. 2001 Nov;22(11):868-73.
23) Ishikawa K, Kyutoku S, Takeuchi E. Free lateral calcaneal flap. Ann Plast Surg.1993 Feb;30(2):167-70.
24) Ebskov L, Rasmussen PB, Erichsen M.[Isolated lesions to the sural nerve. Causes, claims review procedure and compensation].Ugeskr Laeger. 2008 Sep 8;170(37):2885-7. Danish.
25) Adobe Corp. Adobe Photoshop CS5. http://www.adobe.com/nl/products/photoshop/photoshop/
26) Kerver AL, van der Ham AC, Theeuwes HP, Eilers PH, Poublon AR, Kerver AJ, Kleinrensink GJ. The surgical anatomy of the small saphenous vein and adjacent nerves in relation to endovenous thermal ablation. J Vasc Surg. 2012 Apr 11
27) Kerver AL, Carati L. Eilers PHC, Langezaal AC, Kleinrensink GJ, Walbeehm ET. Feasibility of developing a pre-operative test for evaluating the strength of the individual wrist extensors. Journal of plastic reconstructive and aesthetic surgery, 2013: An anatomical study of the ECRL and ECRB.
28) Kerver AL, Leliveld MS, den Hartog D, Verhofstad MH, Kleinrensink GJ. The surgical anatomy of the infrapatellar branch of the saphenous nerve in relation to incisions for anteromedial knee surgery. Journal of bone and joint surgery, 2013.
29) EffectMatrix Software Studio. Magic Morph 1.95. http://www.effectmatrix.com/morphing/
30) Zwipp H, Rammelt S, Barthel S. Calcaneal fractures--open reduction and internal fixation (ORIF). Injury. 2004 Sep;35 Suppl 2:SB46-54.
31) Rak V, Ira D, Masek M. Operative treatment of intra-articular calcaneal fractures with calcaneal plates and its complications. Indian J Orthop. 2009 Jul;43(3):271-80.
32) Chatterjee S, Hadi AS. Regression analysis by example, fourth edition. 2006 Wiley & S Sons. Book publication.

01000100 01101001 01110011
01100011 01110101 01110011
01110011 01101001 01101111
01101110

Discussion and Future Perspectives

Previous chapters show that the CASAM method is a valuable tool for mapping and visualizing complex anatomy of multiple specimens. Anatomical research conducted using CASAM has been published and provides clinicians with comprehensive renditions of difficult anatomy. For instance the complex anatomy of the short saphenous vein and the sural nerve was mapped and summarized in a comprehensible figure, allowing easy identification of a safe zone for thermal ablation of the vein and minimizing the risk of iatrogenic damage to the sural nerve. Therefore these results have been published as a book chapter[1], are cited in guidelines[2-4] and have become part of the international consensus for the treatment of varicose veins[5]. Similarly, research on the infrapatellar nerve has been cited in multiple guidelines for knee surgery[6-8] and other studies conducted using CASAM have also contributed towards answering specific surgical and non-surgical issues. The visual nature of the final renditions made with CASAM are a valuable tool in summarizing complex anatomy. This makes it easy to implement the results in everyday surgical practice, minimizing the gap between basic anatomical research and clinical practice.

Inversely, research questions to which CASAM proved to be the answer were all presented by clinicians, based on problems encountered in daily practice. Therefore it is imperative to have clinicians extensively involved in defining proper research questions and the preparation phase of research projects. Clinicians should not only be involved in the discussion about the main of end-points of research projects but also be actively involved in all other aspects of data acquisition. For example, in the study on venous perforators of the fore-arm, the vascular surgeon pointed out that grouping the different perforating veins by their origin would be more clinically relevant than to map them solely based on their location. Similarly, the trauma surgeon involved in the study of the infrapatellar nerve suggested that knees had to be photographed in 90 degrees flexion to better simulate the actual position of a patient`s leg during surgery. As with all basic research it is imperative to have close interaction with clinicians in the early stages of study design to avoid acquiring insignificant, useless or even incorrect data.

Furthermore, CASAM has been used in more basic research such as nerve mapping of the hind paws of rats. In this study other methods of anatomy mapping were less able to produce the results necessary to answer the research question, proving that CASAM is not only valuable addition to anatomical research, but can also be considered relevant and necessary for research questions that require intricate mapping and comparing of complex anatomy.

The basic principles of CASAM are shown to be valid and the algorithms used have long been employed in other fields of medicine such as radiology. Renditions made with CASAM were compared with results of conventional anatomy mapping in most of the studies presented and results were always comparable. Results between CASAM mapping and conventional measurements in studies on the short saphenous vein and the sural nerve differed less than one millimeter. In that particular study, safe zones computed with CASAM were exactly the same as safe zones calculated conventionally. High risk zones computed to locate the extensor carpi radialis longus and brevis muscles, located in the dorsal forearm, compared extremely well to similar zones calculated conventionally. An advantage of mapping with CASAM is the opportunity to locate an anatomical structure between all measurement sites due to the warping principles and CASAM algorithm. CASAM therefore results in a more accurate, total anatomy overview over conventional anatomy research. In conventional anatomy mapping, the researcher is always limited to the number of measurements taken, whilst with CASAM the complete course of a nerve, artery, vein or muscle can be mapped, resulting in the possibility to collect more data. The possibility to map a complete structure and all its branches allows researchers to compute more detailed models such as point distributions, safe zones, high risk- or target zones and directional anatomy. CASAM meets the surgical need for visual aids when presented with complex anatomical data and furthermore it allows for more comprehensive and representative anatomy models as "more anatomy" can be mapped.

CASAM provides a full description of dissection, photography, warping and the making of final renditions. Hence reproducible and reliable data are acquired. However, currently every step in CASAM is very laborious. The preparation of small anatomical structures, such as nerves, and the specific manner in which they need to be dissected is difficult and tedious. Performing acceptable dissections proved to be difficult even for experienced surgeons without proper instruction by an anatomist. Erroneous dissection results in shifting anatomy when specimens are handled and as such these unstable data cannot be used. Positioning the landmarks manually and computing average dimensions is still time-consuming and the researcher needs to be able to manually input certain algorithms, to automate part of setting the landmarks. Despite the minimized manual input of the web-based version of CASAM assigning landmarks and computing an average dimension still are time consuming tasks and require basic coding skills. Making final renditions is also time consuming as dissected anatomical structures need to be manually highlighted in image processing software such as Photoshop. Furthermore some forms of final renditions need extensive manual input. Again,

the web-based version of CASAM has streamlined this process, making it more time efficient.

With an increase in the number of specimens dissected and mapped, the reliability of the results is also increased. Currently sample sizes in CASAM anatomy studies are comparable to that of studies using conventional ways of mapping anatomy. However, if the time needed to map each specimen is reduced by further automating parts of CASAM, data of more specimens can be added to a final anatomy model. This will greatly increase the representativeness of anatomy models. However, as with all anatomical research, data gathered with CASAM is based on a finite number of anatomical specimens and no amount of dissected specimen will ever provide an anatomical model that is applicable to every patient in all situations. Therefore, renditions such as safe-zones should be used as a guideline to better understand the complex and varying human anatomy and never as a substitute for proper surgical planning or dissection.

The web-based version of CASAM also further improves accessibility. The method has been used numerous times during dissection courses and surgical training at the Skills Lab of the Erasmus MC, University Medical Center Rotterdam, to provide individualized personal feedback to course participants ranging from surgeons in training to surgeons with many years of experience. For

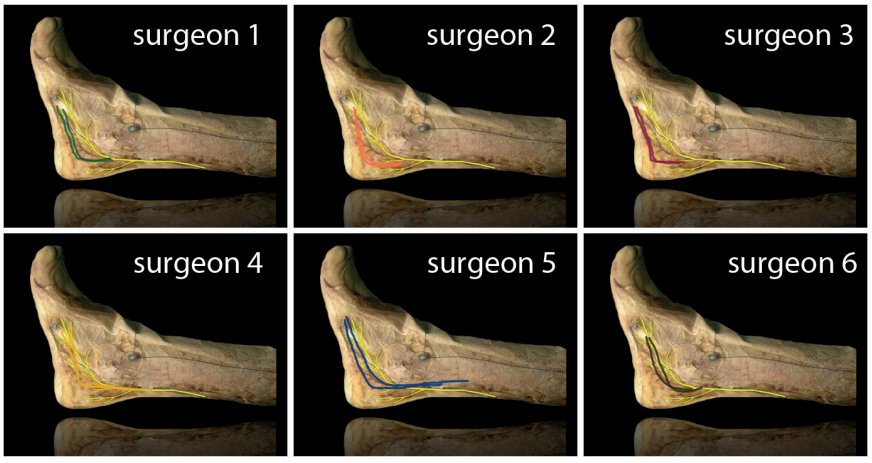

Figure 1. Two incision lines drawn by six different surgeons for an extended lateral approach of the calcaneus. Notice the low intra-surgeon variability but the high inter-surgeon variation. The range of incision lines and the difference between the location and form was then discussed with participants

instance, participants would draw incision lines for a certain surgical approach on multiple embalmed specimens. The drawn incision lines would then be loaded into the web-based version of CASAM and could rapidly be either compared to the gold standard for that surgical approach or to the surgically relevant anatomy. During the course a debriefing was given in which the incision lines of each participant were shown and discussed (Figure 1).

Incision lines of certain professional groups can also be compared; for instance trauma surgeons with orthopedic surgeons or registrars with residents. Also, incision lines drawn at the start of the course can be compared to incision lines drawn at the end of a course, visually monitoring the progress participants made during that course

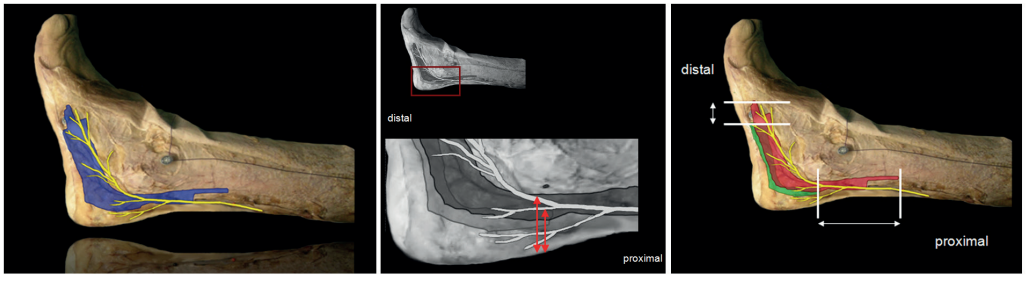

Figure 2. A group of incision lines, relaying the incision lines to anatomical variations and finally giving personalized feedback to a group or individual participants.

Finally, suitable feedback can be given to each individual participant or group of participants as a whole (Figure 2), greatly improving the efficacy of a course by providing individualized visual feedback containing relevant anatomical data provided by the course participants themselves.

The warping algorithms used for the web-based version of CASAM are open access and have been verified and validated previously. In addition, the algorithms used in the original CASAM showed similar warps with final renditions that showed comparable anatomy and safe-zones.

Photo manipulation in science and a proposal for a new image classification system

The use of Photoshop and picture manipulation has been controversial in science for two main reasons. First, in the present era of digital imaging, intentional forgery of digital images is much easier than manipulation of traditional film images. Unfortunately, examples of such intentional forgery of images and pictures are numerous and not only limited to low impact or open access journals. For example, The University of California obtained proof of gross intentional manipulation[16] of images in two papers published in Science[10, 11]. In these papers parts of other images had been duplicated and inserted into the original images to represent actual results. The papers had by then been cited 36 and 161 times respectively and were eventually both withdrawn from the journal.

Secondly, intentional manipulation of digital images becomes more common. Manipulation of images and enhancing the images to make them more comprehensible can be justifiable, yet also treacherous. Simple modifications to the brightness and contrast of a Western blot can seriously alter the results presented (Figure 3).

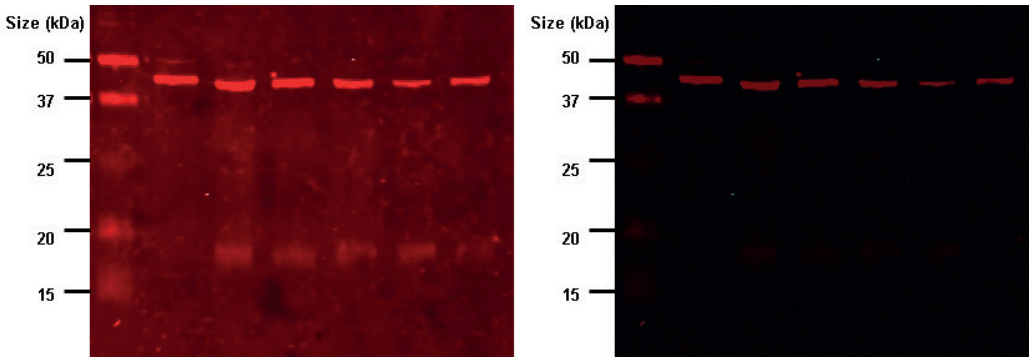

Figure 3. Derived from Tim Vickers[12]
Simple alterations to the original[12] Anti-lipoic acid immunoblot show the completely altered results on the right side.

After years of unregulated image manipulation more major publishers start to provide guidelines to authors for image manipulation and enhancement. The website "ORI" also provides an easy to use "Online learning tool for Research

integrity and Image processing" in which is explained how a researcher should look at images and treat them as conventional data[13].

Most guidelines are based on the four basic guidelines of the Rockefeller University Press[9]:

- No specific feature within an image may be enhanced, obscured, moved, removed, or introduced.
- Adjustments of brightness, contrast, or color balance are acceptable if they are applied to the whole image and as long as they do not obscure, eliminate, or misrepresent any information present in the original.
- The grouping of images from different parts of the same gel, or from different gels, fields, or exposures must be made explicit by the arrangement of the figure (e.g., dividing lines) and in the text of the figure legend.
- If the original data cannot be produced by an author when asked to provide it, acceptance of the manuscript may be revoked.

These (and the extended) guidelines mainly apply to basic research and focus on (stained) microscopic views, histograms, western blots and gel analysis. None of the surgical or anatomical research publishers provide any guidelines regarding image manipulation other than the size and codec of the final output file (jpg, tiff, or pdf). Interestingly, in the field of photo-journalism the ethical issues, related to the digital revolution of photography have long been addressed[14] and ethical guidelines have been established which are updated regularly[15].

Regarding CASAM some extra remarks have to be made. With CASAM it is impossible to strictly follow the ethical codes on image manipulation as described by Rockefeller. For instance, landmarks are digitally added to an image, the image is completely distorted during the warping process, renditions are made in which non-contributing parts of the picture are deleted whilst relevant anatomy is being highlighted, combined and calculations are made on the data. These intentional and contemplated breaches of these ethical codes are of course completely different to the recent damage to credibility of science by publications of intentionally falsified images. However a researcher using CASAM should be well aware of the current commotion surrounding image manipulation in science and should be the guardian of his own integrity on this subject. Any researcher working with CASAM should:

- Provide full disclosure.
- Educate himself on warping.
- Educate himself on image processing; Images need to be treated as data because they are data. Each pixel in each image contains data on its location, the

(x,y) value on the grid, and a numerical value of its color. Therefore an image basically is nothing more than an extensive Excel-spreadsheet in which each box contains information on its location. Therefore any manipulation to an image is just a mathematical function applied to all or some of the boxes/pixels and as such these mathematical procedures need to be recorded. Software such as Photoshop is initially and foremost designed for design and art specialists not for research. Therefore, a scientist should not trust any complex function, such as image filters, without understanding how it affects raw data.

- Keep original, raw data and record the computations you apply to it; having the original files and the adjusted files recorded for each step of the CASAM method ensures reproducibility and the possibility to verify your findings. The researcher is always accountable for the original, raw data. In that respect, also the original anatomical specimen should be kept for 5 years after publication of any published article, containing CASAM data.
- Continuously verify data gathered with CASAM by means of conventional anatomy mapping.

Following these rules, the use of CASAM is a guarantee for valid and 'honest' data. All steps of the procedure can be verified and even the simple and complex mathematical processing can be calculated and verified by editors of scientific journals.

Primarily researchers and research institutes are responsible for high quality research, yet it can be postulated that responsibility for publishing reliable and transparent research is shared with journals and its reviewers. Currently, pictures and images of anatomy are being manipulated, sometimes even without the reader being properly informed. For example, arteries are slightly highlighted or made redder so they are more visible. Although it could be seen as a harmless example, it still is manipulation of data and ideally it should be declared.

Therefore publishers of surgical and/or anatomical journals should also take responsibility and apply clear guidelines for the use and manipulation of images. Preferably photographic images should be categorized comparable with basic research by for instance "levels of evidence". Furthermore editors should take an active role in checking the procedures by which the images are processed.

1) Compiled image. Data of multiple specimens (Figure 4)
   a) >10 specimen
   b) <10 specimen
2) Original image
   a) No image manipulation
   b) Minimal image manipulation (contrast/brightness/levels to the whole picture) (Figure 5)
   c) All other image manipulation (with the exception of moving structures) (Figure 6)
3) Schematic image

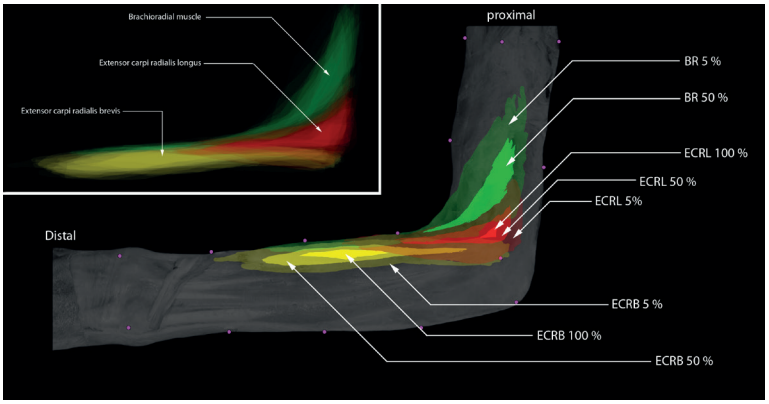

Figure 4. Image category 1a.
A complication of forearm muscles (ECRL, ECRB and BR) of 20 specimens.

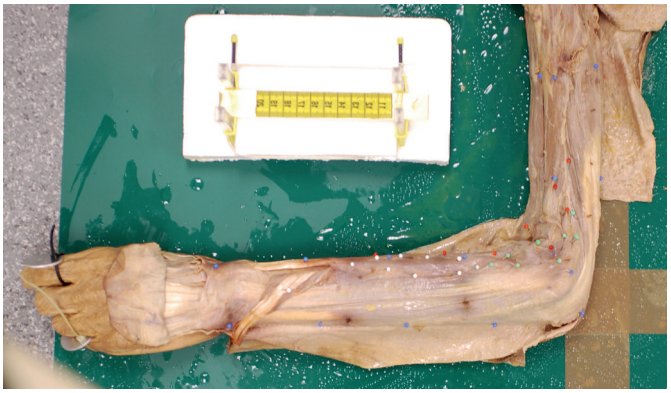

Figure 5. Image category 2b.
Brightness and contrast of the whole picture adjusted for clarification. One specimen in which the forearm muscles (ECRL, ECRB and BR) are dissected.

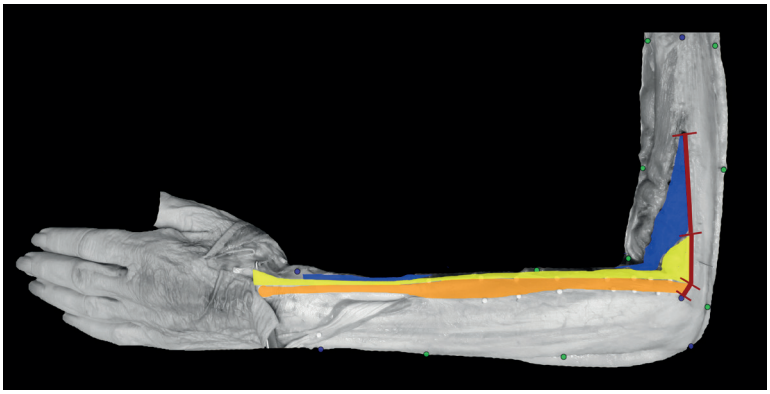

Figure 6. Image category 2c.
The muscles of the forearm of 1 specific specimen are highlighted. The rest of the image is made black and white. Landmarks are highlighted.

3D anatomy with CASAM

CASAM 2D renditions can currently be made of multiple specimens. The 2D renditions are a representation of 3D anatomical specimen. As such, renditions will always be a 2D approximation of a 3D world. As Jason Geng stated; "If a 2D picture is worth a thousand words, then a 3D image is worth a million" [17]. Currently there are some 3D anatomy atlases[18-22]. However the anatomy portrayed in these 3D anatomical models is either based on a CT-scan or MRI scan of a singular specimen or drawings from old anatomy books. Furthermore, using a 3D atlas on a 2D screen has proven to be difficult as users find it hard to navigate the 3D models, making it more difficult to comprehend the anatomical data visualized. One of the solutions to overcome this problem is to create "states". These states are researcher defined presets of 3D images that will show the user the best and most comprehensive view of a certain anatomical structure. Users can choose to change view after a state has been provided to them or revert to a preexisting state if they have lost their bearings. Furthermore, with recent developments in glasses-free 3D screens[23, 24], 3D and virtual reality wearables[25, 26] and concomitant 3D navigational tools, it has become easier to transfer difficult 3D information to a general user. 3D screens and easy 3d navigational tools have already proven to be of value in basic science27 (Figure 7).

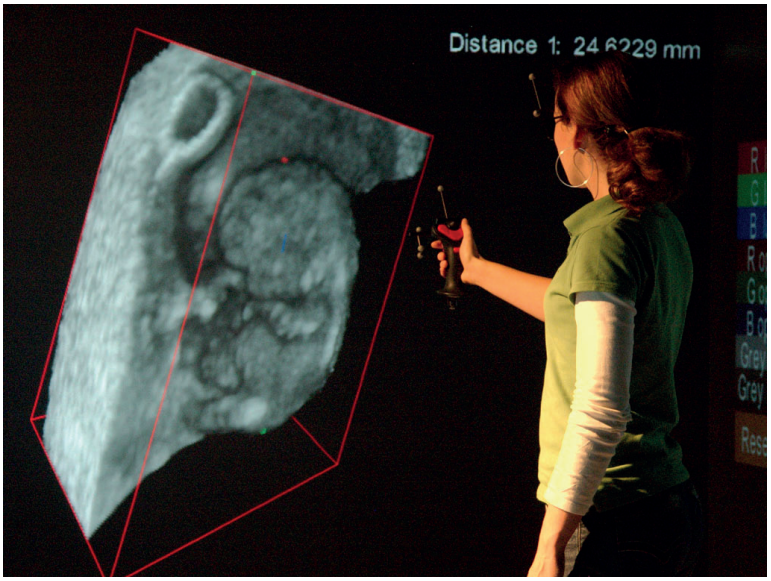

Figure 7. The i-space in the Erasmus MC Rotterdam[7].

Another problem in 3D anatomy often occurs when multiple overlapping structures are visualized simultaneously, automatically leading to a trade-off between the number of anatomical structures or anatomical variations shown and the clarity of the visual data provided. New techniques[28, 29] are being developed with multiple experts in different biomedical domains to create a technique to design focus-and-context visualizations in a fast and intuitive manner.

One of the first steps in 3D visualization of anatomical data is 3D gathering of data. 3D scanners measure the distance to the surface of an object and create a point cloud[30] (Figure 9). The measured points can then be used to compute the shape of an object or specimen. There are several different types of 3D scanners and they are generally divided in "contact" or "non-contact" solutions[31]. Contact scanners require a probe to physically touch a surface and therefore are of limited use when specimens are to be scanned. The non-contact scanners can be divided into "active" or "non-active" scanners. Active scanners emit light, ultrasound or x-ray. Active time-of-flight scanners measure the time it takes for the emitted medium to be reflected back from the specimen to the scanner and active triangulation-scanners use a separate camera to determine the shape and size of the emitted medium on the specimen, thereby calculating the position of the specimen[32]. Time-of-flight scanners have a relatively low accuracy, measured in millimeters, and therefore are of less value to scan specimens. Triangulation scanners are accurate in the order of tenths of micrometers, making it feasible for

those scanners to scan the intrinsic 3D anatomy dissected in human specimens. Another advantage is that triangulation scanners can be hand-held and are becoming more accessible to the general public and become cheaper whilst maintaining great accuracy and scanning speed[33]. More advanced scanners are currently able to scan anatomical specimens with superb accuracy and with high speed (Figure 8)[34].

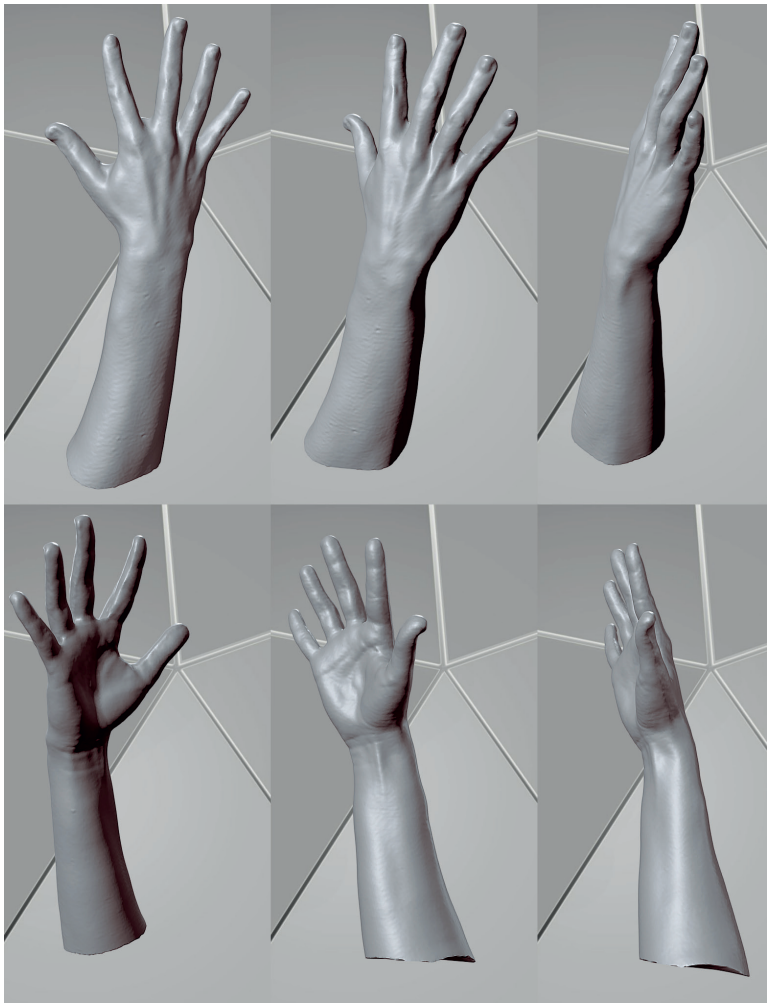

Figure 8. A hand scanned with Artec 3D Eva
Images adapted from Artec[34].

3D scanning produces digital "noise" and a variety of algorithms have already been proposed to reduce the noise in the final renditions. There are two major methods of de-noising 3D renditions; "Mesh de-noising" and "point-set de-noising". The former uses a mesh representation whilst the latter deals with points in the Euclidean space, mostly using the Moving Least Squares method[35, 36] to smoothen the 3D rendition as much as possible with the least amount of local errors. An increasing amount of research is published to contribute to a better smoothing method after 3D scanning[31].

Figure 9. Denoising. Image from[34].
Left; standard Bust model (with triangulated point cloud for the sake of visual clarity)
Right: corresponding model after being denoised.

When the specimens and their relevant anatomy have been scanned and highlighted, an average 3D model needs to be generated similarly to the average 2D model that is used in the current CASAM method. First the anatomical landmarks need to be located. In a Euclidean, 2D space, landmarks are defined on an X and Y axis. In a three dimensional Euclidean space[37] those landmarks are defined on a X, Y and Z axis, in which each of the axes are given and are perpendicular to each other at the origin (0,0,0) (Figure 10). Average landmarks can be computed by computing a 3D averagely shaped specimen.

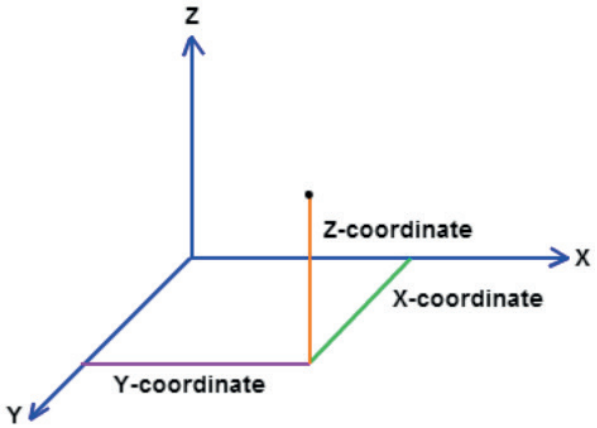

Figure 10. Three dimensional grid system with x, y and Z coordinates.
Image from Wikipedia[37]

Once a 3D average specimen has been computed, the algorithms currently used in the web based version of CASAM can easily be altered to warp the original, scanned 3D models to match the average 3D shape. The thin plate spline models currently used to warp the 2D models in CASAM are equally applicable to warp 3D models[38-40]. The results will comprise of a given number of specimen-, 3D-models, all having the same average shape and size. After relevant anatomy, such as arteries or nerves, have been collected, their 3D locations can be combined and the 3D anatomy of multiple specimens can be visualized in an average specimen as never before.

The advantages of 3D mapping anatomy of multiple specimens and comparing the 3D location of structures as arteries and nerves are paramount. Surgical residents, medical students and even surgeons struggle with the transfer of 2D literature to the 3D patient. Surgical residents will often tell you that an anatomy lesson in a dissection room with real 3D models is much more informative than reading the 2D anatomy atlases. They realize that they need to internalize the 3D relation between anatomical structures to understand anatomical forms and relations. They also realize that they need this internalized 3D information to form the basis for future surgical procedures. The advantages of CASAM generated 3D anatomy renditions are that 3D information of multiple specimens can be combined into an averagely shaped specimen. This allows for much easier visualization of multiple variations of anatomy and 3D renditions showing general areas computed from multiple 3D variations. Figure 11 shows an example. In this

3D model[34] an average facial nerve is shown (yellow line) and the green area for example represents the area in which the facial nerve always runs a sub-fascial course. This 3D image could easily assist a surgeon in planning surgery, giving him 3D anatomical information on safe zones and the difficult anatomy of the facial nerve.

Standardized photography, one of the major difficulties in the current CASAM

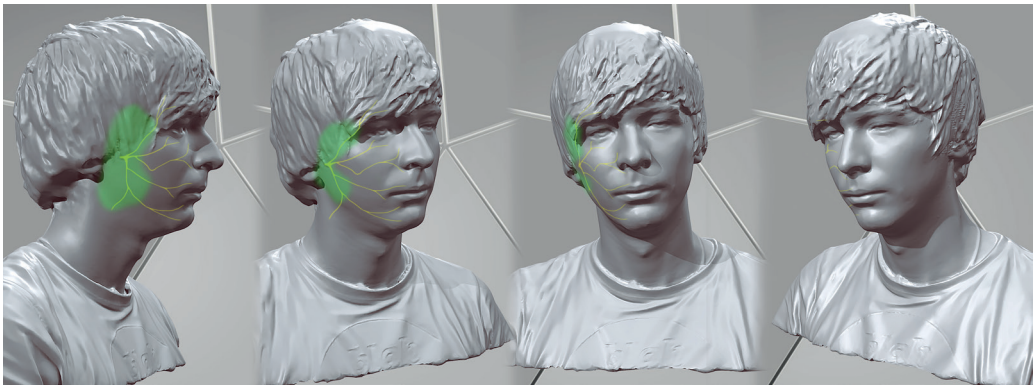

Figure 11. Example picture adapted from Artec[34].
An average facial nerve on a 3D model scanned with Artec Eva[34]. The green area represents the location in which the nerve would run sub-fascially and can therefore be considered as a 3D "safe zone".

iteration, can be overcome using 3D mapping. Currently, minor differences in angulation of a specimen during photography can result in a major disruption of the final rendition. As such, great care needs to be taken to avoid angulation issues and strictly protocolled photography is necessary. With 3D scanning there is no angulation problem since the complete 3D structure of a specimen is scanned and landmarks are located using the three axes in a 3D Euclidean space. This will not only make the CASAM method easier and less time consuming, it will also benefit reproducibility and further improve data reliability.

Automated landmark placement

One of the important steps in CASAM is correct landmark localization. As described in the Materials and Methods, both bony and non-bony landmarks are used for CASAM. Especially the bony landmarks are often difficult to set on a 2D picture. In the anatomy lab in general, they were placed on the actual specimen in order to produce less inter-observer inconsistencies. In the digital picture, manual placement of non-bony landmarks is less difficult. However, it

proved to be very laborious. Especially in complex anatomical models such as hands or paws, many landmarks need to be placed in each individual specimen. Then each individual specimen again needs to be warped to match a computed average and all landmarks need to be located again. Even though part of this process was done using custom algorithms using Autohotkey[41], it still showed to be a tedious job. Currently, in the web-based version of CASAM, landmark placement is only done manually.

One of the ways to make CASAM less difficult to use and more accessible to the general public would be to introduce automated landmark placement. If automated landmark localization algorithms are able to produce reliable and robust results, this would mean that CASAM can be used by more research groups and end-users. It would take less time to produce average warps, which in turn will save time for specimen dissection and final rendition creation.

Automated landmark placement however, is very difficult and has been attempted many times before, for instance in facial landmark detection and face registration[42]. Recently reliability of facial recognition was increased by using registration and a point distribution model[43] similar to the algorithm used in the current web-based version of CASAM. These and other advances have already made their way into medical applications such as MRI and CT algorithms. For instance automatic landmark localization on 3D MRI data of the knee have been proposed claiming that the method is robust but their long-term accuracy and reliability has not been proven yet[44].

Especially in CASAM, if automated landmark placement is utilized, accuracy is paramount. Inaccurate and unreliable landmark placement, both when uploading anatomical data, as well as downloading anatomical data to match a patients dimensions, is detrimental to the end result and might even produce more complications.

Therefore, until now, a combination of manual and automated landmark placement seems most feasible. Bony landmarks, such as a lateral malleolus of the ankle or tibia plateau of the knee, are hard to locate using an algorithm on a 2D photograph or 3D computed specimen model. Therefore these landmarks are better located by hand. Non-bony, shape defining landmarks are easier to be placed automatically. They are not only equidistant to each other based on manually placed bony landmarks but are also located on the outer edge of a specimen. Therefore they are easier to distinguish using an algorithm. This approach is similar to the method proposed by Bromiley et al. from Manchester[39, 40] in which limited user input is required. In this method training data from input by a researcher is used and a final error correction stage, or "landmark check",

is used to minimize manual landmark input in 3D data by a factor of ten. This group also proposed that as larger data sets are annotated and more landmarks of complex models such as hands or paws are used it would further increase the statistical power and reliability of the automated landmark placement, especially when subsequent processing such as Procrustes- and Principle-component analysis[45] are being used. Both of these analyses are currently already used in the web-based version of CASAM. Moreover, the of hybrid landmark placement proposed by Bromiley et al. proved to be more reliable than manual landmark placement. It is suggested that this is mainly due to the fact that currently 3D navigation is still difficult, especially if multiple specific landmarks need to be located with great precision[46].

Recently an algorithm was published on automated placement of craniofacial landmarks needing even less user input[47]. For this method it is only needed to roughly orient the mandibles whilst other craniofacial structures are located automatically. The resulting data have already been used to compare the 3D differences between left and right mandibles[48] but these data would just be as easy to quantify the differences between two or more other anatomic structures such as for instance femurs.

Automated landmark placement, most likely in a hybrid form requiring minimal manual input and final placement correction seems feasible in the near future and would make CASAM more accessible to other and more diverse users. However robust and reliable landmark placement should never be placed above accessibility since accurate setting of landmarks is crucial for the validity and reliability of CASAM.

Ethnical variations in anatomy and international anatomical wet-lab collaboration (central web-server)

The well-known paradigm in surgery “no patient is the same!” has never left the classroom. However, ethnically related anatomical variations are not yet used in common practice of surgery. Despite our population becoming more multi-cultural and multi-ethnical, social paradigms regarding racism seem to restrict medical innovation and possibly could withhold patients with a non-Caucasian background from tailor-made surgery. Therefore further research on ethnical anatomical variance is essential. A web-based version of CASAM can provide a central basis for anatomical research performed and provide a platform in which anatomical research can be compared internationally. The results would be easily accessible to surgeons and help them to further individualize their decision process and surgical approach, resulting in Tailor-made surgery.

Most of the basic anatomical research has been done in the western world, in which the German anatomical tradition was leading until the end of the 19th century. After 1900 the United States took the lead. As a consequence, most anatomical measurements since then are applicable to a Caucasian population. In other words, this means that doctors and surgeons are taught Caucasian anatomy since Caucasian specimens are the basis for common anatomy atlases such as Sobotta and Netter. The anatomy of other ethnicities such as African or Asian are not well recognized. Inversely, recent anatomical data gathered in Asia are added to the international pool of literature and are often used to support the use of new surgical techniques in the western world, even when anatomy obtained from Asian people might not correspond to a Caucasian population. In a world that is becoming more multi-cultural and diverse, ethnical anatomical variations should be recognized and integrated in general practice. Rotterdam, A City in The Netherlands, for instance is a growing Dutch city with a little more than 600.000 inhabitants and has a rich and mixed culture consisting of up to 170 different nationalities[49, 50]. Literature on ethnical differences is abundant and has become common practice in assessing the risk of cardiovascular disease[51], peripheral vascular disease[52], diabetes or colorectal disease[53]. However, In surgery this personalized approach is restricted to a patient`s sex, Body Mass Index and smoking habits. Relevant information such as ethnic background is mostly not taken into account even when it can have a profound impact on complication rates.

We have known for a long time that there are anatomical differences between ethnic groups; skin color for instance being one of the most obvious differences. One of the most studied anatomical variations of racial differences is the anatomy of the nose. Hinderer et all.[54] described three typically ethnic characteristics in nasal anatomy variation; platyrrhine (African), mesorrhine (Asian) and leptorrhine (Caucasian). The measurements used to describe the different nasal variations were previously used in anthropologic literature; for instance “the African nose has thicker skin, a smaller nasal spine, and less cartilage support than the Caucasion nose”; all factors directly influencing the choice of a surgical approach.

Ethnical anatomical variation, however, is not limited to easily observable differences such as facial features or skin color. Recent literature is describing profound differences between people with different ethnical backgrounds in for instance abdominal anatomical dimensions[56] and skeletal muscle properties[57].

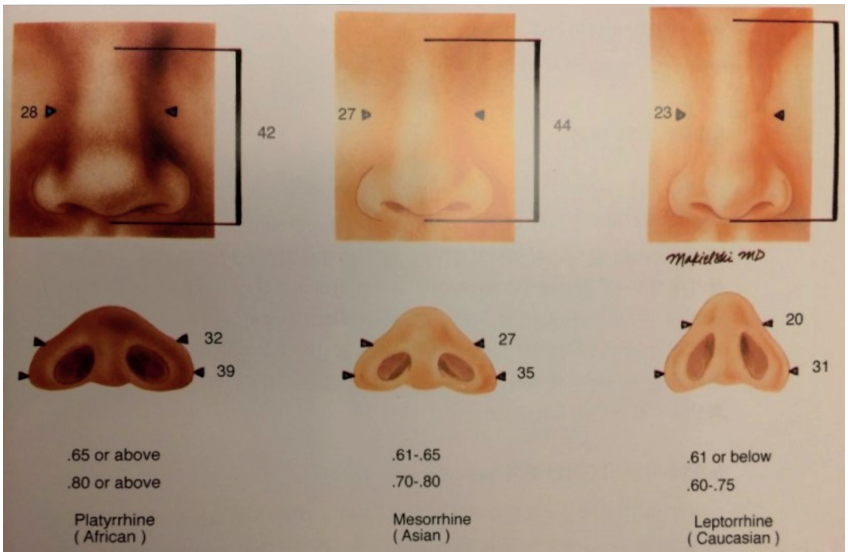

Figure 12. Ethnical variation in nasal anatomy.
From surgical anatomy of the face[54, 55]

Comprehensive knowledge of anatomical variations can save lives. In hepato-billiary surgery for example, anatomic variation is a well-recognized risk for complications and based on anatomic research on Caucasians[58, 59] guidelines were changed and recommendations such as the direction of traction on the gallbladder and the need to identify the cystic duct-common bile duct junction[60] have lowered complication rates considerably. Interestingly the origin and course of the cystic artery varies significantly between Caucasians, Asians (Sri Lanka)[61] and Africans (Uganda[60], Sudanese[62]). Easily accessible data on these racial variations could potentially further reduce complication rates. However, none of these data are currently used in surgical training or in general practice.

Another example in which ethnical variance has played a large role in the development of medical devices is the significant differences in the dimensions of the proximal femur between Asians and Caucasians[63]. In hip fractures requiring a gamma nail it was found that in Asian patients of a short stature there is a profound geometric mismatch between the nail and the femur[64, 65]. This mismatch is mainly due to the different trochanteric and femoral shaft anatomy in Asian people. Not surprisingly, the original nails were developed based on Caucasian measurements. Currently nails are available, based on the femur dimensions of Asians[63] resulting in a better geometrical match between nail and the femur of Asian patients. These specialized nails however have not been in general use in

most Western countries, although research on different geometric fits between Caucasians and Asians is increasing[66].

Similarly dimensions of a forearm are shown to differ between Asians, Africans and Caucasians[67] and as such anatomy of arteries, nerves and muscles will certainly differ. Again, the ethnical background of a patient can be of great assistance during surgery and surgical planning if data on anatomical variations of patients with a similar ethnical background are readily available.

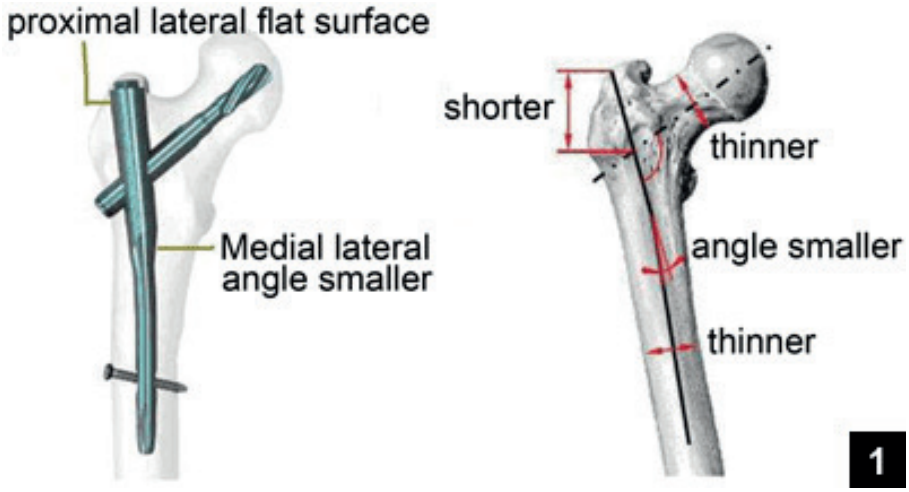

Figure 13. Shape differences in Asain proximal femur.
From Chaoliang[63].

Web-based version of CASAM

In order to map these ethnical differences we need international collaboration between multiple anatomy labs following a standardized protocol. Furthermore these international labs need to be able to communicate and compare anatomical data through a central server. Finally data need to be simplified and made visually comprehensive so this information is easily available and accessible to surgeons.

In order to compare anatomical data, it is paramount that the data should be acquired following a strict protocol. CASAM describes a complete protocol of anatomical data acquisition starting with preparation, dissection, photography, setting landmarks, data extraction and final renditions. In each of the CASAM studies multiple parts of the CASAM protocols were checked and followed by multiple observers providing minimal inter- and intra-observer variation. Landmark placement for instance, was relentlessly controlled in each study. Multiple observers were engaged in locating landmarks in five specimens and if inter-observer variability was more than one millimeter, landmarks

were redefined or omitted and inter-observer variation was re-calculated. With a central server this method can easily be extrapolated for international collaboration. Researchers from different institutions can interpret landmark locations and compare results in order to optimize landmark protocols and insure low inter-observer variability. This would also generate an excellent opportunity to compare ethnic differences. Other parts of the CASAM executive protocols, such as photography, data extraction such as highlighting nerves, or final renditions, are also easily verified if data are gathered centrally. Furthermore, protocols regarding these parts of CASAM can then be further standardized in order to make international anatomical data acquisition as consistent and reliable as possible. Eventually, international protocols for anatomical data acquisition would even allow for optimization of processes; anatomists in one part of the world will dissect specimens and define landmarks while researchers of different institutes will be able to extract data on anatomical structures such as nerves. Also, since data are gathered in a standardized manner, specimens can be used to answer multiple international research questions. This hits two birds with one stone; If for instance an anatomical lab wishes to study the course of the sural nerve (dorsal part of the leg) and another institute wants to investigate the course of the Achilles tendon or short saphenous vein, specimens need only be dissected once and data of nerves, Achilles tendon and veins can all be extrapolated and used since data were gathered in a standardized way. One institute will dissect specimens, locate landmarks and can then upload raw photographs to a central server. Other affiliated research institutes will then be able to download these raw data and extract data on the anatomical structures relevant to their initial research question. This means that research can be done faster and fewer new specimens need to be used for research. It will also further promote international collaboration, resulting in less duplication of research and the possibility of more comprehensive insight in anatomy since researchers are confronted with research questions of other institutes in their general region of interest. On the other hand, the standardization of anatomy protocols will make it possible for researchers to extend the existing database of at least 20 specimens with data from their own research. Hence the database will grow rapidly and reliability of the data will further increase over time.

People in general, but especially surgeons, prefer visually presented data more than numerical data. Therefore the way in which data are visually represented with CASAM should be ideal. Also CASAM allows for an enormous amount of data to be presented in several easily interpretable images, which decreases the

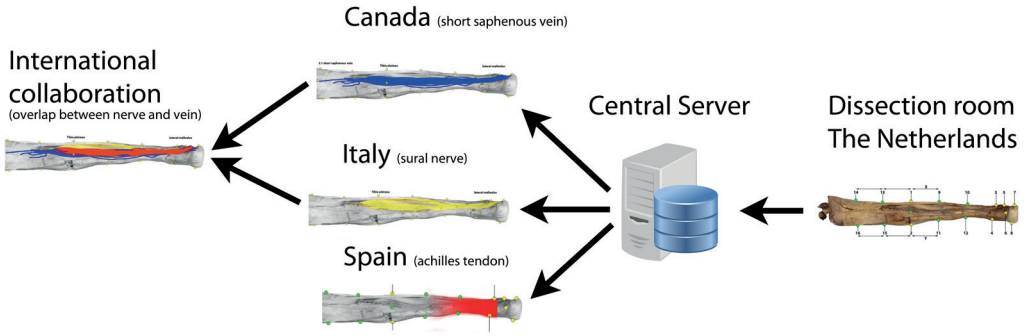

Figure 14. Example of a Web-based anatomy server.
Standardized data acquisition can be used to answer multiple international research questions. The centralized data might also inspire further international collaboration and a more comprehensive anatomy overview applicable to a wider array of surgeons.

distance between surgeon and anatomist. Having a central server harboring easily interpretable and surgically relevant anatomical data should further decrease the distance between surgeon and anatomist. The surgeon will then be able to look up data on anatomical variations or safe zones in the operating room, with the patient right next to him.

The 3D scanning of anatomy and comparing the average results between different ethnicities has already been used and experimented with outside the field of surgery. In the field of new Anthropometrics, a field of study that aims to bridge the gap between design and science, R. Ball et al. scanned over two thousand Chinese heads, computing an average Chinese head that is used for the design of helmets and Asian headwear such as sunglasses (Figure 15)[68].

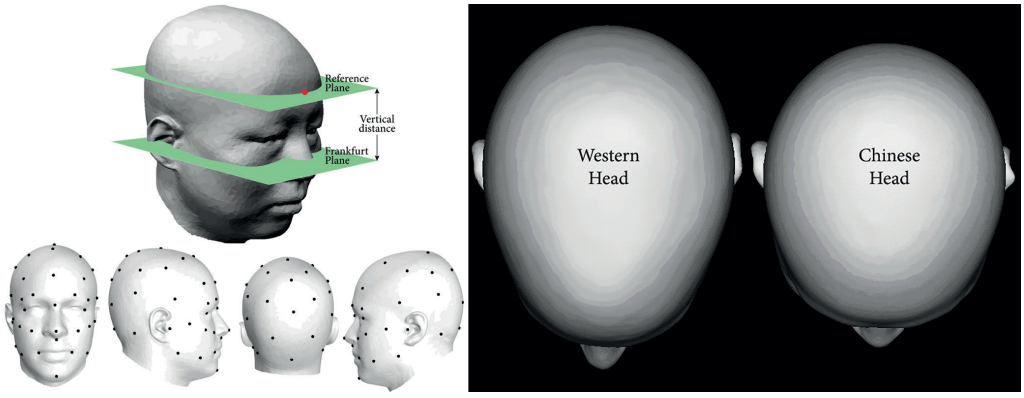

Figure 15. Differences between the shape of a Caucasian head and a Chinese head. Adapted from R. Ball[68]

Whilst Ball and colleagues had to physically go to China to gather 3D models on living Chinese people, a web based version of CASAM could in the future provide the field of "New Anthropometrics" valuable anatomical data of people with different ethnicities, further individualizing the possibilities of design, clothing and safety-wear. These data can be derived from any number of specimens before they are being used for further anatomical research or even specimens that are going to be used for anatomical courses can be scanned before the start of a course.

As the computations used in CASAM are done server-side, previous limitations such as low computing power and the need for high-end firmware are no longer required by end-users such as a surgeon or researcher. This allows research groups with less funding and small budgets to also contribute and benefit from the international anatomical database. It also further improves consistency as the same algorithms are used and can be improved by multiple users and research groups.

In the current web-based version of CASAM users are assigned to different user-groups; administrator, researcher, surgeon and student. Furthermore, each user is assigned access to a certain amount of studies. For instance, a Canadian researcher is assigned to the "research user-group" and is therefore allowed to create a new study on for instance Achilles tendons. He is then allowed to upload anatomical data, place landmarks, warp and make renditions to the Achilles tendon project. He is however not allowed to automatically upload anatomical data to studies of other research groups without the explicit consent of the principal-investigator. Surgeons in the "Surgeon user-group" are allowed to look at the

final renditions of finished studies but are not allowed to add anatomical data or look at unfinished research without the consent of the principal-researcher.

Initially researchers will need to upload unedited photos of specimens. These photos might contain personal information such as birthmarks or tattoos and thus unintendedly reveal recognizable parts of deceased people, possibly violating their privacy. However, after the landmarks and relevant anatomy of the unedited images is derived, the original images can be deleted from the server and only need to be stored on a personal storage device of the researcher or research group. This means that on the server no privacy sensitive information has to be stored. Only numerical data on landmarks and relative anatomy derived from multiple specimens is stored server-side. Obviously, as is common in current research, the original images and data need to be safely stored offline in order to be able to examine correct data input and data handling. Storage is part of the responsibility of the researcher or research-group using CASAM, as is currently conventional in all anatomy research.

Regular backups of anatomical data stored on servers are required to prevent data loss. These backups can easily be done online and multiple fail-saves can be implemented server side. Within CASAM an export feature is also provided. This makes it possible for researchers to export all data from one or multiple projects into an archive. This archive can be stored on disk or generic USB and later used as a back-up in the event of a server failure. The archive can also be uploaded to another server that uses the CASAM technology. This allows for multiple servers in different continents to each have their own research projects whilst still being able to exchange complete projects.

Summarizing, the current web-based version of CASAM can be a very good platform for international collaboration between anatomical laboratories, providing a central, safe and well-optimized forum to compare the human anatomy. It provides a user friendly interface and is easily accessible for anatomy researchers around the world, encouraging international collaboration and a more ethnical approach to anatomical variations. This allows for a more individualized approach to surgery, especially when combined with accessible final renditions summarizing complex anatomy for surgeons in their operating room. Furthermore the research of ethnical differences in anatomy can be used outside the field of surgery, and be of interest to fields such as “new Anthropometrics” to further individualize design.

Personalized teaching (CASAM in the operating room)

This part of Future Perspectives addresses a largely underestimated issue: surgical training and the modern way of teaching psycho motor skills to surgical residents. In the past, training formats based on the 'master-apprentice' relationship between experienced surgeon and novice were adequate. However, these formats require long practicing hours, an intensive relationship between master and apprentice. Originally and ideally, the master should be a 'real' master and not, for instance, a senior resident. Last but not least the patient needs to be a willing 'participant´ in the young surgeon`s learning curve. These factors determine that in modern times these formats are, ethically but also socially no longer acceptable and a discussion about new teaching formats and techniques needs to be initiated, focusing on:

1) Discouraging surgeons from performing surgery in an automated manner
2) Providing surgeons with direct personal feedback
3) Promoting and re-introducing deliberate practice in the theatre of an experienced surgeon.

A web based version of CASAM will be of benefit to the surgical resident as it allows visual, direct and personalized feedback on a well-defined task such as drawing an incision. Furthermore, personalized-, tailor made surgery using a web based version of CASAM in the operating room will not only benefit the individual patient. It will also re-engage the experienced surgeon in deliberate practice instead of automated surgery, exciting him with new surgical approaches and challenge him with renditions of complex anatomy whilst being accessible in theatre, even per-operatively.

To support these possible advantages of a web-based CASAM we must first have a look at the general concepts of learning and expert performance.

As early as Plato, medical teaching and expertise has been described. He described that routine medical procedures should be carried out by a so called 'slave doctor' and that the more intricate medical diagnosis and explanation to the patient should be carried out by an "expert doctor" [69]. To become an expert doctor one needed to have plenty experience in order to have empirically gathered knowledge on how to treat patients with all different kinds of diseases[70]. Expertise was therefore directly linked to age, as it was the accumulation of personal experiences.

In agreement with this hypothesis are more contemporary views on education as described by Galton[71]. He recognized the importance of practice, yet he also

stated there had to be a hereditary, or genetic, maximal level of performance and that the limits by which an individual is bound could not be improved by training.

Automatization, an expert's enemy

Other recent views of skill acquisition[72, 73] seem to be consistent with Galton`s views. They describe the three phases of skill acquisition. In phase one[72] the student mostly follows the teacher and the main goal is to reach a level of mastery that allows for every day, acceptable activity. The student's main focus is to avoid gross mistakes.

In the second phase everyday activities become less exhausting and gross mistakes become rare.

In the third phase performance becomes automated and performance appears smoother. With automation however comes the loss of conscious control over the execution of those skills and change becomes difficult[74]. Therefore in stage 3 a stable plateau of performance is reached[74] which is consistent with Galton`s assumption of a performance limit. However, the most important difference is that the performance limit is not genetic or hereditary but this plateau of performance is reached by automation of everyday tasks. Thus, fast, smooth and often automated performance halts continuous growth of skill during a surgeon's career and the surgeon prematurely reaches a plateau of performance which is often mistakenly perceived as a performance limit. Not hereditary or genetic factors determine this performance limit but the time it takes for the surgeon to automate his everyday tasks.

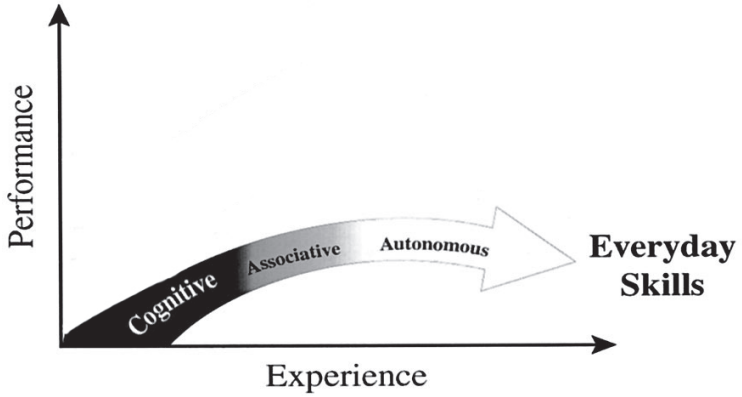

Figure 16. Adapted from Anders Ericsson[74]
The goal for everyday activities is to reach as rapidly as possible a satisfactory level that is stable and "autonomous." After individuals pass through the "cognitive" and "associative" phases, they can generated their performance virtually automatically with a minimal amount of effort (see the gray/white plateau at the bottom of the graph).

An example of this perceived performance limit was described in chapter 3.4. We asked surgeons to draw incision lines and we compared them to the current-day gold standard and the location of surrounding nerves. We concluded that most surgeons did not comply with the gold standard and were at risk of damaging surrounding nerves. When asked for their reasoning most answered derivates of the following: "That is how I learned it. I have done it like this for years". In our opinion this therefore is the result of performance becoming automated and therefore the loss of conscious control of skills learned long before. Most participants in these studies read new literature and research in their field, which was full of adaptations of the gold standard we asked them to draw. However, somehow the knowledge written down in paper did not reach the operating theatre. Experts as described by Ericsson[74] "counteract automaticity by developing increasingly complex mental representations to attain higher levels of control of their performance and will therefore remain within the cognitive and associative phases". Moreover, he describes that some experts, during the course of their career give up seeking excellence, or feel a lack of incitement to keep aiming for excellence and thus revert to automation of their performance, resulting in, premature, arrested development (Figure 17). In summary, only experts consciously avoid automation and constantly try to be in an associative state by challenging and getting challenged by their patients, colleagues and students.

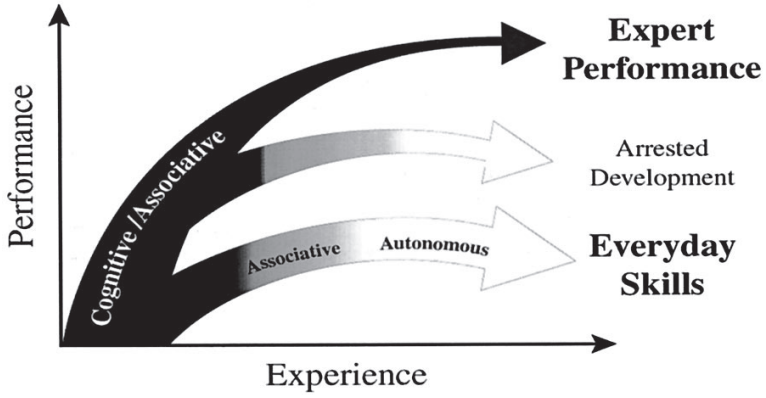

Figure 17. Adapted from Anders Ericsson[74]
Expert performance and arrested development.

Lack of deliberate practice

This raises the question of what qualities make an expert surgeon and how these qualities can be acquired. Generally spoken, an expert is regarded as someone who delivers a consistent superior performance, mainly in representative tasks[74]. However there is no empirical evidence that superior performance can be achieved by extensive experience alone[75-77]. For instance the level of training and years of experience of clinical psychologists is not related to their efficacy and success in treating patients[78]. The same results account for UC Berkley professors of physics[79], software designers[80, 81]. Even experienced wine-experts perform only slightly better than regular wine drinkers[82]. Furthermore[83, 84] no genetic or innate individual characteristics predestined for expert performance but still resistant to modification by training have yet been found. Of course, there is a difference between cognitive tasks, such as being a Berkley Physics professor, and surgical motor skills.

The lack of an internal reference in motor learning determines the flat learning curve in the first phases of motor learning. For example, a person who would only have seen a laparoscopist bringing in an inguinal hernia mesh would be unable to handle the mesh themselves.

Again, in Part 3.2 of this thesis, the studies on experienced surgeons showed no significant relation of performance in drawing a "good" or "bad" incision line, with years of experience or surgical specialty such as trauma- or orthopedic-surgeon. This substantiates the earlier statement that the performance and thus the act of drawing an incision has become automated and that despite plenty of study material had been presented in journals, adequate adaptation of new standards has been proven difficult. In this study only one of all 23 participants drew both incision lines conform the gold standard. When asked to his peers, outside the scope of the study and without the results of the study presented, he was considered an expert on that particular field, e.g. foot-ankle surgery.

If not experience in years, could it be experience per patient that forms an expert surgeon? Ericsson et al.[74] proposed a new way of evaluating expert performance. From the studies described above they deduced that experience in age or experience per patient alone is not sufficient. They stated that the genetic or hereditary performance limit is just the arrest in development driven by automated performance. By studying chess players they found that Deliberate Practice for 4 hours a day over up to 10 years was mostly correlated to tournament ratings[75, 85]. Other studies, unintentionally meeting requirements

for solitary deliberate practice, also consistently found an association with expert performance in chess[86], music[87-89] and sports[90-92]. The act of deliberate practice halts the "migration" to autonomous performance and therefore the student keeps using the cognitive associative functions for problem solving and progresses further towards expert performance.

Deliberate practice consists of:
1) A well-defined task
2) Detailed immediate feedback
3) The possibility to improve and repeat the task.

Using CASAM during wet-lab courses or the web-based version of CASAM during surgery the phases of deliberate practice can be mimicked:

1) Invite the trainee to make an incision line for a certain surgical procedure on a patient or specimen.

2) Using CASAM anatomical feedback of multiple anatomical variations in relation to the incision line drawn is given and the trainee gets detailed immediate feedback. This contrasts to current surgical training in the operating room where detailed anatomical feedback cannot be given on such level. Using a web-based version of CASAM, more feedback can be provided on anatomical variations in relation to a specific incision line.

3) The initial task of drawing an incision line can be repeated in the next patient/specimen or even a picture of the previous patient, ensuring that a trainee can repeat and improve a task until a satisfactory result is achieved.

This application of CASAM would benefit a surgeon in training as it speeds up the learning process. Research shows[71, 72, 74] that expert performance in chess is only achieved if the chess player participates in deliberate practice for 4 hours a day, over a period of ten years. Currently, no surgical resident gets 4 hours of training conform the deliberate practice method whilst literature clearly shows that it minimizes the time to learn a certain task or anatomy. Currently in The Netherlands the amount of years of training for surgical residents is reduced significantly making the contents and methods of the training more important than ever. Also, deliberate practice in surgical courses and surgical "in theatre" training keeps young surgeons longer in a cognitive and associative phase allowing future surgeons to come closer to expert performance.

Similarly to young surgeons, surgeons with more years of experience who have reached an arrested development, or even decline in performance, can be

reengaged after new challenges are brought into the general, automated surgical proceeding. The web-based version of CASAM can be an easy to use platform to re-introduce anatomical variance and different degrees of anatomical complexity, using the actual patient as a teaching canvas. Not only might this reintroduce deliberate practice to a surgeon previously performing automated surgery and in addition, as suggested by literature on academic medicine, reactivate a cognitive and associative phase inducing expert performance in general.

Lack of direct feedback

Experience per patient sometimes lacks direct feedback. When a hemorrhage occurs during surgery it gives the surgeon direct feedback and he is therefore able to directly reconstruct the decision process that led to the event. Using this feedback per patient, during surgery most surgeons start operating more slowly or even give a warning to the operating staff when they intuitively feel that shortly significant blood loss might occur.

However when such a hemorrhage is recognized hours later it becomes more difficult to reconstruct the thinking process that was going on during surgery and therefore fewer lessons can be learnt. Superficial or cutaneous nerve damage is even worse in this regard, as generally iatrogenic damage is mostly noted days or weeks after the surgery has finished. It makes it almost impossible to reconstruct what actually happened during surgery and which decisions led to the damage of the nerve. This makes CASAM mapping of the superficial nerves more important since the usual direct feedback of a hemorrhage does not occur when a nerve is damaged.

Similarly, new research is best read in the operating room itself as intuitive links are made when new information is presented in the context in which they are going to be used.

The time at which results of research are generally being read is considered “spare-time” or during surgical conferences and are often not linked to the actual surgical procedure itself. Therefore it doesn’t entice a surgeon to have a conscious self-reflecting discussion on the current-day performance or approach to the research presented to him. In addition the next day in theatre, the practice itself is automated and in-theater performance is not being linked to the “spare-time readings”. The gap between anatomy research and the in-theater performance needs to be decreased, allowing the surgeon to receive new information in theatre and motivate a conscious decision to make a certain incision or perform a certain surgical approach.

Tailor made surgery and Real-time anatomy projection

A Web-based CASAM server with internationally gathered anatomical 3D data and automated landmark algorithms opens up the possibility for a whole new level of Tailor Made Surgery and personalized surgical planning. Since 3D data are readily available in the operating room and easily accessible for a surgeon, using minimal manual input, it would in theory be possible to map and project this data on the actual patient (Figure 18).

Figure 18. Representation of intra-operative projection of 3D anatomical data of the sural nerve on a patient`s ankle. Adapted image[93]

In order to successfully project 3D anatomical data on a patient interactively several major hurdles have to be overcome during surgery.

Real time-tracking of the patient.

It is undesirable not to be able to move the patient during surgery. Therefore some kind of tracking needs to be implemented to know where the ankle or arm of a patient is in real time so that 3D anatomy can be interactively projected onto the patient. First the location of the patient needs to be relayed to the software. Currently in neurosurgery this has already been achieved and it has been possible for a while to relay 3D anatomical data of a Ct-scan or MRI to a patient during surgery. There are multiple products on the marked such as Brainlab[94] and Brainsight[95]. Most products use laser pointers or actual pointers that the surgeon

needs to use to locate the different parts of the patient. Besides being quite labor intensive, the method has an actual 3D reference model of the patient with the MRI or CT-scan of that patient. In CASAM however there is no reference 3D model for an algorithm to relate the landmarks of the patient. One way to overcome this problem would be to make a 3D scan for each patient operated upon and then warp the average anatomy in the CASAM database. This way, there is a 3D reference and it therefore is much easier for a computer to locate the patient. However, this would introduce an extra step in the CASAM method which would be costly and time-consuming, at the same time making the data less accessible.

Once a patient`s location has been made clear to the computer, the patient has to be tracked when he moves. Current brain surgery products[94-96] use navigators that are being attached to a patient in order to track minimal changes in the position of the patient using a stereotactic camera (Figure 19). Given that these trackers are made for brain-surgery they are very accurate at tracking minimal changes but were not designed to account for major changes in the patient's position.

Figure 19. Trackers attached to a patient being tracked real time by a stereotactic camera. Adapted from Neurolite[95, 96].

In order to realistically and reliably track a patient that is potentially in motion, other methods need to be developed. A high speed and high accuracy option is the use of structured light. Although there are many different forms and methods of real-time 3D tracking with structured light the basis is the same. On an object that needs to be scanned a certain "structured light" is projected. As the light hits the 3D object the form of said light is deformed. A secondary camera registers the deformation of the original "structured light" and can thereby compute a 3D model of the object the light is on (Figure 20).

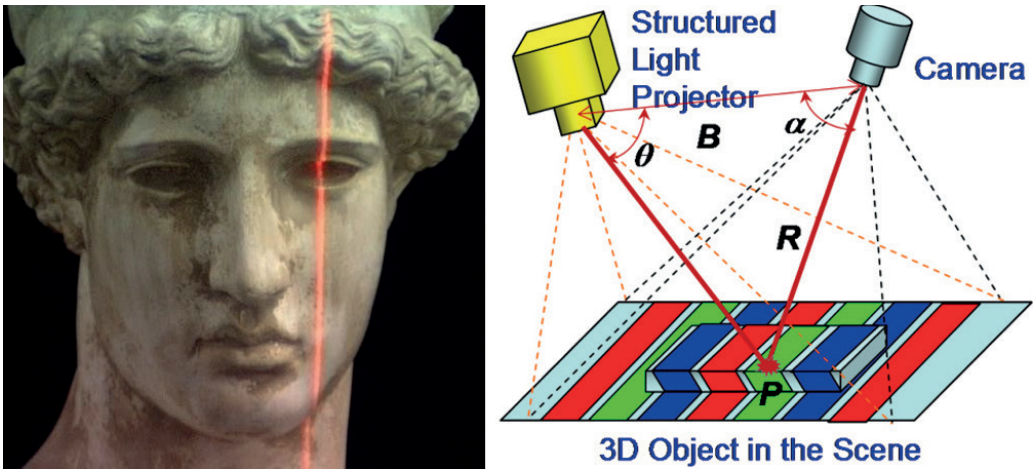

Figure 20. Structured light
Adapted from Jason Geng[97]

Algorithms on 3D mapping using structured light have been progressing quickly and there are many different methods using different forms of light and light structures, as well as light sensors and calibration techniques. In 3d scanning there is a trade-off between accuracy, scanning speed and the resolution of the scan. When using CASAM in theater both accuracy and scanning speed are very important, whilst resolution is of less relevance. Structured light scanning has already been used in many fields such as real-time vehicle crash test scanning and dental surgery[97]. It is also currently used for in-clinic 3D scanning of the female breast necessary for pre-surgical planning for breast augmentation[97]. Structured light has already been used to model repetitive motion[98] of for example heart muscle in mice, being able to not only track muscle movement with very high accuracy but also reveal it real-time in a heart beating 500 times a minute[99].

Besides dynamic tracking of the patient the projector needs to be able to constantly project on the patient from different angles. Instead of moving the projector around constantly when a patient is moved, mirrors can be used to deflect projection. Similar to systems that are designed to track a ball during sports games[100] mirrors can be used. The mirrors can change direction quickly without having to move a much heavier projector creating less projection lag or difficulty to real-time follow a moving patient. Furthermore, the projectors are rapidly becoming smaller. Therefore it is likely that these projectors can be integrated in operating room lighting and that these cameras and projectors will be robotized in the near future.

Real-time projection of anatomical data on patients would be of great benefit during surgery. However, as described by Kleinrensink et al.[101], the posture and motion of a patient`s extremity is of influence on peripheral nerve tension and its location. If data on peripheral nerves are extracted from extended legs, it might not be applicable to extrapolate the data on a flexed leg as the location of the nerves and other structures such as muscles, arteries and veins might be different. Therefore, the impact of movement and extremity position on the location of anatomical structures needs to be thoroughly investigated before real-time use of anatomical data projected on a patient can be used in clinical practice.

REFERENCES

1) Menon, R.R. Lower limb venous anatomy (Book Chapter) 2015. Chronic Venous Disorders of the Lower Limbs: A Surgical Approach.
2) Lugli, M. ELA technique of the small saphenous vein | [Réalisation technique du LEV de la petite veine saphène] 2013. Phlebologie - Annales Vasculaires 66 (2), pp. 50-54
3) Harlander-Locke, M., Jimenez, J.C.,Lawrence, P.F., (...), Gelabert, H.A., Farley, S.M. Management of endovenous heat-induced thrombus using a classification system and treatment algorithm following segmental thermal ablation of the small saphenous vein. 2013 Journal of Vascular Surgery.
4) Uhl, J.-F., Gillot, C. Anatomy and embryology of the small saphenous vein: Nerve relationships and implications for treatment. 2013. Phlebology
5) Joh JH, Kim WS, Jung IM, Park KH, Lee T, Kang JM. Vasc Specialist Int. 2014 Dec;30(4):105-12. doi: 10.5758/vsi.2014.30.4.105. Consensus for the Treatment of Varicose Vein with Radiofrequency Ablation; Consensus Working Group.
6) Kaiser, P., Schmidle, G., Raas, C., Blauth, M. Treatment concept for a traumatic lesion of the prepatellar bursa 2015. Operative Orthopadie und Traumatologie. 27 (5), pp. 427-438
7) Odutola, A., Fick, D., Khan, R. Exposure in revision knee arthroplasty. 2015. Orthopaedics and Trauma.
8) Li, J.-Y., Zhao, Q.-C., Shang, X.-F., Deng, X.-W., Gan, Z.-Y. Autologous hamstring tendon for anterior cruciate ligament reconstruction: Influence of incisions in different directions for cutting the hamstring tendon on the anterior tibial skin sensitivity. 2014. Chinese Journal of Tissue Engineering Research
9) Rossner M, Yamada K. What's in a picture: the temptation of image manipulation. J Cell Biol. 2004;166:11-15.
10) Maile T, Kwoczynski S, Katzenberger RJ, Wassarman DA, Sauer F. TAF1 activates transcription by phosphorylation of serine 33 in histone H2B. Science. 2004 May 14;304(5673):1010-4. RETRACTED ARTICLE
11) Sanchez-Elsner T1, Gou D, Kremmer E, Sauer F. Noncoding RNAs of trithorax response elements recruit Drosophila Ash1 to Ultrabithorax. Science. 2006 Feb 24;311(5764):1118-23. RETARCTED ARTICLE
12) http://en.wikipedia.org/wiki/Western_blot#mediaviewer/File:Anti-lipoic_acid_immunoblot.png Tim Vickers.
13) http://ori.hhs.gov/education/products/RIandImages/default.html
14) Wheeler T. Phototruth or photofiction? : Ethics and media imagery in the digital age. Mahwah, NJ: Lawrence Erlbaum Associates; 2002.
15) https://nppa.org/code_of_ethics
16) http://retractionwatch.com/2014/05/29/science-retracts-two-papers-for-image-manipulation/
17) Jason Geng. Three-dimensional display technologies. OSA Publishing > Advances in Optics and Photonics, Volume 5 Issue 4 Page 456
18) https://www.biodigital.com/
19) http://www.anatomyzone.com/3d_atlas/
20) http://netter3danatomy.com/
21) http://www.anatronica.com/
22) http://www.visiblebody.com/

23) http://www.holografika.com/
24) http://news.mit.edu/2016/glasses-free-3d-larger-scale-0725
25) https://www.oculus.com/
26) https://www.vive.com/eu/
27) http://www.erasmusmc.nl/corp_home/corp_news-center/2011/2011-12/embryos.ispace/
28) N. Lichtenberg. N. Smit, C. Hansen, K. Lawonn. Conference: Eurographics Workshop on Visual Computing for Biology and Medicine. Sline: Seamless Line Illustration for Interactive Biomedical Visualization.
29) N. Smit, A. Kraima, D. Jansma, A. Vilanova. VarVis: Visualizing Anatomical Variation in Branching Structures. Conference: EuroVis, At Groningen.
30) Wetzler. G. Rosman. R. Kimmel. Patch-space Beltrami denoising of 3D point clouds. 2012 IEEE 27-th Convention of Electrical and Electronics Engineers in Israel.
31) Brian Curless. "From Range Scans to 3D Models". ACM SIGGRAPH Computer Graphics. 33 (4): 38–41. doi:10.1145/345370.345399
32) Roy Mayer (1999). Scientific Canadian: Invention and Innovation From Canada's National Research Council. Vancouver: Raincoast Books. ISBN 1-55192-266-5. OCLC 41347212
33) https://www.fuel-3d.com/nl/shop/
34) https://www.artec3d.com/artec-eva#specifications
35) Lancaster P, Salkauskas K. Surfaces generated by moving least squares methods. Mathematics of Computation. 1981;37(155):141–158. doi: 10.1090/S0025-5718-1981-0616367-1.
36) fCheng ZQ, Wang YZ, Li B, Xu K, Dang G, Jin SY. A survey of methods for moving least squares surfaces. In: Proceedings of the Fifth Eurographics / IEEE VGTC conference on Point-Based Graphics; 2008. p. 9–23.
37) https://en.wikipedia.org/wiki/Three-dimensional_space
38) Adrien Bartoli, Mathieu Perriollat, Sylvie Chambon. Generalized Thin-Plate Spline Warps. VI-Technology. http://isit.u-clermont1.fr/~ab/Publications/Bartoli_Perriollat_Chambon_IJCV10.pdf
39) Karol Miller, Poul MF Nielsen. Computational Biomechanics for Medicine. Soft tissues and the musculoskeletal system.
40) Li Zhang, Noah Snavely, Brian Curless, and Steven M. Seitz. Spacetime Faces: High-Resolution Capture for Modeling and Animation. http://grail.cs.washington.edu/wp-content/uploads/2015/08/zhang-2004-sfh.pdf
41) AutoHotkey Foundation LLC. https://autohotkey.com/
42) Perakis P, Passalis G, Theoharis T, Kakadiaris IA. 3d facial landmark detection & face registration.University of Athens, Tech. Rep. 2011 Jan
43) Nair P, Cavallaro A. 3-d face detection, landmark localization, and registration using a point distribution model. Multimedia, IEEE Transactions on. 2009;11(4):611–623.
44) Bauer S, Ritacco LE, Boesch C, Reyes M. Automatic Detection of Anatomical Landmarks on the Knee Joint Using MRI Data. Article in Journal of Magnetic Resonance Imaging 41(1) · January 2015. DOI: 10.1002/jmri.24516 · Source: PubMed
45) Bromiley PA, Schunke AC, Ragheb H, Thacker NA, Tautz D. Semi-automatic landmark point annotation for geometric morphometrics. Frontiers in Zoology. 2014;11(1):61.

46) (Automatic) Identification of 3D landmarks – first steps. PA Bromiley. AC Schunke. D Tautz . NA. Thacker.

47) ED Aneja, SR Vora, ED Camci, LG Shapiro, and TC Cox. Automated Detection of 3D Landmarks for the Elimination of Non-Biological Variation in Geometric Morphometric Analyses. Proc IEEE Int Symp Comput Based Med Syst. 2015 June; 2015: 78–83. doi: 10.1109/CBMS.2015.86

48) Rolfe SM, Camci ED, Mercan E, Shapiro LG, Cox TC. A new tool for quantifying and characterizing asymmetry in bilaterally paired structures. Conf Proc IEEE Eng Med Biol Soc. 2013;2013:2364-7. doi: 10.1109/EMBC.2013.6610013.

49) https://rotterdampartners.nl/pers/facts-and-figures/

50) http://www.oozo.nl/cijfers/rotterdam

51) Kurian AK1, Cardarelli KM. Racial and ethnic differences in cardiovascular disease risk factors: a systematic review. Ethn Dis. 2007 Winter;17(1):143-52.

52) Dillingham TR, Pezzin LE, Mackenzie EJ. Racial differences in the incidence of limb loss secondary to peripheral vascular disease: a population-based study. Phys Med Rehabil. 2002 Sep;83(9):1252-7.

53) http://www.cdc.gov/cancer/colorectal/statistics/race.htm

54) Hinderer K.H. (1971) Fundamentals of Anatomy and Surgery of the Nose. Aesculapius Publishing, Birmingham, AL

55) W.F. Larrabee jr, K.H. Makielski, J.L. Henderson. Book. surgical anatomy of the face, second edition.

56) Parnell BA1, Midia EC, Fielding JR, Robinson BL, Matthews CA. Relationship between race and abdominal anatomy: effect on robotic port placement. Female Pelvic Med Reconstr Surg. 2013 May-Jun;19(3):165-8. doi: 10.1097/SPV.0b013e318288ad6d.

57) Suminski RR1, Mattern CO, Devor ST. Influence of racial origin and skeletal muscle properties on disease prevalence and physical performance. Sports Med. 2002;32(11):667-73.

58) Anson BJ. Anatomical considerations in surgery of the gall bladder. Quarterly bulletin. Northwestern University Medical School, 1963, 30:250–9.

59) Daseler EH et al. The cystic artery and constituents of the hepatic pedicle. A study of 580 specimens. Surgery, gynecology & obstetrics, 1947, 85:47–63.

60) East and Central African Journal of Surgery. Association of Surgeons of East Africa and College of Surgeons of East Central and Southern Africa ISSN: 1024-297X EISSN: 2073-9990 Vol. 12, Num. 1, 2007, pp. 93-98

61) De Silva M, Fernando D. Anatomy of the Calot's triangle and its relevance to laparoscopic cholecystectomy. Ceylon medical journal, 2001, 46(1):33–4.

62) M.A. Bakheit. Eastern Mediterranean Health Journal. Prevalence of variations of the cystic artery in the Sudanese. La Revue de Santé de la Méditerranée orientale, Vol. 15, N° 5 2009

63) Chaoliang Lv, MD; Yue Fang, MS; Lei Liu, MD; Guanglin Wang, MD; Tianfu Yang, BS; Hui Zhang, MD; Yueming Song, MD. The New Proximal Femoral Nail Antirotation-Asia: Early Results. Orthopedics. May 2011 - Volume 34 · Issue 5: e18-e23

64) Hwang JH, Oh JK, Han SH, Shon WY, Oh CW. Mismatch between PFNa and medullary canal causing difficulty in nailing of the pertrochanteric fractures [published online ahead of print September 11, 2008]. Arch Orthop Trauma Surg. 2008; 128(12):1443-1446.

65) Leung KS, Procter P, Robioneck B, Behrens K. Geometric mismatch of the Gamma nail to the Chinese femur. Clin Orthop Relat Res. 1996; (323):42-48.

66) Beat Schmutz, Jayani Amarathunga, Stanley Kmiec, Jr., Prasad Yarlagadda, and Michael Schuetz. Quantification of cephalomedullary nail fit in the femur using 3D computer modelling: a comparison between 1.0 and 1.5m bow designs. J Orthop Surg Res. 2016; 11: 53. Published online 2016 Apr 27. doi: 10.1186/s13018-016-0389-7 PMCID: PMC4848874.

67) Dale R Wagner and Vivian H Heyward. 2000 American Society for Clinical Nutrition. Measures of body composition in blacks and whites: a comparative review. Am J Clin Nutr. 2000 Jun;71(6):1392-402.

68) Roger Ball. SizeChina, a 3d anthropometric Survey of the Chinese Head.
https://id.gatech.edu/people/roger-ball

69) Moulton CA, Regehr G, Mylopoulos M, MacRae HM. Slowing down when you should: a new model of expert judgment. Acad Med. 2007 82(10 Suppl):S109-16

70) Toni Bernhard. How to be sick: Wisdom Publications 2010. A Buddhist-Inspired Guide for the Chronically Ill and Their Caregivers.

71) Galton F. Hereditary Genius: An Inquiry into Its Laws and Consequences. _Originally published in 1869._ London: Julian Friedman Publishers, 1979.

72) Fitts P, Posner MI. Human Performance. Belmont, CA: Brooks/Cole, 1967.

73) Anderson JR. Acquisition of cognitive skill. Psychol Rev. 1982;89:369–406.

74) K. Anders Ericsson. Deliberate Practice and the Acquisition and Maintenance of Expert Performance in Medicine and related Domains. Acad Med. 2004 Oct;79(10 Suppl):S70-81.

75) Ericsson KA, Krampe RT, Tesch-Ro¨mer C. The role of deliberate practice in the acquisition of expert performance. Psychol Rev. 1993;100:363–406.

76) Ericsson KA, Lehmann AC. Expert and exceptional performance: evidence on maximal adaptations on task constraints. Annu Rev Psychol. 1996;47:273–305.

77) Ericsson KA. The scientific study of expert levels of performance: general implications for optimal learning and creativity. High Abil Stud. 1998;9:75–100

78) Dawes RM. House of Cards: Psychology and Psychotherapy Built on Myth. New York: Free Press, 1994.

79) Reif F, Allen S. Cognition for interpreting scientific concepts: a study of acceleration. Cogn Instruct. 1992;9:1–44.

80) Rosson MB. The role of experience in editing. In: Proceedings of INTERACT ’84 IFIP Conference on Hum-Comput Interact. New York: Elsevier, 1985:45:-50.

81) Ashworth CA. Skill as the fit between performer resources and task demands. In: Proceedings of. 14th Annual Cognitive Science Meeting. Hillsdale, NJ: Erlbaum, 1992:444:-9.

82) Valentin D, Pichon M, de Boishebert, Abdi H. What’s in a wine name? When and why do wine experts perform better than novices? Abstr Psychonom Soc. 2000;5:36.

83) Howe MJA, Davidson JW, Sloboda JA. Innate talents: reality or myth? Behav Brain Sci. 1998;21:399–442.

84) Ericsson KA. Basic capacities can be modified or circumvented by deliberate practice: a rejection of talent accounts of expert performance. A commentary on M. J A. Howe, J W Davidson, and J A. Sloboda "Innate Talents: Reality or Myth?" Behav Brain Sci. 1998;21:413–4.

85) Simon HA, Chase WG. Skill in chess. Am Sci. 1973;61:394–403.

86) Charness N, Krampe RT, Mayr U. The role of practice and coaching in entrepreneurial skill domains: an international comparison of life-span chess skill acquisition. In: Ericsson KA (ed). The Road to Excellence: The Acquisition of Expert Performance in the Arts and Sciences, Sports, and Games. Mahwah, NJ: Erlbaum, 1996:51–80.

87) Krampe RT, Ericsson KA. Maintaining excellence: deliberate practice and elite performance in young and older pianists. J Exp Psychol Gen. 1996;125:331–59.

88) Lehmann AC, Ericsson KA. Music performance without preparation: structure and acquisition of expert sight-reading. Psychomusicology. 1996;15:1–29.

89) Sloboda JA. The acquisition of musical performance expertise: deconstructing the "talent" account of individual differences in musical expressivity. In: Ericsson KA. (ed). The Road to Excellence: The Acquisition of Expert Performance in the Arts and Sciences, Sports, and Games. Mahwah, NJ: Erlbaum, 1996:107–26.

90) Starkes JL, Deakin J, Allard F, Hodges NJ, Hayes A. Deliberate practice in sports: what is it anyway? In Ericsson KA (ed). The Road to Excellence: The Acquisition of Expert Performance in the Arts and Sciences, Sports, and Games. Mahwah, NJ: Erlbaum, 1996:81–106.

91) Helsen WF, Starkes JL, Hodges NJ. Team sports and the theory of deliberate practice. J Sport Exerc Psychol. 1998;20:12–34.

92) Ward P, Hodges NJ, Williams AM, Starkes JL. Deliberate practice and expert performance. In: Williams AM, Hodges NJ (eds). Skill Acquisition in Sport. London: Routhledge, 2004:231–58.

93) Dror Paley, MD; Bradley . Lamm, DPM; Dimitris Katsenis, MD; Anil Bhave, PT; John E. Herzenberg, MD. From Treatment of Malunion and Nonunion at the Site of an Ankle Fusion with the Ilizarov Apparatus. J Bone Joint Surg Am, 2006 Mar; 88 (1 suppl 1): 119 -134 .

94) https://www.brainlab.com/en/

95) http://www.neuroconn.de/produkte_neuronavigation_en/

96) http://www.neurolite.ch/en/products/magnetic-stimulation/navigated-tms/tms-navigator-research-edition

97) Jason Geng. Structured-light 3D surface imaging: a tutorial. Advances in Optics and Photonics Vol. 3, Issue 2, pp. 128-160 (2011) https://doi.org/10.1364/AOP.3.000128

98) Xu Y1, Aliaga DG. Modeling Repetitive Motions Using Structured Light. IEEE Trans Vis Comput Graph. 2010 Jul-Aug;16(4):676-89.

99) Jacob I. Laughner, Song Zhang, Hao Li, Connie C. Shao, Igor R. Efimov. Mapping cardiac surface mechanics with structured light imaging. American Journal of Physiology - Heart and Circulatory Physiology Published 15 September 2012 Vol. 303 no. 6, H712-720

100) http://www.medtronic.com/us-en/healthcare-professionals/products/neurological/ surgical-navigation-imaging/ surgical-navigation-systems/

101) G. Kleinrensink. Influence of posture and motion on peripheral nerve tension. Anatomical, biomechanical and clinical aspects. Thesis

01110011 01110101 01101101
01101101 01100001 01110010
01111001 00001010

Summary

To know where you are and where you are going means knowing where you came from. Therefore this thesis starts with a brief Historical overview explaining the thoughts of our predecessors that led to the eventual development of CASAM. In Dissection the works of the founding fathers of modern anatomy and surgery such as "The first known anatomist", "the father of modern Surgery", and "the restorer of anatomy" are described giving an historical overview of human dissection. Averaging describes how scientists such as Leonardo Da Vinci have long tried to capture the shapes of anatomy and reduce them to average and ideal proportions. Warping illustrates "how thinking outside the box" leads to exceptional theories; A Scottish biologist reduced the differences in shapes of related species such as ape and man to simple mathematical functions. In essence this formed the basis for the application of algorithms in the description of variations in anatomy and species.

Current concepts of CASAM are explained in **Part I, Computer Assisted Surgical Anatomy Mapping**. In the first sub-chapters the general principles of Image processing, Geometry and Warping are explained. Secondly their role in the novel anatomy mapping tool CASAM is elucidated when the three phases of the method are explained. First Preparation, photography and landmarks are described. Then in Warping the algorithms and averaging process is outlined and in Renditions the process of computing safe-zones and final renditions summarizing complex anatomy is illustrated.

The application of CASAM in basic surgical research is shown in **Part II, CASAM in Surgical Anatomy**. This part is divided into three subchapters, each describing different sorts of renditions dependent on the clinical research question. In Point distribution model the perforating veins of the lower arm are mapped as they have an impact on survival of Arteriovenous fistulae created for haemodialysis (chapter 2.1).

In Multiple Line model the variations of nerves and arteries are mapped in relation to kidney surgery (chapter 2.2) and ankle surgery (chapter 2.3). In chapter 2.4 regarding knee surgery, not only the superficial nerves are located but their direction is also mapped, encouraging surgeons to rethink the direction of the incision in which the knee is approached. As the wrist is a common site for neuropathic pain after injury of the sensory nerves, two of the radially located superficial nerves were mapped (chapter 2.5). The anatomical relation between these nerves is also quantified as it might explain the high rates of post-injury

neuroma formation and neuropathic pain found in the dorso-radial side of the wrist.

In chapter 2.6 the mapping of a Multiple area model is illustrated summarizing the anatomy of the sural nerve and the short saphenous vein. During thermal ablation, heat from the laser might damage the nerve and initially no safe zone could be defined as both structures are located close to each other. However the nerve partially runs below a protective fascia layer and by mapping this area in 20 specimens, even a 3-D Safe-zone for laser surgery is be defined. A "zone of interest" was mapped for three muscles located near the elbow; by defining a zone in which each muscle is present in all 20 specimens without overlap of other muscles a noninvasive preoperative test for tendon transfers for tetraplegic patients can be developed (chapter 2.7). Finally in chapter 2.8 CASAM is used to completely map the skin innervation of the hindpaw in multiple rats. The likelihood of overlap in skin innervation between the three branches of the sciatic nerve and the saphenous nerve was determined using CASAM.

Examples of the application of CASAM in the second pillar of surgery, teaching, are given in **Part III, Surgical Training.** First, the means by which CASAM is implemented in surgical teaching is discussed in chapters 3.1 and 3.2; the web-based version of CASAM allows for quick processing of incision lines drawn by participants on actual specimen. The photographed incisions can then be related to a "gold standard" or the computed location of multiple arteries and/ or nerves. Hereby residents and surgeons are given personalized and direct feedback, supported by multiple variations of anatomy dissected for research. Interestingly the results presented in this study seem to partially contradict the current perceived benefits of "volume surgery".

Incisions drawn by participants of surgical anatomy courses, or surgeons in general, can be compared and the inter- and intra-surgeon variability can be quantified. In chapter 3.3 incisions drawn for an approach of the tibia are mapped in relation to tibial nailing and chapter 3.4 discusses the inter- and intra surgeon variability in incisions drawn for an approach of the calcaneus in relation to calcaneal surgery. Common variables in the placement of these incision lines such as experience, surgical specialty and exposure to calcaneal surgery are related to how well a surgeon is able to draw an incision conform the "gold standard", showing that experience is not always related to expert performance.

Finally, in Discussion and future perspectives regularly raised reservations regarding CASAM are discussed. Most importantly the disadvantages and main doubts of warping algorithms and their application in CASAM will be related to data verification by means of conventional anatomy mapping. Currently CASAM is a labor intensive process and researchers not only need to learn how to dissect in a certain way but also be capable of basic coding and have a decent understanding of photo manipulation. Furthermore image manipulation is currently not widely accepted in research. Therefore a simple classification system is proposed that categorises the level of image manipulation to ensure that the reader exactly knows to what extent an image has been altered.

CASAM algorithms are ready for 3D and with 3D hardware available for the general public a current lack of 3D atlases comparing the anatomy of multiple specimens can be filled. Automated landmark placement nevertheless is still difficult but with the right amount of manual input it is definitely feasible. Furthermore a central server running CASAM software has the opportunity to provide a platform for international collaboration between anatomical wet-labs resulting in standardized and comparable anatomy research on a large scale. It will further individualize surgical planning as surgeons have straightforward access to easily interpretable 3D renditions representing a huge amount of anatomical data from people with different ethnical backgrounds. This will minimize the gap between basic anatomical research and the clinical surgeon since web-based data is freely accessible in the operating room. In the future, real time projection of surgically relevant anatomical data on individual patients might even be feasible. In theatre, access to anatomy will not only benefit the patient providing tailor-made surgery and personalised surgical planning, but it will also keep the surgeon up to date on anatomy based surgical approaches and keep him engaged in one of the most important fields of surgery; human anatomy.

01010011 01100001 01101101
01100101 01101110 01110110
01100001 01110100 01110100
01101001 01101110 01100111

Samenvatting, Nederlands

“Je weet pas waar je heen kan gaan als je weet waar je vandaan komt”. Daarom begint dit proefschrift met een kort hoofdstuk over de Geschiedenis van de anatomie en visualisatie technieken. In Prepareren worden de werken van de oprichters van moderne anatomie zoals “de eerste anatoom”, “de vader van moderne chirurgie”en “de hersteller van anatomie” beschreven. In Gemiddelden wordt beschreven hoe wetenschappers zoal Leonardo Da Vinci de vorm van het menselijk lichaam proberen samen te vatten in ideale, gemiddelde proporties. Het hoofdstuk Warpen laat zien hoe onderzoekers die buiten de gebaande paden denken exeptionele vooruitgang voortbrengen; een Schotse bioloog liet bijvoorbeeld zien hoe de verschillen in vorm tussen dieren te bevatten zijn in mathematische functies. Sindsdien worden algoritmes gebruikt om de variatie in anatomie tussen verschillende soorten dieren maar ook rassen te beschrijven.

De basis van CASAM wordt uitgelegd in **Deel I, Computer Assisted Surgical Anatomy Mapping**. In het eerste deel van dit hoofdstuk worden de basis principes van Foto-bewerking, geometrie en warpen uitgelegd. Vervolgens wordt hun toepassing in CASAM beschreven en worden de drie verschillende fasen van onderzoek toegelicht. Eerst wordt beschreven hoe Dissectie, Fotografie en het plaatsen van Landmarks in zijn werk gaat. Vervolgens worden de algorithmes voor het Warpen beschreven en wordt uitgelegd hoe de uiteindelijke Rendities worden gemaakt zodat complexe anatomie kan worden samengevat in bijvoorbeeld safe-zones of danger-zones.

De verschillende toepassingen van CASAM op chirurgisch anatomisch onderzoek staan in **Deel II, CASAM in de Chirurgische Anatomie** beschreven. Dit hoofdstuk is onderverdeeld in drie losstaande delen waarbij in elk hoofdstuk andere rendities nodig zijn om een bepaalde klinisch-chirurgische vraagstellingen te beantwoorden. In het hoofdstuk Punt distributie modellen zijn de perforerende venen van den onderarm in kaart gebracht omdat de locatie van deze perforanten impact heeft op de vitaliteit en duurzaameheid van arterio-veneuze fistels gemaakt voor bijvoorbeeld haemodialyse. (hoofdstuk 2.1).

In het hoofdstuk Meerdere lijnen modellen worden de anatomische variaties van zenuwen en arterien in kaart gebracht en gerelateerd aan bijvoorbeeld nierchirurgie (hoofdstuk 2.2) en enkel chirurgie (hoofdstuk 2.3). Hoofdstuk 2.4 gaat over knie-chirurgie en hierin wordt niet alleen de lokatie van oppervlakkige zenuwen beschreven, ook de richting waarin deze zenuwen lopen wordt gevisualiseerd zodat chirurgen worden aangespoord de richting van hun incisies

voor knie chirurgie aan te passen. Ook na letsel van de zenuwen in de dorsale pols komt het relatief vaak voor dat patienten hier neuropatische en invaliderende pijnklachten aan over houden. De nauwe anatomische relatie tussen twee van de oppervlakkige zenuwen wordt in hoofdstuk 2.5 beschreven en kan de hoge incidentie van neuropatische pijn na chirurgie in dit gebied verklaren.

In hoofdstuk 2.6 wordt de anatomie van zowel de nervus suralis als de vena saphena parva (zenuw en vene in het onderbeen) samengevat en weergegeven in een Meerdere gebieden model. Tijdens de ablatie van de de vene bij spataderen kan hitte van de laser de nabijgelegen zenuw beschadigen. Hoewel initieel geen duidelijke safe-zone kon worden beschreven vonden we uiteindelijk dat de zenuw gedeeltelijk onder een beschermende fascie laag ligt. Door alle anatomische data te bundelen kon uiteindelijk een 3D Safe zone voor laser-chirurgie van de vene worden bepaald. Voor drie spieren in de onderarm was juist een “zone of interest” nodig; door data over de locatie van alle spieren in 20 preparaten te bundelen kon een niet invasieve test worden ontwikkeld om de spieren te testen in tetraplegische patienten voordat deze spieren gebruikt worden voor pees/spier transposities (hoofdstuk 2.7). Verder wordt in hoofdstuk 2.8 beschreven hoe met CASAM de volledige innervatie van de achterpoot van meerdere ratten in kaart kon worden gebracht.

Voorbeelden van de toepassing van CASAM in een tweede pilaar van chirurgie, namelijk onderwijs, wordt besproken in **Deel III, Chirurgische training**. In hoofdstukken 3.1 en 3.2 wordt besproken hoe CASAM gemakkelijk kan worden geintegreerd in anatomisch/chirurgisch onderwijs. Met de huidige web-based versie van CASAM kunnen incisie lijnen van verschillende cursisten op verchillende preparaten snel verwerkt worden. Deze incisies kunnen dan bijveoorbeeld vergeleken worden met de gouden standaard voor die operatie of de berekende locatie van verschillende zenuwen, arterien of venen. Op deze manier kunnen chirurgen in opleiding persoonlijke en directe feedback krijgen op hun input en dit vergelijken met de anatomie van niet één, maar meerdere preparaten.

Incisies getekend door chirurgen in opleiding, of door ervaren chirurgen kunnen met CASAM worden vergeleken en de inter- en intra-chirurgische variatie kan worden berekend. In hoofdstuk 3.3 worden incicies voor de benadering van de proximale tibia (knie) in kaart gebracht en in hoofdstuk 3.4 wordt de inter- en intra-chirurgische variatie van incisies voor de laterale benadering van

de calcaneus (hiel) berekend. Veel genoemde variabelen voor correcte incisie plaatsing, zoals ervaringsjaren, chirurgische differentiatie of het aantal ingrepen per jaar, bleken geen invloed te hebben op hoe consistent of hoe "goed" chirurgen een incisie konden plaatsen en laat zien dat ervaring alleen niet genoeg is voor consistente en competente incisie plaatsing.

In **Discussie en toekomstige onderzoeksdoelen** worden allereerst de algemene terughoudendheid en beperkingen besproken van het gebruik van algoritmes en wiskundige formules in basaal anatomisch onderzoek. Ook zullen de resultaten berekend met CASAM worden vergeleken met conventionele manieren van anatomie mapping. Daarnaast wordt besproken dat CASAM vooralsnog een erg bewerkelijke methode van mapping is; de onderzoeker moet niet alleen op een heel specifieke manier prepareren maar ook basale foto-manipulatie begrijpen, alsook basaal kunnen coderen. Verder wordt behandeld dat foto manipulatie vooralsnog niet altijd geaccepeerd is in basaal wetenschappelijk onderzoek, maar wel steeds vaker voorkomt. Daarom beschrijven we een nieuw classificatie systeem dat zowel door onderzoekers als uitgevers kan worden gebruikt zodat de lezers van wetenschappelijke bladen precies weten wat er met een afbeelding is gebeurd.

Momenteel zijn de CASAM algoritmes klaar voor verwerking van 3D beelden. Huidige 3D atlassen zijn vaak niet toerijkend en CASAM kan een aanvulling zijn op huidige 3D atlassen welke vooralsnog allen gebaseerd zijn op één enkel preparaat. Daarnaast zijn samenvattende rendities juist in nog complexere 3D anatomie extra belangrijk. Zeker nu 3D hardware meer bereikbaar is voor de consument kan 3D anatomie nog makkelijker en duidelijker bij de gebruiker of chirurg worden gebracht. Het volledig geautomatiseerd plaatsen van Landmarks is vooralsnog niet haalbaar maar partiele automatisatie met minimale manuele input is zeker bereikbaar. De webbased versie van CASAM loopt vanaf een centrale server en kan daarom een platform zijn voor toekomstige samenwerking tussen internationale anatomie laboratoria en zo de basis vormen voor gestandaardiseerd anatomie onderzoek. Ook legt dit de basis voor geindividualiseerde chirurgische planning omdat chirurgen de beschikking kunnen hebben over grotere data sets van meerdere prepraten met verschillende etnische achtergronden. Zeker als de web-based versie van CASAM makkelijk toegankelijk is in de reguliere operatiekamer kan zo de afstand tussen basaal anatomisch onderzoek en klinische chirurgie worden overbrugd. In de toekomst kan het zelfs mogelijk zijn om rendities van anatomische data realtime te projecteren op individuele patienten. De gemakkelijke beschikbaarheid van anatomie in de operatiekamer zal niet

alleen directe complicaties verminderen maar door bij elke nieuwe patient de complexe anatomie aan de chirurg te tonen blijft deze continu leren en nauw betrokken bij de basis van zijn/haar vakgebied: de menselijke anatomie.

01000001 01110000 01110000
01100101 01101110 01100100
01101001 01100011 01100101
01110011

Appendices

ACKNOWLEDGEMENTS / DANKWOORD

"I blame all of you. Writing this book has been an exercise in sustained suffering. The casual reader may, perhaps, exempt herself from excessive guilt, but for those of you who have played the larger role in prolonging my agonies with your encouragement and support, well…you know who you are, and you owe me." *Brendan Pietsch, assistant professor of religious studies at Nazarbayev University in Astana, Kazakhstan.*

Wetenschappelijk onderzoek doe je niet alleen en zonder de passie en kwaliteiten van mijn collega`s en het begrip van familie en vrienden was dit boek nooit tot stand gekomen.

Beste professor Kleinrensink, lieve Gert-Jan, allereerst wil ik jou bedanken voor je vertrouwen in mij en alle gekke ideeën waarmee ik regelmatig bij je binnenliep. Zoals met alle mensen om je heen haal jij het beste uit mij en ben je in staat geweest om mijn brede interesse te focussen op dit boek en mijn opleiding. Ik bewonder je passie voor onderzoek en onderwijs en hoe je in alle rust iedereen daarin kan begeleiden. Ook op persoonlijk vlak heb jij altijd energie om mij en anderen te helpen. Door de jaren heen ben jij voor mij gegroeid van mentor naar vriend en ik hoop dat we nog vaak met een pilsje kunnen filosoferen over het leven.

Beste dr Walbeehm, Eric, zelden heb ik een zo gepassioneerd chirurg gezien. Vanaf de eerste keer dat jij me op de snijzaal onderwees tot nu krijg ik energie van onze samenwerking en jouw passie is echt ontzettend aanstekelijk. Jij weet de mensen om je heen altijd te pushen om het maximale te proberen te bereiken en in ruil daarvoor krijgen ze een gedreven mentor die om vier uur `s ochtends de artikelen volledig reviseert of een plekje in Wythensaw regelt. Ik hoop dat ik nog heel lang, heel veel van jou mag leren en ik jou nog lang tot mijn mentor en vriend mag rekenen.

Beste dr den Hartog, Dennis, wat kon jij me scherp houden. Met regelmatige mails en telefoontjes wist jij als geen ander druk op de ketel te houden en de neuzen dezelfde kant op te krijgen. Zonder jou had ik er waarschijnlijk nog 9 jaar over gedaan. Als er auteur problemen waren wist ik dat jij het kon fixen. Verder heb jij me altijd verbaasd over hoe je kan multi-tasken en toch moet je nog steeds een keer de tijd nemen om mij dat te leren.

Professor Verhofstad, hartelijk dank voor de jaren van samenwerking. Jij kan als geen ander een stuk dat net niet lekker loopt omzetten in een artikel dat we makkelijk kunnen publiceren en voor iedereen leesbaar is. Ik heb veel respect voor je academische begeleiding in de leerstoel in Rotterdam was voor mij ook geen enkele verrassing.

Professor Hovius, wat u heeft opgezet in Rotterdam is echt ongelooflijk en van mijn Anios tijd in het Erasmus heb ik ontzettend veel kunnen leren. Ook uw begeleiding en advies daarna heb ik erg kunnen waarderen. Verder heb ik u meerdere keren zien lesgeven en presenteren en er zijn maar weinig mensen die dat zo natuurlijk en bevlogen kunnen.

Beste professor Coert, Henk, hartelijk dank voor je begeleiding de afgelopen jaren. In moeilijke tijden wist jij mij mede te inspireren om door te zetten en was je altijd erg begaan. Verder kan ik erg waarderen hoe je me ook begeleid in het uitzetten van mijn (academische) carrière en laat je mensen nadenken over de lange termijn. Ondertussen zijn we samen weer nieuwe onderzoekslijnen aan het uitzetten en ik ben erg benieuwd waar onze samenwerking toe gaat leiden.

Beste dr Hoogbergen, dr van Rappard en stafleden van de plastische chirurgie in Eindhoven. Heel erg bedankt voor het in mij gestelde vertrouwen. Ik heb het zo ontzettend naar mijn zin bij jullie, niet alleen op professioneel vlak maar ook op persoonlijk gebied. De maatschap en assistenten groep is echt een hecht team waar ik graag deel van ben en waardoor ik veel plezier heb in mijn werk en opleiding. Ik kijk er naar uit om na mijn vooropleiding weer bij jullie te beginnen!

Dank ook aan de overige leden van de promotiecommissie; professor Lange, professor Nijs, professor Ulrich en professor Verhagen. Ik wil jullie hartelijk bedanken voor alle tijd die jullie hebben genomen voor de beoordeling van mijn proefschrift en jullie aanwezigheid tijdens de verdediging.

Lieve assistenten plastische chirurgie van Eindhoven, super bedankt voor de heerlijke tijd tot nu toe! Echt een lekker gezellige groep die niet alleen hard kan werken maar ook continu voor elkaar klaar staat. Ik hoop dat we nog lang met elkaar kunnen samenwerken en dat ik nog veel van jullie mag leren!

En natuurlijk ook een bedankje voor de assistenten chirurgie van Eindhoven! Ik heb superveel van jullie geleerd en ook hier weer mooi om zo`n hechte groep

te hebben. Iedereen staat altijd voor elkaar klaar en een feestje is zo geregeld. Alleen die ski-reis nog... drie maal proberen is scheepsrecht!

Dear professor McGrouther, as a plastic surgeon, researcher and mentor you have inspired me. You passionately teach those who are willing to learn and you stimulate young researchers to push their boundaries and keep an open mind. You taught me that being a medical practitioner is more than prescribing medication or perform surgery; it is about teaching the future generation, patients and the general public and optimize the healthcare system as a whole. Meanwhile you are very humble and were always open to critique or discussion. I can't thank you enough for my time in Wythenshaw and Manchester.

Lieve Yvonne, lieve mamma snijzaal. Wat ben ik blij dat wij elkaar hebben leren kennen. Ik heb het ontzettend naar mijn zin gehad op de snijzaal en veel van jou geleerd. Het is bizar hoe goed wij elkaar gelijk weer aanvoelen als we elkaar lang niet hebben gezien en hoe lekker we alle frustraties bij elkaar kwijt kunnen. Ook de avondjes pilzen zal ik niet snel vergeten! Zo ontzettend top dat je mijn paranimf wil zijn.

Lieve Antoinette, dank voor al je hulp en die heerlijke springende gezelligheid. Zo`n plaats als de snijzaal/het skillslab heeft jou gewoon hartstikke nodig! Ik hoop dat je daar nog jaren zit en we samen nog veel cursussen gaan organiseren. Ik kan me geen betere paranimf voorstellen.

Stefan en Berend-Jan super bedankt voor al jullie hulp. Samen houden jullie alles draaiend in de snijzaal en op het skillslab. Zonder jullie geen onderzoek, geen onderwijs en geen cursussen. Jullie staan er altijd voor iedereen (en voor mij zeker ook!). We hebben veel aan jullie te danken.

Natuurlijk ook dank aan alle snijzaal-studenten, Earp-ers en anatomie enthousiastelingen die hebben geholpen om alle anatomie onderzoeken waar te maken. Zonder jullie was ik nog zeker 10 jaar bezig geweest om alles af te maken! Verder zal ik de snijzaal-borrels, late avondjes dissecteren en muziek op repeat-shrijf sessies niet snel vergeten.

Beste Alex Poublon, dank voor al het werk dat we samen hebben gedaan en de onderzoeken die we publiceren. Veel succes als orthopeed en ik weet zeker

dat je binnenkort ook mag promoveren met een prachtig boekje waar je trots op kan zijn.

Beste Joris Harlaar, Mandala Leliveld, Teunette van der Graaf en Martijn ten Berge, dank voor de samenwerking. Het was een eer om alle mooie ideeën en onderzoeksvoorstellen om te zetten in onze mooie publicaties.

Verder wil ik de ICT-helden uit Delft bedanken: N.N. Smit, S.E.F. van Berkel, B. Bijl, J.Y.T. den Hollander, S. Rabbelier, B.M.W. Sedee. Wat hebben jullie hard je best moeten doen voor de web-based versie van CASAM. We hadden eigenlijk maar heel kort de tijd en spraken elkaars taal maar nauwelijks maar het eindresultaat mocht er zijn en zal de basis vormen voor de toekomst. Ik ben hartstikke trots op wat we samen hebben kunnen neerzetten!

Voor mijn tijd in het Maasstad ziekenhuis wil ik graag Jean Bart Jaquet, Ariën Hofman en Rudy Tjong bedanken. Jullie hebben daar een prachtige plastische afdeling neergezet en ik heb daar in korte tijd zo ontzettend veel kunnen leren. De woensdag-ochtend poli met Jean-Bart en de vrijdag middag Schmidt zeevishandel zal ik nooit vergeten!

Beste Mieke en Bert Timmermans, dank voor jullie steun, gastvrijheid en vertrouwen. In Aardenburg vinden Marieke en ik altijd weer een stukje rust waardoor we ons bizar drukke leventje weer even aankunnen. Beste Stefan en Mark, na deze promotie heb ik weer wat meer tijd dus we gaan snel weer barbecueën! Lieve Mietje en Cees, hartelijk bedankt dat jullie deze dakloze arts en onderzoeker een jaar lang onderdak, schaft, gezelligheid, rummicup toernooien en Brabantse taal-les hebben willen geven. Maarten Nas, super bedankt voor je steun en dat je zo`n lieve oom bent voor Marieke. Je bent hier altijd welkom voor een avondje rijsttafel en lekker bijkletsen!

Beste Mark, Jorn en Pascal. Oude en goede vrienden hebben weinig woorden nodig. Bedankt! En nu eerst een pilsje...

Ook wil ik iedereen bedanken die de moed en kracht heeft gehad om zijn of haar lichaam aan de wetenschap ter beschikking te stellen. Door jullie wordt de nieuwe generatie chirurgen goed opgeleid en kunnen we op grote schaal onderzoek doen.

Lieve Martijn, ik ben apetrots op je jongen. Je bent echt super begaan en bekwaam als tandarts en gaat geen uitdaging uit de weg. Ook in Garderen lekker klussen en je vakkennis uitbreiden, super man. Jij beleeft echt elke dag, of je het nou deelt met patienten, je vrienden, familie, of gewoon met de natuur.

Lieve Thymen, ook op jou ben ik apetrots. Je hebt vaak genoeg moeten knokken maar zo zie je maar, de aanhouder wint. Blijf genieten van de kleine dingen en goede vrienden om je heen. Ik ben zo blij dat ik deze dag (verdediging) met jou kan delen want met jou erbij is het altijd een feestje!

Lieve Bert en Margriet, “leading by example” is wat jullie als geen ander kunnen. Van jullie heb ik geleerd hard te werken, alleen dingen te doen die je echt leuk vindt en jezelf ergens met volle overgave en passie in te storten, of het nou sport, piano, werk of onderzoek is. Jullie zijn er altijd voor mij en mijn broertjes geweest en door jullie hebben we veel mooie kansen gekregen. Pa, ook super leuk dat we samen hebben kunnen opereren, lesgeven en onderzoek doen. De onvoorwaardelijke steun die ik kreeg en het begrip had ik ook echt nodig om dit boek af te maken. Ik sta waar ik nu ben door jullie en ik zal dat nooit vergeten.

Lieve Marieke,

01010110 01101111 01101111 01110010 00100000 01101010 01101111 01110101 01110111 00100000 01100001 01100100 01110110 01101001 01100101 01110011 00101100 00100000 01101010 01100101 00100000 01100111 01100101 01100100 01110101 01101100 01100100 00100000 01100101 01101110 00100000 01101010 01100101 00100000 01100111 01100101 01101100 01101111 01101111 01100110 00100000 01101001 01101110 00100000 01101101 01101001 01101010 00101100 00100000 01101111 01101101 01100100 01100001 01110100 00100000 01101010 01101001 01101010 00100000 01101101 01100101 00100000 01100001 01101100 01110100 01101001 01101010 01100100 00100000 01100010 01100101 01100111 01110010 01101001 01101010 01110000 01110100 00101110 00100000 01011010 01101111 01101110 01100100 01100101 01110010 00100000 01101010 01101111 01110101 00100000 01101001 01110011 00100000 01101000 01100101 01110100 00100000 01100001 01101100 01101100 01100101 01101101 01100001 01100001 01101100 00100000 01101110 01101001 01101011 01110011 00100000 01110111 01100001 01100001 01110010 01100100 00100000 01100101 01101110 00100000 01101101 01100101 01110100 00100000 01101010 01101111 01110101 00100000 01101001 01110011 00100000 01100001 01101100 01101100 01100101 01110011 00100000 01100010 01100101 01110100 01100101 01110010 00101110 00100000

"walk a little slower daddy." Said a child so small. "I`m following in your footsteps and I don't want to fall. Sometimes your steps are very fast, Sometimes they`re hard to see; So walk a little slower, Daddy, For you are leading me. Someday when i`m all grown up, You`re what I want to be; Then I will have a little child Who`ll want to follow me. And I would want to lead just right, And know that I was true; So walk a little slower, Daddy, For I must follow you."

ABOUT THE AUTHOR

Anton Kerver was born on April 17th in 1986 in the Utrecht, the Netherlands, and grew up in Rotterdam with his two brothers Martijn and Thymen, with their parents Bert and Margriet. During high school he spend most of his time training for the decathlon in athletics and was able to participate at several national championships. In 2004 he graduated from the Marnix gymnasium and started studying Medicine at the Erasmus University in Rotterdam.

Early in his studies, Anton became interested in research and participated in several studies in medical fields such as rheumatology, pediatric anesthesia, pediatrics and surgery. He also founded and supervised several teams in which students were able to work at outpatient clinics for departments such as gastro-enterology, general internal medicine and rheumatology.

However, not until Anton started working in the anatomy wet-lab, his passion for human anatomy, surgery and eventually plastic surgery was triggered. Under the supervision of Yvonne Steinvoort, he learned to embalm, dissect and teach anatomy. He co-lectured anatomy courses such as the CASH-course and LISA (lowlands institute of surgical anatomy) and co-founded courses such as the advanced first aid course for Dutch military combat life-savers.

Eventually his enthusiasm for teaching sparked the idea for this thesis: Computer Assisted Surgical Anatomy Mapping. Under the mentorship of his promotor Gert-Jan Kleinrensink, Anton conducted anatomy research and started publishing the results of his novel mapping method. He also co-supervised six bachelor students of the faculty of electrical engineering, mathematics and computer science to build a web-based version of CASAM. Meanwhile, on February 12th in 2012, Anton obtained his medical degree cum laude. While finishing the chapters of his thesis he started working as a Plastic Surgery intern at several Dutch hospitals such as the Maasstad hospital, Erasmus MC and Catharina hospital in Eindhoven. In November 2015 Anton was allowed to start his residency in Plastic and Reconstructive Surgery under the supervision of dr. J.H.A. van Rappard and dr M.M. Hoogbergen.

Whilst literally dissecting a human heart Anton met his loving and supporting partner Marieke Timmermans with whom he happily lives in Eindhoven.

PHD PORTFOLIO

Name PhD student:	Anton Kerver
Erasmus MC Department:	Anatomie en Neurowetenschappen
PhD period:	April 2009 - September 2017
Promotor:	Prof.dr. G.J. Kleinrensink
Co-promoteres:	Dr. D. Den Hartog
	Dr. E.T. Walbeehm

Co-Founder

2014 April 24th	"Seminar Reumahand" (rheumatic hand).
2011 – 2014	Advanced. First aid course for Dutch military personnel.
2009 – 2014	Applied anatomy, First aid course. Dutch military.
2009 – 2010	Fractures of the foot/ankle, surgical course for residents.

Teacher

2012 – 2014	CASH-course surgical residents.
2009 – 2014	Anatomy for engineers.
2009 – 2014	Basic Anatomy courses for para-medical personnel
2009 – 2014	Various anatomy courses for medical students.
2008 - 2009	EARP (Erasmus Anatomy Research Program) Tutor

Co-organizer

2012	Atrium: TEP Course.
2009 - 2011	AO basic course. AO cadaver course Rotterdam/Leiden.
2009 – 2010	Various LISA courses

Course-assistant

2009 – 2015	Assisted in various courses as an employee at the dep. of anatomy and neuroscience. Fracture management, endoscopic surgery, IPSEN, Botox injections, knee replacement surgery, shoulder and knee arthroscopy,

Supervision:

Co-supervisor Bachelor-project

2009	CASAM project. Delft university of Technology, Faculty Electrical Engineering, Mathematics and Computer Science. Students: S.E.F.van Berkel, B. Bijl, J.Y.T. den Hollander, S. Rabbelier, B.M.W. Sedee, N.N. Smit.

2009-2012	Co-supervised multiple medical students with their medical research internship/ bachelor essay.

Presentations:

20 May 2010	(Best Abstract Session) Laterale incisie bij de open benadering van de calcaneusfractuur; interchirurgische verschillen en relatie tot de nervus suralis. Chirurgendagen.
15 May 2010	The Inter-surgeon Variation to the Open Lateral Approach of the Calcaneus. ESTES
24 Apr 2010	Een CASAM studie voor de ontwikkeling van een test voor het individueel evalueren van de kracht van de ECRL en ECRB bij tetraplegie patiënten. NVPC, lustrum.
27 Nov 2009	De chirurgische anatomie van de vena saphena parva en omliggende zenuwen in relatie tot endoveneuze lasertherapie. Chirurgendagen.
29 Mar 2009	De chirurgische anatomie van de vena saphena parva en omliggende zenuwen in relatie tot endoveneuze lasertherapie. Vascular rounds.

Poster presentations

08 Apr 2010	De inter-chirurgische variatie bij de Open Laterale benadering van de Calcaneus en de relatie met de Nervus Suralis. SFG wetenschapsdag Rotterdam.
08 Apr 2010	De chirurgische anatomie van de vena saphena parva en omliggende zenuwen in relatie tot endoveneuze lasertherapie. SFG wetenschapsdag Rotterdam,
07 Apr 2010	Computer Assisted Surgical Anatomy Mapping. WEBIST- Ict conference. Valencia.

Memberships

2016 – present	Junior Vereniging Plastische Chirurgie
2015 – present	Nederlandse Vereniging voor Plastische Chirurgie
2013 – present	Nederlandse Anatomen Vereniging

LIST OF PUBLICATIONS

Submitted 2017. The neurovascular anatomy of the lateral hindfoot in relation to incisions for a lateral approach of the ankle and calcaneus. A.L.A Kerver, M.H.J. Verhofstad, A.J.H. Kerver, A.H. van der Veen, D. den Hartog, G.J. Kleinrensink.

Submitted 2017. A CASAM study on the intra- and inter-surgeon variation of incision lines in the lateral approach of the calcaneus in surgical fracture treatment. A.L.A.Kerver, K.W.J. Klop, W.E. Tuinebreijer, D. den Hartog, G.-J. Kleinrensink

Submitted 2017. Optimal surgical approach for the treatment of de Quervain's disease: a surgical-anatomical study. A.R. Poublon, G-J Kleinrensink, A.L.A. Kerver, J.H. Coert, E.T. Walbeehm.

Submitted 2017. External fixators for treatment of distal radius fractures: An anatomical study on an alternative location of the Schanz pins. A.R.. Poublon, E.T. Walbeehm, A.L.A. Kerver, J.H. Coert, G.J. Kleinrensink.

Journal of Plastic Reconstructive and Aesthetic Surgery, 2016. Study of the dorsal cutaneous branch of the ulnar nerve (DCBUN) and its clinical relevance in TFCC repair. Poublon AR, Kraan G, Lau SP, A.L.A. Kerver, Kleinrensink GJ.

Journal of Plastic Reconstructive and Aesthetic Surgery, 2015: The anatomical relationship of the superficial radial nerve and the lateral antebrachial cutaneous nerve: A possible factor in persistent neuropathic pain. Poublon AR, Walbeehm ET, Duraku LS, Eilers PH, A.L.A. Kerver, Kleinrensink GJ, Coert JH.

Journal of neuroscience methods, 2014: Innervation mapping of the hind paw of the rat using Evans Blue extravasation, Optical Surface Mapping and CASAM. Kambiz S, Baas M, Duraku LS, A.L.A. Kerver, Koning AH, Walbeehm ET, Ruigrok TJ.

Journal of bone and joint surgery, 2013: The surgical anatomy of the infrapatellar branch of the saphenous nerve in relation to incisions for anteromedial knee surgery. A.L.A. Kerver, Leliveld MS, den Hartog D, Verhofstad MH, Kleinrensink GJ.

Journal of plastic reconstructive and aesthetic surgery, 2013: An anatomical study of the ECRL and ECRB. Feasibility of developing a pre-operative test for evaluating the strength of the individual wrist extensors. A.L.A. Kerver; L. Carati; P.H.C. Eilers; A.C. Langezaal, G.J. Kleinrensink; E.T. Walbeehm.

Journal of vascular surgery 2012: The surgical anatomy of the small saphenous vein and adjacent nerves in relation to endovenous thermal ablation. A.L.A. Kerver, van der Ham AC, Theeuwes HP, Eilers PH, Poublon AR, Kerver AJ, Kleinrensink GJ.

Pneumologie 2012: Neue horizonte für die mediastinoskopie: Entwicklung einer transoralen mediastinal-chirurgie auf der basis von NOS (natural orifice surgery). Klem W, Wilhelm T, Leschber G, Harlaar JJ, A.L.A. Kerver, Kleinrensink GJ, Nemat AT.

The Journal of Urology: Letter, 2011. Re: Surgical Anatomy of the 10th and 11th Intercostal, and Subcostal Nerves: Prevention of Damage During Lumbotomy: T. van der Graaf, P. C. Verhagen, A.L.A. Kerver and G.J. Kleinrensink J Urol 2011;186:579–583 Teoh Seong Lin, Srijit Das, 2012.

The Journal of Urology, 2011: Surgical Anatomy of the 10th, 11th Intercostal and Subcostal Nerves: Prevention of Damage During Lumbotomy. Teunette van der Graaf , Md, Paul C.M.S. Verhagen, MD, Ph.D, A.L.A. Kerver, MSc. Gert-Jan Kleinrensink, Ph.D.

European journal of vascular surgery, 2011: Perforating Veins: An Anatomical approach to Arteriovenous Fistula Performance in the Forearm. Martijn M.G. ten Berge, MSc, Tik Ien Yo, MD, A.L.A. Kerver, MSc, Andre A.E.A. de Smet, MD and Gert-Jan Kleinrensink, PhD.

Injury Extra 2010: Inter-Surgeon variation in skin incision for tibial nailing in relation to the infrapatellar nerve. A.L.A. Kerver, Leliveld M, Theeuwes HP, Kleinrensink GJ.

Proceedings of the 6th International Conference on Web Information Systems and Technology (WEBIST), 2010: Web-based Computer Assisted Surgical Anatomy Mapping. A.L.A. Kerver, G.J. Kleinrensink, N.N. Smit, S. Rabbelier, B. M. W. Sedee, C.P. Botha.

European Journal of Cardiothorac Surgery, 2010: Development of a new trans-oral endoscopic approach for mediastinal surgery based on 'natural orifice surgery': preclinical studies on surgical technique, feasibility, and safety. Wilhelm T, Klemm W, Leschber G, Harlaar JJ, A.L.A. Kerver, Kleinrensink GJ, Nemat A.

conf paper, 45th congress of the European society for surgical research, 2010: A new endoscopic method for mediastinal surgery with the usage of natural orifice surgery: Anatomical studies on feasibility and surgical technique of the trans-oral endoscopic approach. Wilhelm T, Klemm W, Harlaar JJ, A.L.A. Kerver, Kleinrensink GJ, Nemat A.

Archives Otorhinolaryngology, 2010: Surgical anatomy of the floor of the oral cavity and the cervical spaces as a rationale for trans-oral, minimal-invasive endoscopic surgical procedures: results of anatomical studies. Wilhelm T, Harlaar JJ, A.L.A. Kerver, Kleinrensink GJ, Benhidjeb T.

Der chirurg, 2009: Transoral endoscopic thyroidectomy. Part 2 surgical technique. Wilhelm T, Harlaar JJ, A.L.A. Kerver, Kleinrensink GJ, Benhidjeb T.

Der chirug, 2009: Transoral thyroidectomy. Part 1 rationale and anatomical studies. Wilhelm T, Harlaar JJ, A.L.A. Kerver, Kleinrensink GJ, Benhidjeb T

NOTES

Don’t give yourselves to these unnatural men - machine men with machine minds and machine hearts! You are not machines! You are not cattle! You are men! You have the love of humanity in your hearts! … Let us fight for a world of reason, a world where science and progress will lead to all men’s happiness. (Charlie Chaplin)

THIS THESIS WAS (FINANCIALLY) SUPPORTED BY:

In no particular order